Mauro Mameli

"PULSATING HEAT PIPES Numerical Modeling and Experimental Assessment"

ISBN: 978-88-97413-05-9

UNIVERSITÀ DEGLI STUDI DI BERGAMO

PULSATING HEAT PIPES
Numerical Modeling and Experimental Assessment

Mauro Mameli
Doctoral Thesis

Tesi di Dottorato in Tecnologie per l'energia e l'ambiente

UNIVERSITA' DEGLI STUDI DI BERGAMO
Facoltà di Ingegneria
Dipartimento di Ingegneria Industriale

DOTTORATO DI RICERCA
IN
TECNOLOGIE PER L'ENERGIA E L'AMBIENTE

XXIV ciclo

Anno 2012

PULSATING HEAT PIPES
Numerical Modeling and Experimental Assessment

Doctoral Thesis:
Mauro Mameli

Supervisors:

Prof. Marco Marengo
Dr. Ing. Stefano Zinna
Prof. Sameer Khandekar

Dipartimento di Ingegneria Industriale. Università degli studi di Bergamo
ISBN: 978-88-97413-05-9
Open access copy available at: http://hdl.handle.net/10446/25393

ABSTRACT

The present thesis is the result of a three year research study on the developing and experimental validation of a numerical model for the thermal-hydraulic simulation of Closed Loop Pulsating Heat Pipes. The project has been carried out in the framework of the PRIN-2009 and put the basis for a fruitful collaboration between the University of Bergamo and the Indian Institute of Technology Kanpur (IITK, India).
The first two years were mainly devoted to improve the theoretical model and to the subsequent implementation of new subroutines. During this first stage the model has been validated by means of experimental data available from the literature. In the last year an actual CLPHP test-rig has been designed, built and tested. The outcome of the proprietor experimental apparatus provided new data on the heat transfer capability of two phase flows in mini-channels and allowed to perform a more accurate quantitative comparison with the simulation results.
Although the final version of the numerical model is able to satisfactorily reproduce many trends of actual PHP devices, further work is needed in order to understand some open issues related to the physics and to release a reliable software tool for the PHP design.

KEY WORDS: Pulsating heat pipe, two-phase flow, slug flow, annular flow, numerical modeling.

Dedication

This is the third and last thesis of my student's career and hopefully time has come to channel all my efforts to research.

Undoubtedly this work is dedicated to my parents Daniela and Giuseppe, my sister Sara and my friends Nene, Andrax and Bolo. Their wholehearted support made these last three years the best period of my life.

When I am asked what are the good basis to start a doctoral I always answer that you need three things: a good mentor, a good laboratory and strong will. Fortunately Professor Marco Marengo is a perfect guide, our laboratory has a big potential and I am quite stubborn.

Special thanks go to Professor Piero Colonna who introduced me to the numerical modeling of complex systems, to Dr. Ing. Stefano Zinna who guided me through the meanderings of programming, to Professor Sameer Khandekar who has been "the guru" during my experimental initiation in IITK India; to the colleagues and dear friends Carlo, Chiara, Ilaria, Claudio F., Claudio C. Claudio B., Vito, Antonello, Abhik and Balkrishna for sharing knowledge and real life, and lastly to Mario "tantra" Finazzi an unreachable genius.

Finally I take advantage of this dedication to make a plea to the few who will read this thesis:

I believe that research process is like a chain: experiments are needed to validate the theoretical analysis which, in turn, needs to prove that man is able to understand at least a small part of the infinite complex universe. If analytical, experimental, and computational scientists do not collaborate, this chain is broken and the secrets held within nature will remain undisclosed.

So, please, be curious and humble!

CONTENTS

PART I:

The Pulsating Peat Pipe, knowledge and available technology

Chapter 1

Introduction to two-phase passive thermal management

1.1 Thermal management: available technologies

Heat dissipation, recovery and accumulation is more and more becoming the limiting factor in the advancement of many energy systems. Consider, for instance, the continuous and rapid development of integrated circuit technology[1]. The trend is going towards higher heat generation coupled with smaller packaging volumes, which means dealing with higher heat per surface unit. In this direction, high heat flux capability and lower thermal resistance will drive and not follow the future design.

[1] Moore's law states that the number of transistors in an IC doubles every 18 months

At present many high performance heat transfer technologies are being investigated:

- Two-phase passive systems (the heat pipe technology);
- Micro-channelled cold plates;
- Electro-hydrodynamic and electro-wetting cooling;
- Immersion cooling;
- Liquid jet impingement;
- Spray cooling;
- Solid state cooling;
- Super-lattice and hetero-structure cooling;
- Thermo-ionic and thermo-tunneling cooling;

but only a few already proved to be reliable, durable, cost effective and mature for massive industrial applications.

1.2 Two phase passive systems

The present chapter provides a short excursus on the *two-phase passive technologies*, from the readily available Heat Pipe (HP) to the new-born Pulsating Heat Pipe (PHP) with the aim to focus on the attractiveness of such systems. In general, the operation of modern passive heat transfer devices is based on the combined action of three physical phenomena: phase-change, gravity and capillarity.

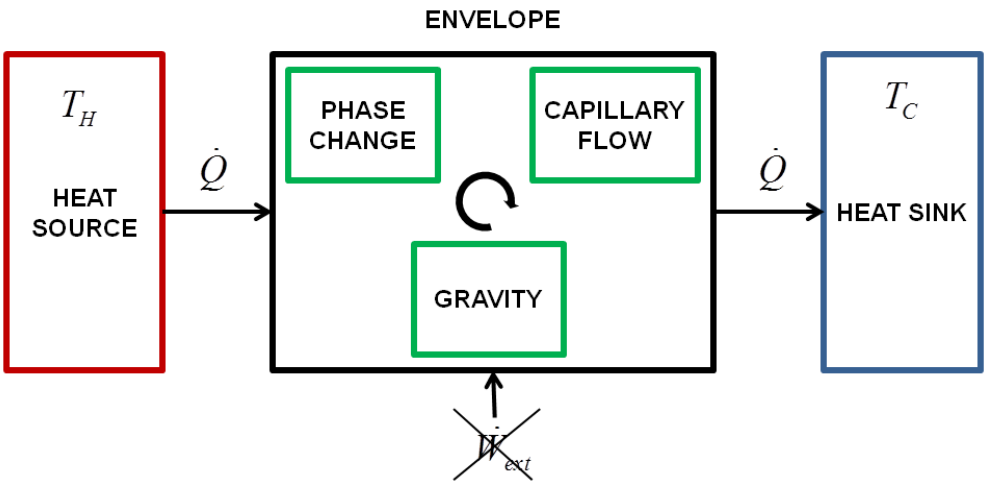

Figure 1. 1: General schematic of two phase capillary driven heat transfer device.

Most of the times the three phenomena are acting together but there may be some extreme conditions where capillary effects are negligible (i.e. thermosyphons) or gravity effects are less important (i.e. sintered HP). Figure 1.1 shows a schematic of a two-phase heat driven transfer device: as long as the proper boundary conditions (the heat source/sink power and the envelope geometry) are present, the mentioned physical phenomena are activated and the heat transfer process is continuous.

With the increased thermal capacity associated with the phase change of a working fluid (Figure 1.2), considerably smaller mass flow rates are required with respect to standard single phase cooling, and the capillary forces, as well as gravity, are able to sustain alone the fluid motion with no need for external mechanical/electric energy. In other words a passive device is fully thermally driven: the heating power activates the evaporation/condensation process and the consequent vapor expansion, together with the capillary/gravity effect on the liquid phase, provide the "pumping power" which is needed to maintain the fluid circulation.

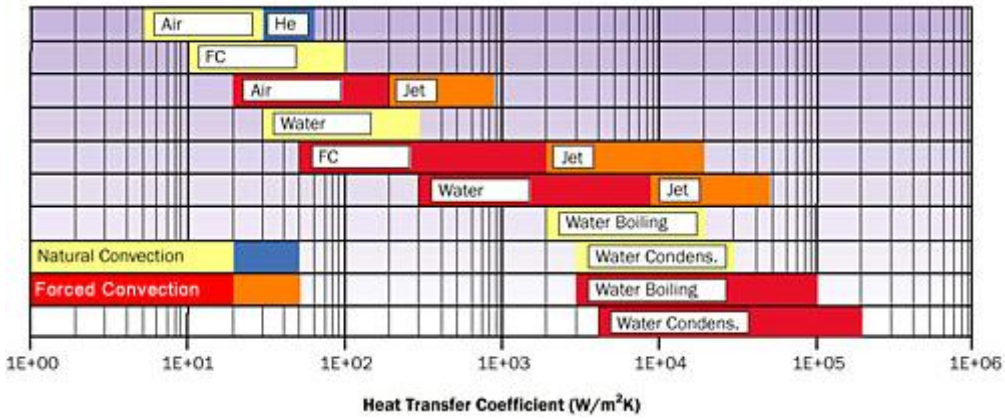

Figure 1. 2: Order of magnitude for heat transfer coefficients depending on cooling technologies.

The passive two-phase heat transfer technology is able to answer to the industry and market demand by providing the following benefits:

- Improved heat transfer capability: higher heat loads, up to some kilowatts, and higher heat fluxes, up to 200W/cm^2 of radial heat flux.
- Improved performance: low thermal resistance, down to 0.01 K/W.
- Lower mass flow rates and related smaller size and weight.
- No need for external pumping work.

- Smaller temperature gradients and nearly isothermal operation regardless of variations in the heat load.
- Ability to work in a wide range of acceleration fields.

Various types of two-phase passive heat transfer devices can be distinguished depending on the peculiar geometry and working principles:

- The heat pipe (HP).
- The capillary pumped loop (CPL) and the loop heat pipe (LHP).
- The thermosyphon (TS).
- The pulsating heat pipe (PHP).

1.3 Historical background

The gravity assisted thermosyphon, widely used since the end of the XIXth century, can be considered as the very first passive heat transfer device and the forefather of the modern devices quoted in the introduction. The lower end of the tube is heated causing the liquid evaporation and the vapor to move to the cold end of the tube where it is condensed. Since condensate is returned to the hot end by gravity, the evaporator must be situated at the lowest point (figure 1.3 a).

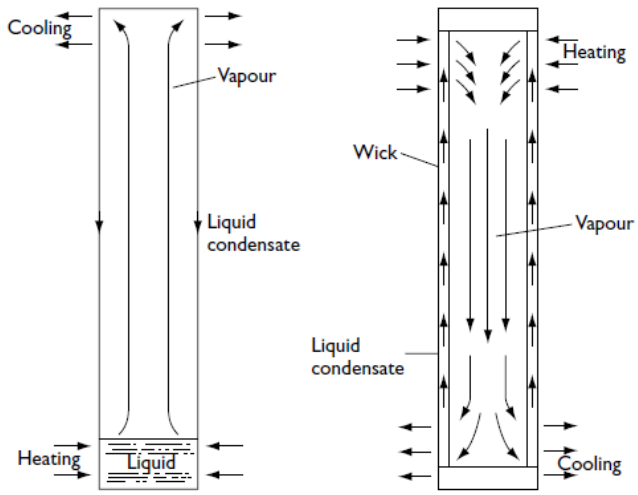

Figure 1. 3: basic operation of Thermosyphon (a) and Heat pipe (b), *Reay and Kew (2006).*

In modern devices this limitation is overcome by means of a wick structure, constructed for example from a few layers of fine gauze, which is fixed to the inside surface and returns the condensate to the evaporator by capillary forces (Fig. 1.3b). In the heat pipe the evaporator position is not restricted and it may be used in any orientation. If, of course, the heat pipe evaporator happens to be in the lowest position, gravitational forces assist the capillary forces.

The name 'heat pipe' was coined by *Grover (1963)* in a patent filed on behalf of the US Atomic Energy Commission, but the same concept was first put forward by Gaugler (1944) of the GM Co. in a patent application published twenty years before. Gaugler proposes a novel heat transfer device to be applied in the refrigeration field, where the liquid returns to the condenser by means of a capillary structure (namely 'a sintered iron wick'). Unfortunately his idea is not developed beyond the patent stage.

Grover's patent is conceptually identical to Gaugler's one, however, he includes a limited theoretical analysis and presents results of experiments carried out on stainless steel heat pipes, incorporating a wire mesh wick and sodium as the working fluid. Grover's heat pipe was successfully employed for supplying heat to the emitters and removing heat from the collectors of thermionic electrical generators.

Shortly after Grover's publication, work is started on liquid metal heat pipes by Dunn at Harwell and Neu and Busse at Ispra (Joint Research Center, Ispra, Italy), where both are developing nuclear-powered thermionic generators.

Interest in the heat pipe concept develops rapidly both for space and terrestrial applications and many experiments are carried out on different working fluids including metals, water, ammonia, acetone, alcohol, nitrogen and helium. At the same time the theory of the heat pipe becomes better understood thanks to the important contribution by *Cotter (1965).*

In the same year the variable conductance heat pipe (VCHP), sometimes called the 'gas-controlled', 'gas-loaded' or 'gas-buffered' heat pipe is developed by *Wyatt (1965).* The VCHP has a unique feature that sets it apart from other types of heat pipe: the ability to maintain a device mounted at the evaporator at a near constant temperature, independent of the amount of power being generated by the device.

Capillary pumped loops (CPL American technology, 1966) and loop heat pipes (LHP Russian technology, 1972) are developed to overcome the

inherent problem of incorporating a long wick with small pore radius in a conventional heat pipe.

Immediately one year after the first successful heat pipe test in space in 1967, the heat pipes is implemented for satellite thermal control on GEOS-B, launched from Vandenburg Air Force Base.

The first Pulsating Heat Pipe was described as Pulsating Heat Pipe (PHP) in the former USSR by *Smyrnov G. F. and Savchenkov G. A. (USSR patent 504065, filed in 1971)*. This PHP was the first wickless system able to operate against gravity and Smyrnov made use of his inventions in refrigeration systems.

The first Heat Pipe international conference is held in Stuttgart in 1973 and, by 1977, the heat pipe technology spreads over as one of the most efficient and convenient 'heat super-conductor' and it becomes established in many applications:

- electronics cooling;
- die casting and injection moulding;
- heat recovery and other energy conserving uses;
- de-icing duties;
- cooking;
- control of manufacturing process temperatures;
- thermal management of spacecraft;
- renewable energy systems (solar collectors and concentrators).

Tamburini (1977) introduces one of the first version of the reverse termosyphon (RTS) called "T-system", which consists of a passive wickless two-phase loop able to operate against gravity. It was proposed indeed for electronic cooling application aboard spacecraft, but no experimental data are reported. First experiments and mathematical modeling of a RTS for solar heating applications are presented by *Nasonov et al. (1980).*

In the early '90s a novel and most known version of PHP enters the scene of passive cooling with a patent by *Akachi (1990)*. The simple and relatively flexible structure based on a millimetric meandering tube (wick is absent) makes it competitive with respect to the standard heat pipe. On the other hand the PHPs are being studied mostly in the academic community because of the intrinsic complexity of its working principles and the still uncertain operating ranges.

1.4 Two-phase passive devices, basic working principles

The PHP results in the technological evolution process resumed in the scheme below.

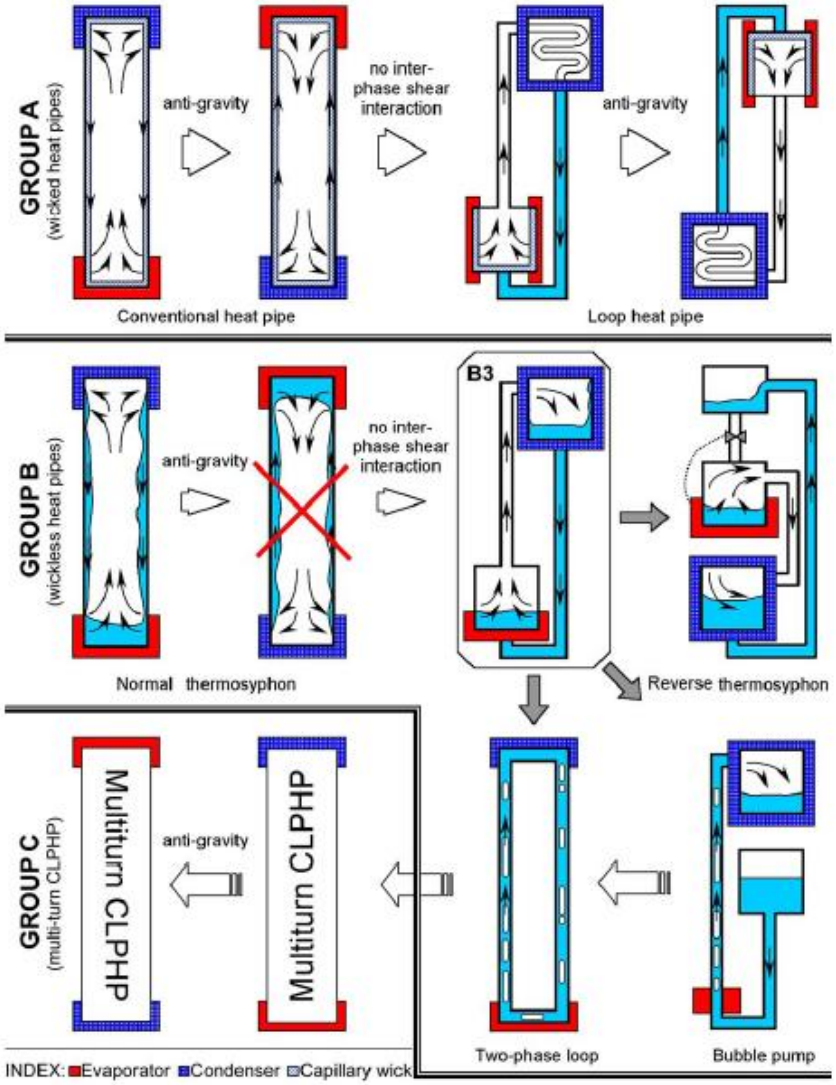

Figure 1. 4: Genealogy of closed passive two-phase systems showing the evolution of multi-turn pulsating heat pipes, *Khandekar & Groll (2008)*.

It is then worthwhile to describe the basic working principles of the PHP forefathers (Conventional Heat Pipe, Loop Heat Pipe, Reverse Termosyphon) in order appreciate the analogies as well as the decisive differences that

significantly distinguish their operation and the course of mathematical analyses.

1.5 Heat Pipe: working principles and performance

The conventional heat pipe belongs to the family of wicked heat pipes (Fig. 1.4). Similarly to all the other two phase passive devices, HPs transport heat from a heat source (evaporator) to a heat sink (condenser) over relatively long distances via the latent heat of vaporization of a working fluid. As shown in Figure 1.4, a heat pipe generally has three sections: an evaporator section, an adiabatic (or transport) section, and a condenser section.

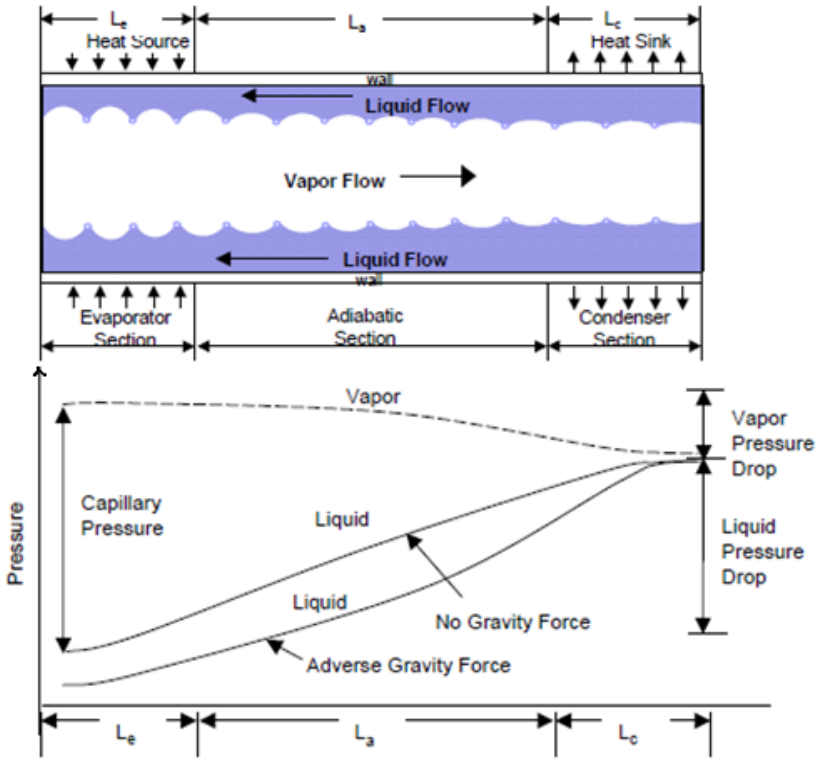

Figure 1. 5: Heat Pipe layout and fluid pressure trends.

The major components of a heat pipe are a sealed container, a wick structure, and a working fluid. The wick structure is located on the HP inner wall surface and it is filled with the liquid phase of the working fluid like a sponge, while vapor phase resides inside the tube core. Furthermore the wick capillary action let the liquid flow from the condenser back to the evaporator

section. As vaporization occurs in the evaporator, the liquid meniscus correspondingly recedes into the wick structure, as shown in Figure 1.4. Similarly, as vapor condenses in the condenser region, the mass addition results in an advanced meniscus. The difference between the capillary radii in the evaporator and condenser ends of the wick structure results in a net pressure difference in the liquid-saturated wick. This pressure difference drives the liquid from the condenser through the wick structure to the evaporator region, thus allowing the overall process to be continuous.

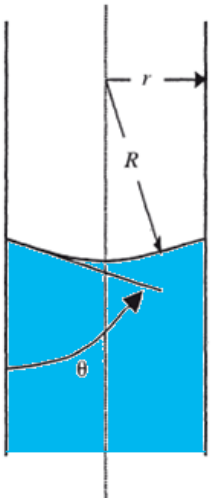

Figure 1. 6: Meniscus in a cylindrical capillary.

Capillary pressure is calculated by means of the Young-Laplace equation as follows:

$$\Delta P_c = \frac{2\sigma}{r_{eff}} \cos\theta \qquad 1.1$$

Where the effective radius of curvature for the wick structure r_{eff} is assumed as the inner radius of a circular tube and θ, the apparent contact angle, is dependent on the fluid–wick pair used. The capillary pressure developed between the evaporator and the condenser is:

$$\left(\Delta P_c\right)_{eva-cond} = \left(\Delta P_c\right)_{eva} - \left(\Delta P_c\right)_{cond} \qquad 1.2$$

Ideally the maximum capillary pressure occurs when the contact angle $\theta = 0°$ in the evaporator (*dry point*) and $\theta = 90°$ in the condenser (*wet point):*

$$\left(\Delta P_c\right)_{\max} = \frac{2\sigma}{r_{eff}} \qquad 1.3$$

This capillary pressure differential circulates the fluid against the friction losses and any adverse body force such as gravity.

1.5.1 Transport limitations

The two categories and basic phenomena for each limit are:

a) Failure

1. *Capillary limit.* When the driving capillary pressure is insufficient to provide adequate liquid flow from the condenser to the evaporator, dry-out of the evaporator wick will occur. Generally, the capillary limit is the primary maximum heat transport limitation of a heat pipe.

2. *Boiling limit (or heat flux limit)*. The boiling limit occurs when the applied evaporator heat flux is sufficient to cause nucleate boiling in the evaporator wick. This creates vapor bubbles that partially block the liquid return and can lead to evaporator wick dry-out.

3. *Entrainment limit.* The entrainment limit refers to the case of high shear forces developed as the vapor passes in the counter-flow direction over the liquid saturated wick, where the liquid may be entrained by the vapor and returned to the condenser. This results in insufficient liquid flow to the wick structure.

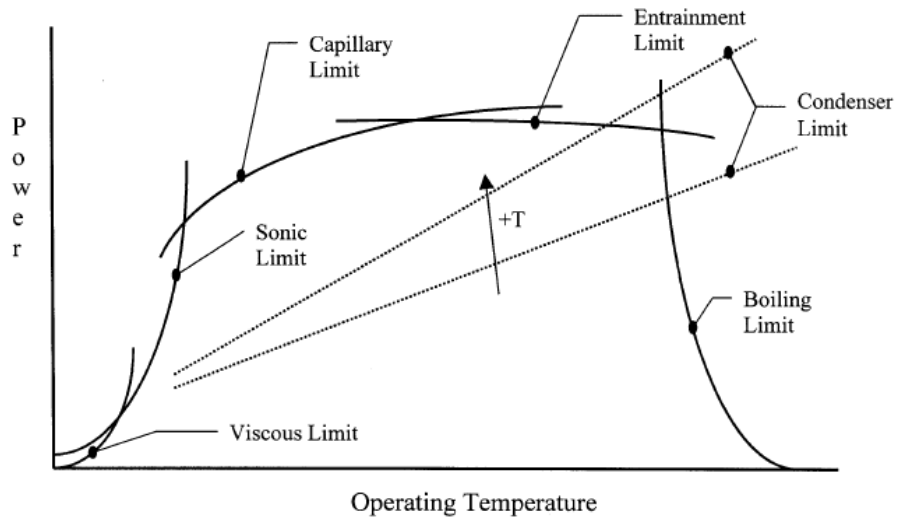

Figure 1. 7: Typical heat pipe performance map, *Reay and Kew (2006).*

b) Non-failure

1. *Viscous limit.* At low operating temperatures the saturation vapor pressure must be almost equal to the pressure drop required to drive the vapor flow in the heat pipe. This results in an insufficient pressure available to drive the vapor.

2. *Sonic limit.* At low vapor densities, the corresponding mass flow rate in the heat pipe may result in very high vapor velocities, the occurrence of choked flow in the vapor passage is be possible.

3. *Condenser limit.* The condenser limit is based on cooling limitations such as radiation or natural convection at the condenser. For example, in the case of radiative cooling, the heat pipe transport may be governed by the condenser surface area, emissivity, and operating temperature.

1.5.2 Performance and operating conditions

For a fixed geometry the HP performance is heavily influenced by the morphology of the wick structure.

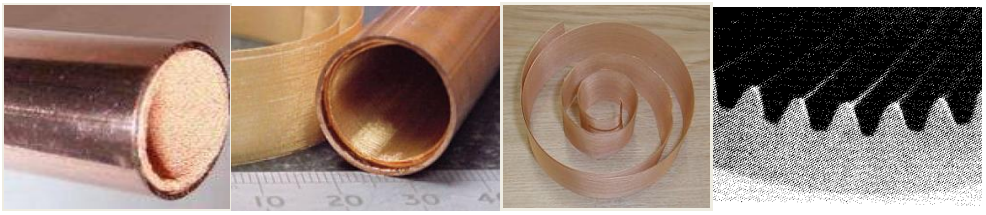

Figure 1. 8: Wick structures: a) sintered powder; b) wire mesh; c) screen mesh; d) axial grooves.

- *Sintered powder*: for standard sintered heat pipes the heat flux limit is typically around 50 W/cm^2. With more specialized wick designs (special powder types and particular shape of the wick structure) heat fluxes up to 250W/cm^2. The sintered HP can work at any orientation.
- *Screen/wire mesh*: heat flux capability between 10 and 15 W/cm^2. High performance between -5° and 90° (vertical, bottom heated) of tilting angle.
- *Grooved HP*: heat flux limit is generally relatively low, 5 to 10W/cm^2, due to the reduced surface area provided for evaporation. Tilting between 0° (horizontal) and 90° (vertical, bottom heated).

The heat pipe temperature range depends mainly on the working fluid residing in the vessel. Table 1.1 shows that the HP is able to cover a wide compass, from cryogenics (helium) to very high temperatures (liquid silver).

Working Fluid	Temperature Range [°C]	Shell Material	Measured axial heat flux [W/cm2]	Measured radial heat flux [W/cm2]
Low Temperature or Cryogenic Heat Pipe Working Fluids				
Helium	-271 to -269	SS, Ti		
Hydrogen	-260 to -230	SS		
Methane	-180 to -100	SS		
Neon	-240 to -230	SS		
Nitrogen	-200 to -160	SS	67 @ -163°C	1.01 @ -163°C
Oxygen	-210 to -130	Al, Ti		
Carbon Dioxide	-50 to 30	Al, SS, Ti		
Mid Range Heat Pipe Working Fluids				
Acetone	-48 to 125	Al, SS		
Ammonia	-75 to 125	Al, SS	295	2.95
Ethane	-150 to 25	Al		
Methanol	-75 to 120	Cu, Monel, Ni, Ti	450 @ 100°C	75.5 @ 100°C
Methylamine	-90 to 125	Al		
Pentane	-125 to 125	Al, SS		
Propylene	-150 to 60	Al, SS		
Water	1 to 325	Cu, Monel, Ni, Ti	670 @ 200°C	146 @ 200°C
High temperature heat pipe fluids				
Mercury +0.02%, Magnesium +0.001%	190 to 550	SS	25100 @ 360°C	181 @ 360°C
Cesium	350 to 925	SS, Inconel, Haynes		
NaK	425 to 825	SS, Inconel, Haynes		
Potassium	400 to 1025	Stainless Steel, Inconel, Haynes	5600 @ 750°C	181 @ 750°C
Sodium	500 to 1225	SS, Inconel, Haynes	9300 @ 850°C	224 @ 850°C
Lithium	925 to 1825	W, Nb	2000 @ 1250°C	207 @ 1250°C
Silver	1625 to 2025	W, Mo	4100	4.13

Table 1. 1: typical cooperating characteristics of heat pipes.

Table 1.2 shows the maximum power transmission ratings for standard HPs available on the market (CRS 5000 series) operating in a horizontal orientation (i.e. virtual zero gravitational influence).

CRS- Series 5000 (Diameter mm)	Maximum Power Handling Capability (Watts)				
	@+20°C	@+40°C	@+60°C	@+80°C	@+120°C
2.0	9.0	11.0	12.0	13.0	14.0
2.5	12.5	16.0	17.5	19.5	21.5
3.0	16.0	23.5	24.5	26.5	29.0
4.0	22.0	27.5	30.5	32.0	37.0
5.0	50.0	58.0	63.0	65.0	68.0
6.0	72.0	86.0	93.0	98.0	108.0
8.0	90.0	108.0	115.0	122.0	134.0
10.0	112.0	134.0	143.0	152.0	169.0
12.0	148.0	178.0	186.0	197.0	218.0

Table 1. 2: Example of heat transfer capability of commercial heat pipes *(courtesy of CRS).*

The temperature ranges given of + 20°C to + 120°C are mean operating temperatures taken at a mid-measurement point between the heat input and heat output sections arranged at either end.

1.6 Capillary Pumped Loop (CPL) and Loop Heat Pipe (LHP)

The capillary pumped loop (CLP) shown in Figure 1.8, consists of an evaporator and a condenser, as in conventional heat pipes, but differs in having separate vapor and liquid lines.

The technical efforts made to overcome liquid–vapor entrainment in heat pipes and, more importantly, in thermosyphons, lead to the isolation of the liquid path from the vapor flow (normally counter current) is beneficial.In the CLP and LHP, these flows are co-current in different parts of the tubing and the wick structure is present only in the evaporator zone.

A unique feature of the LHP with respect to the CLP is the use of a compensation chamber embedded in the evaporator package. This two-phase reservoir helps to establish the LHP pressure and temperature, as well as maintain the inventory of the working fluid within the operating system.

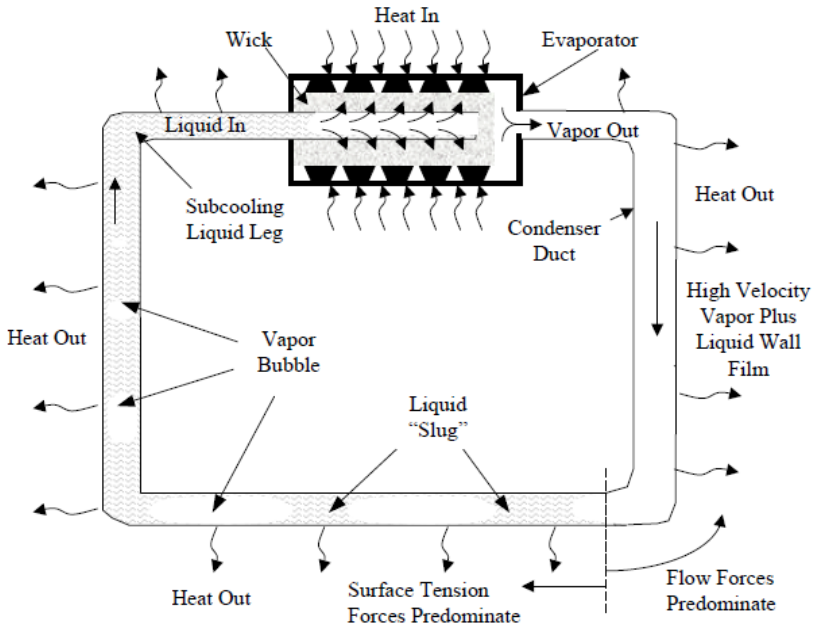

Figure 1. 9: Capillary pumped loop layout (CLP).

A typical LHP evaporator is shown schematically in Figure 1.9. The evaporation in LHPs takes place on the surface of the wick adjacent to the evaporator wall. Vapor removal channels must be incorporated in the wick or evaporator wall to ensure that the vapor can flow from the wick to the vapor line with an acceptable pressure drop. A secondary wick is used to ensure uniform liquid supply to the primary wick and to provide liquid to the wick in the event of transient dry-out.

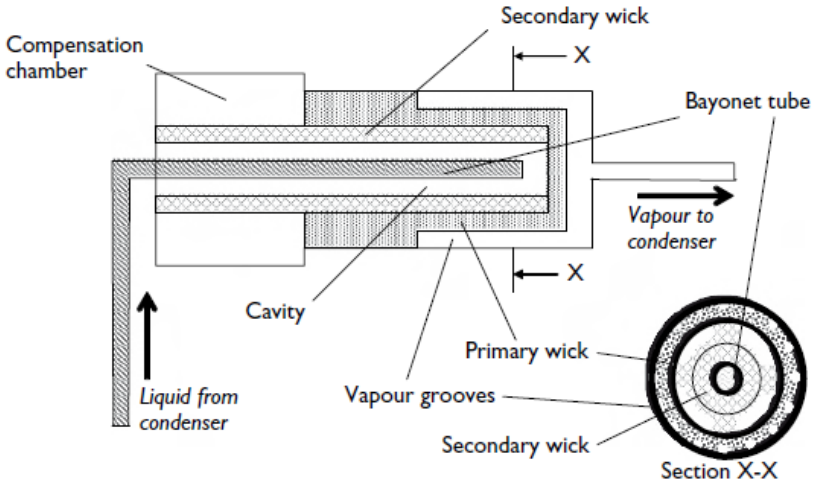

Figure 1. 10: Typical evaporator of a loop heat pipe, Reay and Kew (2006).

The LHP has the features of the classical heat pipe with the following additional advantages:

- High heat transfer capability (heat load up to 7 kW and heat flux up to 70 W/cm^2)
- Capability to transport energy over long distances, up to 23 m, without restriction on the routing of the liquid and vapor lines.
- Ability to operate at different gravity levels, from 0 to 9 g.
- No wick within the transport lines.
- Vapor and liquid flows separated, therefore no entrainment
- May be adapted to allow temperature control.

1.7 The Reverse Thermosyphon

The wick structure is the common and peculiar aspect of the capillary driven two-phase devices presented so far (HP, CLP, LHP). The development of high quality wick structures requires a specific knowhow and represent the main expense in the system. For this reason in the last decades particular attention has been given to wickless devices able to operate against gravity such as reverse thermosyphons (RTS) and Oscillating or Pulsating Heat Pipes (PHPs). In his review *Filippeschi (2006)* shows that more than 50 different versions of reverse thermosyphon can be found in the literature with different names but at last they operate with the same basic governing principles. For this reason he decided to name them Periodic Two-Phase Thermosyphons (PTPT).

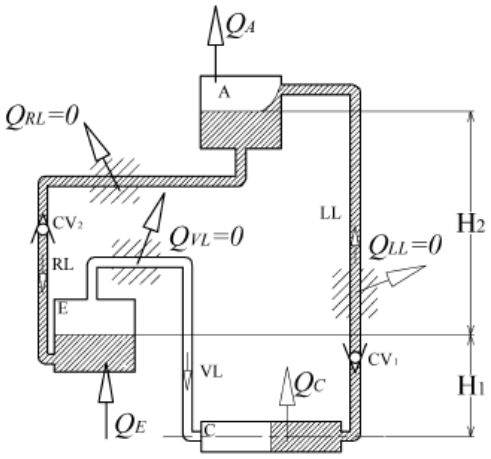

Figure 1. 11: Generic PTPT layout, Filippeschi (2006).

A generic PTPT (Fig. 1) consists of an evaporator *E*, a condenser *C* and a tank separated from the evaporator, called accumulator *A*. These elements are interconnected and constitute a loop. The connecting lines are thermally insulated and they can be named vapor line *VL* (evaporator-condenser), liquid line *LL* (condenser-accumulator) and return line *RL* (accumulator-evaporator). Two check valves are inserted in the loop, the first *CV*1 in the liquid line and the second *CV*2 in the return line. A single cycle of periodic heat and mass transfer can be divided into two main parts: a transfer time, where vapor is transferred from the evaporator to the accumulator through the condenser and a return time, where the liquid collected in the accumulator flows back to the evaporator. Assuming that the fluid inside the evaporator and accumulator is motionless, kinetic terms can be neglected and the heat and mass transfer operation is governed by the following equation:

$$\left(p_E(t)-p_A(t)\right)-\left\{\rho_{C,1}(t)g\left[H_1(t)+H_2(t)\right]-\rho_{E,vap}(t)gH_1(t)\right\}= \int_E^C \rho_{E,vap}(t)dl_f+\int_E^C \rho_{C,liq}(t)dl_f \qquad 1.4$$

where l_f is the specific friction work and H_1 and H_2 are time depending since the fluid level inside all the three vessels may slightly vary. The right-hand term of Eq. (1) represents the friction work. When heat is provided to the evaporator, p_E increases, the left-hand side of Eq. (1.4) becomes greater then right-hand side and vapor is pushed from the evaporator to the condenser. As soon as a volume of vapor leaves the evaporator, part of the liquid collected in the accumulator must return to the evaporator and the starting conditions are restored. In a two-phase thermosyphon the two operations occur simultaneously and a steady state regime is reached, while in a PTPT device these operations occur during two consecutive time periods so that a periodic regime is reached and an antigravity heat and mass transfer becomes possible. In order to restore the starting condition of a single heat transfer cycle either the pressure in the accumulator must increase or the pressure in the evaporator must decrease. In terrestrial applications there is an additional opportunity: by opening a connecting line between the two vapor zones of the evaporator and accumulator, the pressure in the two vessels is equalized and the return of the liquid is gravity-assisted, as long as the accumulator is above the evaporator. Even though PTPT are robust and reliable devices they are affected by the following drawbacks:

- The system layout is more complex than standard HPs.
- A minimum of two electro-valves are needed to control the PTPT heating cycles. Since the opening/closing periods of such valves depend on the heat input level, an electronic control system is also needed.

1.8 The Pulsating Heat Pipe

The Pulsating Heat Pipe by *Akachi (1990)* is the last evolution of the wickless heat pipe technology. The capillary effect is indeed provided by the small dimension of the channel and not by the presence of a wick structure on the internal tube surface (HP, LHP) or by the presence of valves and different storage volumes (Thermosyphon).

Actually the PHP simply consists in a capillary diameter tube bended in many turns, evacuated and partially filled with a working fluid. The flow pattern is another great distinctive feature: liquid and vapor phase are randomly distributed inside a PHP in the form of liquid slugs alternated to vapor plugs (Figure 1.12).

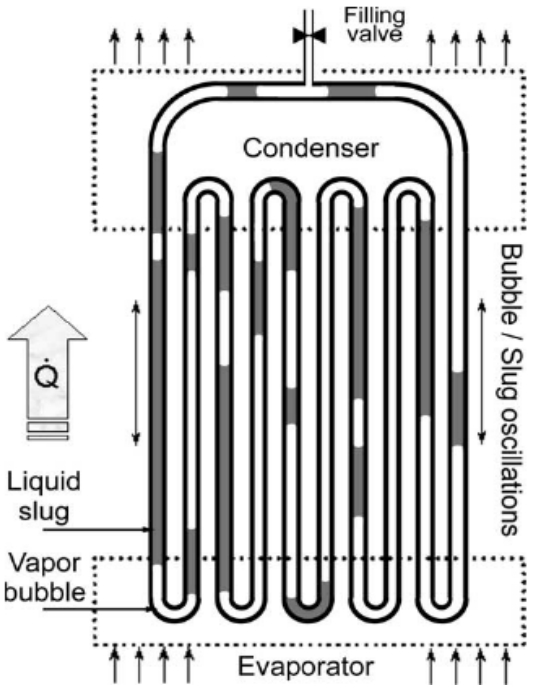

Figure 1. 12: Basic scheme of a Closed Loop Pulsating Heat Pipe, Khandekar (2004).

The device is able to work against gravity without any control valve (if the number of turns is sufficiently high) but unfortunately the fluid motion is intrinsically chaotic and difficult to be predicted by means of a theoretical model. Furthermore a conventional experimental procedure/investigation has not been defined between researchers so experimental data are sometimes contradictory and the PHP working range are not fully established yet. The great potential of having a simple, cheap and flexible structure coupled with the anti-gravity operation is opposed by the lack of reliability, this is the reason why the Pulsating Heat Pipe is still a challenge in the research field.

The next chapter is devoted to clarify what is known about the PHP working principles (Chapter 2); describe the advances and unsolved issues related to the PHP technology (Chapter 3); propose a novel modeling approach (Chapters 4, 5); show the numerical results comprising qualitative and quantitative validation (Chapter 6); describe the design of an original experimental apparatus (Chapter 7); show the output of the experimental investigations (Chapters 8); finally draw the conclusions and a roadmap towards the PHP stable operation (Chapter 9).

Chapter 2

The PHP working principles and potential impact

2.1 Introduction

The present industry demand in terms of favorable operational characteristics coupled with relatively cheaper costs leads to the evolution of novel passive heat transfer devices. The Pulsating Heat Pipe (PHP), originally introduced by *Smyrnov and Savchenkov (1971)* and reproposed in a simpler version by *Akachi (1990),* represents one of the most interesting field of investigation and is projected to meet all present and possibly future specific requirements from electronics cooling to heat recovery.

The subtle complexity of internal thermo-fluidic transport phenomena is quite unique, justifying the need for a completely different research outlook. A comprehensive theory of operation and a reliable database or tools for the design of PHPs still remain unrealized. Nevertheless, since the device is fully thermally driven, cheap and relatively easy to build, the prospects are too promising to be ignored.

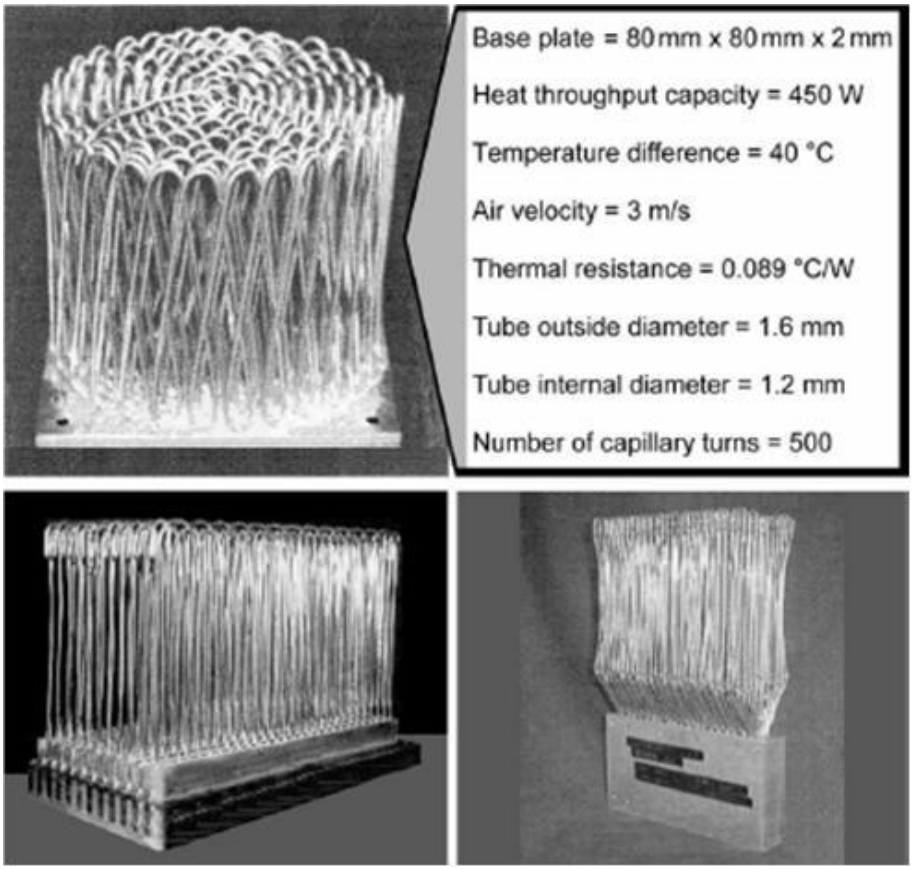

Figure 2. 1: PHP prototypes by Akachi (1993).

2.2 Structure

The Pulsating Heat Pipe (PHP) is a two-phase passive heat transfer device suitable for high heat flux applications. In spite of its name both structure and working principles are very different with respect to the standard Heat Pipe. It consists of a copper capillary tube bent in many turns, which is firstly evacuated, then partially filled with a working fluid and finally sealed. Although a plethora of different 3-D geometries can be found in literature,

the basic PHP geometry usually consists of a planar sequence of U-turns and parallel channels forming a serpentine with the two possible layouts shown in Figure 2.2:

a) Closed Ends PHP (CEPHP): weather tube ends are not connected to each other; sometimes also called Open Loop PHP (OLPHP) .
b) Closed Loop Pulsating Heat Pipe (CLPHP): Tube ends connected to each other in an closed loop.

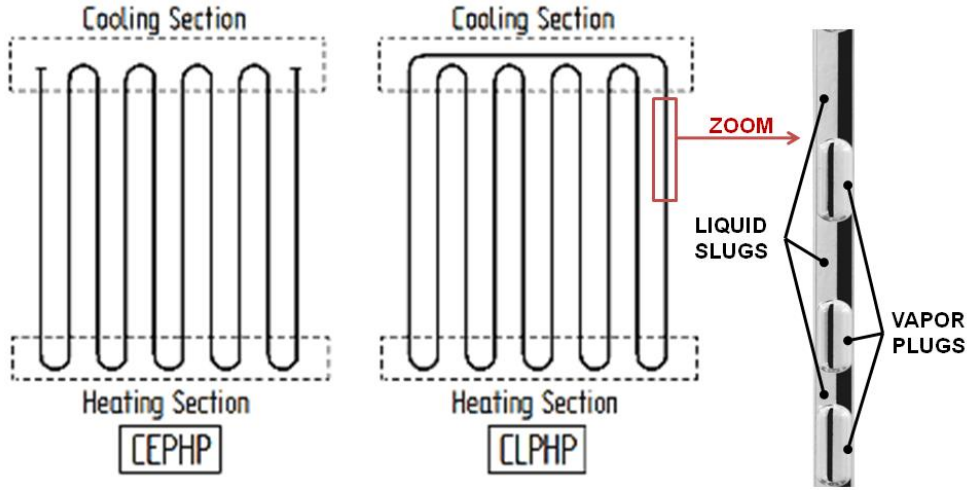

Figure 2. 2: The two main PHP layouts: CEPHP and CLPHP.

Due to the tube capillary dimensions, the working fluid fills the tube as an alternation of liquid slugs and vapor plugs (“slug flow” pattern). Moreover, since the fluid is in saturated conditions, the thermal power provided by the hot source to the heating section causes the evaporation of the thin liquid film which surrounds each vapor plug. The vapor expansion pushes the adjacent liquid through the tube towards the condenser where the adsorbed heat can be released to a cold sink. If the tube is closed end-to-end in a loop the fluid can both oscillate and circulate while in the open loop configuration the fluid can only oscillate.

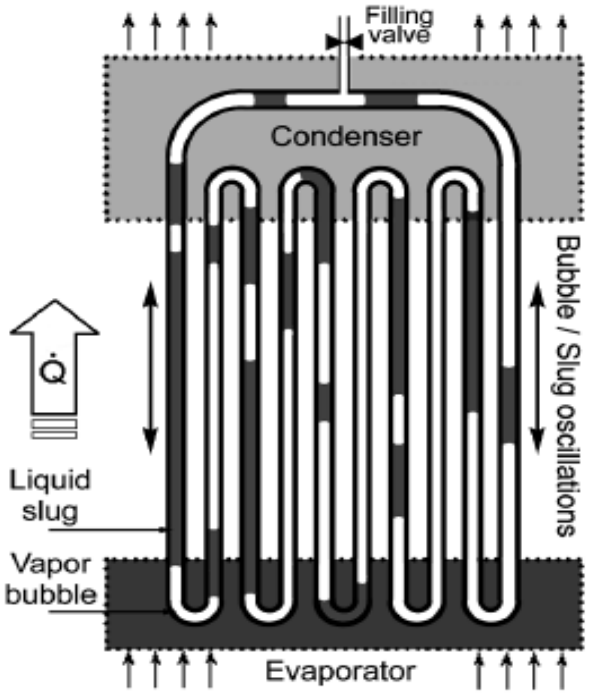

Figure 2. 3: Basic scheme of a Closed Loop Pulsating Heat Pipe

In order to distinguish the PHP from other heat transfer devices (i.e. Heat Pipes, LHP or Thermosyphons), its basic features are listed below and recognizable in Figure 2.3:

- No wick structure (the inner tube surface is smooth).
- No storage volumes in the system.
- At least one heat receiving section called evaporator zone.
- At least one heat dissipating section called condenser zone.
- An optional 'adiabatic' section separating the evaporator and the condenser zone.
- Capillary slug flow characterized by self exited thermally driven oscillations (without external mechanical power source).
- Surface tension predominates although gravity may affect the performances.
- Latent as well as sensible heat transport possible by the self oscillating working fluid.

2.3 Fundamental Processes

Figure 2.4 zooms on a typical liquid-vapour plug system as formed in the PHP and suggests the various forces, heat and mass transfer processes. The analysis of the control volume on a micro scale will manifest much more complicated molecular forces and heat and mass transfer processes than what has been depicted in Figure 2.4. Such a system will be mathematically too complicated and impractical.

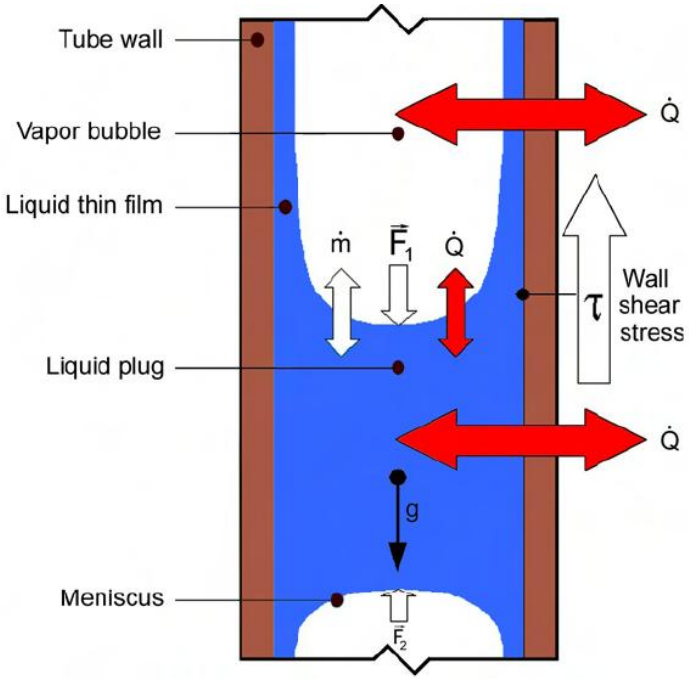

Figure 2. 4: Fundamental transport processes in a PHP, *Khandekar & Groll (2008).*

Therefore only the primary processes have been summarized below:

- The flow pattern in the PHP tubes may be always categorized as capillary slug flow. As the heat input rises the flow pattern may change locally to semi-annular and finally to annular flow.
- Liquid slugs having menisci on its edges are formed due to surface tension forces and the capillary dimensions of the PHP tube. A liquid thin film surround the vapour plugs. The contact angle of the menisci, the liquid thin film stability and its thickness depends on the fluid-solid combination and the operating parameters which are selected. If a liquid plug is moving or tends to move in a specific direction then the leading contact angle (advancing) and the lagging contact angle (receding) may

be different. This happens because the leading edge of the plug moves on a dry surface (depending on the liquid thin film stability and existence) while the lagging edge moves on the just wetted surface. The major contribution of pressure drop in a capillary slug flow comes from the liquid plug and the leading and lagging faces (ends) of the bubble. The in between length of the bubble body does not generally contribute to the overall pressure drop.

- Although surface tension forces predominate, the liquid and vapour plugs move against the gravity vector at an angle depending on the global PHP orientation and the location of the plugs in the up-header or down-header tubes. The extent of the effect of gravity on PHP operation is still not fully established.
- The liquid and vapour plugs are subjected to pressure forces from the adjoining plugs.
- The liquid and vapour plugs experience internal viscous dissipation as well as wall shear stress as they move in the PHP tube. The relative magnitude of these forces will depend on the flow field motion.
- The liquid-vapour plugs may receive and reject heat mostly in the radial direction but also in the axial one, or move without any external heat transfer depending on their location in the tube.
- In the evaporator the liquid plug receives heat and two different phenomena may occur: if the liquid slug enters the evaporator in a sub-cooled condition, sensible heating plays the main role while, if the liquid slug already is in saturated condition, heating is simultaneously followed by evaporation mass transfer to the adjoining vapour bubbles or breaking up of the liquid plug itself with creation of new bubbles in between as a result of nucleate boiling in the slug flow regime. The saturation pressure and temperature thus increase locally.
- When a vapour bubble travels in the evaporator zone evaporation mass transfer from the surrounding liquid film and the adjoining liquid plugs thereby occurs increasing the instantaneous local saturation pressure and temperature and providing the pumping work to the system.
- The above processes as described for the evaporator are repeated in a reverse direction in the condenser.
- In the adiabatic section, while passing from the evaporator to the condenser, the train of vapour-liquid slugs are subjected to a series of

complex heat and mass transfer processes. Essentially non equilibrium conditions exist whereby the high pressure, high temperature saturated liquid-vapour plugs are brought down to low pressure, low temperature saturated conditions existing in the condenser. Internal enthalpy balancing in the form of latent heat takes place by evaporation mass transfer from the liquid to the vapour plugs whereby saturation conditions are always imposed on the system during the bulk transit in the adiabatic section. It is to be noted that there occurs no 'classical steady state' occurs in PHP operation. Instead pressure waves and pulsations are generated in each of the individual tubes which interact with each other possibly generating secondary and ternary reflections with perturbations.

- Heat transfer coefficients are different for the vapour plug, the liquid slug and the liquid film and their analytical calculation is far from being an easy issue.

2.3.1 Thermodynamics background

The device performance primarily depends on the continuous maintenance or sustenance of the non-equilibrium conditions within the system. The liquid and vapour slug transport is because of the pressure pulsations caused in the system. Since these pressure pulsations are fully thermally driven, there is no external mechanical power source required for the fluid transport.

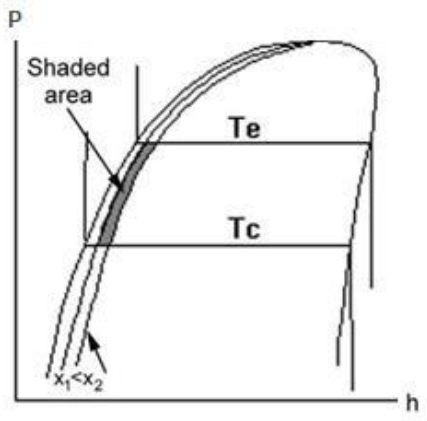

Figure 2. 5: Pressure-Enthalpy diagram of a working fluid control volume in equilibrium conditions, *Khandekar (2004).*

Consider the ideal case when a PHP is isothermal throughout. Under this condition, the liquid and vapour phases in the PHP exist in equilibrium at a saturation pressure corresponding to the fixed temperature (Fig. 2.5).

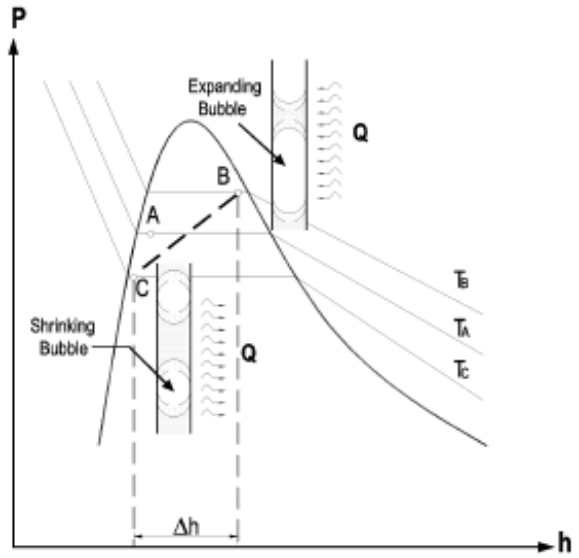

Figure 2. 6: Pressure-Enthalpy diagram of a working fluid control volume in non equilibrium conditions, *Karimi (2004).*

The whole system has constant volume and its total vapour mass quality is rather low (even when the filling ratios are small). From a standard equilibrium analysis it seems that the average thermodynamic state of the whole pulsating heat pipe may only shift inside the shaded area in Figure 2.5. Since the PHP is characterized by strong non-equilibrium phenomena it cannot be satisfactorily described with a single thermodynamic state: there are different local thermodynamic states depending on the different zones. During operation, a temperature gradient prevails between the evaporator and the condenser, causing non-equilibrium pressure conditions.

The heat transfer to the evaporator causes the bubbles in the evaporator to grow continuously and tries to move point A to point B at a higher pressure/temperature and a larger quality (Figure 2.6). This pushes the liquid column toward the low temperature end (condenser). Simultaneously, the condensation at the other end will further enhance the pressure difference between the two ends, and point A is forced to move to point C at a lower pressure/temperature and a smaller quality. In this way a non-equilibrium state is formed between the driving thermal potentials and the system in

return attempts to equalize the internal pressure. Because of the inter-connection of the tube(s), the motion of the liquid slugs and vapour bubbles at one section of the tube towards the condenser also leads to the motion of slugs and bubbles in the other section towards the high temperature (evaporator) in the next section. This works as a restoring force. Thus a self sustained thermally driven oscillating flow is obtained in a PHP. The inter-play between the driving force and restoring force leads to oscillation of the vapour bubbles and liquid slugs in the axial direction.

Further, inherent perturbations present in real systems augment pressure fluctuations in the system. Unlike conventional heat pipes, no steady-state pressure equilibrium can be achieved for an operating PHP. The frequency and amplitude of the oscillations are expected to depend on the heat flow rate and the mass fraction of the liquid in the tube. Through these oscillations, heat which is supplied by the heat source at the evaporator is carried to the condenser and is removed by a heat sink.

2.4 Defining Parameters

2.4.1 Channel diameter

The internal tube diameter is the most important geometrical parameter because it essentially manifests the fundamental definition of CLPHPs.

The slug flow pattern inside the tube is a fundamental working condition because pumping force is generated by the growing bubbles in the evaporator and the collapsing bubbles in the condenser area. Such condition is ensured only if the tube inner diameter is smaller than a critical diameter.

Classical studies of cylindrical bubbles rising in isothermal static fluids states that a bubble rises through the denser liquid because of its buoyancy. The velocity u with which a single cylindrical bubble rises through stagnant liquid in a duct is governed by the interaction between buoyancy and the other forces acting on the bubble because of its shape and motion. If the viscosity of the vapor in the bubble is neglected, the only forces besides buoyancy, which are important, are those from liquid inertia, liquid viscosity and surface tension. The balance between buoyancy and these three forces may be expressed in terms of three non-dimensional groups:

$$Fr = \frac{\rho_l \cdot u_\infty^2}{d \cdot g \cdot (\rho_l - \rho_v)} = \frac{inertia}{buoyancy} \quad 2.1$$

$$Po = \frac{\mu_l \cdot u_\infty}{d^2 \cdot g \cdot (\rho_l - \rho_v)} = \frac{viscous}{buoyancy} \quad 2.2$$

$$Eö = \frac{d^2 \cdot g \cdot (\rho_l - \rho_v)}{\sigma} = \frac{buoyancy}{surface} \quad 2.3$$

The Bond number is frequently used in place of the Eötvös number:

$$Bo = \sqrt{Eö} \quad 2.4$$

In the above equations, *d* is typically the characteristic dimension of the duct cross section. For circular ducts, *d* represents the internal diameter. In situations where viscous forces and surface tension can be neglected, the rise velocity can be correlated only by Equation (2.1) above. Similarly, when viscous force constitutes the only predominant factor, the bubble rise velocity is obtained by the Poiseuille number. The last case, when surface tension dominates, is the case of present interest. Interestingly enough, the Eötvös number has no velocity term in it. So the question is, how this number can be used to find the rise velocity under the dominance of surface tension.

Since the general solution is governed by three non-dimensional parameters as defined above, it can be represented as a two-dimensional plot of any two chosen dimensional groups with the remaining third independent group as a parameter. The three parameters may also be combined to generate new dimensionless quantities for convenience. For example, a convenient property group is frequently used and is defined as:

$$Y = \frac{Po^4 \cdot Eo^3}{Fr^2} = \frac{g \cdot \mu_l^4}{\rho_l \cdot \sigma} \quad 2.5$$

When the above problem was first attempted analytically, it was thought that the Fr and Eö numbers should tend to zero together *(Bretherton, 1960).* In simpler terms this means that for a given fluid-bubble system, as the tube diameter is reduced, thereby making Eö approach zero, the bubble rise velocity should follow the trend and become zero when Eö=0. The experimental observations have negated this hypothesis and showed that there is a critical value of Eö below which no rise takes place at all (i.e. u=0).

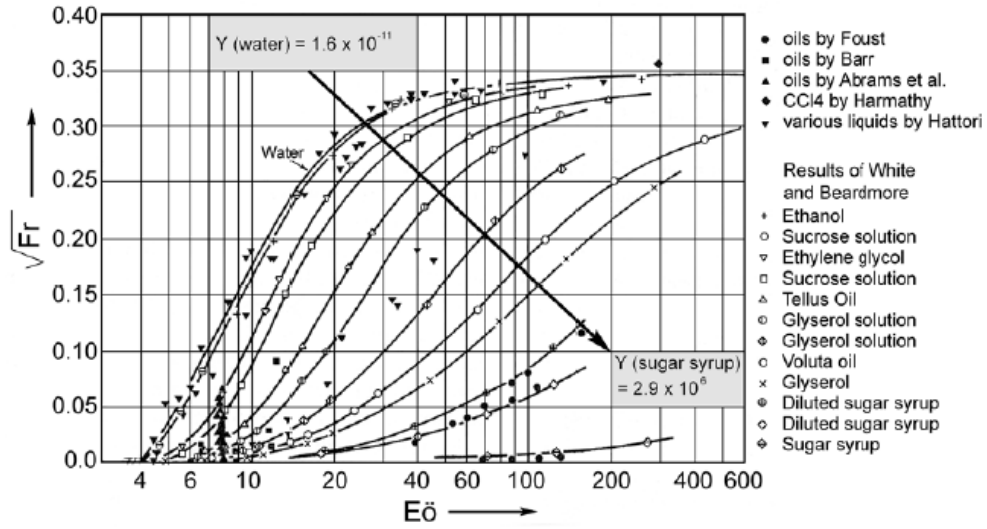

Figure 2. 7: Parametric experimental results for rise velocity of cylindrical bubble in various stagnant liquids contained in a channel, *(White and Breadmore, 1962).*

Figure 4 shows experimental data for a wide range of fluids in adiabatic conditions as reported by *White and Beardmore (1962).* Main conclusions of present interest are:

- As Eö increases beyond a particular value (around 70 for many common fluids e.g. water, ethanol etc.), the terminal bubble velocity approaches a constant value. The viscous forces and surface tension can be neglected and Equation (2.1) takes the form $Fr \approx 0.345$.
- Below $E\ddot{o} \approx 70$, the terminal velocity continuously decreases.
- Around $E\ddot{o} \approx 4$, the terminal velocity becomes zero. This is the surface tension dominated zone given exclusively by Eq. (2.3), i.e.:

$$E\ddot{o}_{crit} = \frac{{d_{crit}}^2 \cdot g \cdot (\rho_l - \rho_v)}{\sigma} \approx 4 \rightarrow d_{crit} \approx 2\sqrt{\frac{\sigma}{(\rho_l - \rho_v) \cdot g}} \qquad 2.6$$

where σ, g, and ρ are surface tension, gravitational acceleration, and density, respectively. If $d < d_{crit}$ surface tension forces tend to dominate and stable liquid slugs are formed.

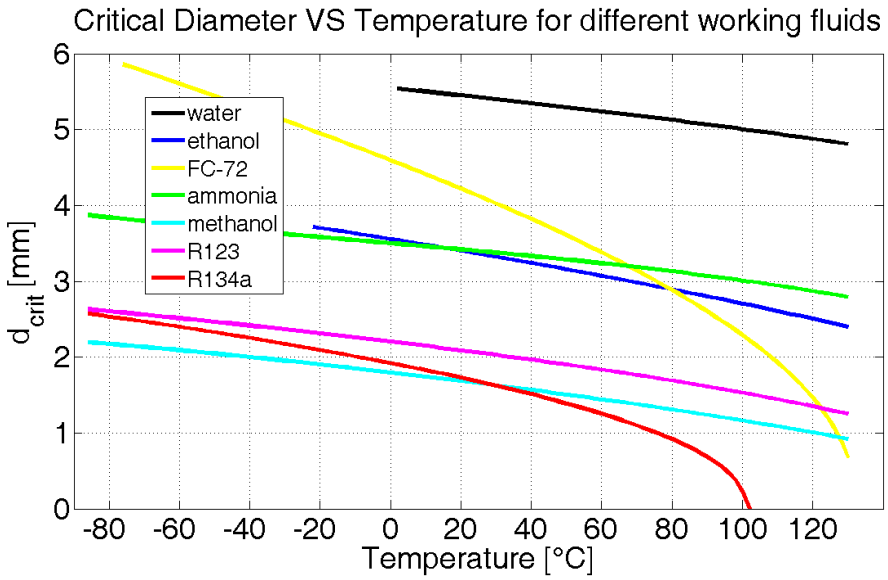

Figure 2. 8: critical diameter over temperature for different working fluids.

As the PHP tube diameter increases beyond d_{crit}, the surface tension is reduced and all the working fluid will tend to stratify by gravity and the heat pipe will stop functioning as a PHP and the device may operate as an interconnected array of two-phase thermosyphons. Obviously, rather than a certain fixed diameter which classifies the boundary between classical thermosyphons and CLPHPs, there is a finite transition zone and optimum liquid pumping will be achieved at a certain diameter below which the pressure drop overshadows the pump yield.

2.4.2 Heat input

For a defined CLPHP geometry of the device, the input heat flux is directly responsible for the type of flow pattern which will exist in the channel. The operating heat flux may also affect the level of perturbations inside a CLPHP thereby affecting the thermal performance of the device.

Experimental studies on CLPHPs, coupled with visualization, have indeed indicated towards this trend. Figure 2.9 shows a typical phenomenological trend for a partially filled device (about 50%-70%). The figure is representative of a range of working fluids like water, ethanol and R-123. The qualitative zones, as shown, may vary with actual fill charge, geometry and working fluid.

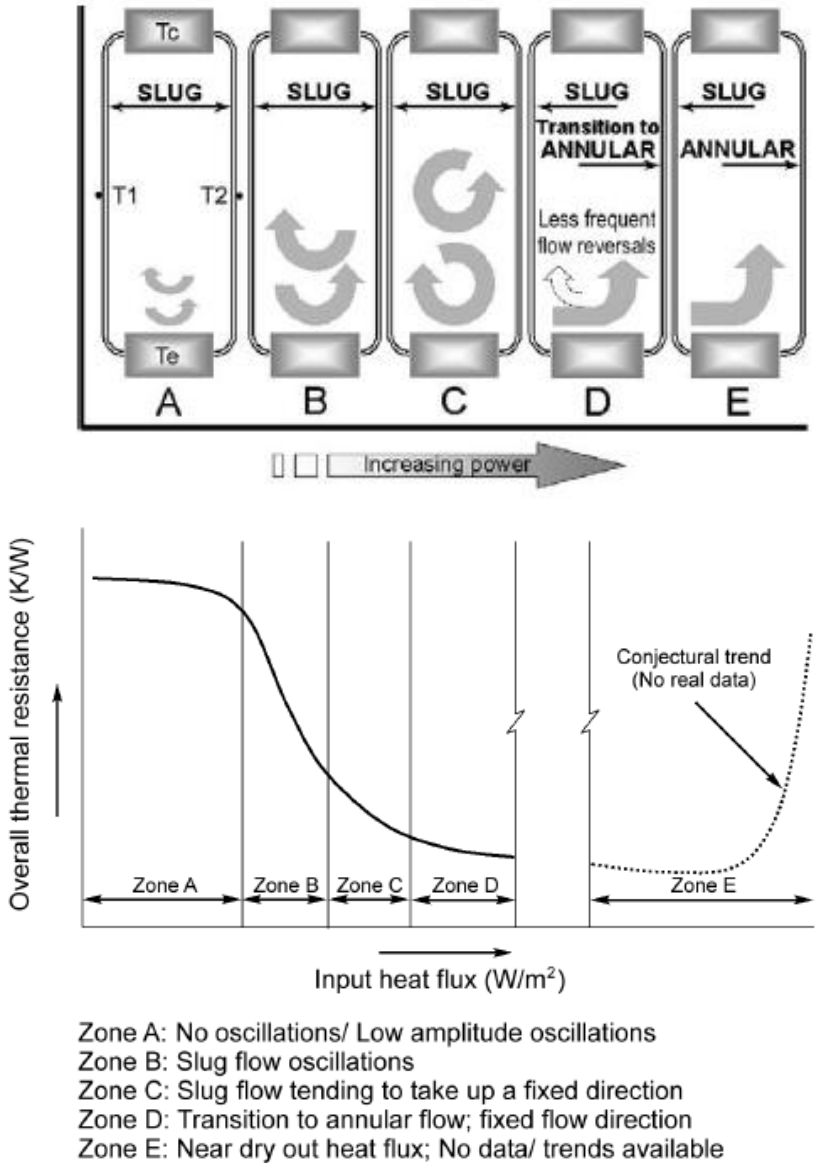

Figure 2. 9: Phenomenological trends for the effect of input heat flux, *Groll and Khandekar (2004).*

Visualization experiments, in parallel, have also supported these trends *(Khandekar, 2003).* Low input heat fluxes are not capable of generating enough perturbations and the resulting bubble pumping action is extremely restricted. The bubbles only oscillate with a high frequency and low amplitude. There are periods of 'no action' intermission stage followed by some small bulk activity phase. Overall, this scenario results in a poor

performance (i.e. very high thermal resistance). As the heat input is increased, slug flow oscillations commence whose amplitudes increase with increasing heat flux and become comparable to the length of the device. This improves the heat transfer coefficient to a marked degree. As the heat flux is further increased, the oscillating flow tends to take a fixed direction. The thermal resistance further reduces. Still higher input heat fluxes result in a transition of slug flow to annular flow at the outlet of the evaporator U-bends (figure 2.9).

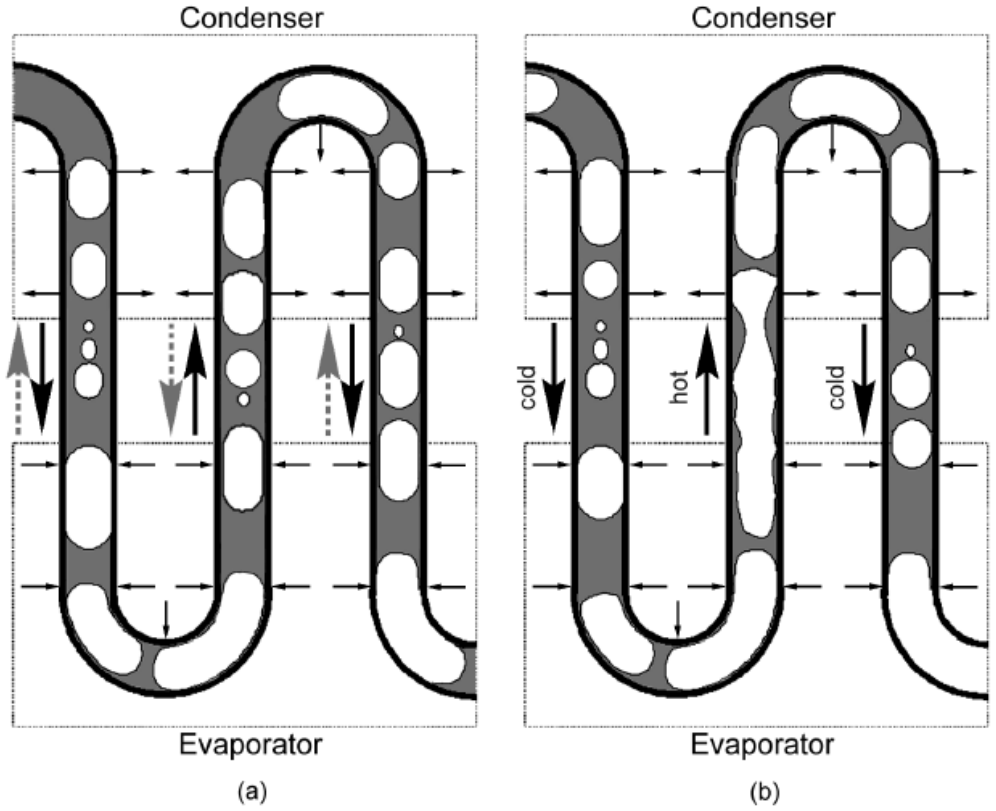

Figure 2. 10: Flow patterns in a CLPHP (a) oscillating slug flow in all tubes (b) alternate tubes with slug and annular flow *(Groll and Khandekar, 2003).*

This is true even for cases C and D. The bulk flow takes a fixed direction which does not reverse with time. The alternating tube sections are then hot and cold, with cold bubbly/slug flow coming down from the condenser to the evaporator in one tube and annular/semi-annular flow in the adjacent tube forming the outlet of the evaporator U-tube. This shows that the pulsating unstable slug flow behavior is again stabilized after a certain higher input heat flux. Interestingly, in such a case, best performance of CLPHP (lowest

thermal resistance) is observed. This is logical since the evaporator U-sections experience convective boiling through the thin liquid film rather than nucleate type boiling in slug flow regime. Thus, the best performing closed loop pulsating heat pipe is not a "pure" PHP device anymore. Further increase in heat flux leads to some sort of evaporator dry-out phenomenon but quantitative experimental data and phenomenological trends are not available in these near dry-out zones. It is indeed worthwhile to concentrate efforts in this direction. Thus it is confirmed that the input heat flux governs the degree of pulsations in the device and essentially acts as a demarcation parameter.

2.4.3 Filling ratio

The filling ratio (FR) of a CLPHP is defined as the ratio of working fluid volume actually present in the device to that of the total volume of the device (say at room temperature). Thus, a given CLPHP has two operational extremities with respect to the filling ratio, an empty device without any working fluid i.e. FR = 0 and a fully filled device i.e. FR = 1. It is obvious that at FR = 0, the empty CLPHP tubes constitute inefficient conduction fins and obviously have a very high thermal resistance. A fully filled PHP (FR = 1) is identical in operation to a single-phase thermosyphon. There exist no bubbles in the tube and so no 'pulsating' effect is present. Substantial sensible heat transfer can still take place due to liquid circulation in the tubes by thermally induced buoyancy. In between these two extremities lies the present area of interest. In this region also there exist three distinct sub-regions: (a) Nearly 100% fill ratio: In this mode there are only very few bubbles present rest being all liquid phase. These bubbles are not sufficient to generate the required perturbations and the overall degree of freedom is very small. The buoyancy induced liquid circulation, which was present in a 100% filled PHP, gets hindered due to additional flow resistance due to a few bubbles. Thus, the device performance is seriously hampered and the thermal resistance is much higher than for FR = 1. (b) Nearly 0% fill ratio: In this mode there is very little liquid to form enough distinct slugs and there is a tendency towards dry-out of the evaporator. The operational characteristics are unstable. The device may, under some operating conditions, work as a two-phase thermosyphon array.

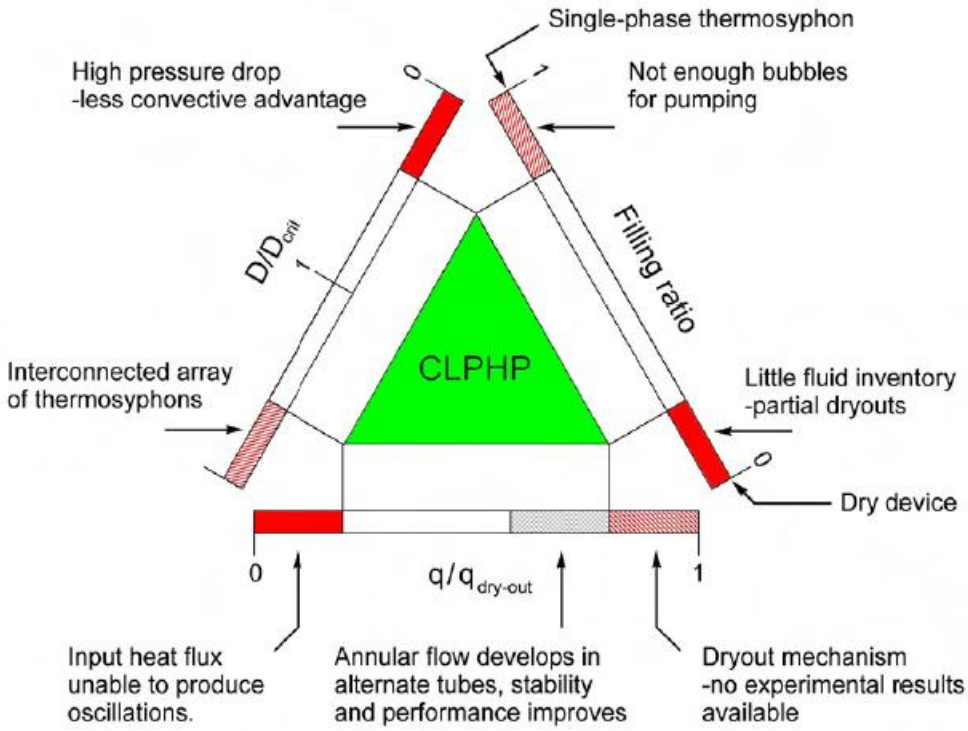

Figure 2. 11: Boundary conditions for CLPHP operation *(Khandekar 2004).*

(c) PHP true working range: Between about 10% to 90% fill charge the PHP operates as a true pulsating device. The exact range will differ for different working fluids, operating parameters and constructional details. The more bubbles (lower fill charges), the higher is the degree of freedom but simultaneously there is less liquid mass for sensible heat transfer. Less bubbles (higher fill charges) cause less perturbations and the bubble pumping action is reduced thereby lowering the performance. Thus an optimum fill charge exists. It can therefore be concluded that the filling ratio is also an independent parameter which defines a closed loop pulsating heat pipe.

2.4.4 Working Fluid Properties

• *Surface tension*. Higher surface tensions will increase the maximum allowable diameter and also the pressure drop in the tube. Larger diameter will allow improved performance, but an increased pressure drop will require greater bubble pumping and thus a higher heat input to maintain pulsating flow.

• *Latent heat*. A low latent heat will cause the liquid to evaporate more quickly at a given temperature and a higher vapor pressure; the liquid slug oscillating velocities may be increased and the heat transfer performance of the PHP also improved; on the other hand the dry-out phenomenon may occur at lower heat input levels.
• *Specific heat*. A high specific heat will increase the amount of sensible heat transferred. Because in most of the cases a great percentage of the total heat transfer in a PHP is due to sensible heat, a fluid with a high specific heat is desirable.
• *Viscosity*. A low dynamic viscosity will reduce shear stress along the wall and will consequently reduce pressure drop in the tube. This will reduce the heat input required to maintain a pulsating flow. The rate of change in pressure with respect to temperature at saturated conditions $\left(dP/dT\right)_{sat}$. This property affects the rate at which bubbles grow and collapse with respect to changes in temperature. At a high value of $\left(dP/dT\right)_{sat}$, the difference between vapor pressures in the evaporator and condenser will be increased and the performance of a PHP will be improved by enhanced oscillatory motion of liquid slugs.

2.4.5 Number of Turns

The number of turns in the PHP may affect thermal performance making negligible the effect of gravity. By increasing the number of turns, there are more distinct locations for heat to be applied and more local pressure drops. The higher level of local perturbations helps to avoid vapor phase recoiling in the evaporator and liquid merging in the condenser. The uneven distribution of liquid slugs and vapor plugs inside heating and cooling sections is necessary to create differences in pressure at each turn which drive the pulsating flow. If a PHP only has a few turns, it may not operate in the horizontal or top heat modes but a PHP with many turns can operate at any orientation because of the perturbations in each turn. There may be a critical number of turns which allows horizontal operation and an optimum number of turns allowing an independent orientation operation. These are not fixed values but they are undoubtedly functions of the other fundamental parameters such as inner diameter, heat flux level, filling ratio and working fluid.

2.4.6 Inclination Angle

PHP performance may or may not change with inclination angle. The dependence on orientation is coupled to the number of turns. Experimental results have shown that performance is generally better in a vertical bottom heated orientation, and some PHPs with only a few turns do not operate at horizontal orientations *(Charoensawan and Terdtoon, 2008)*. Other experiments, usually using PHPs with many turns, greater than 40 turns, *(Akachi et al. 1997, Maezawa et al 1997)*, have shown that performance is practically independent of inclination angle. The inclination angle is usually measured with respect to the horizontal direction:

- Bottom heat mode (BHM): vertical operation with evaporator on bottom and condenser on top (90°).
- Horizontal: no height difference between evaporator and condenser (0°)
- Top Heat Mode: vertical operation with evaporator on top and condenser on bottom (-90°).

2.4.7 Size and Capacity of Evaporator and Condenser

These parameters can affect the overall heat transfer of the PHP and could change the flow patterns within the heat pipe. Below a particular onset heat flux from the evaporator, the fluid in the PHP will not pulsate. Also, if the condenser cannot dissipate enough heat, it will limit the maximum heat transfer from the PHP. *Rittidech et al. (2003)* investigated the effect of the evaporator length on the heat flux of a CEPHP, whether *Panyoyay et al. (2008)* investigated the effect of the evaporator length on maximum heat flux of an inclined CLPHP. Both of them showed that the heat flux capability increases when the evaporator length decreases at every inclination angle. This is because when the evaporator length is small, the heated length of each U-turn in the evaporator is also small: it is easier for the fluid to transit the U-turn completely and to be “refreshed” with other colder fluid coming from the adiabatic/condenser regions. If the evaporator length is higher, vapor pressure may not be strong enough to push the fluid towards the condenser, the vapor plugs residing in the U-turn recoils and dry-out occurs at lower heat fluxes. It is likely that the closed loop configuration is less affected by the evaporator length since the fluid is not as confined as in the closed end configuration.

2.5 Closure: Open issues

Presently the PHP technology is still under research because of some lacks in its physical comprehension and characterization. Some open issues are listed here below:

- the role of latent and sensible heat;
- the existence of different flow patterns besides the pure slug-flow and their influence on the heat transfer performance;
- The characteristic oscillation frequency: does it always exist? Does it affect the thermal efficiency?
- Oscillating VS circulating working mode: is circulation always desirable for the PHP?
- The combined effect of gravity and the number of turns;
- The effective existence of multiple pseudo-steady-states for large number of turns.

The aim of this thesis is to answer to the previous questions or, at least, try to propose a roadmaps towards a better understanding of the PHP optimal operation.

Chapter 3

Chronicle of PHP modeling and experiments

3.1 Introduction

The Pulsating Heat Pipe (PHP) technology is quite young, nevertheless more than a hundred and fifty documents comprising journal papers, conference papers, reviews (Table 3.1), reports and patents (Table 3.2) were published in the last two decades, since it was introduced in its modern version by *Akachi (1990)*.

A detailed chronicle of the PHP modeling and experimental investigations is provided in the present chapter. At the end, as per the review by *Zhang & Faghri (2007)*, all the relevant publications outcomes are resumed in a table. The chart may represent a useful handbook for anyone who wants to approach the PHP technology advances through its crude scientific historical background.

Author, year	Title of the reviews
(Delil, 2001)	Pulsating & oscillating heat transfer devices in acceleration environments from micro-gravity to super-gravity
(Weislogel, 2002)	Passive Oscillatory Heat Transfer Systems
(Khandekar et al. 2002)	Mathematical modeling of Pulsating Heat Pipes, state of art and future challenges
(Groll & Khandekar, 2003)	Pulsating Heat Pipes: Progress and Prospects
(Khandekar & Groll, 2004)	Pulsating Heat Pipes: attractive entrants in the family of closed passive two-phase systems
(Karimi et al. 2004)	Review and Assesment of Pulsating Heat Pipe Mechanism for High Heat Flux Electronic Cooling
(Zhang & Faghri, 2007)	Advances and Unsolved Issues in Pulsating Heat Pipes

Table 3. 1: List of the literature reviews on the Pulsating Heat Pipe.

Author, year	Patent title (number)
(Smyrnov & Savchenkov 1971)	(USSR patent 504065, filed in 1971)
(Akachi 1990)	Structure of a heat pipe (US patent 4,921,041)
(Akachi 1993)	Structure of a micro heat pipe (US patent 5,219,020)
(Akachi 1996)	L-type heat sink (US patent 5,490,558)
(Akachi 1997a)	Ribbon like plate heat pipe (patent 5,642,775)
(Akachi 1997b)	Tunnel plate type heat pipe (US patent 5,697,428)
(Akachi 1998)	Method of manufacturing tunnel plate type heat pipe (US patent 5,737,840)
(Akachi 2000)	Heat transfer device having metal band formed with longitudinal holes (US patent 6,026,890)
(Smyrnov 2004)	Method of action of the PHP, its construction and the devices on its base (US 6,672,373)
(Asfia et al. 2007)	Cooling apparatus system and associated method (US 7,345,877)

Table 3. 2: PHP related patents.

3.2 PHP theoretical, analytical and numerical modeling

Since Akachi registered his first patents in the early ‘90s, many researchers are trying to develop mathematical and numerical models of PHP. The first attempts were made by *Akachi et al. (1996)* and were mainly focused on the analysis of the fluid pressure oscillation observed

experimentally. A purely analytical model based on the self-excited sinusoidal signal is used to explain how the pressure oscillation works as the fundamental function to complete the vapor-liquid circulation cycle. The first numerical model has been proposed by *Wong et al. (1999)* who mainly focused on the hydrodynamics of the CEPHP hydrodynamic: each liquid and vapor volumes of the slug train were described by a set of first order, nonlinear differential equations (mass and momentum). The pipe was assumed as adiabatic and a pressure pulse applied to the first plug at one end of the PHP represented the driving force for the flow motion and it was a given input; *Dobson & Harms (1999)* developed a lumped parameter model for the CEPHP where the fluid inside the tube consisted in a central liquid slug surrounded at each side by a vapor plug. The energy equations were considered for the vapor plugs, the liquid slugs were adiabatic and the attention was mainly focused on the hydrodynamic of the inner fluid; *Hosoda et al. (1999)* proposed one of the first CLPHP numerical model. It consisted in a single closed loop with two vapor volumes and two liquid volumes where momentum and energy equation (both axial and radial direction) were considered for the liquid phase only. The single vapor plug propagation process was investigated and an attempt of experimental validation for the fluid pressure and temperature was also presented; *Zuo et al. (1999, 2001)* developed a detailed model for the temporal displacement of the liquid slugs, lately updated with a detailed heat transfer section. Experimental validation is shown only for the thermal performance response with respect to the filling ratio and it is not very clear how a smooth tube PHP model can be validated if the experimental data are coming from a flat plate type PHP with embedded porous wick.

Shafii et al. (2001) presented a similar lagrangian multi-plug model both for the CEPHP and the CLPHP. Although the model considers many characteristic parameters and represents the first complete model, results show that gravity has no significant effect on the performance of CEPHP in top heat mode (i.e. with the heater in the above part of the PHP) and that the total number of vapor plugs always reduced to the total number of heating sections, which is in contrast with the experimental evidence. *Shafii et al. (2002)* numerically investigated the heat transfer through the liquid film which surrounds the vapor volumes in a PHP with open end concluding that heat transfer in a PHP is due mainly to the exchange of sensible heat (ed. This is true only for low heat fluxes and in case of pure slug flow regime);

Zhang et al. (2002) focused on the hydrodynamics of a single liquid slug in a U-turn miniature tube; *Zhang and Faghri (2003)* proposed another multi-plug model of a CEPHP and investigated the effect of the number of turns on the fluid oscillation frequency. *Holley and Faghri (2005)* proposed one of the most comprehensive numerical models for the CLPHP which considered also the effect of the diameter variation along the tube length. A detailed description of the numerical procedure as well as a careful qualitative validation was given. *Sakulchangsatjatai et al. (2008)* proposed one of the most exhaustive models of CEPHP. They updated *Zhang and Faghri (2003)* model with empirical assumptions on nucleate boiling frequency, bubble length and liquid film thickness coming from their experimental visualization campaign. Qualitative and quantitative validation was given for evaporator temperatures, inclination angles and input heat fluxes; *Khandekar and Groll (2008)* suggested a lumped parameters model for the CLPHP (single loop) but the assumption of homogeneous fog-flow seems more suitable for thermosyphons than PHP. Finally some attempts of modeling the PHP by artificial neural networks (ANN) can be found in literature *(Khandekar and Cui 2002, Lee and Chang 2009, Chen et al. 2009)*. ANN is a mathematical tool based on statistical regression and needs to be trained with a huge number of experimental test data. The main disadvantage is that the algorithms are not linked to the physical phenomena heading the dynamics of the system and can only predict the PHP behavior in the range of the particular experimental test data. The non-linear analysis performed by *(Song and Xu 2009)* states that PHPs are deterministic chaotic systems and that prediction ability of the system is finite but still PHPs have complex relationship between correlation dimensions and number of turns.

Very recently *Das et al. (2010)* developed an evaporation/condensation model of single liquid slug/vapor bubble that allows the large amplitude oscillations (as observed experimentally) to be explained. *Nikolayev (2011)* updated the previous model in order to treat an arbitrary number of bubbles and branches. Several phenomena occurring inside the PHP are taken into account: coalescence of liquid plugs, film junction or rupture, etc. The model reproduces some of the experimentally observed regimes of functioning of the PHP such as chaotic or intermittent oscillations of large amplitudes. Even though a model for the solid domain (tube wall) as well as a quantitative validation are missing, the use of an object oriented method represents a step forward with respect to all the previous codes.

Mameli et. al (2011) updated the model by *Holley and Faghri (2005).* The local pressure drops related to the presence of bends are accounted for and an attempt of quantitative validation is also shown. The above work is thoroughly explained in the second part of the present thesis work.

3.3 Towards stable operation of PHPs: Pure oscillation VS net circulation

The existence of dominant oscillation frequencies is one of the most actual issues related to PHPs. From an analytical point of view, the quest for a characteristic oscillation frequency while modeling PHP may be misleading because fluid motion inside real PHPs is quite chaotic and far from having only one dominant frequency. From a practical point of view, basic research should spend more efforts to state clearly if and how oscillation frequency affects the heat transfer capability of a fluid. By the time being it has been proved (see also Chapter 8) that a net fluid circulation, together with an oscillating component, is desirable in terms of stability and heat transfer performance. Furthermore in case of net circulation a dominant frequency is hardly recognizable. Many theoretical and experimental works have been devoted to the fluid circulation enhancement. Some examples are provided below.

3.3.1 Use of Check valves

Check valves have been already introduced by *Akachi (1990)* in his first patent as a way to avoid phase recoiling and promote fluid net circulation. *Rittidech et al. (2007)* investigated the optimum ratio between number of turns and number of check valves. *Wannapakhe et al. (2010)* and *Bhuwakietkumjohn and Rittidech (2010)* coupled the use of valves with silver nano-fluids. Actually phase recoiling, occurring when all the vapor phase resides in the evaporator zone and all the liquid phase fills the condenser, is less evident but fluid circulation is damped by the local pressure drops introduced by the check valves. The increase of the system complexity in this direction is not worthily repaid by the small increase of performance.

3.3.2 Varying the channel diameter

Holley and Faghri (2005) developed a numerical code for the analysis of a PHP with capillary wick and varying channel diameter. Results indicate that

heat transfer can be enhanced when the diameter of the channel is varied along the channel length, thereby providing increased range of heat load capability, less sensitivity to gravity, and in some cases smaller temperature differential.

Liu et al. (2007) built two special configurations of PHP, one with alternately varying channel diameter, the other equipped with one section of thicker tube, advantageous in establishing and maintaining reliable circulation of the working fluid. The thermal performance of the PHPs was examined over a range of working conditions. Comparing with the normal PHP with uniform diameter, either of the improved PHPs exhibited higher thermal performance.

Varying the channel diameter along the flow path; build a PHP as an alternated sequence of channels with different diameters or with thicker walls, is undoubtedly better than using check valves but still further complexity is added to the PHP production process.

3.4 Novel materials and working fluids

Lin et al. (2009) built a flat plate polydimethylsiloxane (PDMS) PHP in order to perform both the thermal and the visual investigation. Thermal conductivity of PDMS is very low (k = 0.2 W/mK) indeed evaporator and condenser zone were made of copper. Even if the performance is very poor, the idea is promising as the manufacturing process is simple and the cost is low. A valuable future alternative to PDMS could be represented by high conductive polymers (k = 20 W/mK); in such a way, copper blocks in the heat transfer section may be avoided and the structure could gain flexibility.

Recently many efforts have been spent on the investigation of PHP working with nano-fluids. *Wilson (2006)* found that the thermal conductivity for the diamond nano-fluid was 1.0 W/mK comparing with the thermal conductivity of 0.6 W/mK for HPLC grade water and stated that the nano-fluid provided a significant increase in thermal conductivity, which is supposed to be a primary reason for the significantly increased heat transport capability in the OHP. If such a small increase in the fluid thermal conductivity is able to increase the PHP performance, it would be interesting to test a PHP operating with mercury (k = 8.4 W/mK) as working fluid.

Lin et al. (2008) investigated the effect of silver nano-fluid on PHP thermal performance, in particular they compared pure water with a 20 nm

silver nano-fluid at different concentration (100 ppm and 450 ppm in water solution). The best efficiency is achieved with 100 ppm, while the 450 ppm concentration operates worse than pure water. The author put the blame on the higher fluid viscosity.

Qu et al. (2010) performed an experimental investigation on the thermal performance of an oscillating heat pipe (OHP) charged with base water and spherical Al_2O_3 particles of 56 nm in diameter. The very interesting research output is that the change of surface condition at the evaporator due to nanoparticle settlement was found to be the major reason for the enhanced thermal performance of the alumina nanofluid-charged OHP.

Ji et al. (2011) experimentally investigated the particle shape effect on the heat transfer performance of an PHP. Platelet (9 nm), blade (60 nm), cylinder (80 nm), and brick (40 nm) were studied and the maximum heat transport capability of the OHP was reached by means of cylinder-like alumina nanoparticles.

3.5 PHP direct applications

Miyazaki (2005) developed a series of flexible CLPHP for notebook personal computer cooling that can dissipate heat from the CPUs to the rear surface of the foldable display. The wing type design with 1.2 mm channel diameter and 12 turns achieved a thermal conductance of 3.5 W/K and a maximum heat transport capability of 100 W which are reasonably thought to be a sufficient potential for such kind of application.

Rittidech and Wannapakne (2007) investigated a flat plate solar collector in conjunction with a CEPHP operating with R134a as a working fluid and showed that this solution offers a reasonably efficient and cost effective alternative to conventional solar collector system that use heat pipes with the additional advantages of corrosion free operation and absence of icing problems during winter months.

Yang et al. (2009) showed the possibility of embedding the PHP as an integrated structure or heat spreader, in order to provide a higher overall thermal conductance to the host substrate. The influence of various operating parameters, including volumetric filling ratio of the working fluid, input heat flux and operating orientation, on the thermo-hydrodynamic performance, were investigated and successful operation at all orientations with respect to gravity was achieved.

Maydanik et al. (2009) built a compact cooler for electronics on the basis of CLPHP. The operation of the cooler has been investigated with water, methanol and R141b as working fluids at a uniform and concentrated supply of a heat load in different heating modes. A reliable operation of the device has been demonstrated in the range of heat loads from 5 to 250 W. With a heat load equals to 125W concentrated on a section of the thermal interface limited by an area of 1 cm^2, a minimum value of thermal resistance equal to 0.62 °C/W was attained when methanol was used as a working fluid.

Khandekar (2010) presented two PHP based heat exchangers: a temperature controlled liquid-liquid module which can be suitable for process waste heat recovery and a heat flux controlled air cooled module that can handle high power electronics applications. Both the devices could reach a maximum heat throughput of 800W and overall thermal resistances have been found to be of the order of 0.2 K/W or lower. For the low values of heat throughput, the air cooled PHP module performs better (in terms of thermal resistance and effective thermal conductivity) in gravity supported orientation than in anti-gravity orientation. As the applied heat flux increases, gravity does not play a significant role; comparable thermal resistances are obtained in both orientations. *Nuntaphan et al. (2010)* showed that the performance of a wire-on-tube heat exchanger can be enhanced by 10% if the wire-fin is replaced with a PHP.

3.6 PHP publications handbook (1996-2011)

Table 3.3 resumes the most relevant publications. The symbol "*" indicates that the article has been also quoted in the latest available review by *Zhang and Faghri (2007)*.

Author, year	Exp./Num. Approach; industrial appl. (if any)	Envelope Layout (material)	Configuration (n° of chann.)	Inclination angle [deg]	Cross section (I. D. [mm])	Working fluid	Filling Ratio	Heat Input [W]	Conclusions/comments
(Akachi et al. 1996)*	(EXP)	Tube (Cu)	Open (254-1000)	-	Circular (0.7-1.2)	R142b	0.5	70-100-450	Thermal resistance is independent of q and theta if n° of channels >80
(Maezawa et al. 1997)	(EXP)	Tube (Cu)	Open (80)	90 / 0 / -90	Circular (2)	Water, R142b	0.5	50 - 1000	R142b performs better than water. BHM better than THM. Oscillation has no specific periodical feature
(Miyazaki et al. 1996)*	(EXP/NUM) differential relationship between oscillation and pressure propagation wave	Pube (Cu)	closed (60)	90 / 0 / -90	Circular (1)	R142b	0.25 - 0.7	20 - 180	Optimized filling ratio (FR) for BHM and THM are 70% and 35% respectively. A symmetrical wave is obtained at proper charge ratio
(Miyazaki et al. 1998)*	(NUM) wave equation of pressure is derived. A continuous distribution of void fraction is assumed a priori	Plate (Cu)	closed (-)		-	-	-	-	The progressive wave for a closed loop and a standing wave for a open can be obtained from the wave equation
(Miyazaki et al. 1999)*	(EXP)	Plate (Cu, PC)	closed (50)	-90	Rectangular (-)	R142b	0.42	-	Measured wave velocities fairly agreed with eq.(14)
(Nishio et al. 1999)*	(EXP/NUM)	Tube (glass)	closed (4)	90	Circular (1.8 - 2.4 - 5.0)	Water, soap suds, ethanol, R142b	0.2 - 1.0	70	best performance with FR=0.35, thermal conductivity is 500 times copper. Better performance than standard HP with the same diameter.
(Gi et al. 1999)*	(EXP)	Tube (teflon)	closed/open (10)	30 / 50	Circular (2)	R142b	0.2 - 0.5 / 0.3 - 0.7	60-100	flow visualization
(Hosoda et al. 1999)*	(EXP/NUM) numerical solution of 1-D Liquid slug and vapor plug	Tube (glass)	closed (20)	90	Circular (1.2)	Water	0.3 - 0.9	80 - 220	best performance with FR=0.6. Numerical results overestimate pressure but oscillation is simulated
(Lee et al. 1999)*	(EXP)	plate (brass, acrylic)	closed (8)	30 / 90	rectangular (1.5)	ethanol	0.2 - 0.8	-	only fluid oscillation is observed (no net circulation). Most active in BHM with FR=0.4-0.6
(Zuo et al. 1999)*	(EXP/NUM) hydrodynamics modeled as vibrating sistem (sprig-mass-damper)	plate (Cu)	closed	0 - 90	triangular (-)	Water	0.4 - 0.8	5 - 250	even fluid distribution and smaller temperature fluctuation thanks to the wick. Thermal resistance=0.16K/W at FR=0.7

Table 3. 3: Summary of modeling and experiments on pulsating heat pipes (PHP) from 1996 to 2011 (continued)

Author, year	Exp./Num. Approach; industrial appl. (if any)	Envelope Layout (material)	Configuration (n° of chann.)	Inclination angle [deg]	Cross section (I. D. [mm])	Working fluid	Filling Ratio	Heat input	Conclusions/comments
(R. T. Dobson & Harms 1999)*	(EXP/NUM) explicit finite difference for equation of motion and heat transfer	tube (Cu)	open loop with open end	0	circular (3.34)	-	-	-	the system is mounted on a put-put boat, one end is opened and dipped into water. Thrust produced is 0.0027N
(Kisev et al. 1999)*	(EXP)	SS, -	open (46)	0	1.1	acetone	0.6	15 - 300	increasing acceleration from -6 to 12g evap. temperature increased by 30%
(T.N. Wong et al. 1999)*	(NUM) mass and momentum balance in a lagrangian frame (only hydrodynamics, tube is adiabatic)	-	open (4)	0	circular (-)	-	0.5	-	the pressure pulse induces the fluid oscillation which is damped out by friction between wall and fluid
(Van Es & Woering 2000)	(EXP)	plate(Al), tube(glass)	open (48)	-	square (1x1) circular (1)	acetone,FC-87,ethanol water	-	up to 110	Flat plate PHP better than conductive cooling systems but not better then liquid pumped in high-g. heaper in any case
(Lin et al. 2000)*	(EXP)	tube (Cu)	open (40)	0 / 90	circular (1.75)	acetone	0.25 - 0.5	140 - 2040	optimum FR=0.38. No operation when FR=0.25. Horizontal position gives the best performance
(Lin et al. 2001)*	(EXP)	tube (Cu)	open (40)	0 / 90	circular (1.75)	FC-72 , FC-75	0.3 - 0.5	140 - 2040	optimum FR=0.5. FC-72 better than FC-75. Performance independent of orientation
(L. Lin 2001)	(EXP)	tube (Cu)	open (40),1 eva. in the middle and 2 cond.	0 / 90	circular (1.75)	acetone, FC-72 , FC-76	0.25, 0.32 ,0.38, 0.5	140 - 2040	resume of the previous two. Acetone works better then fluoro-chemicals
(Swanepoel 2001)	(EXP/NUM) mass, momentum, energy explicit, htc are constant	tube(glass, SS, Al)	open(2), open(16), closed (18)	0 - 90	circular (3.34)	water, ammonia	-	up to 100	modeling based on dobson's approach and many experiments with different layouts
(Zuo et al. 2001)*	(EXP/NUM) mass momentum and energy 1-D transient 2phase flow with SIMPLEC scheme	plate (Cu)	closed	-	rectangular (-)	Water	0.4 - 0.8		experiments shows that performance is sensitive to FR. Numerical results are not shown.
(Tong et al. 2001)*	(EXP)	tube (glass)	closed (14)	0 / 90	circular (1.8)	methanol	0.6	50	circulation (both clock-wise and counter-clock) was observed and circulation velocity increases with the heat input level.

Author, year	Exp./Num. Approach; industrial appl. (if any)	Envelope Layout (material)	Configuration (n° of chann.)	Inclination angle [deg]	Cross section (I. D. [mm])	Working fluid	Filling Ratio	Heat input	Conclusions/comments
(Shafii et al. 2001)*	(NUM) mass, momentum and energy equations for each LS and VP	-	open/closed (4)	-90	circular (1.5 - 3)	water	0.614, 0.8947	0-80	numerical results say that 95% of heat transferred is sensible heat and that gravity is negligible
(Shafii et al. 2002)*	(NUM) evaporation and condensation of liquid thin film analyzed	-	open/closed (4)	-	circular (1.5 - 3)	water	0.6421, 0.895	0-119	heat transfer mainly due to sensible heat. Higher surface tension results in a slight increase in total heat transfer. No operation at high FR.
(Cai et al. 2002)*	(EXP)	tube (Cu, quartz)	closed/open (12-50)	45	circular (2.2 , 2.4)	ethanol, water, acetone, ammonia	0.5 , 0.4 - 0.6	100 - 600	propagation and extinction of bubbles are observed. Low latent heat fluids are recommended to promote oscillatory motion
(Cao & Gao 2002)	(EXP)	plate (Al)	closed (36)	0,10,30,90	triangular (3)	water, methanol	0.45,0.55 , 0.65	256	maximum heat fluxes achieved are about 40 W/cm2 for methanol and 110 W/cm2 for water
(S. Khandekar & Cui 2002)*	(NUM/EXP)	tube (Cu)	closed(10)	90	circular(2)	ethanol	0.0 - 1.0	5 to 60	ANN is trained by experiments. Effects of diameter, n° of turns, length, theta, fluid prop. Are not in the model
(S Khandekar, M Groll, et al. 2002)*	(EXP)	tube (Cu, glass)	closed (10)	0 / 45 / 90	circular (2)	Water, ethanol	0 - 1.0	5 - 15	Bubble formation and collapse are discussed
(Ma et al. 2002)*	(NUM/EXP) LS oscillation described by a balance of thermally driven capillary fractional and elastic restoring force	tube (Cu)	open (4)	0	circular (1.67)	acetone	-	5-20	minimum onset temperature difference is 15°C. Range of operational temperature difference is studied. Model underpredicts temperature drops
(Zhang et al. 2002)*	(NUM) numerical investigation of LS and VP pulsating flow in a miniature U-tube	-	open (1)	0	circular(-)	-	-	-	numerical overall heat transfer is dominated by sensible heat transfer. Oscillation frequency and amplitude not affected by surface tension
(Zhang & Faghri 2002)*	(NUM) thin film evaporation and condensation solved to get latent heat transfer coefficient	-	open (2)	-90	circular(-)	-	-	-	The amplitude and frequency of oscillation were correlated to the heat transfer coefficients and temperature difference.

Author, year	Exp./Num. Approach; industrial appl. (if any)	Envelope Layout (material)	Configuration (n° of chann.)	Inclination angle [deg]	Cross section (I. D. [mm])	Working fluid	Filling Ratio	Heat input	Conclusions/comments
(Zhang & Faghri 2003)*	(NUM) Liquid–vapor pulsating flow in a U-shaped miniature tube is investigated.	-	open (any)	-90	circular(-)	-	-	-	Amplitude and frequency decrease with the lengths of the heating and cooling sections. Increasing the FR resulted in a decrease of amplitudes and an increase of frequency.
(Charoensawan et al. 2003)*	(EXP)	tube (Cu)	closed (10,14,22,32,4)	0 / 90	circular (1.0 - 2.0)	water,ethanol,R123	0.5	500 - 1100	Gravity has a significant effect on performance. Minimum n° of turns is needed for a horizontal PHP to operate. Performance improves by increasing the diameter and the n° of turns.
(Khandekar et al. 2003)*	(EXP)	tube(glass)	closed (20-58)	0 / 90	circular (2)	R123	0.5	-	Flow oscillates with low amplitude/high frequency at horizontal mode. Capillary slug and semi-annular/ annular flow depend on heat input and inclination angle. Experimental results are correlated using empirical model.
(Khandekar et al. 2003)*	(EXP)	tube (Cu)	closed (2)	0 / 90	circular (2)	ethanol	0 - 1.0	14.8 - 74.4	Optimum charge ratios for three fluids are 30, 20, and 35%, respectively. Orientation affects performance. Horizontal mode did not work.
(Rittidech et al. 2003)*	(EXP)	tube (Cu)	open (38-84)	0	circular (0.55 - 2.03)	ethanol,water,R123	0.5	58	For R-123, heat flux increases with increasing diameter, but the trend is the opposite for ethanol. Correlation for heat transfer was proposed based on experiments.
(Kim et al. 2002)	(EXP)	plate(brass)	closed (20)	30 / 60 / 90	square (1.5 x 1.5)	R142b	0.2 - 0.4 - 0.6 - 0.8	-	best performance when FR=0.4 and theta=90°. Pressure wave has a sinusoidal waveform with frequency between 0.1 and 1.5 Hz
(Kim et al. 2003)	(EXP)	plate(brass)	closed/open (8), closed (20)	30 / 60 / 90	square (1.5 x 1.5)	R142b	0.2 - 0.4 - 0.6 - 0.8	-	oscillation and circulation more active
(Dobson 2003)	(NUM/EXP)lumped mass momentum energy with explicit scheme	-	unlooped with open end (2)	0	circular (3.34)	water	-	-	thermal to thrust efficiency practically zero. Numerical model drastically overpredict mass fluxes
(Khandekar 2004)*	(EXP)	tube (Cu)	closed (2)	90	circular (2)	ethanol	0.6	14.8 - 74.4	single closed loop PHP did not operate in horizontal mode. Capillary slug flow and annular flow depends on heat input.

Author, year	Exp./Num. Approach; industrial appl. (if any)	Envelope Layout (material)	Configuration (n° of chann.)	Inclination angle [deg]	Cross section (I. D. [mm])	Working fluid	Filling Ratio	Heat input	Conclusions/comments
(Zhang & Faghri 2004)*	(EXP)	tube (Cu)	closed open (6)	90	circular (1.18)	FC-72 , ethanol, water	0.6 - 0.9	5 - 60	Open loop PHP did not work. A minimum heat input is necessary to initiate pulsating flow. CLPHP optimum charge ratio is 70% for all three fluids.
(Liang & HB Ma 2004)*	only momentum equation for 1VP and 1LS, pipe is adiabatic	-	-	-	-	-	-	-	Isentropic bulk modulus generates stronger oscillations than the isothermal bulk modulus.
(Gu et al. 2004)*	(EXP)	plate(Al)	closed (96)	-	square (1 x 1)	R114 (R134a?)	0.5 - 0.6	1.4 - 5.9	PHP performed better in microgravity than normal or hyper gravity. New equation of critical diameter in microgravity is developed.
(Riehl 2004)*	(EXP)	tube (Cu)	open (13)	0 / 90	circular (1.5)	acetone, ethanol, isopropyl alcohol, methanol, water	0.5	10 - 50	Performance is better when operating in a horizontal orientation. Better performances were obtained when acetone was used in vertical orientation and methanol was used on horizontal orientation.
(Sakulchangsatjatai et al. 2004)*	(NUM) mass momentum and energy very similar to shafii 2001 but good attempt for validation	-	open(-)/closed(-)	-90	-	-	-	-	Model is same as Shafii et al. (2001). The predicted heat transfer rate is compared to experimental results in literature.
(R Dobson 2004)*	(NUM/EXP)lumped mass momentum energy with explicit scheme	tube (Cu)	unlooped with open end (2)	0	circular (3.34)	water	-	-	The dominate forces for liquid plug motion are vapor pressure difference, friction and gravity.
(Dobson 2005)*	(NUM/EXP)lumped mass momentum energy with explicit scheme	-	unlooped with open end (2)	0	circular (3.34)	water	-	-	Use of an open PHP to pump water. Mass flow rate of the pump is 0.2 mg/s for 100 mm height.
(Rittidech et al. 2005)*	(EXP)	tube (Cu)	open (16-32)	-	circular (2)	water,R123	0.5	1460 - 3504	PHPs were used as an air pre-heater for energy thrift in a dryer. Performance improves with increasing evaporator temperature. PHP with R-123 performs better than PHP with water.
(Katpradit et al. 2005)*	(EXP)	tube (Cu)	open (10,20,30)	0 / 90	circular (0.66 , 1.06 , 2.03)	R123,ethanol,water	0.5	-	Heat flux increases with decreasing evaporator length, increasing latent heat and number of turns. Correlation to predict heat transfer rate was proposed.

Author, year	Exp./Num. Approach; industrial appl. (if any)	Envelope Layout (material)	Configuration (n° of chann.)	Inclination angle [deg]	Cross section (I. D. [mm])	Working fluid	Filling Ratio	Heat input	Conclusions/comments
(J. L. Xu et al. 2005)*	(EXP)	tube (Cu, glass)	closed (8)	90	circular (2)	water, methanol	0.7	10 - 30	Flow circulation was observed. Flows in some channels are in the opposite direction of bulk circulation
(J. L. Xu & X. M. Zhang 2005)*	(EXP)	tube (Cu)	closed (8)	90	circular (2)	FC-72	0.7	10 - 25.6	Both startup and steady thermal oscillations were studied. Oscillation flow at low heating power displays random behavior and becomes quasi periodic at high heat power.
(Gu et al. 2005)	(EXP)	tube(teflon), plate(Al)	closed (40), closed (96)	0 / 90 / -90	circular (1.6?)	R114	0.5-0.7	1.4 - 5.9	improved heat transfer performance under reduced gravity than under normal or hyper-gravity. In my opinion 20 seconds are not enough to reach pseudo-steady in a flat plate PHP due to inertia.
(Holley & Faghri 2005)*	(NUM) mass momentum energy for a PHP with varying diameter and capillary wick	tube with thin porous wick (Cu)	closed (2, 6)	-90 / -45 / 0 / 45 / 90	circular (varying along the flow path)	water	0.30 - 0.65	30 - 80	Varying diameter between parallel channels induces flow circulation and may increase heat transfer capacity. BHM performed better than THM. Sensitivity to gravity decreases when increasing the number of channels.
(Kim et al. 2005)	(NUM) same as Shafi et a. (2001), only different evap. and cond. correlations	-	open (-)	-90	circular (1.5 - 3)	-	-	(const. Thot, Tcold)	diameter, surface tension, FR, have significant effects on the PHP performance
(Rittidech et al. 2005)	(EXP)	tube (Cu)	open (14)	90	circular (2)	R134a	0.5	58	experimental prototype of a CEOHP CPU-heat sink has better thermal performance than conventional heat sink.
(Miyazaki 2005)	(EXP)	tube (Cu, teflon)	closed (16,24)	0 / 90	circular (1.0 - 1.2 - 1.7)	R134a	0.7	0 - 100	results show that flexible oscillating heat pipe may be used to transport dissipated heat from CPUs to the rear surface of the foldable display
(Cai et al. 2006)*	(EXP)	tube (Cu, SS)	-	0	circular (1.397 , 1.568)	water	0.4 - 0.55 - 0.7	100 - 400	Minimal temperature difference and fluctuation appear at operating temperature between 120◦C and 160◦C.
(Ma et al. 2006)*	(EXP)	tube (Cu)	closed loop	90	circular (1.65)	water with diamond nano-particles	0.5	5 - 336	At 100W, the temperature difference can be reduced from 42◦C to 25◦C for the nano-fluid OHP as opposed to the pure water OHP.

Author, year	Exp./Num. Approach; industrial appl. (if any)	Envelope Layout (material)	Configuration (n° of chann.)	Inclination angle [deg]	Cross section (I. D. [mm])	Working fluid	Filling Ratio	Heat input	Conclusions/comments
(Ma et al. 2006)*	(NUM) spring mass damper like ZUO 1999, pulsation frequency imposed a priory. (low level)	-	-	0	circular(1.65)	water, acetone	0.5	-	Oscillation depends on FR, total characteristic length, diameter, temperature difference between the evap. and cond. sections, working fluid, and operating temperature.
(Ma & Zhang 2006)	(NUM/EXP) multivariate variance analysis (statistical approach similar to ANN)	tube (Cu)	closed (10)	0 to 90	circular (2)	water	03. to 0.7	40-200	Only FR, inclination angle, and heating water flow rate are discussed as affecting variables
(Charoensawan et al. 2007)*	(EXP) nondimensional purely empirical correlation for heat transfer of PHP	tube (Cu)	closed (10, 22, 32, 52)	0	circular (1 , 1.5 , 2)	water,ethanol	0.3 - 0.5 - 0.8	-	Prandtl number of liquid, Karman number, modified Jacob number, bond number, Kutateladze number are identified as influential numbers, STD of the empirical correlation is ±30%.
(Qu et al. 2007)*	(EXP)	tube (Cu)	closed (16)	90 / -90	square, triangular (1 - 1.5)	water	0.25 - 0.4	-	PHP with triangle channel performs better than with square channel. PHP with 1.5 mm channel performs better than that with 1 mm channel.
(Chiang et al. 2007)*	(EXP)	(?) Al	open (26,36)	90 / 0	square (-), triangle(-)	ethanol, acetone, nanofluids	0.2 - 0.8	<200	Optimal FR varies with number of ports. Addition of nano-particles slightly improve PHP performance.
(Khandekar & Gupta 2007)*	(NUM) heat conduction in the radiator plate solved with fluent	plate(Al)	closed (22)	90 / 0	circular (2)	water	0.5	20 - 62.5	Embedded PHP can be beneficial only if the conductivity of the plate is low.
(Liu et al. 2007)	(EXP)	tube(glass)	closed (8)	90	circular (alternated 1.6 - 2.0)	eyhanol	0.1 - 0.7	10 - 125	As the flow path geometry of a PHP becomes less symmetric (alternately varying channel diameter), the likelihood of circulatory flow increases and PHP exhibits better performance.
(Rittidech et al. 2007)	(EXP)	tube (Cu)	open (10)+Check Valves	90	circular (1.77)	water,ethanol,R123	0.5	-	heat-flux increases with Rcv and decreases with the aspect ratio. A Correlation for the vertical PHP heat-transfer rate has been proposed
(Rittidech & Wannapakne 2007)	(EXP) direct application	tube (Cu)	open (24)	18	circular (3)	R134a	0.5	-	An efficiency of about 62% was attained (comparable to that of the solar collector by heat pipe). Other advantages of the system include simple construction, corrosion free operation and elimination of winter icing problems

Author, year	Exp./Num. Approach; industrial appl. (if any)	Envelope Layout (material)	Configuration (n° of chann.)	Inclination angle [deg]	Cross section (I. D. [mm])	Working fluid	Filling Ratio	Heat input	Conclusions/comments
(Qu & Ma 2007)	(EXP/NUM) heat transfer model only for the PHP start-up phenomena	tube (glass)	open (2)	90	circular (3)	water	-	-	The startup performance can be improved by using a rougher surface, controlling vapor bubble type, and selecting a right working fluid.
(de Souza et al. 2007)	(EXP)	tube (Cu)	closed (14)	-12.5 - 90	circular (1.5)	CO2	0.25 - 0.5 - 0.75	25 - 100	CLPHP working between -20ºC and 5º C, with CO2 as the working fluid had adequate performance for all tests, up to the power level of 25W
(Van Es et al. 2007)	(EXP)	plate (Al), circular (SS)	open (48), -(20)	0	square (1x1) circular (1.6)	Acetone	0.7	40	half based on NLR experiments and half on the PHP heat-switch. three dimensionless numbers are introduced to capture the PHP working range
(Lin et al. 2008)	(EXP)	tube (Cu)	closed (10)	90	circular (2.4)	water with silver nano-particles	0.2 - 0.8	5 - 85	benefits brought by the higher fluid mean thermal conductivity are opposed by higher viscosity. Silver nano-fluids give no sensible advantage.
(Sakulchangsatjatai et al. 2008)	(NUM/EXP) updated version of the model done in 2004 based on Shafi et al. 2001	tube (glass)	open (4)	0-90	circular (2)	R123	0.5	-	Probably the first model which has been validated both qualitatively and quantitatively.
(Han et al. 2008)	(NUM/EXP) theoretical investigation of the thin film evaporation process	tube (Cu)	closed (12)	0 (?)	circular (1)	Nitrogen	-	30 - 120	experimental and numerical investigation of a PHP for cryogenic applications
(Yang et al. 2008)	(EXP)	tube (Cu)	closed (40)	90	circular (1.0 - 2.0)	R123	0.3 - 0.7	50 - 570	Both CLPHPs with 1 mm or 2 mm ID operated successfully in all three heat modes and showed excellent performances up to 32W/cm^2 radial heat flux
(Khandekar & Groll 2008)	(NUM) two-phase flow modeling of a single-loop gravity supported PHP is attempted considering a homogeneous fog-flow steady model.	tube (Cu)	closed (2)	0 / 90	circular (2)	ethanol	0.4 - 0.6	10 - 50	the effective thermal resistance of the device can then be determined by using correlations for convective boiling and condensation in the respective sections of the device
(Chen et al. 2009)	(EXP/NUM) Based on a neural network, an approach of nonlinear autoregressive moving average model with exogenous inputs.	tube (Cu)	closed (10)	90	circular (2)	water	0.1 - 0.6 - 0.9	20, 60, 100	Although the predicted results follow the measured results well, the physical interpretability of the model is lost

Author, year	Exp./Num. Approach; industrial appl. (if any)	Envelope Layout (material)	Configuration (n° of chann.)	Inclination angle [deg]	Cross section (I. D. [mm])	Working fluid	Filling Ratio	Heat input	Conclusions/comments
(Givler & Martinez 2009)	(NUM) FLOW-3D software (VoF), liquid film is absent, constant heat transfer coefficients	tube (Cu)	sigle straight tube/closed(2,4)	-	circular (3)	water	0.42-0.45	0.0065 -	some qualitative trend and image is shown but the model validation is absent.
(Song & Xu 2009)	(NUM/EXP) PHP is modeled with the autocorrelation functions (ACF) approach.	tube (Cu)	closed (8, 12, 18)	5 - 90	circular (1.2)	water,FC-72	0.5 - 0.8		the analysis states that PHPs are deterministic chaotic systems and identifies three typical attractor functions
(Yang et al. 2009)	(EXP)	plate(Al)	closed (40, 60)	-90 / 0 / 90	square (1 x 1 - 2 x 2)	ethanol	0.05 - 0.95	50 - 430	For horizontal and THM, optimum FR of about 50% – 65% , while in BHM: for higher heat loads, the maximum performance is not very sensitive to FR in the range 40% – 70%. Bigger channel and BHM showed the best performance
(Khandekar et al. 2009)	(EXP)	tube (Cu,glass)	single closed loop	90	circular (2)	ethanol	0.6	20	The single closed loop PHP exhibits multiple quasi-steady steady states. Dominant oscillation frequencies are in the range of 0.1 to 3.0 Hz
(Lee & Chang 2009)	(NUM/EXP) non-linear autoregressive ANN method is used to analyze the thermal dynamics of a PHP in time and frequency domains.	tube (glass)	closed (10)	90	circular (2)	water	0.5	30, 70, 110	the trained model should be tested with other experimental data to check its consistency.
(Lin et al. 2009)	(EXP)	plate (PDMS, PCP)	closed (12)	90	circular(2)	methanol	0.5	3 - 9	preliminary experimental results of using polydimethylsiloxane (PDMS) to manufacture a transparent flat plate pulsating heat pipe.
(Lin, Wang, et al. 2009)	(EXP)	tube (Cu)	closed(8)	90	circular(1.3)	ethanol, water, FS-39E micro-capsule fluid	0.4 - 0.8	5-80	Comparing with pure water and ethanol, FS-39E microcapsule fluid can enhance heat transport capability, The best concentration of FS-39E is 1 wt%.
(Savino et al. 2009)	(EXP/NUM) The system is simulated with teh VOF approach using fluent.	tube (glass)	single tube	90 / 45 / 0	circular(5)	water, ethanol,EG, heptanol, mixtures	-	4 -7-10	a single tube is filled with "self rewetting fluids". Inverse Marangoni effect is exploited to promote fluid motion during horizontal operation.
(Maydanik et al. 2009)	(EXP) direct application	Tube(Cu)	Closed(34),3D spiral shape with fins	90	Circular(1.2)	water, methanol and R141b	-	5 to 250W	When heat input (125W) is concentrated on 1 cm^2, a minimum value of thermal resistance equal to 0.62 °K/W

Author, year	Exp./Num. Approach; industrial appl. (if any)	Envelope Layout (material)	Configuration (n° of chann.)	Inclination angle [deg]	Cross section (I. D. [mm])	Working fluid	Filling Ratio	Heat input	Conclusions/comments
(Qu et al. 2010)	Thermal performance of an oscillating heat pipe with Al_2O_3–water nanofluids								
(Wannapakhe et al. 2010)	(EXP)	tube (Cu)	closed (80) + check valves	0, 20, 40, 60, 80, and 90	circular(2)	Water+silver nanopart.	0.5		best performance in BHM and silver nano-fluid concentration 0.5 %w/v
(Bhuwakietkumjohn & Rittidech 2010)	(EXP)	tube (glass)	closed (20) + check valves	90	circular(2.4)	ethanol with silver nano-particles	0.5		flow patterns of a CLPHP with check valves using ethanol and a silver nano-ethanol. The mixture showed higher heat flux than pure ethanol
(Kammuang-Lue et al. 2010)	(EXP)	tube (Cu)	closed (150)	0	circular(1.06)	R134a	0.5	-	derivation of an empirical correlation to predict the maximum heat flux of a horizontal CLPHP. coefficient of determination and standard deviation of 0.68 and ±35% respectively
(Nuntaphan et al. 2010)	(EXP) direct application	tube(Cu)	open(34) x 2	90*	circular(2.45)	R123, methanol, acetone	0.3		the heat transfer rate of wire-on-tube heat exchanger can be enhanced by 10% by means of an oscillating heat pipe
(Das et al. 2010)	(NUM/EXP) based on SHAFII et al. (2001) and Dobson (2004).	tube(glass)	single tube	0	circular(2)	n-pentane	-	-	Implementation of evaporation/condensation model that allows the large amplitude oscillations (as observed experimentally) to be explained
(Khandekar 2010)	(EXP) two set-ups: temperature controlled and heat flux controlled	Tube(Cu)	Closed(120), closed(224)	90, -90	Circular(1.8), circular(2)	ethanol	0, 0.4, 0.6, 0.8	Up to 1300W	Heat flux controlled configuration is better suited for PHP applications. These devices can handle large heat fluxes with low thermal resistance.
(Ji et al. 2011)	(EXP)	tube(Cu)	closed (12)	90	circular(1.65)	EG+water+ alumina nano-particles			Heat transfer performance depends on particle shape and volume fraction. Best performance is achieved with cylinder like alumina nano-particles.
(Nikolayev 2011)	(NUM) based on Dobson, object oriented code	Fluid only							
(Mameli et al. 2011)	(NUM) evolution of Holley et. al (2005). Works with different fluids, considers the pressure losses at the bends	tube (Cu)	closed (4), (10), (40)	0, 45, 90	circular (2)	ethanol, acetone, r134a, FC-72	0.5		first attempts of both qualitative and quantitative model validation.

PART II:

Theoretical modeling and numerical simulations

Chapter 4

The model by Holley and Faghri

4.1 Introduction

The present chapter provides a detailed description of the theoretical model by *Holley and Faghri (2005)* developed for the analysis of closed loop heat pipes with capillary wick and varying channel diameter. This model has been chosen as starting point for the development of the novel and improved model presented in the next chapter.

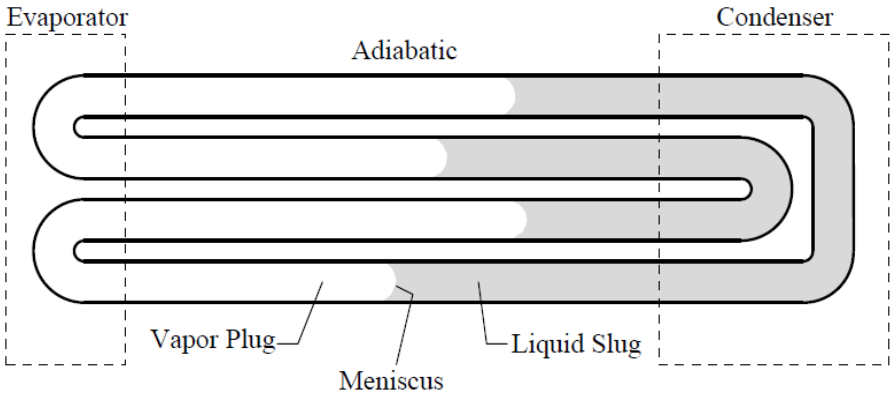

Figure 4. 1: Schematic of a pulsating heat pipe with four parallel tubes.

4.2 Theoretical model

Holley and Faghri (2005) developed a one dimensional model of a CLPHP with capillary wick and varying channel diameter working with water. The working fluid is always in the form of liquid slugs and vapor plugs which are always alternated (Fig. 4.2).

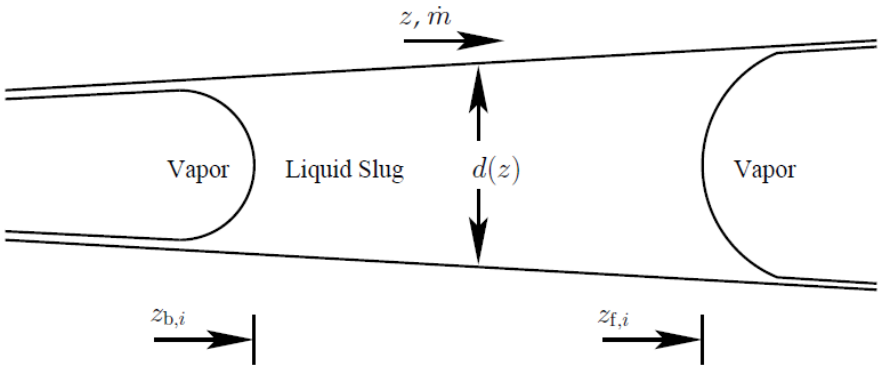

Figure 4. 2: Schematic of a liquid slug in the PHP model.

The tube wall is subdivided into control volumes which are fixed in space (Eulerian approach), while the fluid control volumes follow each liquid slug and vapor plug (Lagrangian approach) which are moving, expanding, nucleating and collapsing. Fluid motion is governed by the momentum equation applied to each liquid slug while vapor is supposed to be an ideal gas. Temperature in the fluid and wall is determined by accounting for energy balance. The energy equation is applied individually to the wall and wick, liquid slugs, and vapor plugs. The three energy equations are coupled by

convective heat transfer terms with appropriate heat transfer coefficients. Latent and sensible heat transfer occur between the tube wall and fluid. Boiling, evaporation, and condensation comprise latent heat transfer. Sensible heat transfer occurs by conduction or convection with laminar or turbulent flow. Within the liquid slugs heat is conducted in the axial direction. Heat transfers also from the vapor plugs to the slug menisci. Within the tube wall heat is allowed to conduct in the axial direction. On the tube external surface constant heat input per unit length is applied at the evaporator while convective boundary condition with constant heat transfer coefficient is applied at the condenser section. No heat transfer occurs at the adiabatic section.

Assumptions are stated as follows.

1. Spatial and time derivatives of density and viscosity are assumed negligible in order to simplify the analysis with regard to the momentum equation. However, all the fluid thermo-physical properties are evaluated as functions of temperature in saturated conditions.
2. The mass flow rate of each liquid slug is constant along its length at a given time.
3. The model is one-dimensional, with the axial dimension along the flow path considered for momentum and heat transfer; heat transfer transverse to the flow path is lumped.
4. The menisci of the liquid slugs are assumed to maintain a spherical meniscus shape with zero contact angle at the wall.
5. Surface tension is evaluated at the plug temperature.
6. The effect of the turns is neglected.
7. The pressure within each vapor plug is assumed uniform.
8. Vapor exists at saturated conditions.
9. There is negligible flow friction corresponding to the vapor plugs.

The fluid and solid domains are governed by the following equations:

4.2.1 Momentum equation for the i-th liquid slug

Regarding the hydrodynamics, each liquid slug is treated as single control volume which is governed by a simplified version of the momentum equation for incompressible flow:

$$\rho \frac{Du}{Dt} = \rho g \cos\theta - \frac{\partial P}{\partial z} + \frac{4\tau}{d} \tag{4.1}$$

Where $\frac{Du}{Dt} = \left(\frac{\partial u}{\partial t} + u \frac{\partial u}{\partial z} \right)$ is the total derivative. By means of assumptions (1) and (2) and writing the slug velocity as $u = \dot{m}/\rho A$, equation (4.1) is integrated and rearranged as follows:

$$\frac{d\dot{m}}{dt} \int_b^f \frac{1}{A} dz + \frac{\dot{m}^2}{2} \left[\frac{1}{\left(\rho A^2\right)_f} - \frac{1}{\left(\rho A^2\right)_b} \right] = \int_b^f \rho g \cos\theta dz - \left(P_f - P_b \right) + 4 \int_b^f \frac{\tau}{d} dz \tag{4.2}$$

The first and second terms on the left hand side are pressure differences due to acceleration as a result of mass flow rate change and dilatation (slug elongation or shortening) respectively. The terms on the right hand side refer to the hydrostatic pressure difference, difference between pressures at the slug menisci, and pressure difference due to shear. There are two contributions to the pressure at the end of a liquid slug. One is the vapor pressure, which is assumed to be at the saturation pressure at the temperature of the vapor plug per Assumptions 7 and 8 while the second is the pressure rise across the meniscus surface due to capillary pressure, the radius for which is dependent on axial location

$$\left(P_f - P_b \right) = \left[P_{sat}\left(T_v\right) + \frac{2\sigma}{r} A \right]_f - \left[P_{sat}\left(T_v\right) + \frac{2\sigma}{r} A \right]_b \tag{4.3}$$

The shear term in Equation (4.2) is treated semi-empirically. The flow is considered to be either fully developed laminar or turbulent. Local values of shear along the i^{th} slug are determined for Hagen–Poiseuille (exact) flow or for turbulent flow (empirical) in a rough pipe. For turbulent flow roughness is considered as a result of the wick. The size of a powder particle for a sintered powder wick, or a capillary pore for a sintered filamentary wick, is chosen as the size for the roughness features. The Colebrook correlation accounts for surface roughness and is used for turbulent flow.

$$\tau = \frac{1}{2} C \rho u^2 \rightarrow \tau = \frac{C \dot{m}^2}{2 \rho A^2} \tag{4.4}$$

where the friction factor is evaluated for the laminar and turbulent regimes as follows:

$$\begin{cases} C = 16/\mathrm{Re}_l & \mathrm{Re}_l < 2000 \\ \dfrac{1}{2\sqrt{C}} = 1.74 - 2\log_{10}\left(\dfrac{2k_s}{d} + \dfrac{18.7}{\mathrm{Re}_l \, 2\sqrt{C}} \right) & \mathrm{Re}_l \geq 2000 \end{cases} \quad \text{when} \tag{4.5}$$

4.2.2 Energy equation for the i-th liquid slug

The energy balance for the liquid is based on heat conduction within the fluid and heat transfer to and from the wall. The formulation is Lagrangian, and there is no axial convection.

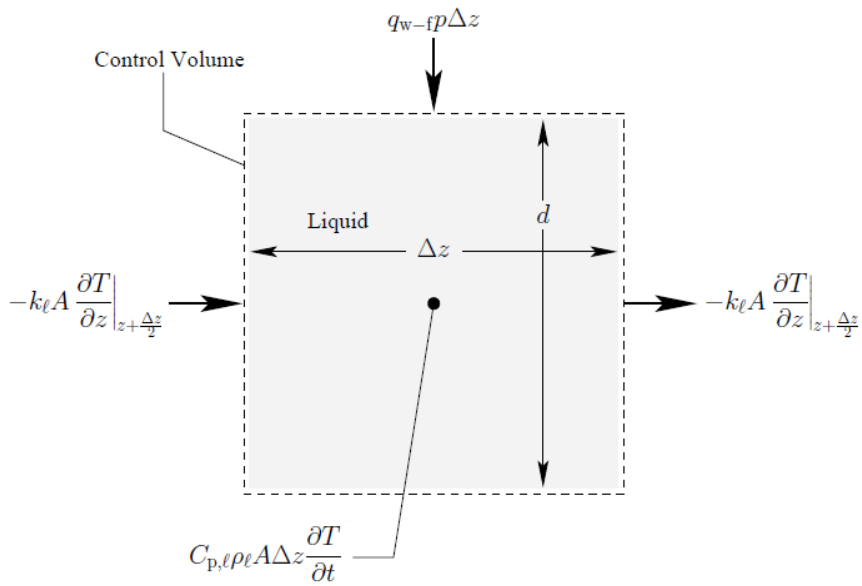

Figure 4. 3: Heat storage and flow into and out of an elemental control volume of liquid slug.

The following partial differential equation accounts for heat storage and axial conduction within the fluid; the heat transfer between the wall and fluid $q_{w\text{-}f}$ is lumped (see the paragraph 4.2.5).

$$\left[c_{p,l}\rho_l A_{cr}\frac{\partial T_l}{\partial t} = q_{w-f}\,p + k_l A_{cr}\frac{\partial^2 T_l}{\partial z^2} \right]_i \tag{4.6}$$

Regarding heat conduction, liquid slugs are no more treated with the lumped approach: each liquid slug is divided into n_s nodes and the temperature for each grid is evaluated by integrating eq (4.6). The remaining spatial derivative is determined using a first order central difference. Values of heat transfer between the wall and fluid are interpolated based on the representative values of adjacent grids.

4.2.3 Energy equation for the j-th vapor plug

The following partial differential equation accounts for heat storage within the entire vapor plug, for the heat transferred between vapor and the tube wall $q_{w\text{-}f}$ and for axial conduction with the neighbouring liquid slugs.

$$\left[\begin{aligned} &(z_{f,j} - z_{b,j})A_{cr}\frac{\partial}{\partial t}\left(H_g \frac{P_{sat}(T_v)}{RT_v} \right) = \\ &= q_{w-f}\,p(z_{f,j} - z_{b,j}) + k_l A_l \left.\frac{\partial T_l}{\partial z}\right|_{z_{f,i-1}} - k_l A_l \left.\frac{\partial T_l}{\partial z}\right|_{z_{b,i}} \end{aligned} \right]_j \tag{4.7}$$

Forward and backward first order differences are used for conduction at the menisci.

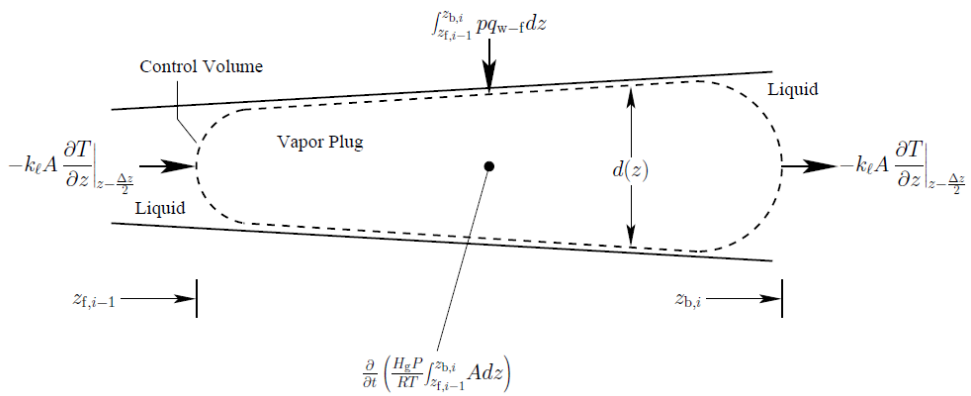

Figure 4. 4: Heat storage and flow into and out of a control volume comprising a vapor plug.

4.2.4 Energy equation for the wall

Holley and Faghri (2005) assume that the internal tube surface is covered by a thin wick and that the liquid film surrounding each vapor bubble is always filling the porous structure. The following partial differential equation accounts for heat storage and axial conduction within the wall and the wick filled by liquid, as per equation (4.6) and (4.7) the heat transfer between the wall and fluid $q_{w\text{-}f}$ is lumped (see the paragraph 4.2.5).

$$\left\{c_{p,w}\rho_w\left[A_w+(\varepsilon-1)A_{wk}\right]+c_{p,l}\rho_l\varepsilon A_{wk}\right\}\frac{\partial T_w}{\partial t}= \\ =q_{ex}p_0-q_{w-f}p+\left(k_wA_w+k_lA_{wk}\right)\frac{\partial^2 T_w}{\partial z^2} \tag{4.8}$$

where $$q_{ex}=\begin{cases} q_{ev} & \textit{evaporator} \\ 0 & \textit{adiabatic} \\ h_\infty(T_\infty-T_w) & \textit{condenser} \end{cases}$$

The outer wall perimeter is $p_0=\pi d+(2\delta_w+2\delta_{wk})$

The entire wall tube is divided into n_w nodes and the temperature for each wall grid is evaluated by integrating Equation (4.8).

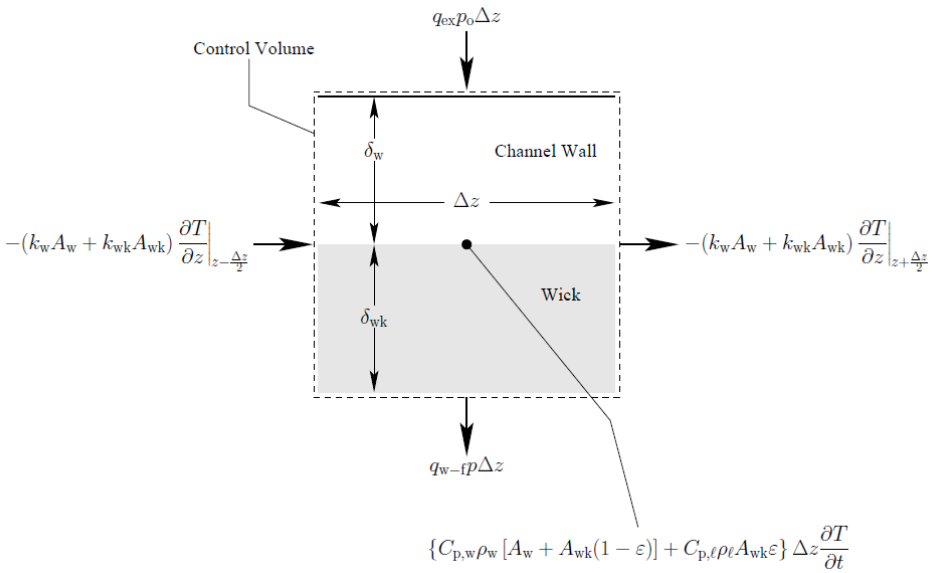

Figure 4. 5 : Heat storage and flow into and out of an elemental control volume of wall and wick.

The remaining spatial derivative is determined using a first order central difference. Values of heat transfer between the wall and fluid are interpolated based on the representative values of adjacent grids.

4.2.5 Heat transfer equations

The heat flux from the wall to the fluid is:

$$q_{w-f} = h(T_w - T_f) \tag{4.9}$$

Where h is the heat transfer coefficient, having different expression whether the fluid is in the form of liquid slug of or vapor plug. The temperature difference is that between the wall and liquid saturation temperature. The boiling heat transfer coefficient is applied under certain conditions to heat transfer from the wall to the fluid, whether vapor or liquid. *Webb (1994)* reports a comparison in boiling heat flux for smooth and porous metal surfaces. The temperature difference required to produce a given heat flux is reduced by a factor of 10 for pool boiling of water on a porous rather than a smooth metal surface. To apply the data reported by Webb to a boiling heat transfer coefficient for the present model, a linear fit is computed from those data:

$$h_b = \left[213(T_w - T_f) - 80.4 \right] \cdot 10^3 \, W/m^2 K \tag{4.10}$$

The boiling heat transfer coefficient applies when it exceeds the evaporation or sensible heat transfer coefficients. Evaporation and condensation occur between the liquid layer in the wick and a vapor plug. The same heat transfer coefficient is used for both evaporation and condensation, and it is based on the thickness and conductivity of the wick as saturated with working fluid. Measurements of heat transfer coefficients for water undergoing complete condensation by *Begg et al. (2003)* indicated that the primary mode of heat transport was conduction through a liquid film on the tube wall for water in tube diameters consistent with the PHPs modeled here. In the current study, the presence of the wick will lead to an even thicker and slower moving liquid layer than the film in the condensation experiments. It is expected that modes of heat transfer other than conduction through the liquid layer will be negligible. The evaporation and condensation heat transfer coefficient through the liquid layer is:

$$h_{c,e} = k_{wk} / \delta_{wk} \tag{4.11}$$

The effective conductivity of the wick for various wick types can be found in *Faghri (1995).* For sensible heat transfer to laminar flow the Nusselt number is assumed a constant 4.36 for fully developed flow with constant heat flux. Under certain conditions Nusselt numbers vary from 3.66, for fully developed laminar flow with an isothermal wall, to over 40 for the hydrodynamic entrance region of a tube with constant heat flux. In the present study the temperature and velocity profiles in the fluid are unknown, so the assumption is made for fully developed laminar flow subject to constant heat flux. For sensible heat transfer to turbulent flow the roughness of the wick is taken into account. The Gnielinski correlation applies a friction factor that varies with roughness. The Colebrook correlation used in Eq. (4.5) provides the needed friction factor. Reynolds and Prandtl numbers are taken at local flow conditions along with the friction factor for the Gnielinski correlation:

$$Nu = \frac{(C/2)\cdot(\mathrm{Re}-10^3)\,\mathrm{Pr}}{1+12.7(C/2)^{1/2}\left(\mathrm{Pr}^{2/3}-1\right)} \tag{4.12}$$

Where C is the friction coefficient.

which is stated to hold for $0.5 < \mathrm{Pr} < 106$ and $2300 < \mathrm{Re} < 5\cdot 10^6$. For this study the Gnielinski correlation will be applied for $\mathrm{Re} \geq 2000$. The sensible heat transfer coefficient, along with conduction through the wick is analogous to the sum of two resistances in parallel:

$$h_s = \left[\frac{k_{wk}}{\delta_{wk}} + \frac{Nu\cdot d}{k_l}\right]^{-1} \tag{4.13}$$

4.3 Numerical Procedure

First, several design and computational parameters and operating and initial conditions are defined.

1. Design parameters:
   a. Channel: fill ratio, length, surface roughness feature size, and diameter as a function of length.

b. Wall: density, specific heat, thermal conductivity, thickness, wick thickness, wick thermal conductivity.

2. Computational parameters: maximum time step, minimum time step refinement factor, convergence criterion, trapezoidal integration length step, maximum allowable plug temperature change between time steps, and simulation time. In order to handle derivatives, the wall and each liquid slug are represented by one-dimensional computational grids. The grids for the liquid slugs are allowed to move. The number of grid nodes comprising wall and liquid are specified here as well.
3. Operating conditions: ambient temperature, condenser heat transfer coefficient, initial temperature, total heat input rate, and functions of length: evaporator, adiabatic and condenser locations and gravity angle.
4. The Nusselt number for laminar slug flow is set for the simulation.
5. Initial conditions:
   a. The liquid begins as one slug, and time, mass flow rate and pressure differentials on the slug are set to zero.
   b. The total internal volume of the heat pipe is calculated by trapezoidal integration. The length step Δz from Step 2 and N are iteratively increased until the condition below is satisfied.

$$V_t = \frac{\Delta z}{2}\sum_{n=1}^{N}\left\{A\left[(n-1)\Delta z + A(n)\Delta z\right]\right\}\frac{\Delta z_0}{2}\left[A(L-\Delta z_0)+A(L)\right] \tag{4.14}$$

   Such that $L = N\Delta z + \Delta z_0$ and $\Delta z_0 < \Delta z$

   c. The initial positions of the menisci are calculated by integration in the manner of Step b.

$z_b = 0 \quad z_f = N\Delta z + \Delta z_0$ Such that $\Delta z_0 < \Delta z$

$$\frac{\Delta z}{2}\sum_{n=1}^{N}\left\{A\left[(n-1)\Delta z + A(n)\Delta z\right]\right\}\frac{\Delta z_0}{2}\left[A(L-\Delta z_0)+A(L)\right] = \gamma V_t \tag{4.15}$$

   d. The mass of the slug is integrated using area as a function of length and liquid density as a function of temperature.

$$m = \frac{\Delta z}{2}\sum_{n=1}^{N}\left\{(\rho A)\left[z_b + (n-1)\Delta z\right] + (\rho A)(z_b + n\Delta z)\right\}\cdot$$
$$\cdot\frac{\Delta z_0}{2}\left[(\rho A)(z_f) + (\rho A)(z_f - \Delta z_0)\right] \tag{4.16}$$

   Such that $z_f - z_b = N\Delta z + \Delta z_0$ and $\Delta z_0 < \Delta z$

Several quantities are integrated in the following steps. For this purpose adaptive Simpson quadrature is applied. The integral is approximated to the n[th] iteration as:

$$\int_a^b f(z)\,dz \approx \frac{1}{3}F_n$$

$$F_n = \frac{1}{2}\left[F_{n-1} + \frac{2C_n - C_{n-1}}{2^{n-2}}\right],\ F_0 = f(a) + f(b),\ C_0 = 0, \qquad (4.17)$$

$$C_n = \sum_{k=1}^{2^{n-1}} f\left\langle a + \frac{(b-a)(2k-1)}{2^n}\right\rangle$$

The brackets $\langle\ \rangle$ denote a function that allows for circulation and is defined as:

$$\begin{cases} z < 0 \rightarrow \langle z\rangle = z + L \\ z > 0 \rightarrow \langle z\rangle = z - L \\ else \rightarrow \langle z\rangle = z \end{cases} \qquad (4.18)$$

The quadrature is iterated for increments of n, and when results from two subsequent iterations agree within the convergence criterion, the latter value is taken as the integral.

e. The evaporator heat flux is calculated based on the total heat input rate and combined evaporator section length:

$$q_e = Q_e\left[\int_0^L \begin{Bmatrix} 1(evaporator)\,p \\ 0(otherwise)\,p \end{Bmatrix} dz\right]^{-1} \qquad (4.19)$$

f. Locations of grid boundaries in the liquid slugs are determined. Slugs are represented by a number of equal mass increments. The rear boundary of the first mass increment in each slug is the back meniscus. The forward boundary is located using the secant method. The first two points for the secant method are $z' = z_b$ and $z' = \langle z_b - m'/n_s\rho A\rangle$ with $m' = \int_{z_b}^{z'} \rho A dz$. Subsequent values of z' are obtained using the secant method. The value of the forward boundary is taken when $\left[n_s m'(z') - m\right]/m$ satisfies the convergence criterion.

The representative location for each grid is taken as the midpoint between the grid boundaries. Density is evaluated at the temperature found by linearly interpolating adjacent grid values. Forward and backward extrapolation is used near the menisci where points do not lie between the representative locations of two adjacent grids. Area is a function of location as indicated in Step 1a. The location of the forward meniscus is set equal to the forward boundary of the last mass increment.

g. The volumes of the vapor plugs are calculated by $V_{p,i} = \int_{z_f,i-1}^{z_b,i} \rho A dz$

The time iteration loop begins here.

6. The time step refinement factor is determined. If a collision between adjacent slugs is anticipated before the next time step, the time step is reduced to synchronize the collision with the next time step, which serves to reduce overlap of the menisci.

$$C_{t,i} = \frac{\left\langle z_{b,i} - z_{f,i-1} \right\rangle}{\Delta t \left[\left. \frac{m}{(\rho A)_f} \right|_{i-1} - \left. \frac{m}{(\rho A)_b} \right|_i \right]} \tag{4.20}$$

7. The differential pressure due to gravity across each slug is determined as indicated in Equation (4.2).
8. The differential pressure across each slug due to shear is calculated per Equations (4.2) and (4.4).
9. The incremental change in mass flow rate is calculated using Equation (4.2) with the results of the previous three steps.
10. The displacements of the back menisci positions are calculated based on mass flow rate and time step by convergence of the following equation

$$\Delta z_i = \frac{\Delta t}{2} i \left(\frac{\dot{m} + \Delta \dot{m}}{\rho_l \left[T_l \left(z_{b,i} + \Delta z_i \right) A \left\langle z_{b,i} + \Delta z_i \right\rangle \right]} + \frac{\dot{m}}{\rho_l \left[T_l \left(z_{b,i} \right) A \left\langle z_{b,i} \right\rangle \right]} \right) \tag{4.21}$$

The initial estimate to the above equation is

$$\Delta z_i = \frac{\Delta t}{2}\left(\frac{\dot{m} + \Delta\dot{m}}{\rho_l \left[T_l\left(z_{b,i}\right) A\left\langle z_{b,i} \right\rangle \right]} \right) \tag{4.22}$$

The back meniscus position is updated as $z_{b,i} = \left\langle z_{b,i} + \Delta z_i \right\rangle$.

11. Slug grid boundaries and the front slug menisci are located as done in Step 4f.
12. Heat transfer from the wall to the fluid at each wall grid is determined using Equation (4.9).
13. The temperature for each wall grid is evaluated by integrating Equation (4.8) along the grid length. The remaining spatial derivative is determined using a first order central difference. Values of heat transfer between the wall and fluid are interpolated based on the representative values of adjacent grids.
14. The temperature of the vapor plugs is determined using Equation (4.7). Heat transfer values from the wall to fluid are interpolated. For the spatial temperature derivatives, forward and backward first order differences are used for conduction at the menisci. Since temperature is a function of other values on the left hand side of Equation (4.7), the equation is solved iteratively until the convergence criterion is satisfied. If the temperature change in a vapor plug from one time step to the next exceeds the allowable amount (set in Step 2), the time step refinement factor is divided by ten and the simulation proceeds from Step 6.
15. The temperatures of the grids in each liquid slug are determined by integrating Equation (4.6) along the length of each grid. For the conduction term backward, central or forward, first order differences are used based on whether the grid is a first, middle or last grid along the slug. Heat flux from the wall to the fluid is integrated with interpolated values.
16. The merging of liquid slugs is accounted for. If the spacing between any two adjacent menisci is zero, or if there is overlap, the two liquid slugs are combined and the number of liquid slugs is reduced by one. The mass flow rate for the combined slug is determined by summing the momenta.

$$\dot{m} = \frac{L_{i-1}\dot{m}_{i-1} - L_i\dot{m}_i}{L_{i-1} - L_i} \tag{4.23}$$

17. The formation of new vapor plugs has been taken into account only in terms of pure nucleation inside the liquid phase. The exact interaction between the wall and fluid in the boiling process has still to be implemented. By the time being:

    - The temperature of each liquid sub-volume is compared to the temperatures of the vapor plugs adjacent to the liquid slug.
    - The maximum grid boundary temperature is chosen as the location where a new vapor plug is formed if that temperature exceeds one or the other adjacent plug temperatures. The mass flow rate is the same for both segments of the slug.
    - The temperature of the plug is set to the fluid temperature at that location.

    The other criterion for locating the new vapor plugs is to compare the saturation pressure associated with the liquid slug grid boundary temperature to the pressure of the adjacent vapor bubble grid boundary.

$$\left[P_{sat}(T_l)\right]_{n_s} > \max\left[\left(P_{sat}(T_v) + \frac{2\sigma}{r}\right)_j ; \left(P_{sat}(T_v) + \frac{2\sigma}{r}\right)_{j+1}\right] \tag{4.24}$$

    If the above condition occurs, a new vapor plug will be created and, if there is sufficient vapor pressure in the plug, the plug will grow, otherwise it will collapse and the two adjacent liquid slugs will merge again in step 16.

18. Calculation resumes from Step 5 until the end time is reached.

4.4 Closure

Although a number of input parameters can be varied in order to simulate different CLPHP (external and internal tube diameter, evaporator and condenser length, filling ratio, inclination angle with respect to gravity, heat input at the evaporator, cooling medium heat transfer coefficient), the model by *Holley and Faghri (2005)* is still limited by the following major issues:

1. The model artifact to consider a thin capillary wick is not representative

of the usual PHP which usually has a smooth inner tube surface.

2. The heat transfer model was suitable for water only.
3. The model allows to investigate only PHP with a small number of turns.
4. The local pressure drops due to the presence of turns are not considered in the momentum equation for the liquid slug.
5. Only qualitative validation has been provided.

The following Chapter describes all the modifications which have been developed in order to solve the above issues.

Chapter 5

The new model for the simulation of the PHP thermohydraulic behavior

5.1 Introduction

The major weak points of the model by *Holley and Faghri (2005)*, summarized in the end of Chapter 4, have been faced as follows:

1. The model artifact to consider a thin capillary wick, which is not representative of the usual PHP has been eliminated.
2. The heat transfer model was completely rewritten and new working fluid libraries have been implemented.
3. A new subroutine for the automatic generation of the PHP geometry starting from the user inputs have been added in order to investigate PHPs with different number of turns.
4. The local pressure drops due to the presence of turns have been implemented in the momentum equation for the i-th liquid slug.

The present chapter describes how each single point has been treated and implemented in the theoretical and numerical model.

5.2 Structure modifications

In the original code the authors assume that the internal tube surface is covered by a thin porous wick and that the liquid film surrounding each vapor bubble is always filling the porous structure. Since most of the prototypes and the experimental apparati are built with smooth tubes without any wick (this is also the most attractive feature of the CLPHP with respect to the standard heat pipe) the wick is not considered in the present work and the energy equation for the wall (4.8) is simplified as follows:

$$c_{p,w}\rho_w A_w \frac{\partial T_w}{\partial t} = q_{ex}\, p_0 - q_{w-f}\, p + k_w A_w \frac{\partial^2 T_w}{\partial z^2} \qquad (5.1)$$

Even if the energy equation for the wall is simpler then the original, there is a new issue related to the liquid film. The liquid film thickness is no more fixed by the wick structure but must be evaluated. The procedure is descripted in paragraph 5.4.

5.3 Geometry modifications

In the base model the definition of the PHP geometry (i.e. the angle between flow direction and gravity direction, the evaporator, adiabatic and condenser tube portions along the whole tube length) had to be carried out point-to-point by the user. This can be easily done for a simple geometry such as a single closed loop PHP but it becomes too laborious when the number of turns increases. The code has been updated with a dedicated subroutine: a “comb geometry” CLPHP is automatically built as far as the following six parameters are set by the user (fig.3):

- L_{ev} = Evaporator section length.
- L_{co} = Condenser section length.
- L_{ad} = Adiabatic section length.
- L_1 = Characteristic distance between turn and bend.
- r_t = Radius of all bends and turns.
- N_t = Number of turns (180°).

This avoids time consuming operations and allows to perform numerical investigation on CLPHPs with a larger number of turns, rarely done by the models quoted in literature.

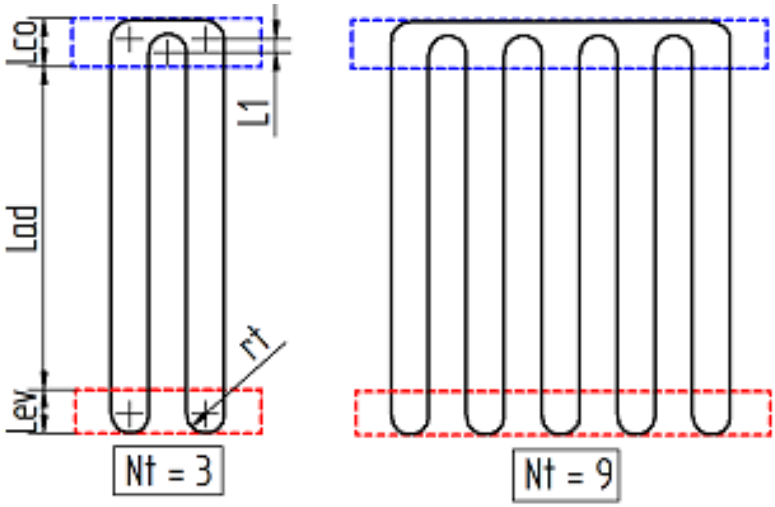

Figure 5. 1: CLPHP geometry input parameters: two cases with 3 and 9 turns, respectively.

Holley and Faghri (2005) investigated the single loop and a five turns geometry weather in the present work four different layouts have been tested: Nt = 3, 9, 39, and the single loop as well. Furthermore, the single loop and the PHP with 39 turns are set in order to simulate two real experimental devices as described in Chapter 6.

5.4 Different working fluids

A new subroutine allows the user to choose between seven different working fluids.

FLUID	Tmin [°C]	Tmax [°C]
Water	5	305
Ethanol	-18	202
FC-72 (C6F14)	2	152
R123	-73	167
Methanol	-53	197
R134a	-103	87
Ammonia	-53	107

Table 5. 1: List of the working fluids temperature limit

In particular, the following thermodynamic properties both for liquid and vapor in saturated conditions have been calculated for each fluid with the NIST REFPROP 8.0, *Lemmon et al. (2007)* in the temperature range specified in table 2: $C_{p,l}(T_{sat})$; $C_{p,v}(T_{sat})$; $H_l(T_{sat})$; $H_v(T_{sat})$; $k_l(T_{sat})$; $k_v(T_{sat})$; $\mu_l(T_{sat})$; $\mu_v(T_{sat})$; $P_{sat}(T_{sat})$; P_{cr}; $\rho_l(T_{sat})$; $\rho_v(T_{sat})$; $\sigma_l(T_{sat})$; $T_{sat}(P_{sat})$. A five degree polynomial fitting (eq. 5.1) have been performed in the PHP temperature range by means of a Matlab® code for every fluid property calculated above.

$$fp(T) = c_0 + c_1 T + c_2 T^2 + c_3 T^3 + c_4 T^4 + c_5 T^5 \tag{5.2}$$

where $fp(T)$ is the fluid property, T is the fluid temperature, c_j are the fitting coefficients (the Matlab® code outputs). One file containing the fitting coefficients is produced for each fluid. Finally, once the fluid name is set in the new subroutine of the present model, the program reads the fitting coefficients from the Matlab® output files and updates the general functions in the Fortran code devoted to the fluid properties calculation which have the same form of equation 5.1, but in this case T and c_j are the inputs.

5.5 Heat transfer modification

The heat transfer strategy adopted in the original code was deeply modified. The thin porous wick layer has been eliminated and the assumption of a liquid film trapped into the porous wick is no more valid. More general heat transfer correlations that can be applied to different working fluids have been added. Following, the assumptions regarding the liquid film thickness as well as the heat transfer computational procedure are described in more detail.

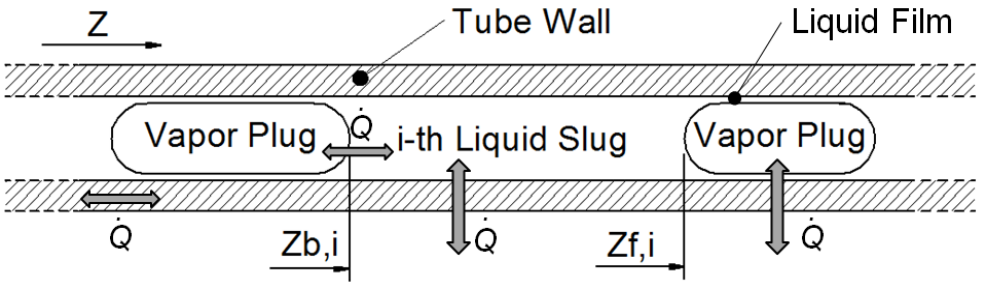

Figure 5. 2: Heat transfer modes in the novel model

Regarding the single phase, the laminar constant Nusselt (when $\mathrm{Re}_l \le 2000$) and Gnielinski correlation (when $\mathrm{Re}_l > 2000$) were implemented in the original code. Since the PHP local flow regimes are rarely stationary and furthermore the fluid is rarely approaching a thermally developed zone, the laminar correlation can be improved. In the present model the single phase heat transfer coefficients have been set as follows:

- When $\mathrm{Re}_l \le 2000$ the thermally developing laminar flow correlation by *Shah and London (1979)* has been implemented:

$$h_l = \begin{cases} \left(\frac{k_l}{d}\right)\cdot 1.953\cdot\left(\mathrm{Re}_l\,\mathrm{Pr}_l\,\frac{d}{L_x}\right)^{1/3} & \text{when } \left(\mathrm{Re}_l\,\mathrm{Pr}_l\,\frac{d}{L_x}\right)\ge 33.3 \\ \left(\frac{k_l}{d}\right)\left(4.364+0.0722\,\mathrm{Re}_l\,\mathrm{Pr}_l\,\frac{d}{L_x}\right) & \text{when } \left(\mathrm{Re}_l\,\mathrm{Pr}_l\,\frac{d}{L_x}\right)< 33.3 \end{cases} \tag{5.3}$$

  Where the developing length L_x is here equal to the evaporator/condenser tube length.

- When the flow is transient/turbolent ($2000 < \mathrm{Re}_l < 10000$) the Gnielinski correlation has been implemented:

$$h_l = \left(\frac{k_l}{d}\right)\left[\frac{(f/8)\left(\mathrm{Re}_l - 10^3\right)\mathrm{Pr}_l}{1+12.7(f/8)^{1/2}\left(\mathrm{Pr}_l^{2/3}-1\right)}\right] \tag{5.4}$$

  Where f is the friction coefficient calculated by the Colebrook correlation.

- When the flow is fully turbulent ($\mathrm{Re}_l \ge 10000$) the Dittus-Boelter correlation has been implemented:

$$h_l = \left(\frac{k_l}{d}\right)0.023\,\mathrm{Re}_l^{\,0.8}\,\mathrm{Pr}_l^{\,n} \tag{5.5}$$

  where n = 0.4 if $T_{wall} > T_{fluid}$ and n = 0.3 if $T_{wall} < T_{fluid}$.

With regard to the phase change heat transfer the original code implemented a linear fit of experimental data valid for water only (eq. 4.10). In the present work the more general correlation by *Gungor and Winterton (1987)* has been implemented:

$$h_b = h_l \left\{ 1 + 3000 Bo^{0.86} + \left[\frac{x}{1-x} \right]^{0.75} \left(\frac{\rho_l}{\rho_v} \right)^{0.41} \right\} \tag{5.6}$$

Where $Bo = \frac{q'' A_{cross}}{|\dot{m}| H_{lv}}$ is the boiling number, x the vapor mass quality of the heated zones and h_l is the single phase sensible heat transfer coefficient evaluated for the different flow regimes (Eqs. 5.3, 5.4, 5.5).

Furthermore the correlation for internal convective condensation by *Shah (1975)* has been added:

$$h_c = h_l \left[(1-x)^{0.8} + \frac{3.8 x^{0.76} (1-x)^{0.04}}{(P/P_{cr})} \right] \tag{5.7}$$

where x is the vapor mass quality of the cooled zones and again h_l is the single phase sensible heat transfer coefficient evaluated for the different flow regimes (Eqs. 5.3, 5.4, 5.5).

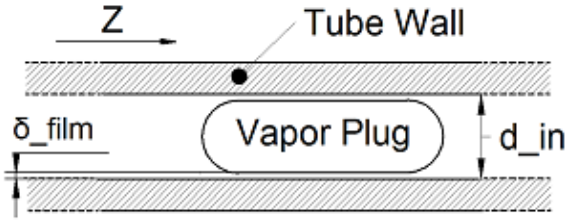

Figure 5. 3: Liquid film surrounding a vapor plug.

The strategy adopted for the heat transfer modeling is based on a *non homogeneous approach* where the liquid slugs and the vapor plugs are treated separately. In particular each vapor plug is considered as homogeneous two-phase flow where the liquid phase sorrounds the vapor phase in the form of a liquid film and each liquid slug is considered as completely liquid. Hence, although the liquid film is not considered in the hydrodynamics of the model (a vapor plug is treated as an ideal gas control volume), the presence of a liquid film sorrounding the vapor plug is considered in the heat transfer procedure. Assuming that no dry-outs occur, slug flow regime is always present and that the liquid film thickness is constant along the vapor plug (fig.4), the vapor mass quality x_{vp} can be

evaluated as a function of the liquid film thickness δ_{film} and the local fluid saturated temperature T_{sat} as follows:

$$x_{vp} = \frac{m_v}{m_t} = \frac{V_v \rho_v (T_{sat})}{V_v \rho_v (T_{sat}) + V_l \rho_l (T_{sat})} = \\ = \frac{\left(\frac{d}{2} - \delta_{film}\right)^2 \rho_v (T_{sat})}{\left[\left(\frac{d}{2} - \delta_{film}\right)^2 \rho_v (T_{sat})\right] + \left\{\left(\frac{d}{2}\right)^2 - \left[\left(\frac{d}{2} - \delta_{film}\right)^2\right] \rho_l (T_{sat})\right\}} \tag{5.8}$$

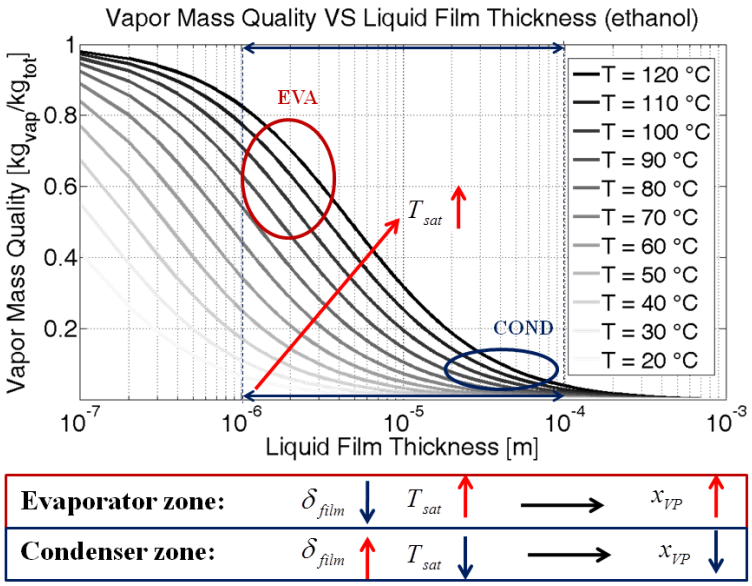

Figure 5. 4: Vapor mass quality against liquid film thickness for ethanol at different temperatures.

Figure 5.4 shows the vapor mass quality (Eq. 5.8) for ethanol at different saturated temperatures. Regarding the liquid film thickness, the last available measurements by *Han et al (2009)* for a 1.305mm internal diameter tube working with air and ethanol in adiabatic conditions show that the valid range for δ_{film} is between 1 and 100 μm. In the evaporator zone the liquid film thickness il smaller weather the fluid temperature is higher so it is reasonable that $x_{vp,ev}$ lies in a higher range. A vapor plug travelling the condenser has a higher liquid film thickness at lower temperatures thus $x_{vp,co}$ should be lower as shown in Figure 5.4 .

$q''\left[\frac{W}{cm^2}\right]$	4				8				12				16			
$T_{sat}[°C]$	*min*		*max*		*min*		*Max*		*min*		*max*		*min*		*max*	
	23		55		34		70		54		87		76		117	
$x_{vp}\left[\frac{kg_{vap}}{kg_{tot}}\right]$ **Range**	*min*	*max*	*min*	*max*	*min*	*max*	*min*	*max*	*min*	*max*	*min*	*max*	*min*	*max*	*min*	*max*
	0.0007	0.0772	0.0036	0.2960	0.0013	0.1320	0.0065	0.4343	0.0034	0.2867	0.0130	0.6074	0.0083	0.4944	0.0355	0.8116
$x_{vp}\left[\frac{kg_{vap}}{kg_{tot}}\right]$ **Chosen value**	*cond*		*eva*		*cond*		*eva*		*cond*		*eva*		*cond*		*eva*	
	0.001		**0.01**		**0.01**		**0.1**		**0.1**		**0.5**		**0.4**		**0.8**	

Table 5. 2: Heat input fluxes, fluid working temperature ranges (from previous numerical investigations), vapor mass quality ranges and vapor mass quality values (bold) chosen for the numerical simulation.

In order to set punctual values for $x_{vp,ev}$ and $x_{vp,co}$, at different heat input levels (this also means different saturated temperatures ranges), the model has been set in order to simulate the experimental data by *Khandekar et al. (2004)*. Different simulations has been performed tuning the values of the vapor mass quality with the aim of reproducing the experimental data. The chosen values at each heat input are shown in table 5.2. For sake of clarity let's analyze a single case: at each heat input level the extrapolated values for the average fluid temperature in the evaporator and condenser are $T_{sat,\max}$ and $T_{sat,\min}$; these temperature values together with the liquid film thickness range by Han et al are fed into Eq. 5.8 and the plausible ranges for $x_{vp,\max}(T_{sat})$ and $x_{vp,\min}(T_{sat})$ are evaluated. The punctual values of $x_{vp,ev}$ and $x_{vp,co}$ are chosen inside these ranges in order that the numerical results compare reasonably well with the experimental data. The computational procedure for the calculation of different heat transfer coefficients (HTC) is set as follows.

In case of Liquid Slug:

- if $T_{wall} > T_{fluid}$ the liquid slug is supposed to be in the incipient boiling condition. So the subroutine sets the boiling HTC (Eq. 5.6) with $x_{vp} = 0$.
- if $T_{wall} < T_{fluid}$ the liquid slug is simply cooled by mean of sensible heat transfer mode and the subroutine sets the single phase liquid heat transfer coefficients (Eqs. 5.3, 5.4, 5.5).

In case of Vapor Plug:

- if $T_{wall} > T_{fluid}$ the subroutine sets the boiling HTC (Eq.5.6) with values of $x_{vp,ev}$ from table 1.
- if $T_{wall} < T_{fluid}$ liquid film is condensing, thus the subroutine sets condensation HTC (Eq. 5.7) with lower values of $x_{vp,co}$ from table 5.2.

5.6 Pressure losses due to bends and turns

In the previous theoretical models the effects of bends and turns have been taken into account only in terms of change of the flow direction with respect to gravity and in terms of the alternation of hot and cold zones but the local pressure losses related to the bends and turns have always been

neglected. Experimental investigations on a CLPHP working in the horizontal position by *Charoensawan and Terdtoon (2008)* showed that, if the number of turns is less than a critical number, there is no fluid motion. The fact that a device with a big number of turns works in the horizontal position is than indictable to the bigger alternation of hot and cold zones but also to the presence of local pressure losses. For this reason the effect of local pressure losses should be considered and one of the main novelties of the present numerical model is that a proper pressure drop term ΔP_K has been added in the momentum equation for the i-th liquid slug. When the channel cross section is constant the momentum equation (4.2) defined in chapter 4 is furthermore simplified and, after integrating along the liquid slug length, it results in:

$$\left[\frac{d\dot{m}_l}{dt} = A_{cr} \left(\Delta P_g - \Delta P_v + \Delta P_\tau + \Delta P_K \right) \right]_i \tag{5.9}$$

The different pressure terms on the right hand side are respectively due to:

Gravity force

$$\Delta P_g = \rho_l g \cos\theta \tag{5.10}$$

where theta is the angle between the gravity vector and the flow direction.

Adjacent vapour plugs expansion/compression

$$\Delta P_v = \left[P_{sat}\left(T_v\right) \right]_{j+1} - \left[P_{sat}\left(T_v\right) \right]_j \Big/ L_l \tag{5.11}$$

where L_l is the length of each liquid slug.

Viscous shear

$$\Delta P_\tau = \frac{f}{2d} \rho_l u_l^{\,2} \tag{5.12}$$

where the friction coefficient is evaluated for the laminar and turbulent regimes by means of the Colebrook equation:

$$f = 64 / \mathrm{Re}_l \quad \text{when} \quad \mathrm{Re}_l < 2000 \tag{5.13}$$

$$\frac{1}{\sqrt{f}} = 1.74 - 2\log_{10}\left(\frac{2\varepsilon}{d} + \frac{18.6}{\mathrm{Re}_l\sqrt{f}}\right) \quad \text{when} \quad \mathrm{Re}_l \geq 2000$$

Where $\mathrm{Re}_l = \rho_l u_l d/\mu_l$ is the Reynolds number related to each liquid slug.

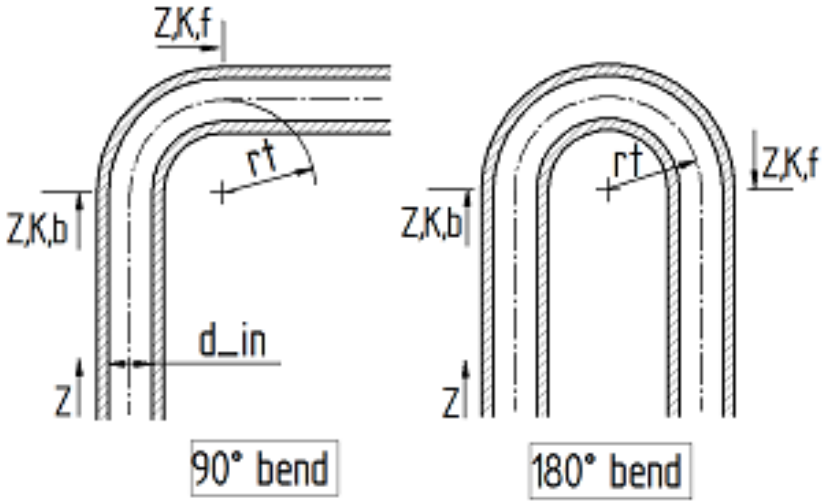

Figure 5. 5: Geometry of 90° bend and 180° turn in the CLPHP.

Local pressure drop due to the presence of bends and turns

$$\Delta P_K = \sum_{k=1}^{N_t} \frac{K_k}{2d} \rho_l u_l^{\,2} \tag{5.14}$$

and K_k is the loss coefficient due to the k-th turn according to *Darby (1999,2001):*

$$K_k = \frac{K_{\mathrm{Re}}}{\mathrm{Re}_l} + K_r\left(1 + \frac{K_d}{(d/0.0254)^{0.3}}\right) \tag{5.15}$$

This empirical correlation depends on three main parameters ($K_{\mathrm{Re}}, K_r, K_d$), on the Reynolds number and on the exact geometry of the bend. This term is non-zero only if the i-th liquid slug is passing in between the turn boundaries $\left\lfloor Z_{K,b}; Z_{K,f} \right\rfloor_k$ (fig.5.5). The values adopted for the three parameters in case of 90° bend and 180° are listed in the bend-type table below.

Fitting type	r_t/d_{in}	K_{Re}	K_r	K_d
bend 90°	1.25	800	0.091	4
Turn 180°	1.25	1000	0.1	4

Table 5. 3: 3-K constants for loss coefficients for bends and turns according to *Darby (1999,2001).*

The 3-K method considers that the flow regime may be variable: K_j is indeed unaffected by Reynolds number when $\mathrm{Re} >> K_{\mathrm{Re}}$ (turbulent flow), however K_j grows as soon as $\mathrm{Re} < K_{\mathrm{Re}}$ and this is a fundamental issue since the flow inside the PHP is often laminar. The K_r constant is linked to the fitting curvature ratio r_t/d_{in} and the fitting type: small curves are more sensitive to the surface roughness thus K_j is greater for smaller bends of a given type. Furthermore the $d_{in}/0.0254$ correction accounts for the size differences: K_j is higher for small diameters and nearly constant for large sizes. The bends and turns lengths are discretized: if one liquid slug is partially occupying one curve, it consequently undergoes a lower pressure drop. Finally the summation on the *j* curves indicates that a single liquid slug can be passing through more than one bend/turn in the same time.

Next Chapter shows the numerical investigation campaign and both qualitative and quantitative validation of the numerical results are provided by direct comparison with experimental data available in literature as well as self-produced (see Chapters 7 and 8).

Chapter 6

Numerical investigations

6.1 Introduction

The main objective of the numerical simulation campaign is to provide a qualitative and quantitative validation to the model presented in the previous chapter. The present chapter has been subdivided depending on the PHP different geometries and on the tested parameters as follows:

- Effects of different liquid properties on a simple geometry.
- Effects of the local pressure losses due to meanderings combined with the effect of having different working fluids and different number of turns.
- Effect of orientation and gravity.
- Simulation of a multi-turn PHP.

6.2 Effects of different liquid properties on a simple geometry

A Closed Loop Pulsating Heat Pipe (CLPHP) is characterized by a strong thermo-hydrodynamic coupling governing its thermal performance. To better understand its operational characteristics, *Khandekar (2004)* built a two-phase loop with a copper capillary tube (ID = 2.0 mm) having no internal wick structure. The loop (Figure 6.1) is heated at one end and cooled at the other and partially made up of glass in the adiabatic zone to assist visualization. The working fluid employed is ethanol.

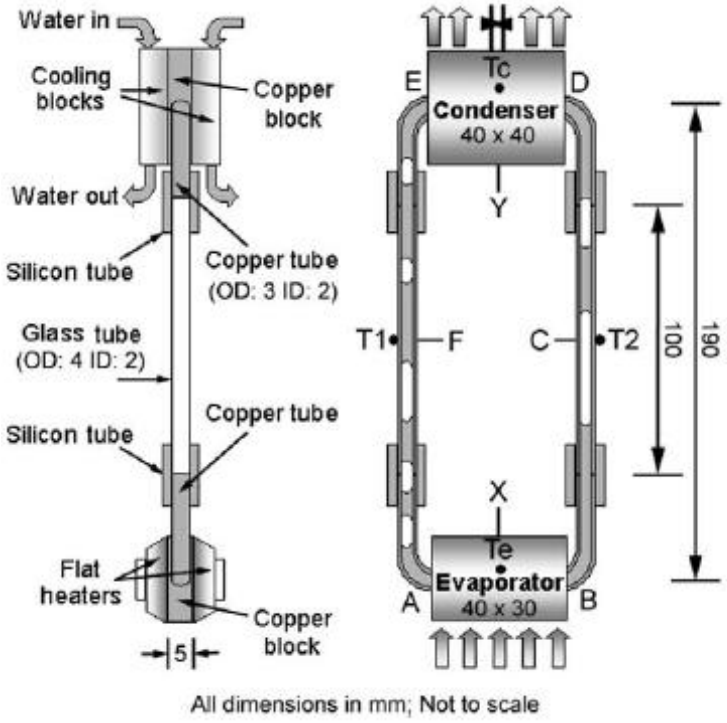

Figure 6. 1: Scheme of the single closed loop PHP test cell built by *Khandekar (2004).*

The code input parameters (geometry, initial conditions, boundary conditions and computational parameters) are set in order to simulate the thermal-hydraulic behavior of the single closed loop PHP experimental test-rig shown above. Note that the parameters listed below (Table 6.1) have been used also for the evaluation of the vapor mass quality in Chapter 5.

INPUT PARAMETER	VALUE
Tube thermal conductivity	400 [W/mK]
Tube specific heat capacity	389 [J/kgK]
Tube density	8960 [kg/m^3]
Internal tube diameter	2 [mm]
external tube diameter	3 [mm]
Inner surface roughness	5 [μm]
Evaporator section length	40 [mm]
Condenser section length	40 [mm]
Adiabatic section length	190 [mm]
filling ratio	0.6 [-]
External cooling temperature	20 [°C]
Initial temperature (fluid and tube)	30 [°C]
Initial number of Liquid Slugs and Vapour Plugs	6 [-]
Heat inputs	14.8, 32.1, 44.2 [W]
Computational time step	0.0001 [s]
Number of grids for the wall domain	460 [-]
Number of grids for the liquid domain	225 [-]
Convergence criterion	0.001 [-]

Table 6. 1: Code input parameters.

Khandekar (2004) investigates the effect of increasing the heat input rate on the hydrodynamics and the heat transfer capability of a single closed loop PHP in vertical position (condenser above the evaporator). In particular he observes the fluid motion and flow pattern through the transparent adiabatic zone and measures the temperature trends in the evaporator and adiabatic section by mean of thermocouples. An increase of the heat input rate leads to increase the amplitude of flow oscillation (Case A, B); than a net circulation of the fluid is more evident as well as flow reversals (Case C); Increasing again the heat rate input leads to a transition of the flow pattern from complete slug flow to annular flow (Case D and E). In such final conditions, liquid and vapor are separated and the device operates more likely a thermosyphon than a PHP.

Figure 6. 2: An Insight into thermo-hydrodynamic coupling inside a losed loop PHP, *Khandekar (2004)*

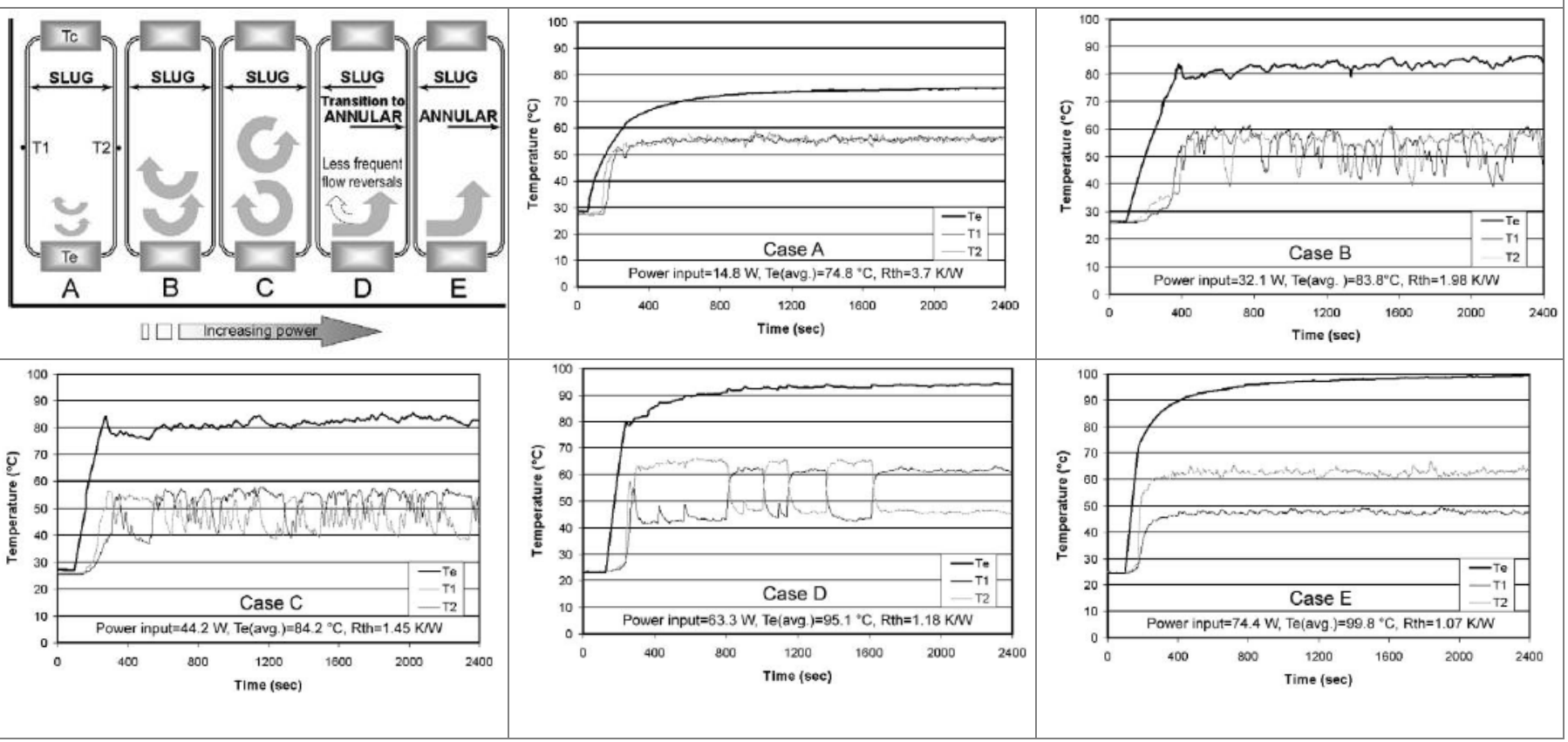

Figure 6. 3: Numerical results: temporal trend of the maximum tube temperature.

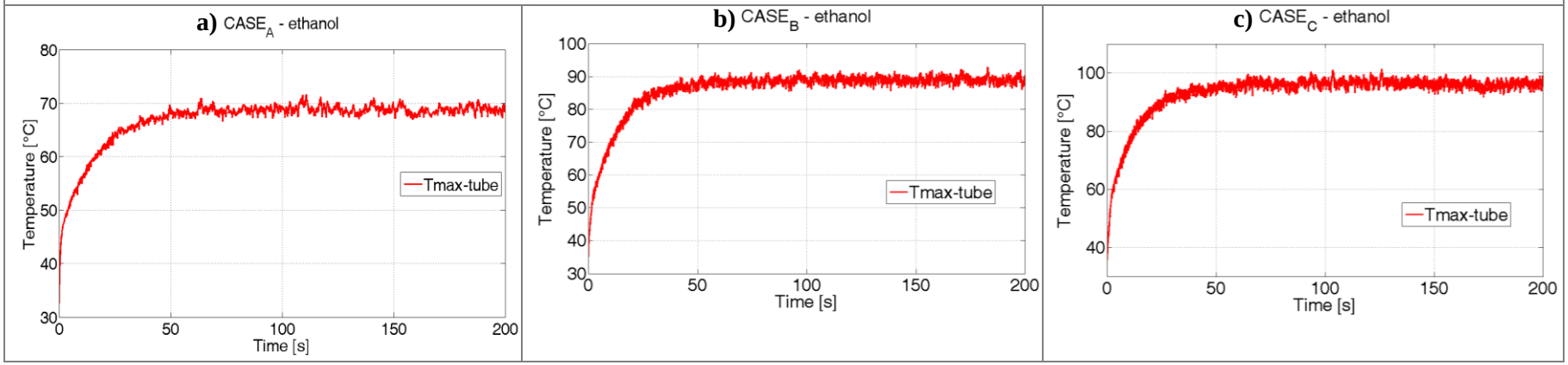

Figure 6. 4: Numerical results: temporal trend of the total liquid momentum.

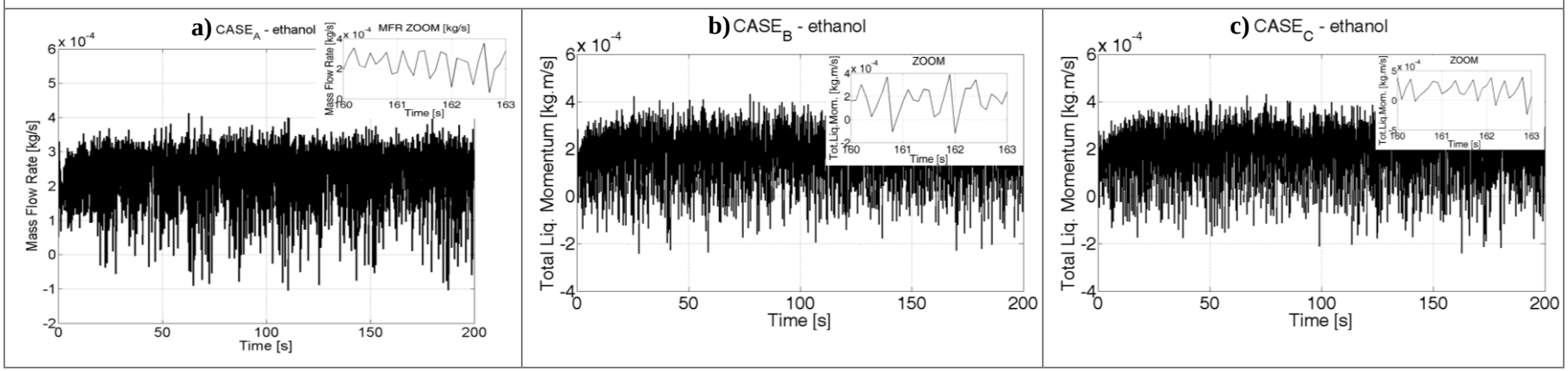

Cases A, B and C are simulated with the numerical code, while cases D and E are not: in these last two cases slug flow regime is no more present and all the liquid phase lies in one of the two vertical branches while the vapor phase lies in the other.

The code output parameters are chosen depending on their criticality and the possibility of matching with experimental measurements. For the single test cases the temporal trend of the maximum tube temperature $T_{w,\max}$ and the total momentum of the liquid phase $M_{l,tot}$ are plotted over time. $T_{w,\max}$ is easy to be measured and must be monitored since the evaporator zone is usually in contact with components that should work under a threshold temperature. On the other hand for $M_{l,tot}$ it is more difficult to find reliable experimental data, but it gives important information about the flow field inside the device: oscillation, circulation, reversals and eventual stops, and it is a common variable for comparison with other numerical simulations. The previous two parameters were also used to obtain three other representative quantities:

- when a pseudo-steady state has reached (after a transient period, the average component of the wall temperature settles to a constant value even if oscillations around such mean value is still present), $T_{w,\max}$ was averaged in time obtaining the mean maximum wall temperature $\overline{T}_{w,\max}$;
- the overall equivalent thermal resistance have been calculated:

$$R_{eq} = \left(\overline{T}_{w,\max} - \overline{T}_{w,\min}\right) / \dot{Q}_t \qquad (6.1)$$

  where $\overline{T}_{w,\min}$ is the average of the minimum tube wall temperature in the cooling section.
- a Fast Fourier Transform (FFT) has been performed on the total momentum in order to obtain the dominant frequency of the fluid oscillations.

The end time is set to 200s for every simulation, since all cases shows a transient of about 60 seconds. The longer transient period of about 600 seconds reported in the experimental results (Figure 6.2) is due to the thermal inertia of the heating section elements (i.e. heaters, copper block and thermal insulation) which are not included in the numerical model. Nevertheless the average value of the evaporator temperature in pseudo-steady state regime

extrapolated from the numerical results compares quite well with the data measured by Khandekar as shown in table 6.2.

	$\bar{T}_{w,\max}$ (exp.)	$\bar{T}_{w,\max}$ (num.)	Error
CASE A (14.8W)	74.8 °C	68.9 °C	-7.8%
CASE B (32.1W)	83.8 °C	88.9 °C	6.2%
CASE A (44.2W)	84.2 °C	96.5 °C	14.7%

Table 6. 2: Mean maximum tube temperature percentage difference between Khandekar's measurements and the simulations output values.

Case C represents the transitory situation between slug and annular flow regimes and it is also the limit case for the presented numerical model where the slug flow regime is assumed a priori. This fact also explains the higher error percentage between experimental data and numerical results for Case C. In one of his most recent works on the single closed loop PHP *(Khandekar et al. 2009)* analyze the spectral content of quasi-steady state pressure signals. They conclude that the dominant frequencies of flow oscillations are in the range of 0.1 to 3.0Hz. For this reason the FFT analysis with a sample frequency of 20Hz is performed on the numerical results concerning the total liquid momentum (Figure 6.3, below) which is directly connected with the fluid pressure variation in time. Table 6.3 shows that the dominant frequencies for the three simulated cases with ethanol are within this range.

	dominant frequencies [Hz]
CASE A (14.8W)	2.54
CASE B (32.1W)	2.30
CASE A (44.2W)	2.24

Table 6. 3: Dominant frequencies of total liquid momentum oscillation for the three simulated cases with ethanol.

Finally, in his experimental work, Khandekar also concluded that, as soon as the slug flow regime is maintained, the internal thermo-fluidics observed in a two-phase single loop is also observed in a multi-turn CLPHP. For this reason the present numerical model, which is able to simulate the thermo-fluid characteristics of a single loop closed PHP, is undoubtedly the first validated step for the creation of a multi-turn CLPHP design tool.

The model input parameters are then fixed on the basis of the good results obtained with ethanol and the same simulations are performed different

working fluids: methanol, FC-72 and R123. Temperature trends and total liquid momentum oscillations obtained when simulating with the other fluids are similar to those obtained with ethanol, thus the results for the different fluids are resumed in two plots: Figure 6.5 shows the mean maximum tube temperature in quasi-steady state conditions at different heat inputs and Figure 6.6 shows the PHP equivalent thermal resistance.

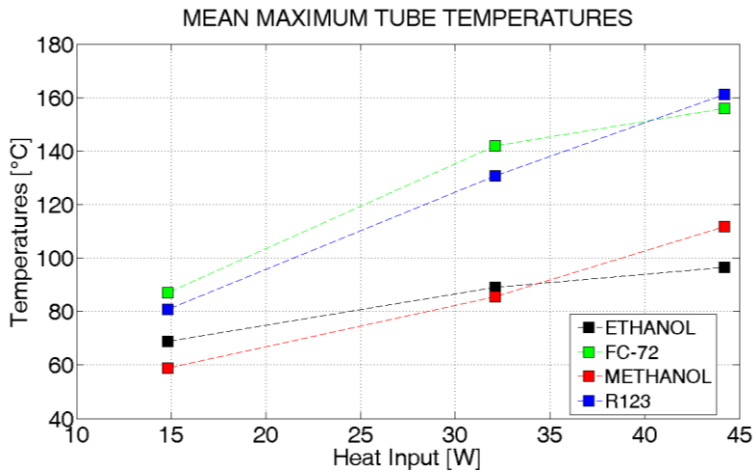

Figure 6. 5: Numerical results: mean maximum tube temperatures in steady state conditions.

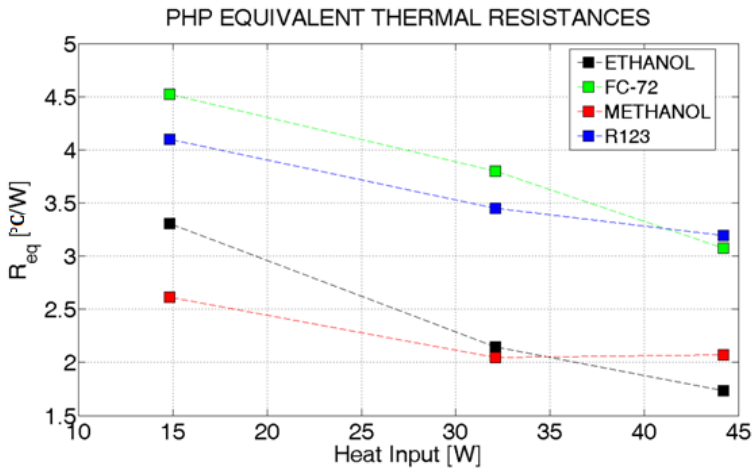

Figure 6. 6: Numerical results: mean equivalent thermal resistances in steady state conditions.

In general the equivalent thermal resistance diminishes when the heat input is increased but it is evident from Figure 6.6 that the thermal performance is reaching an asymptotic threshold. From this point over, the

PHP begins to work more likely as a thermosyphon and its performance is no more enhanced by the heat input increase. A high mean maximum tube temperature in the evaporator is of course not desirable and from figure 6.5 it seems that the refrigerants fluids (FC-72 and R123) are working worse than alcohols. Actually in this temperature range alchools are favoured by their lower density, higher thermal conductivity, specific heat and surface tension (see table 7). It is very likely that a low temperature application would be more suitable for FC-72 and R123.

FLUID	ρ_l	$c_{p,l}$	h_{lv}	k_l	μ_l	σ_l
ethanol	783,82	2596,7	919700	0,16469	0,00104	0,02154
methanol	784,51	2546,1	1166200	0,20018	0,00052	0,02210
FC-72	1687,6	1049,7	92096	0,057737	0,00064	0,01091
R123	1459,1	1021,9	170600	0,075902	0,00040	0,01495

Table 6. 4: Saturated liquid properties evaluated at T = 27 °C.

6.2.1 Closure

The single two-phase loop which is the basic constitutive element of a multi-turn CLPHP *(Khandekar, 2004)* has been simulated and the following conclusions can be deduced:

- The error percentage on the mean evaporator maximum temperature between numerical results and the experimental data are within the 15% despite the lack of information both about the liquid film thickness which surrounds the vapour plugs in the different zones of the PHP.
- The FFT analysis which has been performed on the numerical results related to total liquid momentum, which is directly connected with the fluid pressure variation in time, confirms that the dominant frequencies of flow oscillations are in the range of 0.1 to 3.0Hz.
- The same PHP geometry and working conditions have been simulated for methanol, FC-72 and R123 and the model shows satisfactory qualitative results both for the thermal and for the dynamic behavior.
- The present numerical model can be adapted to perform simulations also on multi-turn CLPHP which are proved to be an attractive solution for many industrial thermal management issues.

6.3 Effects of the local pressure losses due to meanderings combined with the effect of having different working fluids and different number of turns

A comparative study is performed on two PHPs with three and nine U-turns, Table 6.5 resumes the code input parameters.

INPUT PARAMETER	3 turns	9 turns
Working fluids	Ethanol, FC-72, R123	
Tube material	copper	
Internal tube diameter, $d_{in}[mm]$	2	
external tube diameter, $d_{out}[mm]$	3	
Inner surface roughness, $r_{fs}[\mu m]$	50	
Curvature radius of all bends and turns, $r_t[mm]$	2.5	
Adiabatic section length, $L_{ad}[mm]$	102	
Evaporator section length, $L_{ev}[mm]$	8.5	
Condenser section length, $L_{co}[mm]$	8.5	
Total length, $L_{tot}[mm]$	440	1100
Evaporator heat exchange area, $A_{rad,ev}[cm^2]$	2.49	6.23
Initial temperature $T_0[°C]$	30	
Filling ratio, $\gamma[-]$	0.6	
Tilting angle with respect to gravity direction, [deg]	0 (BHM); 90 (horizontal)	
Ext. heat transfer coefficient $h_\infty[W/m^2K]$	*(constant temperature boundary condition)*	
External cooling temperature, $T_\infty[°C]$	20	
Losses due to the presence of bends, ΔP_K	OFF	ON
Total heat input, $\dot{Q}_{ev}[W]$	10; 20; 30; 40	25; 50; 75; 100
Maximum computational time step, [s]	$1x10^{-4}$	
Minimum time step refinement factor, [s]	$1x10^{-6}$	
Number of grids for the wall domain, [-]	440	1100
Number of grids for the liquid domain, [-]	225	
Convergence criterion on integration methods (Simpson, trapezoidal, secant) [-]	$1x10^{-3}$	

Table 6. 5: Code input parameters.

According to figure 6.7 the input heat flux $q''\left[W/cm^2\right]$ can be calculated as follows for each geometry:

$$q''=\frac{\dot{Q}_{ev}}{A_{rad,ev}} \text{ where } A_{rad,ev}=\left(\pi r_t+2L_2\right)*\pi d_i \tag{6.1}$$

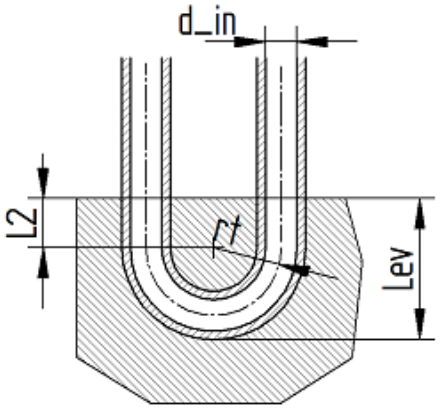

Figure 6. 7: Detail of a turn dipped into the evaporator zone: calculation of the radial heat flux input.

The effect on the PHP thermal performance of several parameters is investigated: accounting for the local pressure losses (ΔP_K"*ON*") and neglecting them *(*ΔP_K"*OFF*"*)*. The PHPs are operated with three different working fluids, namely ethanol, FC-72, R123, and four different heat input levels. In order to investigate also the combined effect of local pressure drops on the PHP orientation, two inclination angles are considered: 0° when the PHP lies in the horizontal position (Horizontal H); 90° when the PHP is in vertical position and the evaporator is located below the condenser (Bottom Heat Mode BHM).

6.3.1 Effect of the local pressure losses

In order to appreciate the effect of local pressure losses on a wide range of test cases, the three representative quantities (Frequency**,** $\overline{T}_{w,\max}$ and R_{eq}) are plotted over the input heat flux, for three different fluids: ethanol in black, FC-72 in green and R123 in blue. The sequence above (Figures 6.8 a, b, c) shows the behavior of the CLPHP with three turns in bottom heat mode while the sequence below (Figures 6.9 a, b, c), shows the CLPHP with 9 turns.

Figure 6. 8: Numerical results for the PHP with **three** turns in bottom heat mode. a) Dominant oscillation frequencies; b) Mean maximum temperatures; c) Equivalent thermal resistances.

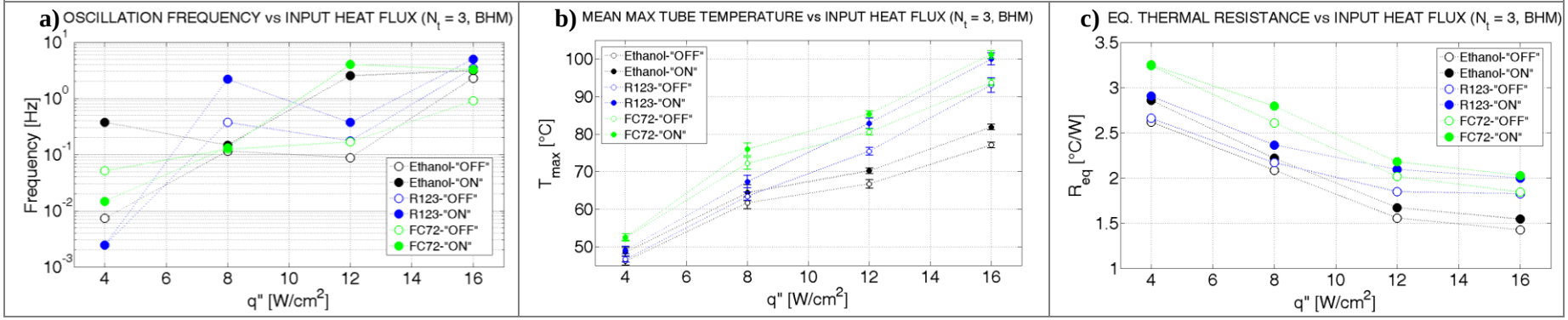

Figure 6. 9: Numerical results for the PHP with **nine** turns in bottom heat mode. a) Dominant oscillation frequencies; b) Mean maximum temperatures; c) Equivalent thermal resistances.

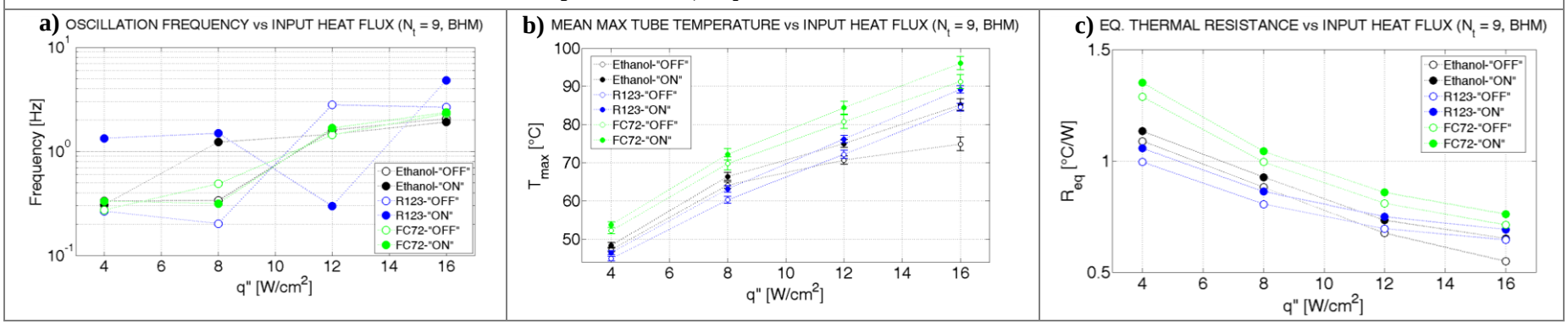

It is clear that the local pressure losses have a non negligible effect both on the hydrodynamic and thermal performance of the CLPHP. When the fluid is travelling through bends and turns undergoes a local deceleration which causes a decrease of the local convective heat transfer. A less efficient heat transfer between fluid and tube wall leads to an increase of the mean maximum temperatures (Figures 6.8b, 6.9b). The equivalent thermal resistance is always underestimated if the model disregards the local pressure losses (Figures 6.8c, 6.9c) and the effect is more evident for higher heat fluxes.

The momentum damping caused by the local pressure drops has also an influence on the dominant oscillation frequencies of the total momentum, even if a general trend cannot be found (Figure 6.8a). This leads to conclude that an increase or decrease of the local fluctuation frequency (not the amplitude) in the flow motion is not directly linked to the CLPHP thermal performances. The same effects are appreciable on the CLPHP with nine turns in bottom heat mode as shown in Figure 6.9a.

Chareonsawan and Terdtoon (2008) esperimentally demonstrate that a CLPHP in the horizontal position does not work if the number of turns is less than a critical number (i.e. $N_t = 5$). All the numerical test cases with three turns in the horizontal position, both losses "ON" and "OFF", are not working as predicted by experiments. The fluid flow inside the CLPHP damps out and completely stops after 100 seconds (fig. 6.10a).

Actually, if the number of turns is too small, there is a minor alternation of hot and cold zones and a minor presence of local pressure drops, so it is easier for the liquid slugs to merge and form bigger ones that are not evenly distributed along the tube length. In this junction vapor expansion may not be sufficient to push the adjacent liquid slugs and all the vapor plugs merge in the evaporator zone and all the liquid recoils in the condenser zone, no new liquid slugs are generated, the fluid motion stops and the device works only by conduction within the copper tube and the maximum tube temperature consequently rises towards higher values (fig. 6.10b).

An interesting result comes from the CLPHP with nine turns: both "ON" and "OFF" test cases works in the horizontal position till $q'' = 12\left[W/cm^2\right]$ but when input heat flux is set to $q'' = 16\left[W/cm^2\right]$ the flow motion stops if losses are neglected while the model with $\Delta P_K "ON"$ is still working as shown in Figures 6.10c and 6.11c.

Figure 6. 10: Numerical results: temporal trend of the maximum tube temperature.

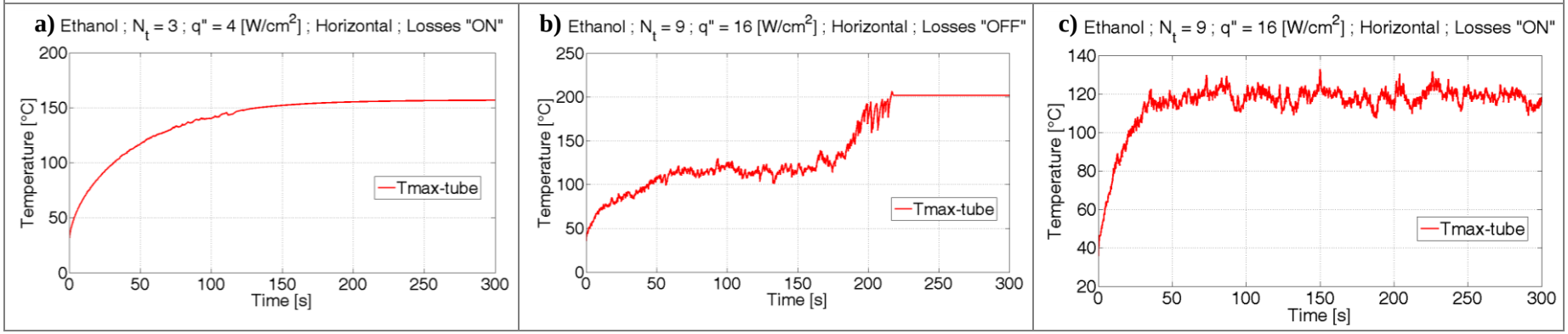

Figure 6. 11: Numerical results: temporal trend of the total liquid momentum.

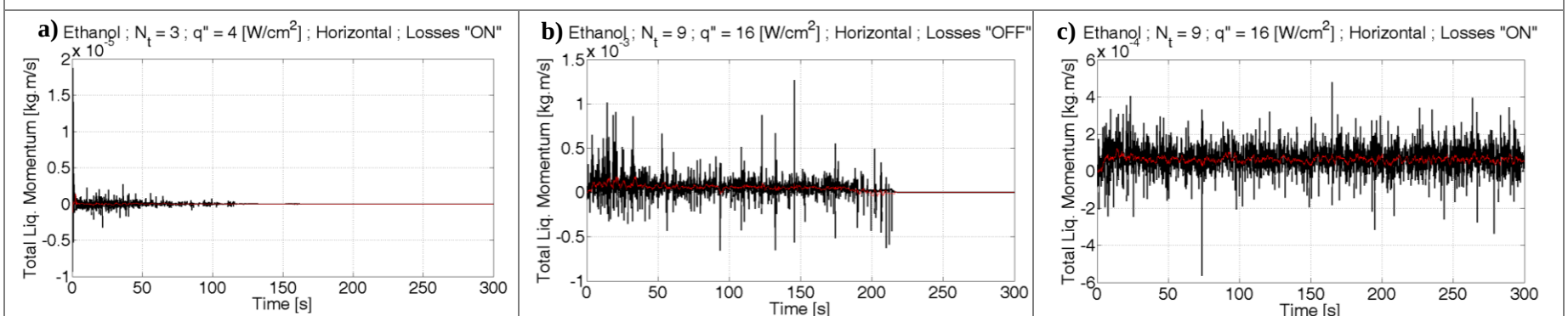

At higher heat inputs the vapor phase has a stronger tendency to accumulate in the evaporator zone and the liquid phase has a stronger tendency to recoil in the condenser zone increasing the probability of dry-outs and stop of the fluid motion. Hence the presence of local pressure losses (whose effect is also stronger at high input heat fluxes) leads on one hand to a worst heat transfer efficiency but on the other hand to avoid the phase accumulation and to work in a wider range of conditions.

6.3.2 Effect of the number of turns

Nine turns CLPHP has many advantages with respect to the one with three turns:

- It is able to work also in the horizontal heat mode.
- Its thermal resistance is lower.
- Performance is slightly less affected by the heat input level.
- There overall efficiency is less influenced by the fluid.

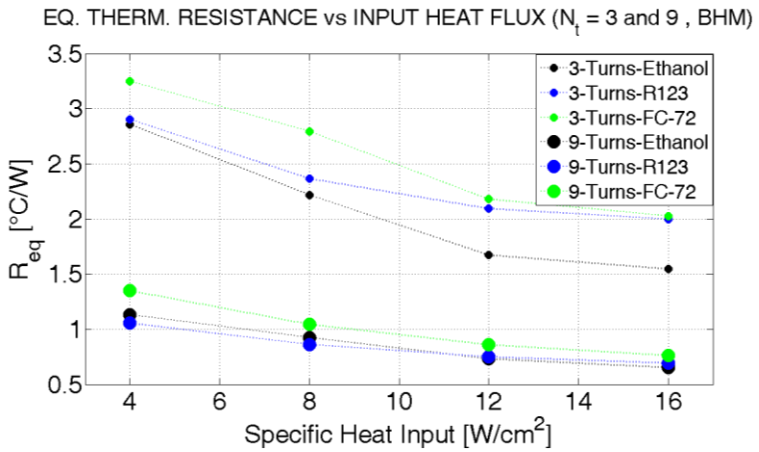

Figure 6. 12: Equivalent Thermal Resistence VS Specific heat input for the 3 and 9 turns CLPHP in Bottom heat Mode considering local pressure losses.

These positive characteristics are due to the chaotic flow motion and the more homogeneous distribution of the two phases within the device. On the other hand when the number of turns is smaller the liquid slugs oscillates but in the meanwhile they all follow the same direction so the liquid phase may easily undergo circulation and flow reversals (Figures 6.13b, 6.14b).

Figure 6. 13: Numerical results: temporal trend of the maximum tube temperature.

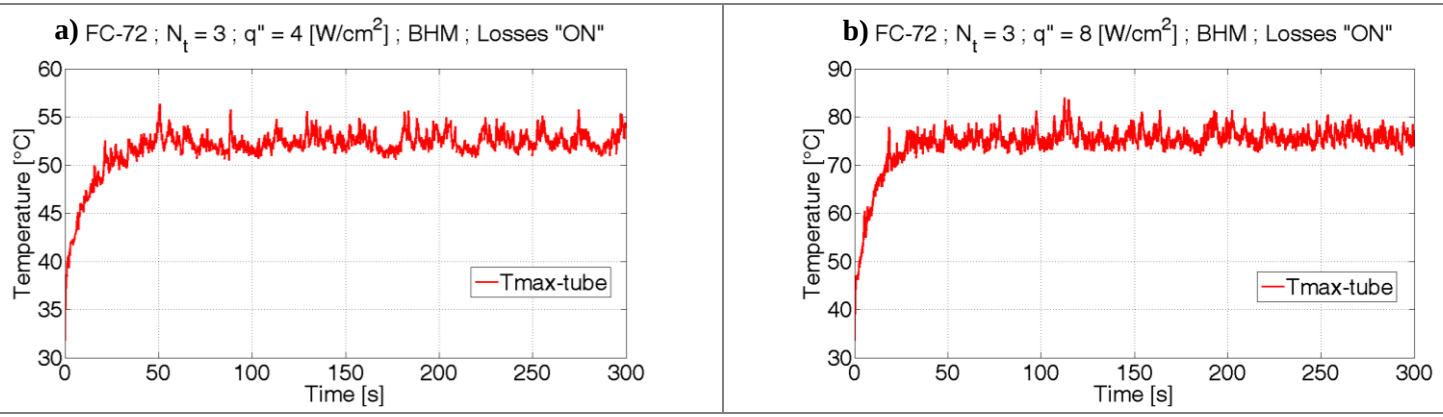

Figure 6. 14: Numerical results: temporal trend of the total liquid momentum.

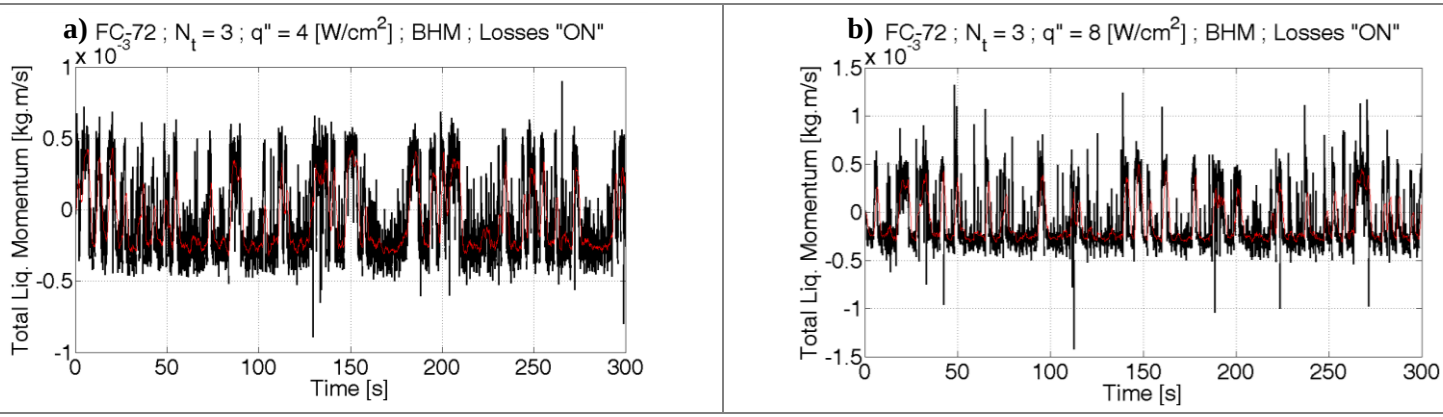

Figure 6. 15: Numerical results: temporal trend of the maximum tube temperature.

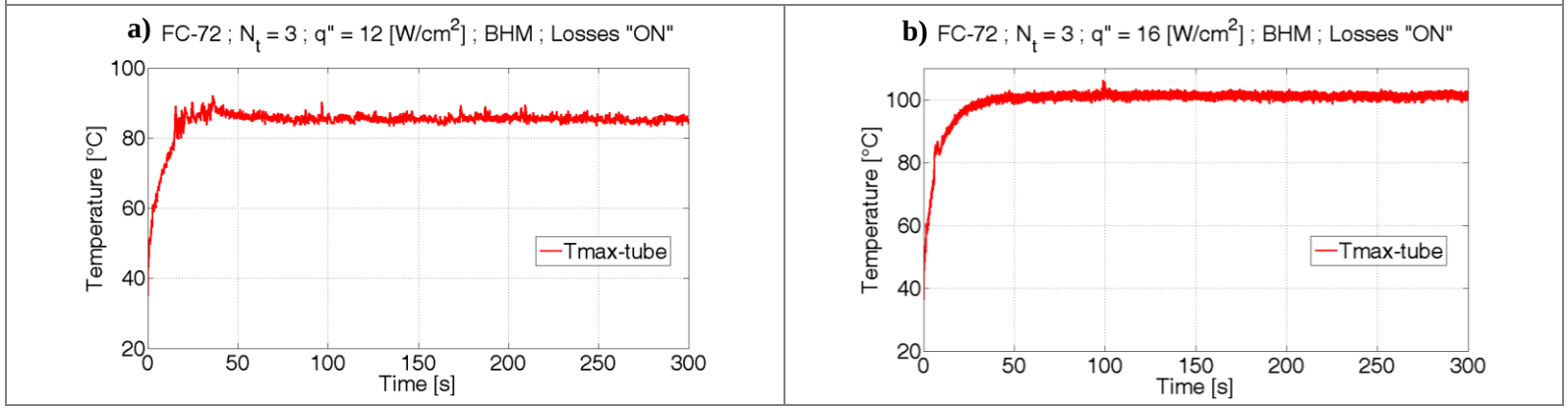

Figure 6. 16: Numerical results: temporal trend of the total liquid momentum.

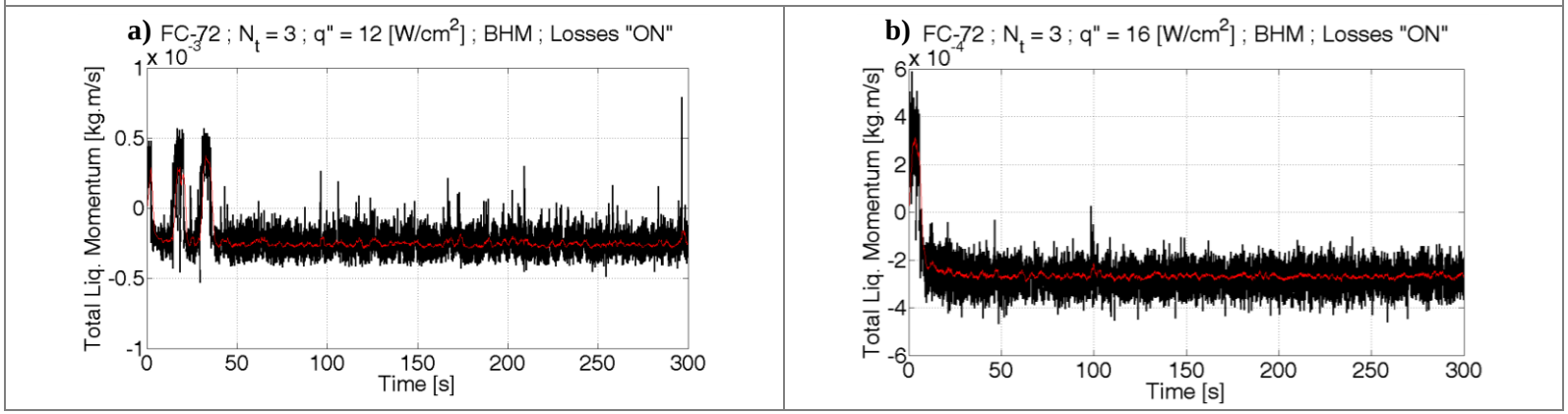

The existence of flow reversals at low input heat fluxes is shown also in *Khandekar (2004)*. The spectral analysis performed on the numerical results (fig. 8a, 9a) highlights that the oscillation frequency is sometimes lower that the usual range (0.1 - 3Hz) for the CLPHP with three turns. Focusing on the total liquid momentum (Figure 6.14a) it is evident that a lower dominant frequency is imputable to the continuous flow reversals occurring within the device. When the input heat flux is increased to 8 W/cm^2, the fluid flow inside the three turns CLPHP changes radically.

Figures 6.14b and 6.15b show that the total liquid momentum keeps on switching between positive and negative values always maintaining an oscillating component. This means that the circulatory motion component undergoes continuous flow reversals. Even if the system reaches a sort of pseudo steady state after about 50 seconds, temperature is still strongly oscillating around a mean value of about 64°C with local maximum peaks at 71-72°C corresponding to the flow reversals and periods of relatively stable temperature when the circulatory motion component is more stable. During the flow inversions the fluid motion is slower, consequently the poorer convective heat transfer affects the maximum tube temperature which rises locally (Figures 6.13a, 6.13b). Increasing the heat input to 12-16 W/cm^2, the vapor expansion in the evaporator zone is strong enough to avoid flow reversal and the circulatory motion component is more stable (Figures 6.16a, 6.16b) as well as the maximum tube temperature (Figures 6.15a, 6.15b).

6.3.3 Closure

- Local pressure losses due to bends and turns affect the device operation especially in the horizontal mode and for high heat input levels. Neglecting the effect of local pressure drop leads to overestimate the PHP overall thermal performance.
- Flow reversals have a negative influence on the thermal performance, while an increase or decrease of the local fluctuations frequency in the flow motion is not linked to the heat transfer efficiency.
- When flow reversal are not predominant, the characteristic frequencies of flow oscillations are in the range of 0.1 to 3Hz , which is confirmed by experimental data in literature.
- Numerical results show that the CLPHP with three turns is not working in the horizontal position, while the test case with nine turns is able to

operate, experimentally confirmed by *Charoensawan and Terdtoon (2007)*.

6.4 Effect of the inclination angle and gravity level.

6.4.1 Inclination angle

The PHP with nine turns (N_t = 9) is investigated at three different orientations: vertical (BHM), 45° and horizontal. Figure 6.17 shows the values of $\overline{T}_{w,\max}$ and the standard deviation bar relative to the temperature oscillation for each test case.

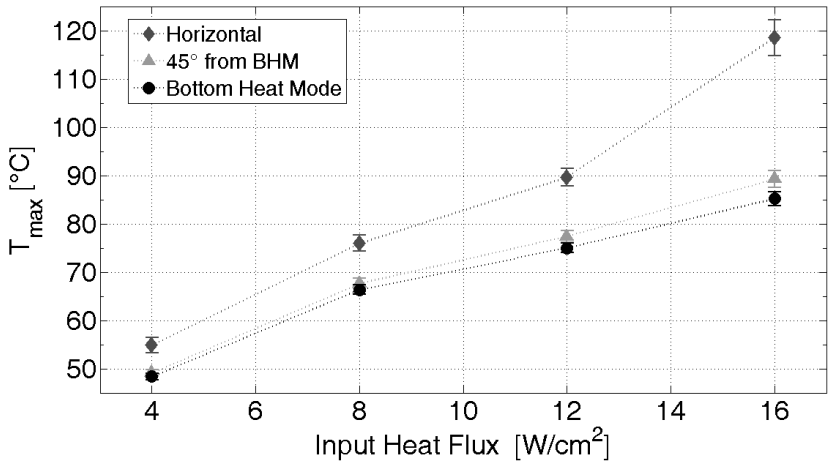

Figure 6. 17: mean maximum tube temperature VS heat input flux for the 9 turns CLPHP at different orientations.

The tilted and horizontal PHP with 9 turns are working but, since the total liquid momentum is less and less assisted by gravity forces the fluid motion becomes less vigorous and oscillation amplitude has lower values. Consequently the convective heat transfer coefficient of the liquid phase is lower and this results in higher mean maximum tube temperatures as expected from experimental evidence.

In all cases the equivalent thermal resistance (Figure 6.18) decreases with the heat flux. The PHP which is working in the horizontal mode reaches a minimum in the thermal resistance and a further heat input increase worsen the PHP performance. Experimental evidence suggests that beyond this heat input level dry-out will occur.

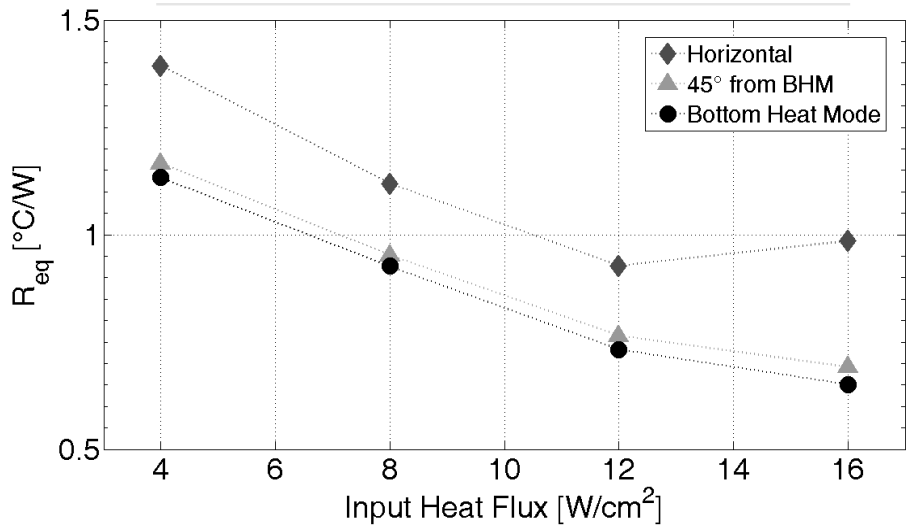

Figure 6. 18: equivalent thermal resistance VS heat input flux for the 9 turns CLPHP at different orientations.

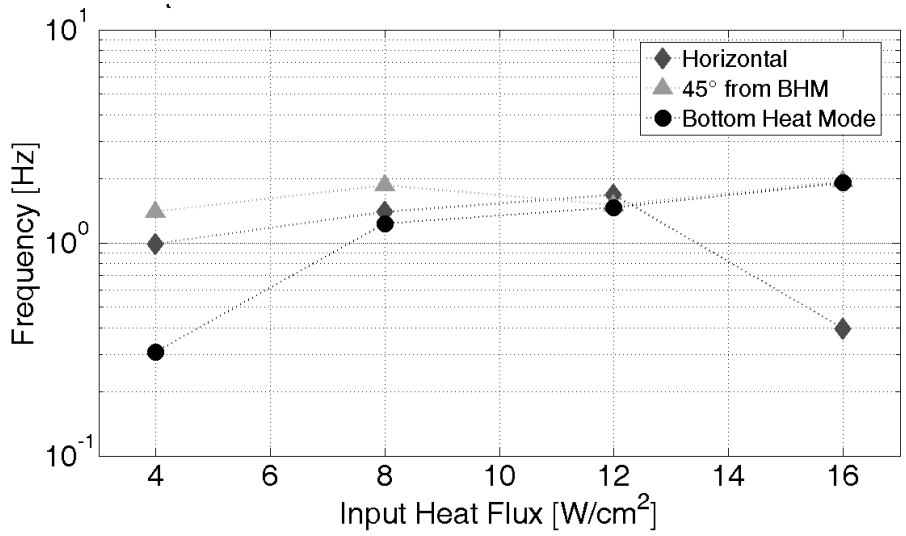

Figure 6. 19: dominant frequency of the total liquid momentum oscillation VS heat input flux for the 9 turns CLPHP at different orientations.

6.4.2 Effect of the gravity level

In this section the CLPHP with nine turns (N_t = 9) in vertical position (BHM) is simulated for different gravity levels and different heat input rates. As expected, the trends obtained by decreasing the gravity level (Figures 6.20, 6.21 and 6.22), are comparable to the tilted PHP trends.

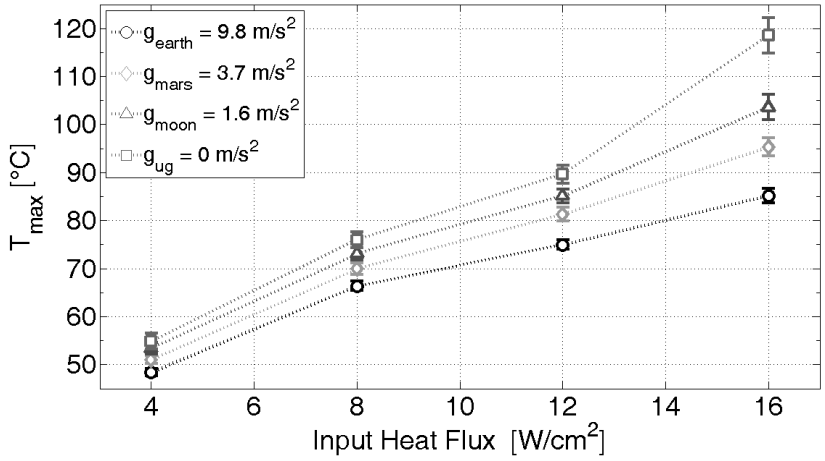

Figure 6. 20: mean maximum tube temperature VS heat input flux for the 9 turns CLPHP at different gravity levels.

From the numerical investigation it seems that by decreasing the gravity level the maximum efficiency occurs at lower heat input fluxes. Figure 6.21 shows that the PHP with nine turns reaches the minimum equivalent thermal resistance at around *q"= 12[W/cm^2]* at 0-g which is still comparable to the grooved and screen mesh heat pipes heat fluxes capabilities.

Oscillation frequencies are also in the range but without a clear effect of gravity. In general higher frequencies results for higher heat inputs.

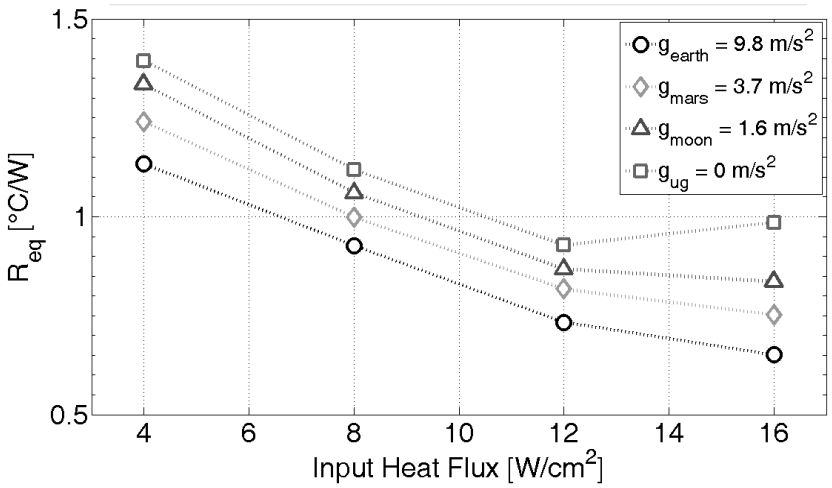

Figure 6. 21: equivalent thermal resistance VS heat input flux for the 9 turns CLPHP at different gravity levels.

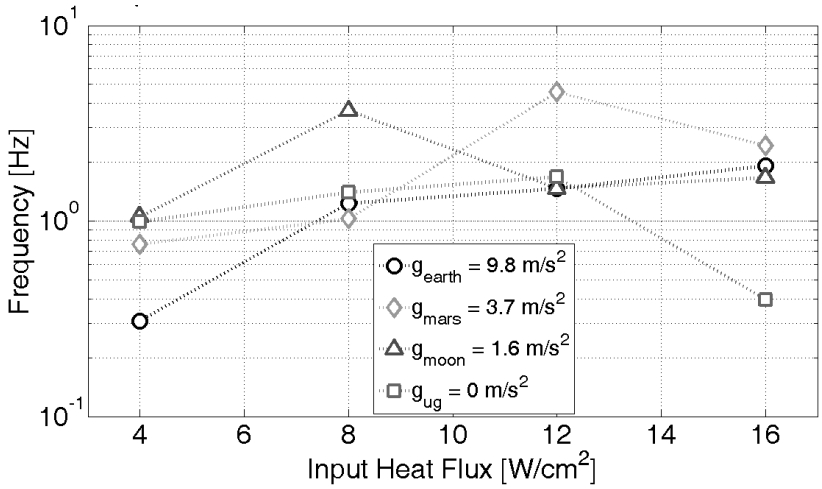

Figure 6. 22: dominant frequency of the total liquid momentum oscillation VS heat input flux for the 9 turns CLPHP at different gravity levels.

If the experimental results will confirm that the horizontal operation under normal gravity is also representative of the zero gravity condition, the CLPHP could be considered a suitable candidate not only for ground but also for aerospace applications. The PHP performance in 0-g will be lower than the gravity assisted mode (Bottom Heat Mode) but it will be also independent from the inclination angle.

6.4.3 Closure

- The simulated CLPHP with three turns can only operate if gravity assisted (Bottom Heat Mode) while the CLPHP with nine turns works also in the Horizontal position even if with a lower thermal performance.
- The test cases with nine turns are still sensitive to the effect of gravity and the bottom heat mode is more efficient then the horizontal mode as confirmed by experimental evidence.
- Dominant frequencies of flow oscillations are in the range of 0.3 to 2.5Hz (quantitatively confirmed by experimental data). If the PHP is operating in the “pure oscillation mode” higher oscillation frequencies are connected to a better PHP thermal performance. However, CLPHPs operate best in the "circulation mode" where oscillation frequencies are not influencing the performance.
- If future experimental results will confirm that the horizontal operation under normal gravity is also representative of the zero gravity condition,

the CLPHP could represent a suitable candidate not only for ground but also for space applications.

6.5 Quantitative validation on a complex geometry

In order to provide a quantitative validation of the present model, the geometrical features and boundary conditions of the apparatus built and experimentally investigated by *Yang et al. (2008)* have been extrapolated and used as input parameters for the present code.

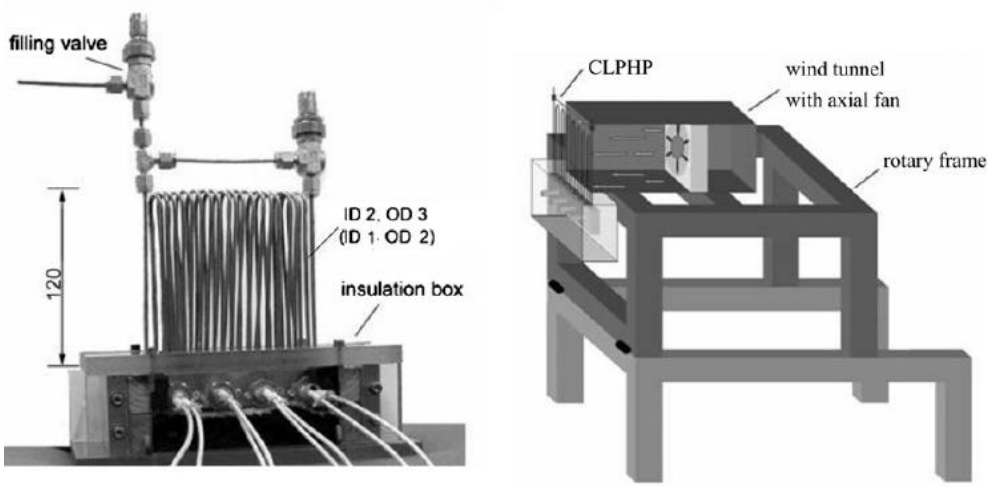

Figure 6. 23: Experimental test-rig by *Yang et al. (2008).*

This device (Figure 6.23) is definitely closer to a practical application: not only the number of turns is considerably high ($N_t = 39$) but also the boundary conditions are different from the previous cases; indeed the heat is provided on an extremely small surface (the evaporator length is only 7 mm) while all the remaining length is entirely devoted to the heat release by mean of air cooling. On the basis of the estimation of the air side heat transfer coefficient carried out by *Khandekar (2010),* a value of $h_{ex} = 90 W/m^2 K$ have been chosen for the external cooling medium. All the other geometrical features as well as the boundary conditions have been extrapolated (see table 4) and four numerical simulations have been run.

INPUT PARAMETER	39 turns
Working fluids	R123
Tube material	copper
Internal tube diameter, $d_{in}[mm]$	2
external tube diameter, $d_{out}[mm]$	3
Inner surface roughness, $r_{fs}[\mu m]$	50
Curvature radius of all bends and turns, $r_t[mm]$	2.5
Adiabatic section length, $L_{ad}[mm]$	0
Evaporator section length, $L_{ev}[mm]$	7
Condenser section length, $L_{co}[mm]$	113
Total length, $L_{tot}[mm]$	5040
Evaporator heat exchange area, $A_{rad,ev}[cm^2]$	25.13
Initial temperature $T_0[°C]$	30
Filling ratio, $\gamma[-]$	0.5
Tilting angle with respect to gravity direction, [deg]	0 (BHM)
Ext. heat transfer coefficient $h_\infty[W/m^2K]$	90
External cooling temperature, $T_\infty[°C]$	27
Losses due to the presence of bends, ΔP_K	ON
Total heat input, $\dot{Q}_{ev}[W]$	100; 200; 300; 400
Maximum computational time step, [s]	$1x10^{-3}$
Minimum time step refinement factor, [s]	$1x10^{-6}$
Number of grids for the wall domain, [-]	5040
Number of grids for the liquid domain, [-]	225
Convergence criterion on integration methods (Simpson, trapezoidal, secant) [-]	$1x10^{-3}$

Table 6. 6: Code input parameters based on the CLPHP built by *Yang et al. (2008)*.

Figure 6.24 and 6.25 show relatively the comparison between two trends of the average maximum temperature and the overall thermal resistance at each heat input level: the experimental results obtained by *Yang et al. (2008)* on the multi-turn CLPHP (black dots) and the the numerical results obtained by the present model fed with the same geometry and boundary conditions (white dots).

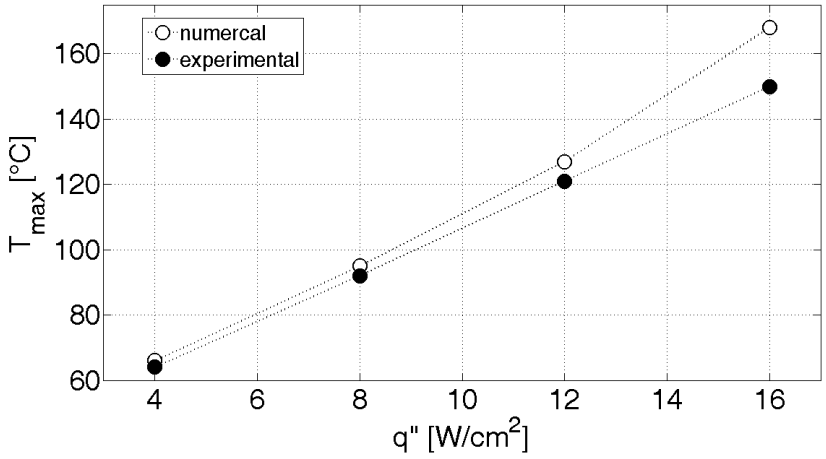

Figure 6. 24: average maximum temperature of a multi-turn CLPHP operating in Bottom Heat Mode, comparison between numerical and experimental obtained by *Yang et al. (2008).*

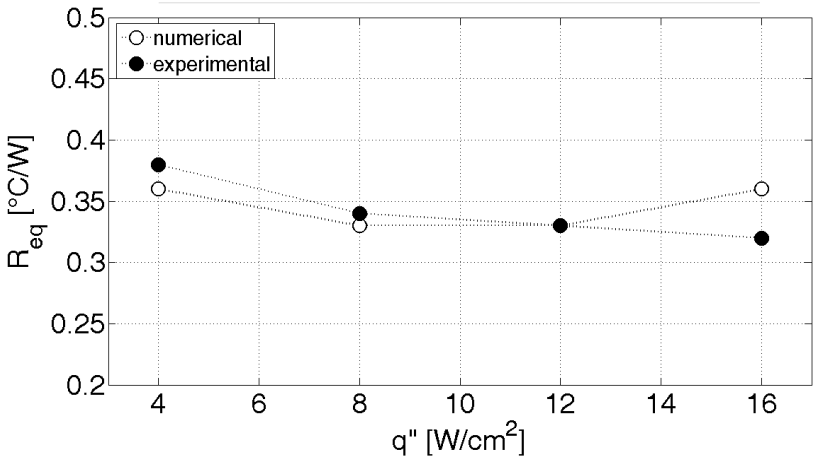

Figure 6. 25: overall thermal resistance of a multi-turn CLPHP operating in Bottom Heat Mode, comparison between numerical results and the experimental data obtained by *Yang et al. (2008).*

As shown in Table 6.7 the present model is able to represent the thermal behavior of the PHP within the 3% of error for the first two cases. The error increases for the last two cases, 5% and 11%, because when the heat input level rises, the experimental evidence shows that the flow pattern inside the device is no more a pure alternation of liquid slugs and vapor plugs.

q'' [W/cm^2]	Q [W]	Te_{exp} [°C]	Te_{num} [°C]	$R_{eq\text{-}exp}$ [°C/W]	$R_{eq\text{-}num}$ [°C/W]	Err. on R_{eq} [%]
4	100	65	63	0.38	0.36	5.26
8	200	95	93	0.34	0.33	2.94
12	300	126	127	0.33	0.33	1.01
16	400	155	170	0.32	0.36	11.72

Table 6. 7: Numerical results VS Experimental data.

A transition of the local phase distribution from slug flow to annular flow corresponds to an increase of the local heat transfer coefficient thus, since the present model does not take into account this flow pattern variation, numerical results tend to underestimate the local heat transfer coefficients and consequently to overestimate the average maximum tube temperature.

There may be another source of error related to the fact that the heat losses at the evaporator are not taken into account in the experimental work. For this reason particular attention should be paid in the test-rig design in order to minimize the heat losses or develop a calibration method so as to estimate the exact heat input rate.

PART III:

Experimental campaign and model validation

Chapter 7

Experimental apparatus, design and assembly

7.1 Introduction

The present chapter provides a detailed description of the experimental test-rig which has been preliminary designed at the Thermal Physics laboratories of the University of Bergamo and successively built and tested at the Refrigeration and Air Conditioning laboratories of the Indian Institute of Technology Kanpur.

Aware of the strong thermo-hydrodynamic coupling inside the PHP, the set-up has been designed to facilitate parametric investigations as well as simultaneous flow visualizations. Although clearly inspired by *Khandekar et al. 2009*, the geometry of the present CLPHP has been conceived in order to avoid the occurrence of multiple steady states. The presence of three U-turns and four parallel channels increases the level of perturbations thereby diminishing the probability of phase recoiling and consequent complete stop-over of the fluid motion. Figure 7.1 shows an overall view of the experimental test-rig.

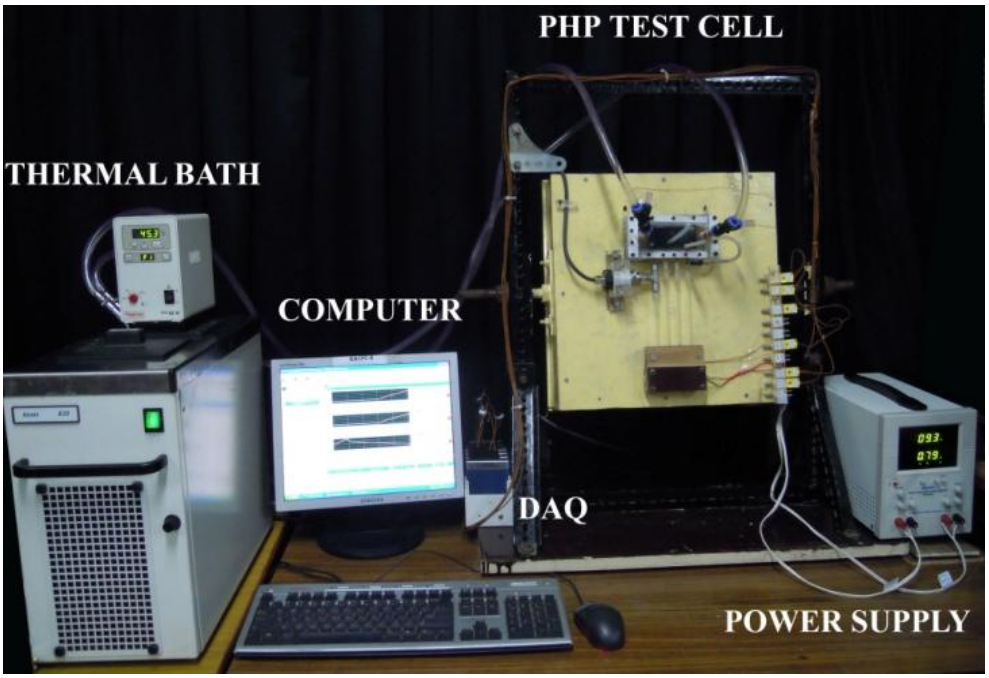

Figure 7. 1: Pulsating Heat Pipe experimental test-rig.

One of the most outstanding features of the present apparatus consists in the implementation of two thermocouples for measuring the fluid temperature in the evaporator section. The local measurement of the two phase flow temperature, together with the wall temperature at the same location and the heat input flux, provides an esteem of the local heat transfer coefficient in a chaotic flow boiling process. These data are not readily available in literature yet.

7.2 Test Cell

The CLPHP is divided in three main sections:

i) The evaporator zone, where the device receives a controlled heat input by means of electric heaters.

ii) The adiabatic zone, ideally insulated from the environment.

iii) The condenser zone where the PHP releases the heat by means of a liquid cooled heat sink.

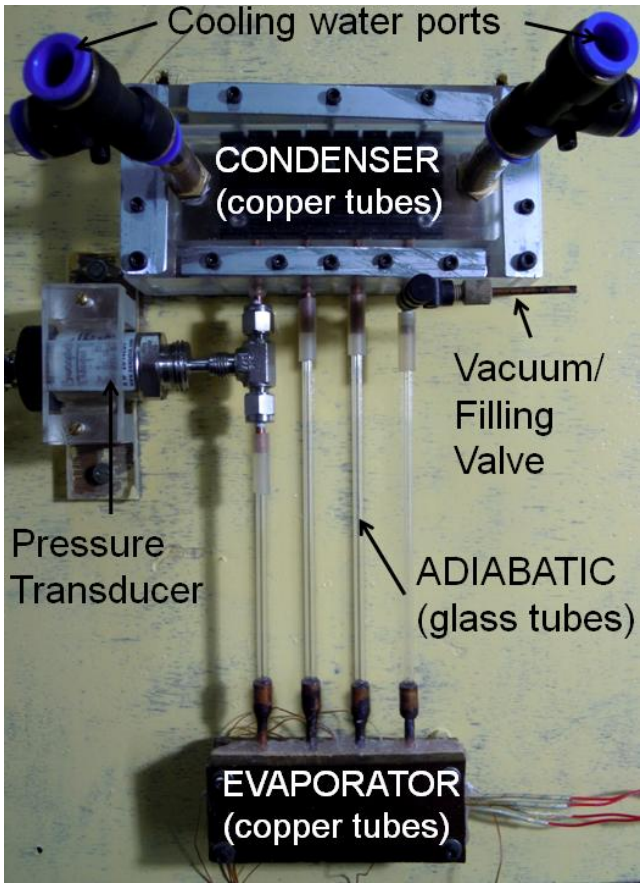

INPUT PARAMETER	VALUE
Working fluid	ethanol
Tube material	copper
Tube I.D.	2 [mm]
Tube O.D.	4 [mm]
Evapaporator length	25 [mm]
Condenser length	35 [mm]
Adiabatic length	202 [mm]
Filling ratio	0.65 [-]
Cool. Medium temperature	15 [°C]
Initial temperature	27 [°C]
Heat input levels	20 to 110 [W]

Figure 7. 2: Pulsating heat pipe test-cell

The tubes in the evaporator and in the condenser sections are made of copper in order to minimize the thermal resistance between the tube and the heat input/output zones while the straight tubes in the adiabatic section are made of borosilicate glass for the purpose of visualization. All tubes have 4.0 mm O.D. and 2.0 mm I.D.; a smaller copper tube (3 mm O.D., 2 mm I.D.) has been brazed on the main tube of the condenser section in order to connect the vacuum/filling valve (M/s Upchurch Scientific®).

A pressure transducer (Swagelok®, PTI-S-AC5-12AS) is plugged in the left external branch of the adiabatic section by means of a T-connector (Swagelok®).

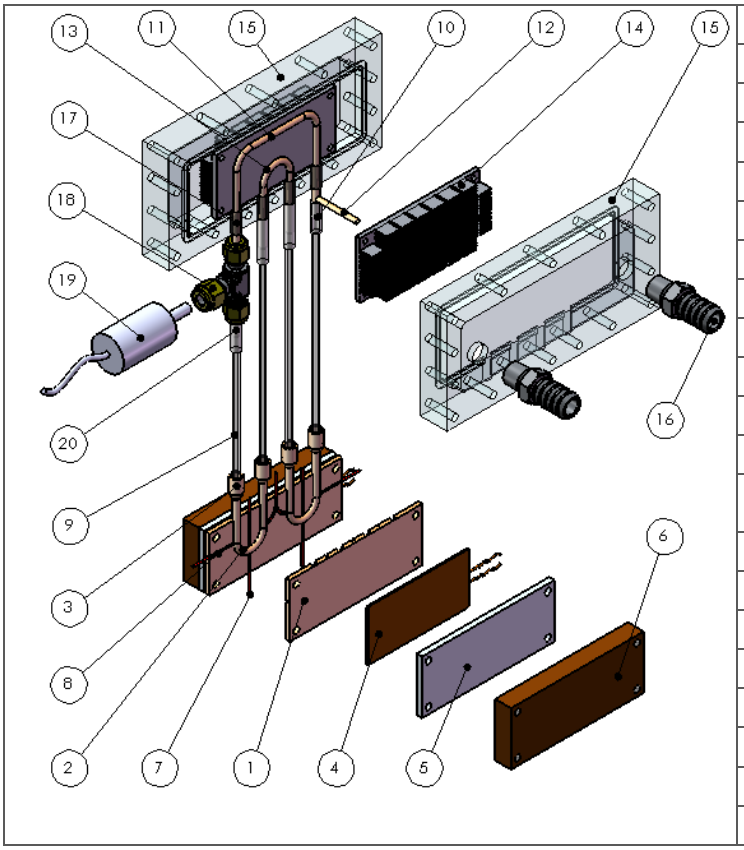

N°	ITEM
1	Eva. copper plate
2	Eva. copper U-turns
3	Copper joint
4	Heater
5	Mica sheet
6	Bakelite back plate
7	TC fluid side
8	TC wall side
9	Glass tube
10	Silicon joint
11	Condenser tube
12	Branch (vacuum/filling)
13	Cond. copper tube
14	Heat sink
15	Cooler shell
16	Cooler connector
17	Silicon seal
18	T-junction
19	Pressure transducer
20	Copper fitting

Figure 7. 3: Exploded view of the Closed loop pulsating heat pipe test-cell.

The copper tubes in the condenser section are connected to the glass tubes simply by fitting a small silicon tube (5mm O.D., 3mm I.D.). This approach is not suitable to the copper/glass connections in the evaporator zone due to the high temperatures. In this case the following procedure has been applied (Figure 7.4):

- a copper joint is located at each end of the U-turns by mean of a steel ring and brazed;
- the glass tubes are inserted in the copper fitting and coupled to the copper tubes by mean of a O-ring;
- High temperature proof polymeric resin fills the remaining gap between the copper fitting and the glass tube above the O-ring thus ensuring a good seal.

Technical drawings are available in Annex II.

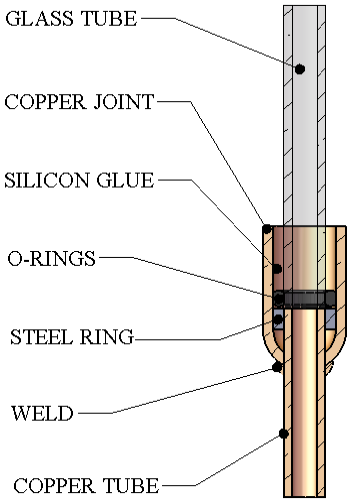

Figure 7. 4: Copper/glass tubes coupling method.

7.2.1 Evaporator section

Two symmetric copper plates (100x40x3 mm) have been built and circular cross section channels have been milled to embed the copper U-turns. The main novelty of the present PHP set-up is that the two copper U-turns in the evaporator section have been drilled (1.0 mm blind hole at the top of the curvature) and two thermocouples (Omega®, K type, bead dimension of 0.3 mm, accuracy ± 0.2 °C after calibration), for measuring the fluid temperature, have been located inside the tube through the hole and fixed with thermal cement (Omega®), as shown in Figure 7.5.

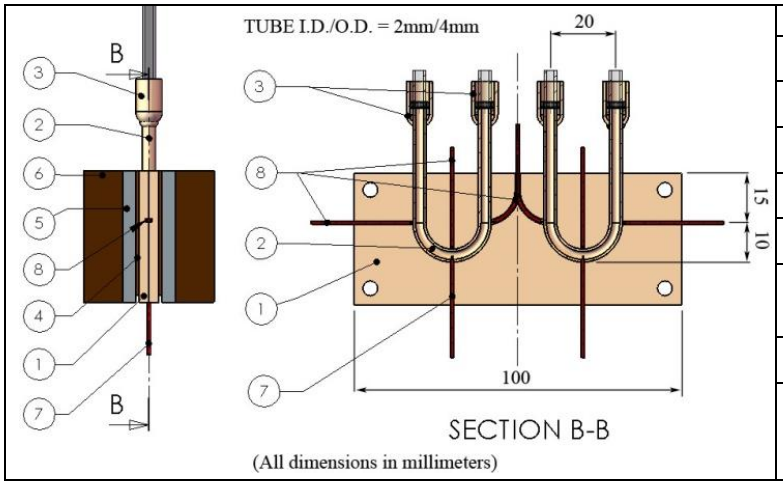

N°	ITEM
1	Copper plate
2	Copper U-turns
3	Copper joint
4	Heater
5	Mica sheet
6	Bakelite back plate
7	TC-fluid side
8	TC-wall side

Figure 7. 5: Detail and section of the evaporator block.

Proper thermal contact between the U-turns and the copper plates is obtained using a high conductive paste. Six thermocouples have been located on the external tube wall by means of small square channels milled on the copper plates. The assembly of the two plates and the U-turns forms the evaporator copper block. Two flat flexible heaters (Minco®, HR5383R10.7L12B) have been placed at each side of the evaporator block.

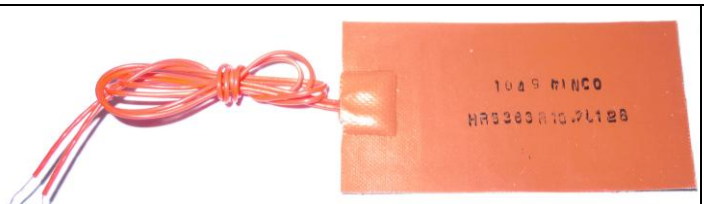

Main features:

- Voltage range: 0-30 V
- Ampere range: 0-3 A
- Resistance: 10.7 Ohms
- Dimensions: 38.1x76.2mm
- Max. temperature:180°C
- Max. heat throughput: 70W

Figure 7. 6: Flexible heater.

Insulation is provided by two Mica fiber sheets (thickness: 3 mm) and two Bakelite® back plates (thickness: 12 mm). Electric power is provided to the heaters by means of a dual tracking power supply (Scientific®) with DC current output (0 to 30V, 0 to 3 A).

7.2.2 Condenser section

The copper tubes in the condenser section are also embedded into a block with the same procedure described for the evaporator.

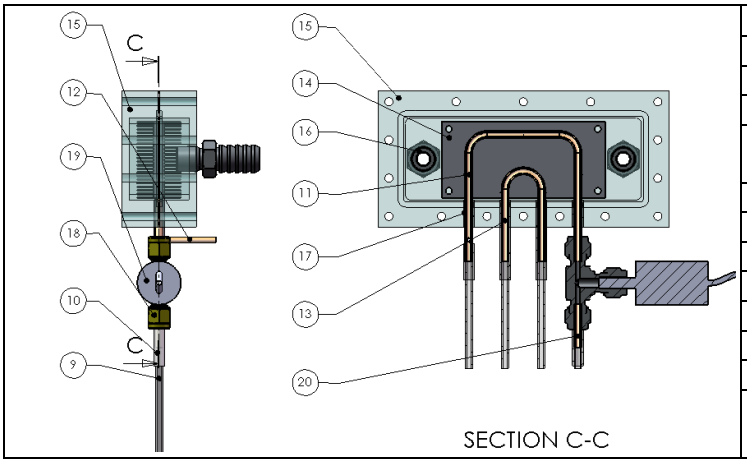

N°	ITEM
9	Glass tube
10	Silicon joint
11	Condenser tube
12	Branch (vacuum/fill)
13	Condenser tube
14	Heat sink
15	Cooler shell
16	Cooler connector
17	Silicon seal
18	T-junction
19	Pressure transducer
20	Copper fitting

Figure 7. 7: Detail and section of the condenser.

In this case the block consists in two symmetric aluminum heat. The condenser block itself fits into a custom Policarbonate shell made of two transparent plates (160 mm x 75 mm x 20 mm) engraved in the Thermal

Physics laboratory by mean of a Roland® EGX-400 micro-milling machine. Four holes allow the copper tube branches to come out the shell and connect with the adiabatic section.
From a simple steady analysis on the heat convection (equation 7.1) it is clear (Figure 7.8) that the condenser is not able to dissipate the total heat throughput only by means of convection over the smooth tube surface.

$$\dot{Q}_{tot} = \dot{Q}_{conv} = h_{ext} \cdot A_{ex} \cdot \Delta T_{w-f} \qquad 7.1$$

Where $\dot{Q}_{tot}$ *[W]* is the maximum deliverable heat throughput that can be dissipated, h_{ext} is an optimistic esteemation of the external HTC for the cooling fluid, A_{ext} is the condenser external surface and ΔT_{w-f} is the temperature difference between the condenser solid wall and the external cooling medium (in previous experiments this value rarely goes beyond 30 K when the cooling medium is water).

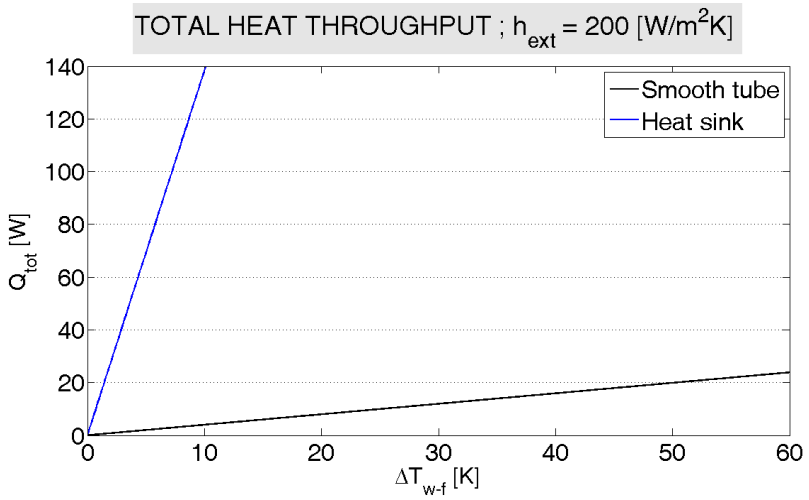

Figure 7. 8: Total heat throughput as a function of wall-fluid temperature difference for two different surfaces (smooth tubes, heat sink) keeping a constant HTC.

In case of smooth tubes the external surface is 0.001987 m^2 and the maximum deliverable heat throughput is 10W with a temperature difference of 30 K. In order to obtain the desired heat throughput with a lower temperature difference and without changing the condenser length, a custom finned heat sink has been designed and manufactured by cutting a single unit (Alpha®, UB90-15B) into two symmetric parts (Figure 7.9). The main

geometric features are listed below (see also the mechanical draw in Annex II):

- Lower plate: 90x42x4mm
- Fin: 9mm
- Total external area: A_{ext_hs} = 0.0691446 m^2

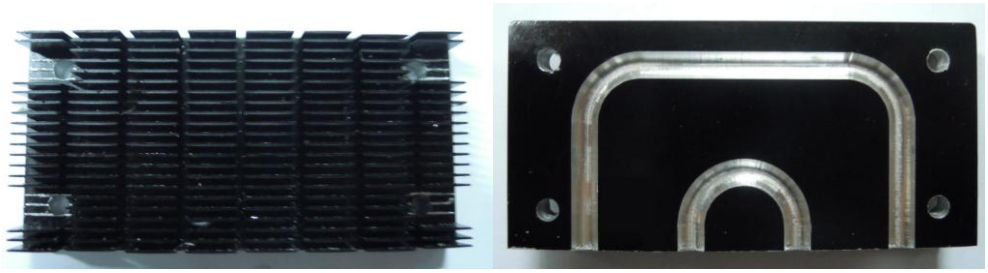

Figure 7. 9: Finned heat sink implemented in the condenser zone.

Assuming the same external HTC, the heat sink is able to dissipate the total heat throughput if ΔT_{w-f} = 10K (blue line in Figure 7.8). A further FEM analysis has been conducted with COMSOL multi-physics® in order to verify the previous overall calculation. In this case the total heat input is imposed in the form of a heat flux boundary condition on the heat sink circular cross section seats ($q''= Q_{tot}/A_{ext\_st} = 70500\ W/m^2$);

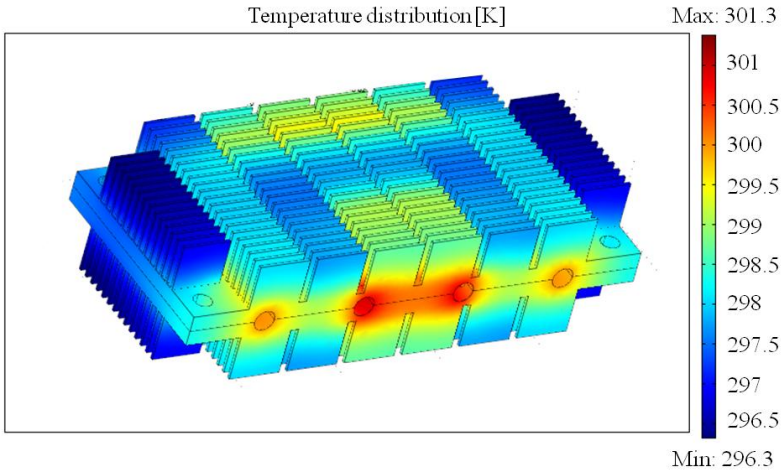

Figure 7. 10: Heat sink temperature distribution (FEM analysis).

The mixed boundary conditions (convective heat transfer coefficient h_{ext} = *200 W/m^{2}K* and cooling medium temperature T_{ext}=*288.15K)* have been imposed on the entire external heat sink surface. The FEM solver provides the heat sink temperature distribution; the local ΔT_{w-f} varies in a range

between 8 and 13 K as expected. Cooling water is kept at constant temperature of 15°C ±1°C by a thermal bath and circulated through the condenser (Haake®, DC-10, K20).

Main features

- Operating temperature: –30 to 100 °C
- Temperature accuracy: ± 0.02 K
- Heater capacity @ 230V / 115V: 2000 /1200 W
- Pump maximum relative pressure: 300 mbar
- Circulation capacity (open): 17 l/min
- Max. flow rate during circulation using 12 mm ø hoses: 12.5 l/min

Figure 7. 11: Thermal bath and recirculation pump

7.2.3 Adiabatic section

The adiabatic zone is made of four straight borosilicate glass tubes for the purpose of fluid visualization.

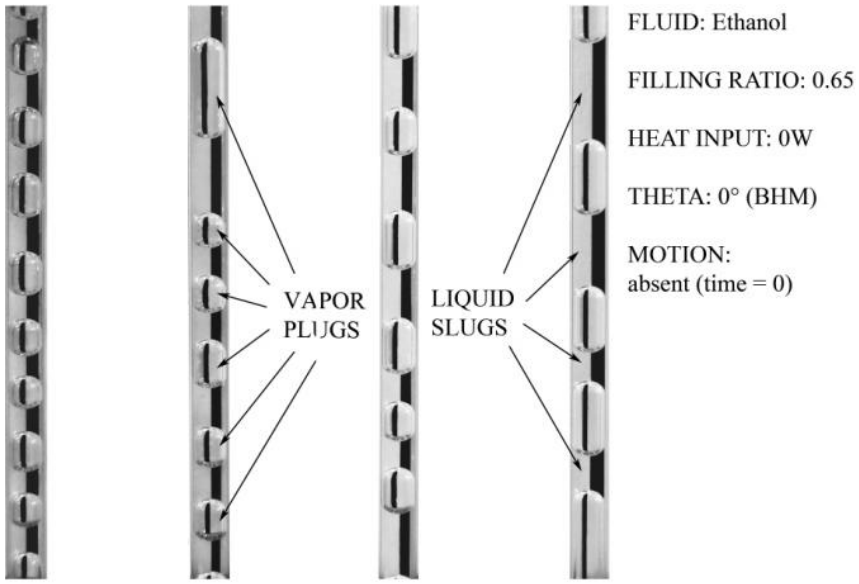

Figure 7. 12: White screen with black stripes visualization technique

A white screen with four black stripes (one for each transparent tube) is placed behind the adiabatic section; the two phases are clearly distinguishable thanks to the different refraction coefficient of liquid and vapor. Fluid motion and flow patterns have been captured with a camera (Nikon®, model: Dx40) in a 100 mm x 100 mm window just above the evaporator section. Fig. 7.12 shows the typical liquid slugs and vapor plug distribution after the filling procedure.

7.3 Base structure

The apparatus is mounted on a plate that can be tilted in order to change its orientation with respect to gravity. Since the number of turns of the present PHP is small, a sensitive decrease of both thermal performance and working range is expected when the device is tilted from the Bottom heat mode to the horizontal heat mode.

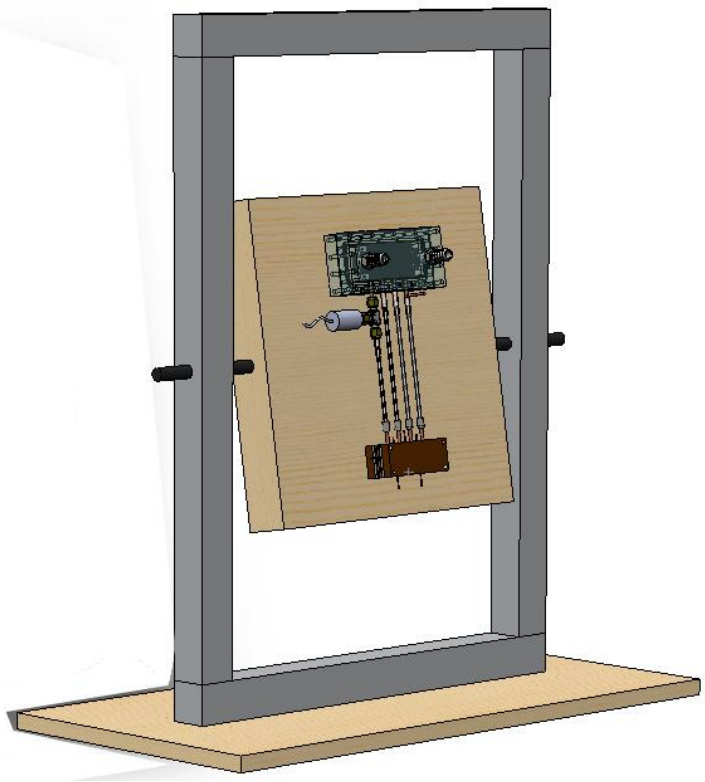

Figure 7. 13: Base structure with tilting plate

7.4 Vacuum and filling procedure

Vacuum as well as the filling procedure are carried out through a micro-metering (M/s Upchurch Scientific®) made of a sturdy PEEK polymer with a through hole of 0.5 mm. The central port has been mounted on the PHP while the other port is alternatively connected to the vacuum system first and finally to the filling system.

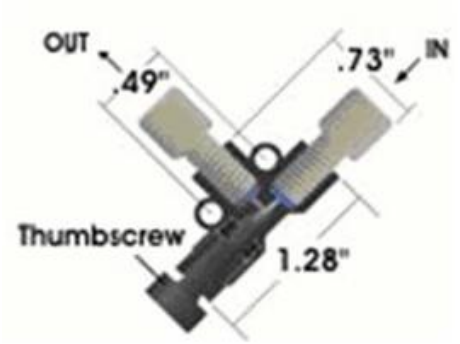

Figure 7. 14: Micro-metering valve for the vacuum/filling purpose.

In order to obtain the desired vacuum level two different vacuum pumps are connected in parallel to the PHP filling valve. The turbo-molecular pump (Varian®, V70) can go up to 10^{-9} mbar but a certain level of vacuum is required for its effective and safe use.

	• Ultimate total pressure: 2*10-3 mbar • Nominal rotation speed: 1500 rpm at 50 Hz
	• Ultimate vacuum level: 10^{-9} mbar • Rotation speed: 75000 rpm • Start-up time: $\leq$ 60 second

Figure 7. 15: Screw/turbo vacuum pumps combo system

A vacuum level of 10^{-3} mbar is created first by means of a primary rotary vane type pump (Varian®, DS-102). While the primary pump is still running, the turbo-molecular pump is activated and both pumps run in parallel. In order to check the vacuum level during the evacuation process two pressure gauges are connected to the pumping system by mean of a T-junction and monitored with a multi-gauge controller.

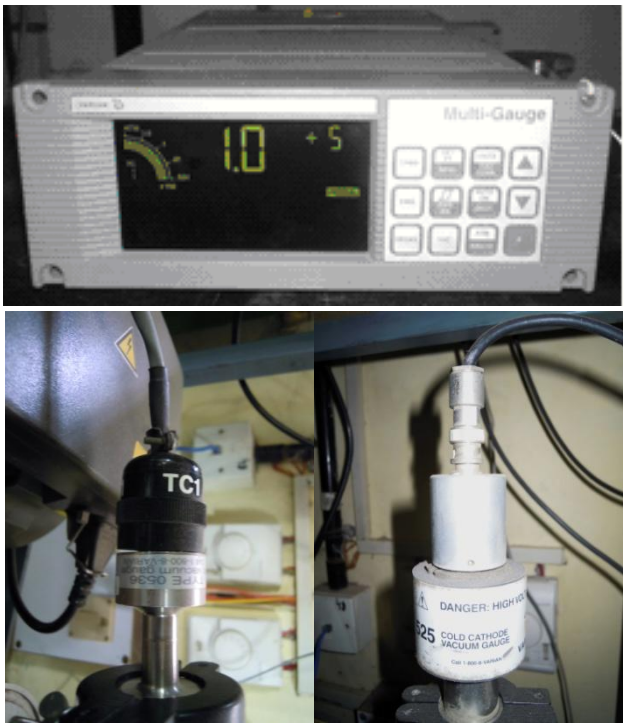

Figure 7. 16: multi pressure gauge controller, vacuum gauge and 525 Cold Cathode Ionization Gauge Tube.

When the pressure level inside the test-rig is less than 0.01 Pa (10^{-4} mbar) the PHP valve is closed and pumps are shut down in reverse manner for safety. The vacuum level inside the PHP is checked again by mean of the pressure transducer (Swagelok®, PTI-S-AC5-12AS) plugged in the left external branch of the adiabatic section.

Main features

- Pressure range: 0 to 6 bar
- Input signal: 0 to 30 V (DC)
- Output signal: 4 to 20 mA
- Connection type: 6 mm Swagelok® tube adapter
- Accuracy: ± ≤ 0.5% LPC of span (0.25% BFSL)
- Hysteresis: ≤ 0.1 % of span
- Repeatibility: ≤ 0.05 % of span

Figure 7. 17: Pressure transducer for measuring the working fluid pressure

The filling procedure is conducted by mean of a syringe (maximum capacity 10 cm^3) which is filled with the working fluid and connected to the filling port (the same used for evacuate the system). After eliminating all the air entrainment, the filling valve is opened and the working fluid is automatically sucked inside the device thanks to the pressure difference.

7.5 Data Acquisition System

The Data acquisition system is totally made of components by National Instruments®. In particular the thermocouples signals have been acquired with three NI-9211® modules connected to the PC via a NI-cDAQ9172® chassis. The pressure transducer current output have been connected in parallel to a 1 Ohm standard reference resistance. The voltage signal have been acquired with a NI-9213® module combined with a NI-USB-9162® chassis. Since the characteristic frequency range of the PHP oscillating phenomena is 0.1 and 3 Hz [-], a minimum DAQ sample rate of 6Hz is requested by the Nyquist criterium. The maximum sample rate for the temperature signal was 6.25Hz and 8.33Hz for the pressure signal.

All the data have been monitored and recorded using Labview Signal Express 2009®.

Chapter 8

Experimental Campaign

8.1 Introduction

The experimental campaign has been carried out with three main targets:

i) Explain the different working modes of the present CLPHP by combining the analysis of the temperature/pressure trends and the fluid flow pattern visualization.

ii) Provide an estimation of the local heat transfer coefficient in the evaporator section by measuring the temperature difference between the tube wall and the working fluid.

iii) Investigate the effect of different parameters, such as the working fluid and the orientation with respect to gravity, on PHP the thermal performance.

8.2 Experimental Procedure

Every experiment is conducted with the following procedure.

a) Preliminary operations:

1) The peripheral devices (PC, DAQ, thermal bath, power supplies) are switched on. Power supply is in stand-by (no electric power is provided to the heater yet). The thermal bath is activated in order to reach a steady cooling water temperature.
2) The working fluid used for the previous experiment is evacuated by mean of an old robust belt vacuum pump. (Note that this is a weak point in the present design. It is strongly recommended to plan for a secondary port in order to avoid the use of a vacuum pump for this purpose and simplify the operation).
3) Once the PHP is no more filled with any fluid, it is evacuated by mean of the vacuum pump system described in the previous Chapter. When the vacuum level is below 0.02 Pa, the vacuum/filling valve is closed and the system is disconnected.
4) A 5 ml syringe is filled with working fluid and it is connected to the vacuum/filling valve by mean of a silicon tube. The syringe piston is then removed and the air trapped in the tube connection is eliminated by tapping the tube. The filling valve is slowly opened in such a way that the working fluid can enter the PHP thanks to the pressure difference. When 2.8ml of fluid, corresponding to a filling ratio of 0.65, are inside the PHP, the filling valve is closed.

b) Main operations:

1) A picture at time t = 0s is taken.
2) The acquisition system is enabled and data are recorded.
3) The power supply voltage is increased in order to provide the desired amount of heat to the device. The actual heat input level is kept until the pseudo-steady state is reached (until the mean value of the evaporator tube wall temperature is constant). For the present tes-rig transients are completely overcome after 20 minutes.
4) Pictures of the actual flow pattern regimes occurring inside the device are taken.
5) The heat input level is increased with a step of 10 Watts.

6) Steps from 2 to 5 are repeated till the device reaches the dry-out condition. The last heat input level (CHF, Critical Heat Flux) is the most dangerous because of the sudden decrease of thermal performance and the consequent increase of the evaporator wall temperature. If dry-out occurs the power supply must be shut off in a few seconds and the experiment is over.

8.3 Heat input and related working modes

The first and very important parameter to play with is the heat power provided to the evaporator zone by means of the electric heaters. *Khandekar and Terdtoon (2004)* showed that the CLPHP may work in different modes (oscillation/circulation) depending on the heat input level and that different flow patterns occur when the heat input is increased.

In order to recognize the heat input range of the present geometry a series of experiments have been performed starting from different heat input levels and a common trend due to the initial heat flux has been recognized: for low initial heat input levels (from 0 to 30 W) the device behavior is mainly unstable and cannot reach a pseudo steady state even if the heat input is then increased during the experiments; for high initial heat input levels (from 40 W) the device behavior is more stable and pseudo steady state can be reached at each heat input level. For this reason, two sets of experiment have been chosen, as representatives of the two situations mentioned above.

- Experiment 1: in order to show the unstable behavior of the PHP for low initial start-up heat inputs (starting from 20 W);
- Experiment 2: in order to show that, for this simple geometry, a critical start-up heat flux is needed to commence a more stable and acceptable flow behavior that allows the estimation of the local heat transfer coefficient for each heat input level and link it with the corresponding internal two-phase flow patterns.

In all the tests, the PHP has been kept in vertical position with the evaporator zone at the bottom and the condenser at the top (Bottom Heat Mode, BHM).

8.3.1 Experiment 1: unstable behaviour

The heat input level has been increased with step of 10 W, from an initial heat input level of 40W. The wall and fluid temperature trends in the left U-

turn in the evaporator section are shown in Figure 8.1. Different heat input levels are also marked on the time line.

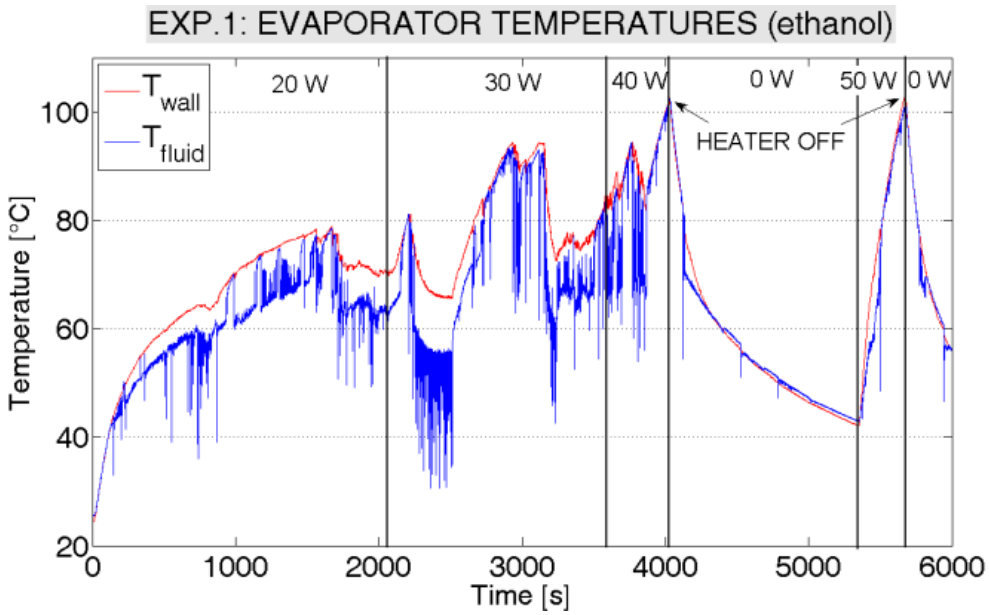

Figure 8. 1: Experiment 1, temporal evolution of evaporator wall and fluid temperatures for different heat inputs.

It is noticeable that the fluid motion can be also identified by the oscillation of the fluid temperature; in particular, the low peaks (or troughs) are related to the passage of a cold liquid slug coming from the condenser section and the higher temperature peaks represent vapor plugs which are residing in the evaporator U-turns and being heated.

Looking closely on the first heat input period (Figure 8.2), four different zones have been selected, depending on the flow motion. During the start-up (up to 700 s), the fluid motion is very poor and it is mainly due to the merging of the smaller vapor plugs; slug flow with a small oscillation amplitude is present in all branches. As soon as the local fluid temperature reaches ~ 60°C and the bigger vapor plugs approach the evaporator, fluid oscillation becomes more vigorous (first box in Figure 8.2) and remains stable till the plugs and slugs distribution is unevenly distributed inside the PHP. It is evident that when the oscillation amplitude is larger, the convection is enhanced and the wall cooling is certainly more efficient.

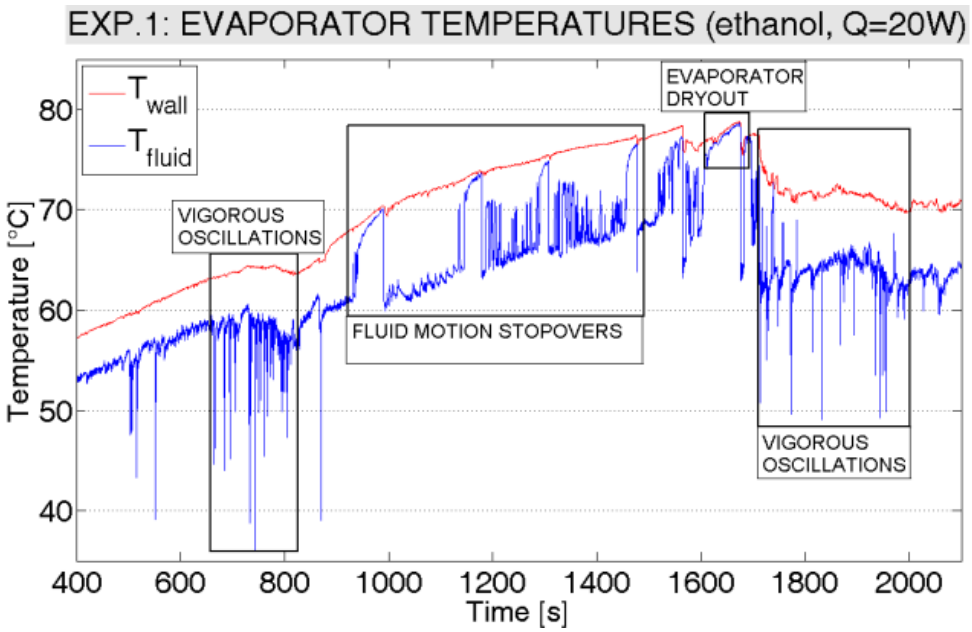

Figure 8. 2: Experiment 1, temporal evolution of evaporator wall and fluid temperature, zoom on Q = 20W.

After about 900 seconds, some big vapor plugs tend to reside/stay in the evaporator section and correspondingly big liquid slugs are seen in the condenser. This is a classic meta-stable distribution that damps the fluid oscillations: the vapor plugs residing in the evaporator are heated up and the PHP heat transfer performance is very low. If fluid temperature and pressure are still relatively low, only a small quantity of colder liquid, in the form of liquid film draining from the hanging menisci, is able to reach the evaporator and only a small fluid pulsation is restored. If the slug and plug distribution is again balanced, this stopover phenomenon repeats (second box in Figure 8.2) and both wall and fluid temperature keep on rising because of the low heat transfer rate.

If the fluid temperature goes beyond a threshold (between 70 and 75°C) and fluid motion is still poor, all the liquid film surrounding the vapor plugs evaporates and dry-out occurs (third box in Figure 8.2) and the fluid temperature reaches the wall temperature. At this point many different scenarios may occur. At low heat input levels, flow instability may restore an uneven plug and slug distribution and also more vigorous oscillations (fourth box in Figure 8.2).

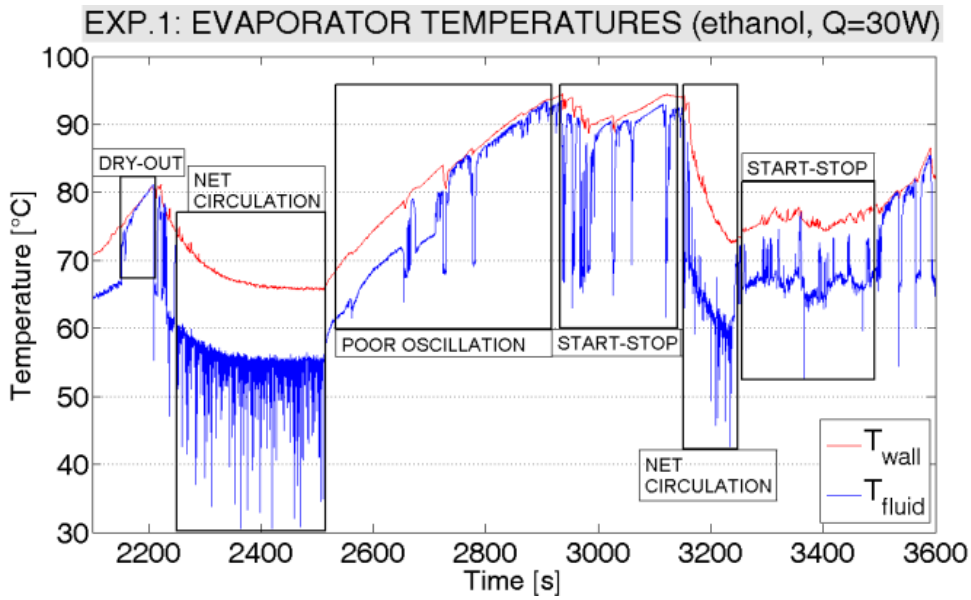

Figure 8. 3: Experiment 1, temporal evolution of evaporator wall and fluid temperature, zoom on Q = 30 W.

At this stage, raising the heat input level to 30 W does not improve the behavior and may lead to a new dry-out (first box in Figure 8.3). More so, such a condition may also evolve abruptly in a fluid net circulation, never present for lower heat inputs, characterized by lower temperatures and consequently with the best efficiency (second box in Figure 8.3). When the fluid and wall temperatures decrease, also the fluid pressure decreases and the net circulation of the fluid cannot be supported anymore. The device starts working as a sort of a heat switch: fluid temperature and pressure rise when fluid oscillations are poor and again decrease, when more vigorous flow motion is activated. Sometimes, as shown in Figure 8.4, dry-outs may not evolve at all, at 40 W the poor fluid motion leads to a faster temperature increase and to a consolidation of the inefficient slug and plug position. The power supply has been switched off and again switched on at 50 W but the previous even distribution lead to another fast dry-out.

The impossibility of getting a steady-state and therefore an acceptable stable thermal performance is mainly due to the simple geometry of the present test-rig. It has been documented by *Charoensawan and Terdtoon (2008)* that this unstable behavior can be mitigated, or even eliminated, by increasing the number of U-turns. By doing this, the number of heated and

cooled section, as well as the local pressure fluctuations due to bends and turns also increase.

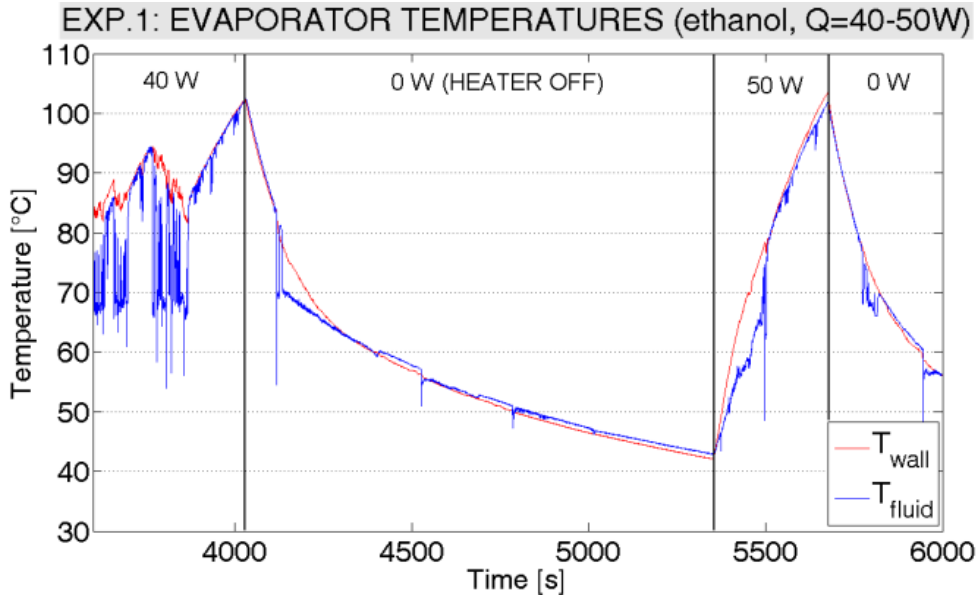

Figure 8. 4: Exp.1, evaporator wall and fluid temperature,(Q=40-50W).

This leads to an intrinsic higher probability of liquid slug break-ups and uneven distribution of plugs and slugs, which indeed is the desired pre-requisite of stable thermal performance of a PHP.

8.3.2 Experiment 2: stable behavior

8.3.2.1 Wall and fluid temperatures at different heat input levels

The heat input level has been increased with step of 10 W, from an initial heat input level of 40W. Figure 8.5 shows the temporal trend of the wall and fluid temperatures in the evaporator zone. Looking at Figure 8.5 it is clear that a critical initial heat flux at the evaporator is necessary to sustain a stable condition right from the start. Indeed, even if at 40W (q" = 5.2 W/cm^2) the device still operates in the 'Heat Switch Mode' described for experiment 1, from 50 W to 100 W (q" = 6.5 to 13.0 W/cm^2) the net circulating flow is definitely dominant in the PHP without any unstable events, as noted in Experiment 1.

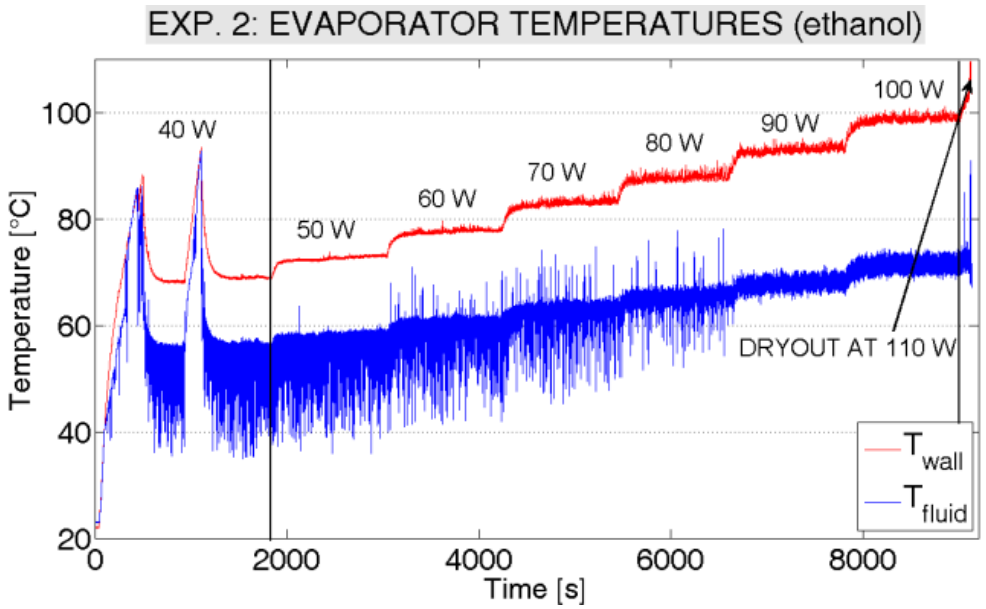

Figure 8. 5: Exp.2, temporal trend of the evap. wall and fluid temperatures.

Each heat input level has been kept for at least twenty minutes in order to be sure that the pseudo steady state was reached (Figure 8.6). The present PHP is able to dissipate up to 100W maintaining the evaporator wall temperature below 100°C.

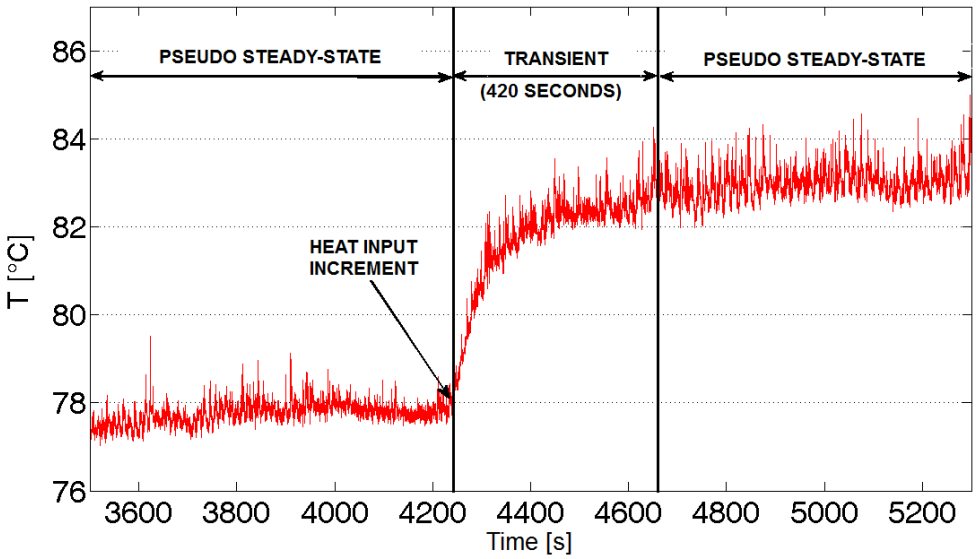

Figure 8. 6: Transient time of the present test-rig.

The transient period of such a PHP is around 420 seconds as shown in Figure 8.6.

8.3.2.2 Fluid pressure and spectral analysis

In order to show that the net fluid circulation is always accompanied by oscillation, the fluid pressure signal over time has been plotted in Figure 8.7.

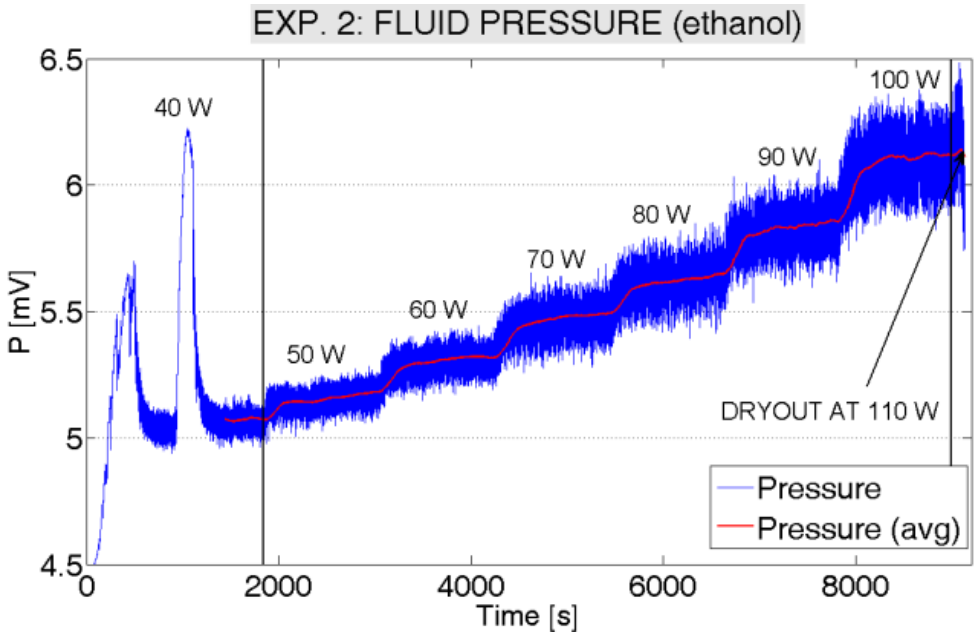

Figure 8. 7: Experiment 2, temporal evolution of local fluid pressure signal for different heat inputs.

The amplitude of the fluid pressure oscillation increases with the heat input level. Another clear observation is that during the second pressure ramp there are no oscillations (Figure 8.7), therefore at this point the fluid motion is very poor resulting in a local dry-out. The vapour phase accumulates in the evaporator weather the liquid recoils in the condenser section as confirmed by visualization (Figure 8.8).

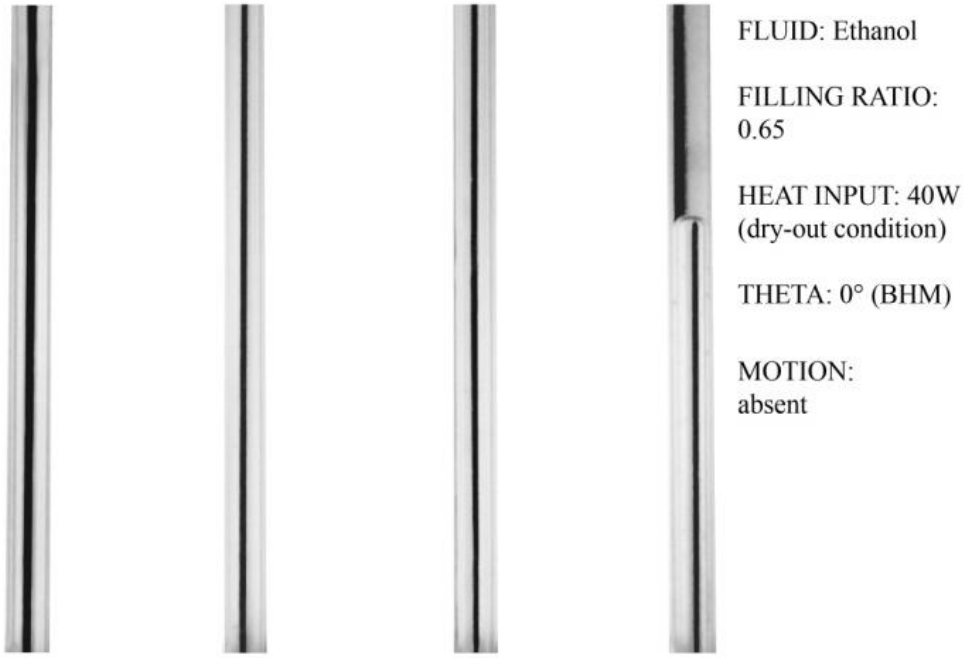

Figure 8. 8: Experiment 2, local dry-out during the start-up.

Since the fluid oscillation is directly connected to the fluid pressure fluctuation, the spectral analysis of pressure signal provides interesting information regarding the existence of dominant or "characteristic" frequencies. A Fast Fourier Transform with a sampling time equals to 0.12 s (8.33 Hz) is performed at each heat input level. The valid frequency range is between 0 and 4 Hz as requested by the Nyquist criterium.

Looking at the presented results (Figure 8.9) a dominant frequency is hardly recognizable. Even though the amplitude of pressure fluctuation increases with the heat input level, it seems that when a net fluid circulation is present (all the six cases shown in Figure 8.9), the oscillating component, does not exhibit any regular behavior in terms of frequency.

Figure 8. 9: Fast Fourier Transform Analysis on pressure signal at different heat input levels

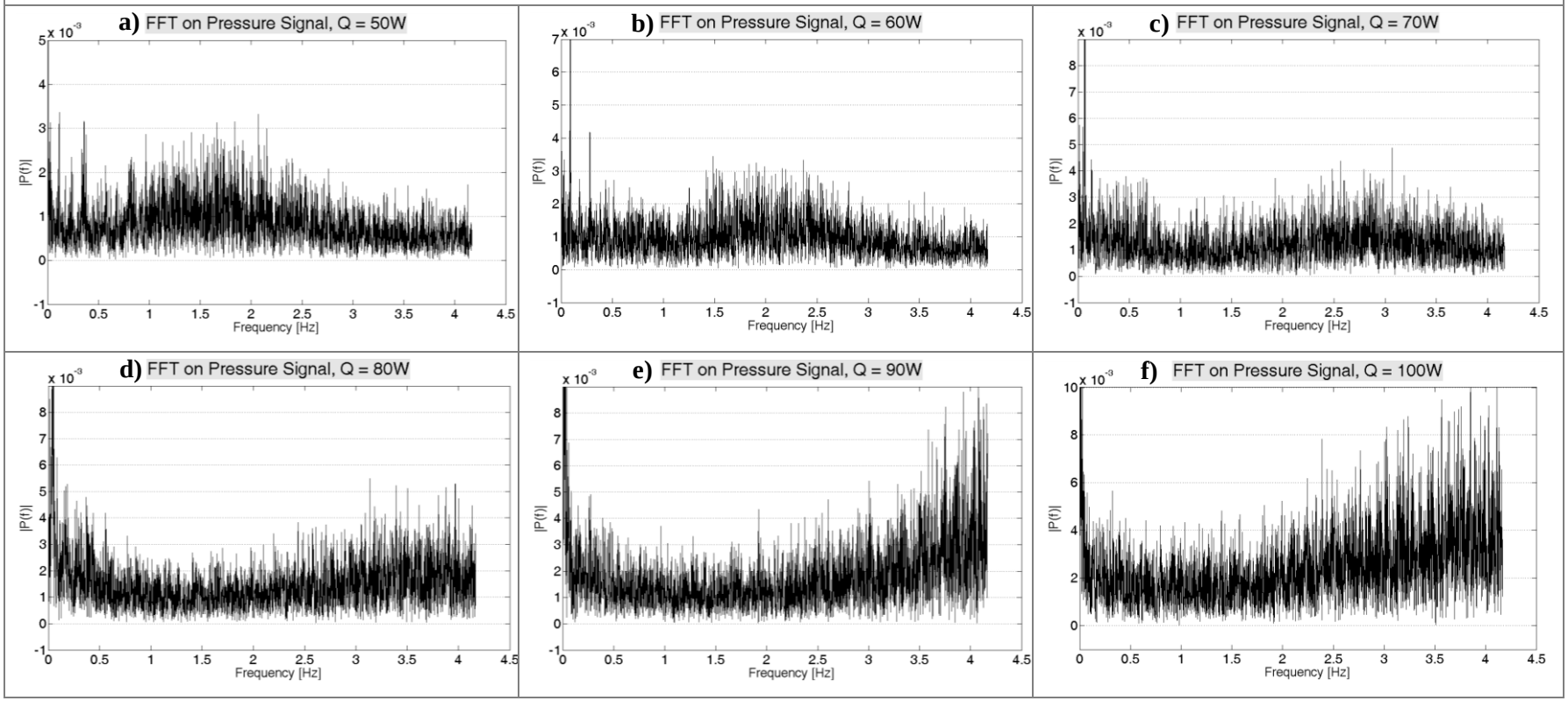

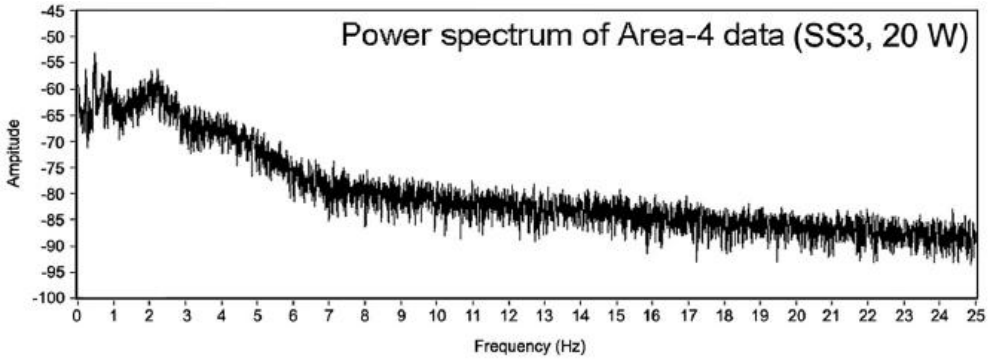

Figure 8. 10: Power spectrum of a steady state area when the single loop PHP is working in net circulation mode, *Khandekar et al. (2009).*

Khandekar et al. (2009) performed the same analysis on the single loop PHP concluding that *"..dominant frequencies of flow oscillations are in the range of 0.1 to 3.0 Hz with each quasi-steady state exhibiting a characteristic power spectrum.*" but, looking at the steady state when their PHP was working with a net circulation, it is also very hard to say what is the fluid oscillation dominant frequency (Figure 8.10). The authors state that the unidirectional flow circulation correspond to the best thermal performance, which is in line with the present experimental analysis: It seems that for simple geometries the "Circulating Heat Pipe" works better then "Pulsating Heat Pipe". It would be worthwhile to find a cost effective solution in order to force a multi-turn PHP to work in this circulating mode.

8.3.2.3 Heat transfer coefficient esteem and PHP overall performance

During Experiment 2 a pseudo steady state occur at each heat input level and this is a necessary condition for the local heat transfer coefficient calculation (Eq. 8.1):

$$\tilde{h}_{ev} = \frac{\dot{Q}}{\Delta T_{w-f} * A_{ev}} [W / m^2 K] \qquad (8.1)$$

where, ΔT_{w-f} is the difference between the wall and fluid temperatures, plotted in Figure 8.5. The local heat transfer coefficient in the evaporator zone (blue line) and its moving average (red line) are shown in Figure 8.11. The plot also corresponds to the five different flow patterns which have been recognized during the PHP operation and captured by the camera.

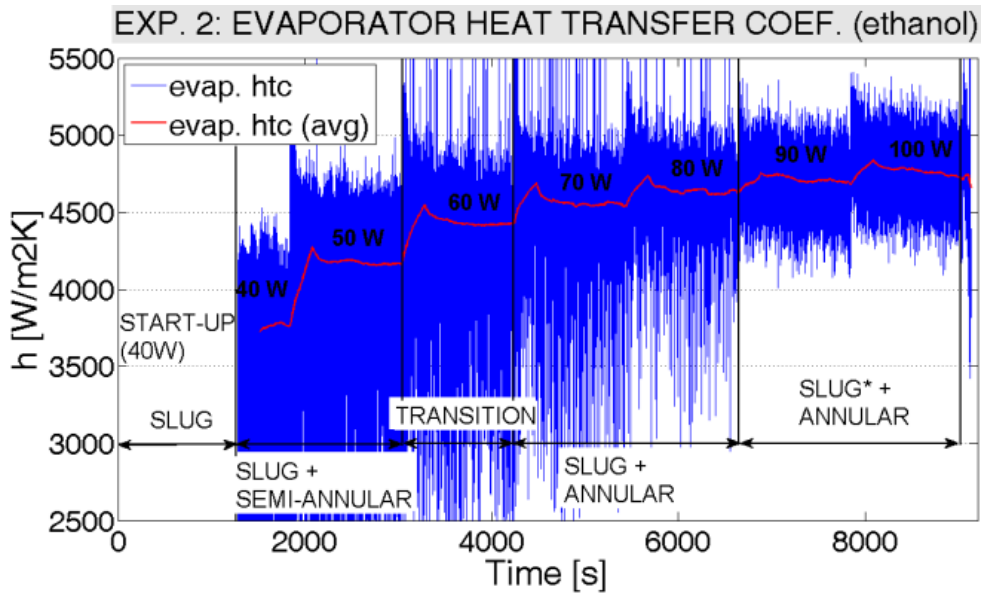

Figure 8. 11: Exp. 2, temporal evolution of local heat transfer coefficient and flow regimes for different heat inputs.

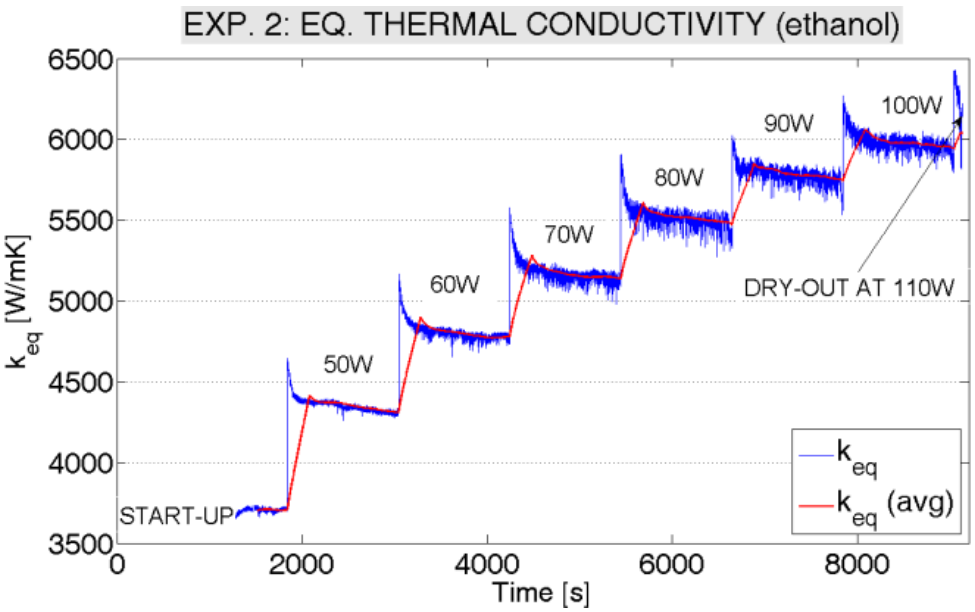

Figure 8. 12: Exp. 2, equivalent thermal conductivity over time for each heat input level.

In order to appreciate the overall performance of such device, the overall thermal conductivity has been calculated as follows:

$$k_{eq} = \frac{\dot{Q}}{A_{cr}} \frac{L_{tot}}{\Delta T_{w-c}} \tag{8.1}$$

where, $A_{cr} = n \cdot \pi \cdot d_{out}^{\ 2} / 4$ is the total radial PHP cross section area, L_{tot} is the distance between the hot source and the cooling one and ΔT_{w-c} is the difference between the wall temperature (hot side) and the average temperature of the cooling water in the condenser zone (cold side). When a net circulation occurs, the overall thermal conductivity is comprised between 4310 W/mK and 5920 W/mK which means that the device is working from 10 to 14 times better than pure copper (Figure 8.12).

This value can be easily compared with the thermal conductivity of the substrate material by defining a enhancement factor EF= k_{eq}/ k_s and also with the values extrapolated from other test-rigs in literature (Tab. 8.1). In spite of its simple geometry the present PHP shows an appealing performance.

Author	**material / support**	**L_{tot} [m]**	**n [-]**	**A_{cr} [m^2]**	**$\dot{Q}_{max}$ [W]**	**ΔT_{w-c} [K]**	**k_eq [W/m.K]**	**EF [-]**
Akachi (1993)	copper / tube d_{out} = 3mm	0,46	160	0,00113	2000	90	9038	22,6
Yang et al. (2008)	copper / tube d_{out} = 3mm	0,12	40	0,00028	400	123	1380	3,4
Yang et al. (2009)	aluminium / plate	0,18	66	0,00036	400	75	2666	10,6
Lin et al. (2009)	PDMS / plate	0,06	12	0,00112	8	80	5	29,0
Mameli et al. (2011)	copper / tube d_{out} = 4mm	0,2	4	5e-5	100	84	5920	14,8

Table 8. 1: Equivalent thermal conductivity and enhancement factors for different PHPs.

Another interesting information provided by Table 8.1 is that the polymeric PHP has a big potential in terms of enhancement factor. In order to improve also the overall thermal conductivity, which is still too low, it would be worthy to investigate PHPs made of high conductive polymers. In this case the substrate material thermal conductivity is in the order of 20W/mK. Supposing an EF = 20, the high conductive polymeric PHP could achieve an equivalent thermal conductivity comparable to the pure copper, with the advantages of being lighter and more flexible.

8.3.2.4 Flow pattern visualization

A set of images has been recorded in order to capture the different flow patterns. The visualization analysis is described here below:

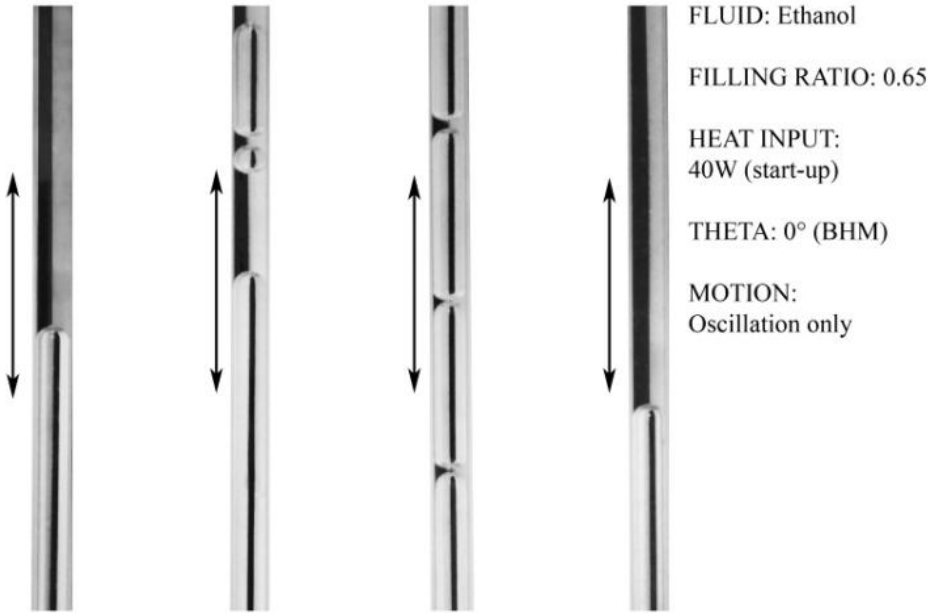

Figure 8. 13: Exp. 2, flow pattern during the start-up period (SLUG FLOW).

During the start-up (Figure 8.13) the flow pattern is completely slug in all the four branches and the flow motion is mainly oscillating. As mentioned for Experiment 1, this stage is characterized by merging of the smaller vapor plugs and formation of bigger ones.

When the heat input level is between 40 W and 50 W, net flow circulation becomes a constant feature. If a vapor plug coming from the a slug flow down-comer is passing through the heated section (i.e., left evaporator U-turn), a part of its liquid film evaporates into the vapor plugs and the resulting vapor pressure becomes strong enough to push the adjacent liquid slug through the next branch up to the condenser section. This is exactly what is happening in the second branch of Figure 8.8, where a liquid slug is being pushed against gravity by the vapour expansion occurring in the left evaporator U-turn.

Due to symmetry, the same phenomena are also happening in the third and fourth branches and, since the device is closed in a loop, the vapour pressure in the last branch pushes the fluid up to the condenser and then again down in the first branch (flow direction is explicitly shown in Figure 8.14).

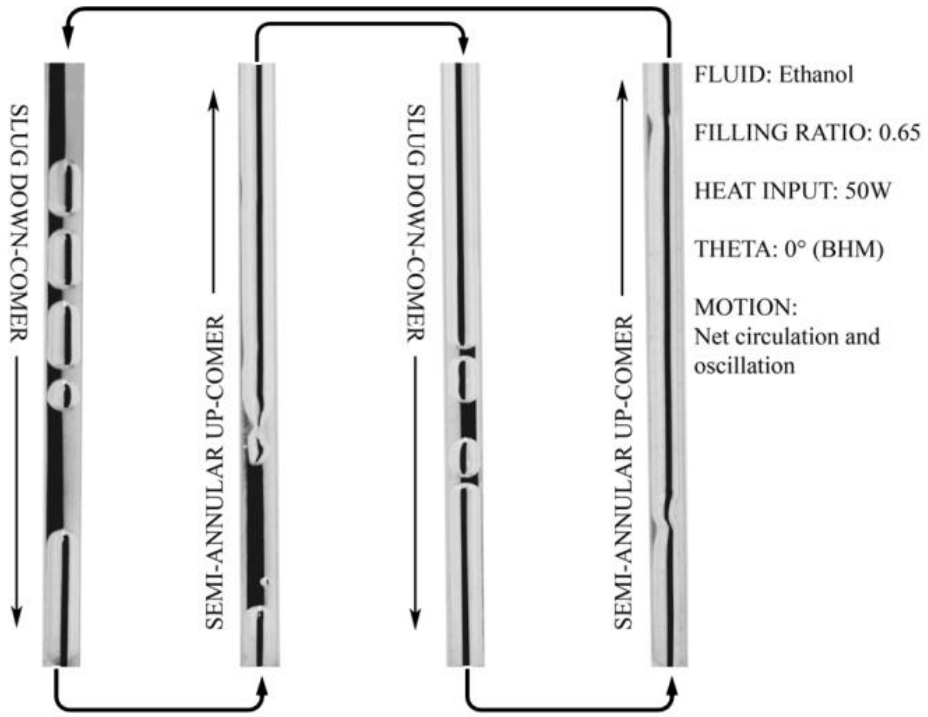

Figure 8. 14: Experiment 2, flow pattern during the pseudo steady state at 40-50W (SLUG + SEMI-ANNULAR).

Thus, owing to a well defined flow circulation, a conspicuous amount of liquid, may be in the form of liquid slugs or in the form of a thin liquid film surrounding each vapour plug, is always available in the evaporator section. Regarding the flow pattern, the first and third branches are always pure slug down-comer and the second and fourth branches are characterized by a semi-annular flow pattern, consisting of long annular periods alternated with some occasional transits of the liquid slugs. When the heat input level goes up to 60 W (Figure 8.15) a flow pattern transition occurs in the two up-comers.

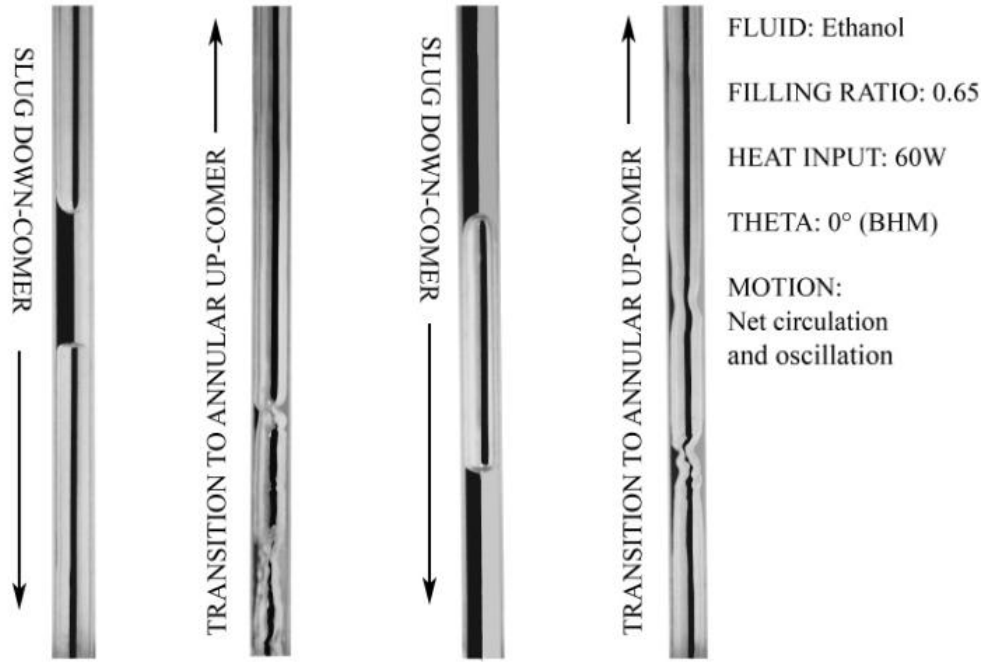

Figure 8. 15: Experiment 2, flow pattern during the pseudo steady state at 60W (TRANSITION from semi-annular to annular up-comers).

The vapour pressure, and the resulting inertia force thereof, in the evaporator section, is now able to break most of the liquid slug menisci bridges and therefore the flow pattern in the two up-comers is changing from semi-annular to pure annular. The liquid film is thick and wavy and a higher amount of the heat transfer is due to the latent heat of vaporization; a 6% gain of the local heat transfer coefficient is recorded with respect to the previous heat input level.

When the heat input level is augmented to 70 W (Figure 8.16) and then to 80 W the fluid, which is going up through the second and third branch, has reached the fully annular flow pattern. The liquid film is thinner and less surface waviness is recorded. The local heat transfer coefficient growth is pretty much lower with respect to the previous case (respectively 3.4% and 2.2%) confirming the fact that most of the local heat transfer is due to latent heat and the system is about to reach its maximum potential.

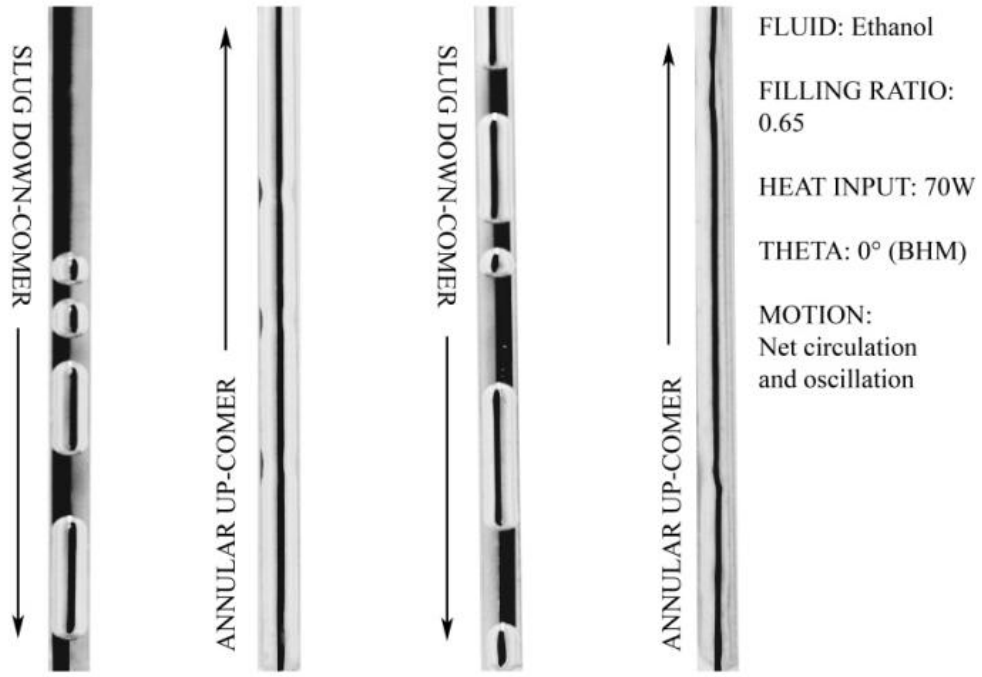

Figure 8. 16: Experiment 2, flow pattern during the pseudo steady state at 70W (SLUG + ANNULAR).

Finally, the last two stable pseudo steady states (90 W and 100 W) are again characterized by annular up-comers and slug-flow down-comers. In these cases, the liquid film in the two up-comers is very thin and, in spite the pressure signal is widely oscillating (liquid slugs in the third down-comer are getting deformed by the strong oscillation), the fluid temperature in the evaporator is not having large variations as before: the high heat power is now able to evaporate the great majority of the liquid coming from the slug down-comer without any vapor reflux (Figure 8.17).

The local heat transfer coefficient is now coming to an asymptotic value and the gain with respect to the previous cases is only around 1%. If the heat input level is increased to 110 W, the slug down-comers are not able to provide a sufficient amount of fresh liquid phase and an abrupt dry-out occurs in a few minutes.

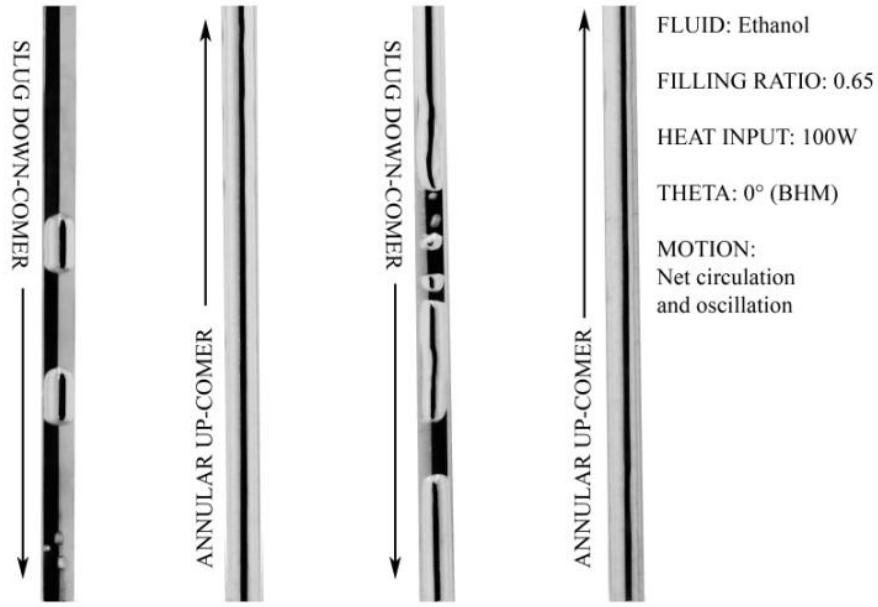

Figure 8. 17: Exp. 2, flow pattern during the pseudo steady state at 100W; SLUG (*unstable film thickness) + ANNULAR.

8.4 Azeotrope mixture of ethanol-water

Flow boiling of binary mixtures is inherently more complicated than the pure fluid counterpart since the composite thermo-physical properties of the mixture may substantially vary from those determined from linear mixing laws, and the bulk liquid contact angle, an important quantity required for understanding boiling mechanism, usually shows highly non-linear behavior with concentration. Very limited number of experimental studies on flow boiling of binary mixtures in mini and micro-channels exist. Most existing studies are limited to single-phase flow only. No explicit heat transfer equation and flow pattern studies are available for binary mixtures, especially of ethanol–water mixtures. In particular, the ethanol-water azeotrope (respectively ethanol 95.5% and water 4.5% by weight) has a constant boiling point which is lower than either of its constituents. Actually it boils at 78.2°C at ambient pressure while pure ethanol an pure water boils respectively at 78.4°C and 100°C (Figure 8.18).

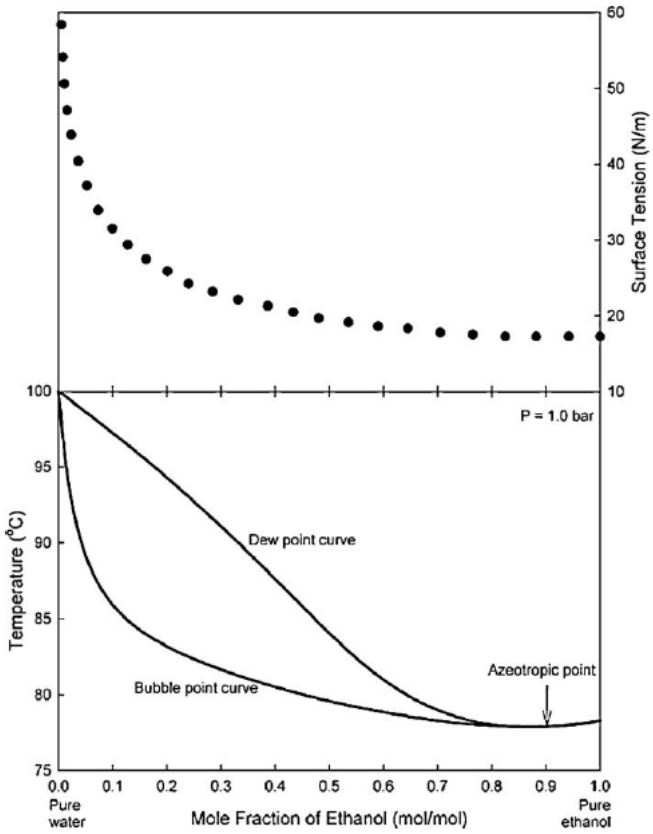

Figure 8. 18: Bubble point and dew point temperature and corresponding surface tension variation (top graph) of ethanol–water mixture.

In order to check if the mentioned mixture may enhance the PHP performance with respect to pure ethanol, the same experiment described in section 8.3 is performed with the azeotrope as working fluid. The overall thermal resistance has been estimated as follows:

$$R_{eq} = \frac{\left(T_{w,\max} - T_{\infty}\right)}{\dot{Q}_t}[W/mK] \tag{8.2}$$

where $T_{w,\max}$ is the evaporator wall temperature, T_{∞} is the cooling medium temperature and $\dot{Q}_t$ is the total heat input power. Figure 8.19 shows the temporal trend of the equivalent thermal resistance calculated by means of equation 8.3 for the PHP operated with pure ethanol (black line) and the PHP charged with the azeotrope (green line). As noticeable no sensible difference has been recorded.

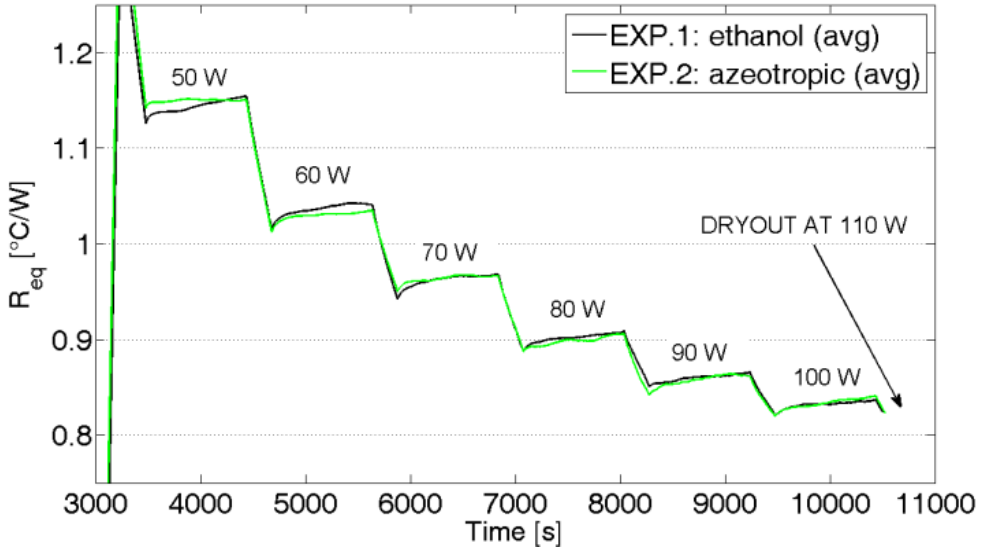

Figure 8. 19: Temporal evolution of the overall thermal resistance for different heat inputs.

Further research on binary and ternary mixture is needed to provide more data and check if the PHP efficiency may be enhanced.

8.5 Tilting angle analysis

The PHP filled with ethanol (constant filling ratio of 0.65) has been tested in six different orientations: from the Bottom Heat Mode (i.e. vertical position with the evaporator zone situated below the condenser) to the horizontal position with steps of 30°. For each position the heat input level is increased with step of 10W starting from the minimum heat input level which allows a stable behavior, to the maximum heat input level which causes the dry-out of the fluid inside the evaporator zone.

Wall and fluid temperature in the evaporator zone, the pressure signal and the different flow patterns in the transparent adiabatic zone, have been recorded. As per experiment 2 described in section 8.3, the following different flow patterns are recognized:

- S: fully slug flow in all the four branches (unstable behavior);
- SA: semi-annular flow in the two up-comers;
- T: transition from semi-annular to fully annular flow in the two up-comers;
- A: fully annular flow in the two up-comers;

- D: Dry-out condition and consequent.

The flow patterns occurring inside the PHP for each tilting angle and each heat input level are resumed in table 8.2.

		Heat input level [W]										
		10	20	30	40	50	60	70	80	90	100	110
Inclination	BHM	-	-	-	S	SA	T	A	A	A	A	D
	30°	-	-	S	SA	SA	T	A	A	A	A	D
	45°	-	S	SA	SA	T	A	A	A	D	-	-
	60°	-	S	SA	SA	T	A	A	D	-	-	-
	75°	S	SA	SA	T	A	D	-	-	-	-	-
	H	-	-	-	-	-	-	-	-	-	-	-

Table 8. 2: Flow patterns for each tilting angle and each heat input level.

It is noticeable that every orientation has its own working range in terms of heat input level. This range shrinks and shifts to lower heat power values as the tilting angle increases. The performance of PHP with such a simple geometry is heavily affected by the inclination with respect to gravity, indeed the device is not operating at all in the horizontal position

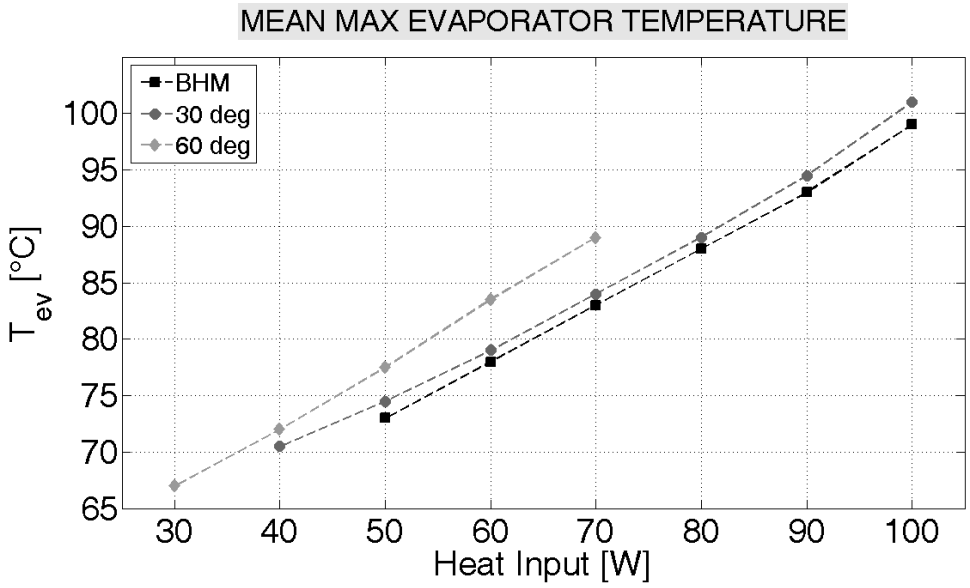

Figure 8. 20: Maximum mean evaporator temperature for tilting angles equal to BHM, 30° and 60°.

For sake of clarity the average value of the wall temperature at each heat input level is plotted only for three orientations, respectively BHM, 30° and

60° (Figure 8.20). The PHP tilted with an angle of 30° works at slightly higher temperatures resulting in a slightly lower equivalent thermal conductivity but the heat input working range is wider: the stable behavior is already active at 40W.

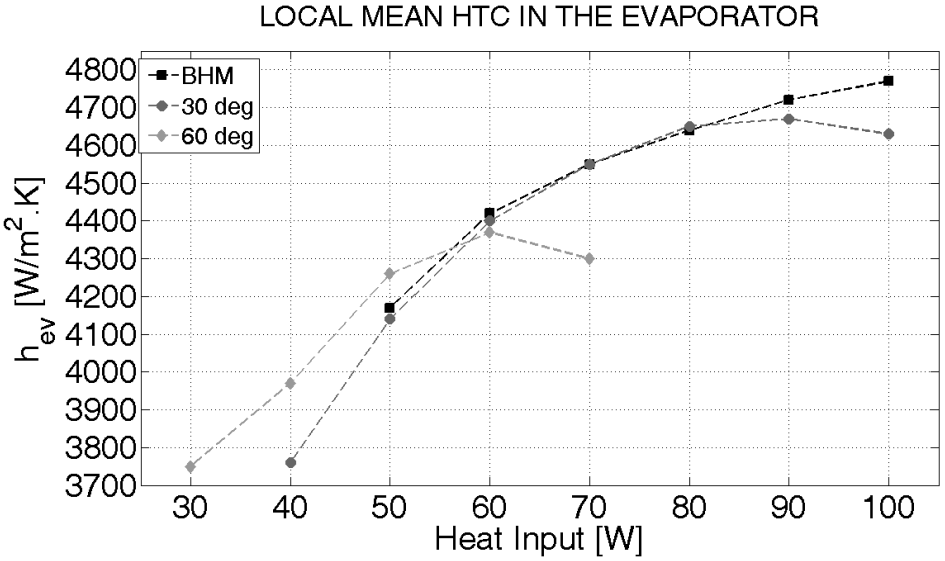

Figure 8. 21: Local heat transfer coefficient in the evaporator for tilting angles equal to BHM, 30° and 60°.

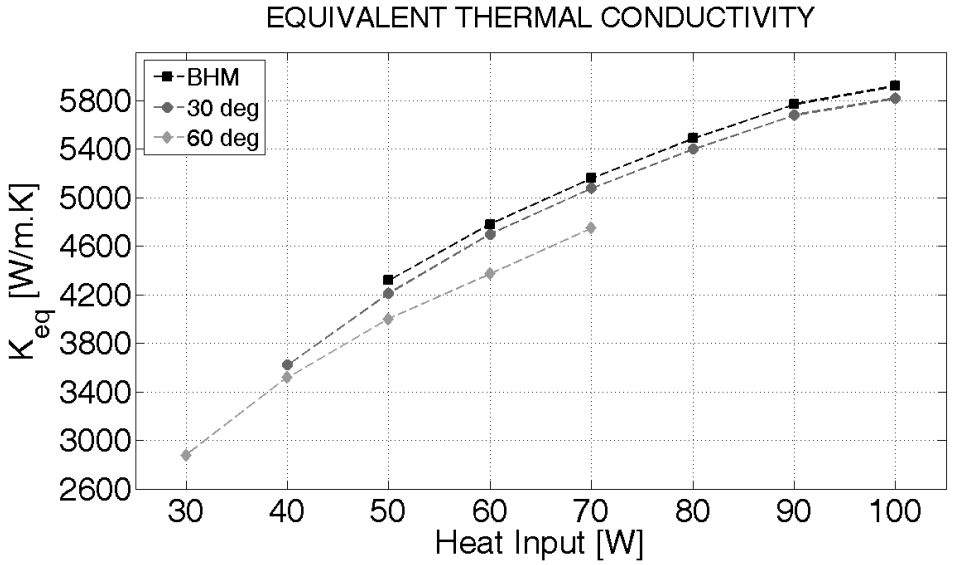

Figure 8. 22: Overall equivalent thermal conductivity for tilting angles equal to BHM, 30° and 60°.

Increasing the inclination to 60°, fluid is less assisted my gravity, its motion is less vigorous, resulting in poorer convective heat transfer as shown in Figure 8.22. The heat flux capability is lower (30W to 70W) but interestingly the device operation is stable at lower heat input levels.

Undoubtedly the target of a reliable and efficient heat transfer device is not to be affected by orientation. Increase the number of turns and decrease the channel internal diameter may help in achieving the target but may also inhibit the net circulation of the fluid inside the device. A parametric assessment on how to maintain the alternation of annular up-comer, slug down-comer working mode on a multi-turn CLPHP is one of the most outstanding cue for future experiments.

8.6 Model validation with actual experimental data

Finally the numerical model is set with the actual PHP test-rig characteristics listed in Table 8.3 and experiment 2 has been simulated.

INPUT PARAMETER	VALUE
Working fluid	ethanol
Tube material	copper
Internal tube diameter	2 [mm]
external tube diameter	4 [mm]
Inner surface roughness	5 [μm]
Evaporator section length	25 [mm]
Condenser section length	35 [mm]
Adiabatic section length	202 [mm]
filling ratio	0.65 [-]
Cooling medium temperature	15 [°C]
Cooling medium HTC	10000 [W/m^{2}K]
Initial temperature (fluid and wall)	27 [°C]
Initial number of Liquid Slugs and Vapour Plugs	6 [-]
Heat input levels	50,60,70,80,90,100 [W]
Computational time step	0.0001 [s]
Number of grids for the wall domain	1168 [-]
Number of grids for the liquid domain	225 [-]
Convergence criterion	0.001 [-]

Table 8. 3: Code input parameters.

Table 8.4 shows the chosen values for the vapor mass quality assigned to the vapor plugs travelling in the evaporator section (x_{ev}) and in the condenser section (x_{co}) on the basis of the numerical analysis performed in Chapter 5.

Q =50W (q"=6,4W/cm^2)		Q =60W (q"=7,7W/cm^2)		Q =70W (q"=9W/cm^2)		Q =80W (q"=10,3W/cm^2)		Q =90W (q"=11,5W/cm^2)		Q =100W (q"=12,8W/cm^2)	
x_{ev}	x_{co}	x_{ev}	x_{co}	x_{ev}	x_{co}	x_{ev}	x_{co}	x_{ev}	x_{co}	x_{ev}	x_{co}
0.05	0.005	0.1	0.01	0.3	0.05	0.4	0.1	0.5	0.1	0.6	0.2

Table 8. 4: Vapor mass quality of the vapor plugs travelling in the evaporator (x_{ev}) and condenser (x_{co}) for the different heat input levels.

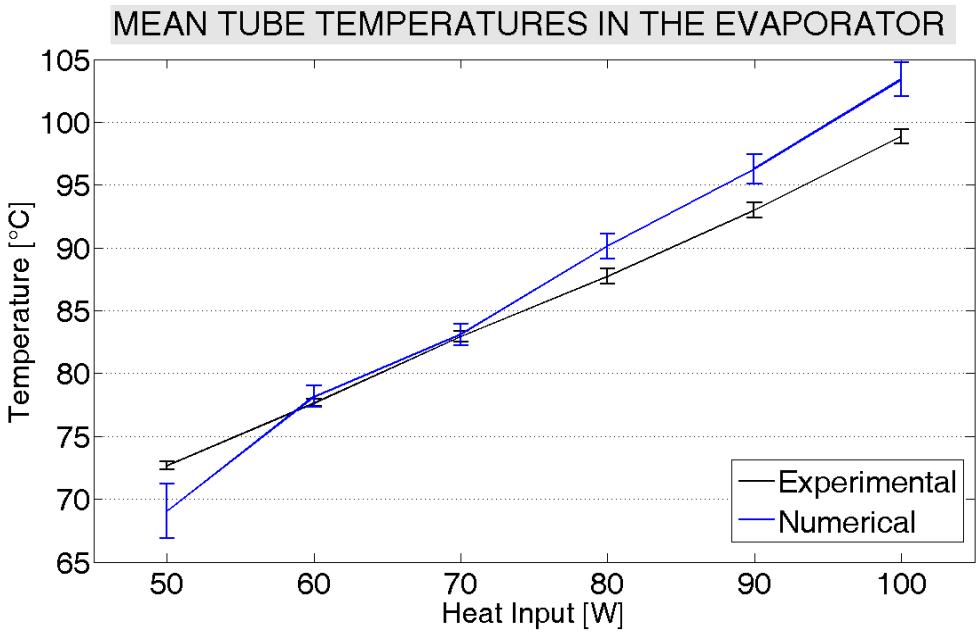

Figure 8. 23: Comparison between numerical results and actual experimental data.

The mismatch of the numerical results on the mean tube temperature in the evaporator is always less than 5°C (Figure 8.23). The higher error at high heat flux levels is due to two causes:

- Numerical: the model assumption of pure slug flow regime may not be suitable when the fluid up-comers goes fully annular. An experimental campaign should be devoted to investigate if the transition from semi-annular to annular flow occurs at a critical heat flux level so as to update the numerical model.

- Experimental: at high heat input level, in spite of the insulation, the evaporator releases part of the heat power to the environment, if the heat losses are not taken into account properly, temperatures are overestimated by the model.

The response to many other sensible parameters (i.e. tilting angle, filling ratio) still needs to be checked. Nevertheless the roadmap towards quantitative validation of the numerical model is traced and future work will be devoted to further improvements.

Chapter 9

Conclusions and future developments

9.1 Achievements of the research activity

The twofold aim of the present research activity is to develop a model for the thermal-hydraulic simulation of a Pulsating Heat Pipe and provide, by means of experiments, sensible data for the model validation.

The model by *Holley and Faghri (2005)* has been chosen as starting point and widely improved by means of a novel non homogeneous heat transfer approach where the vapor mass quality of the vapor plugs is the only tuning parameter *(Mameli et al. 2011a).* This model was able to simulate the thermal-hydraulic behavior of the single closed loop PHP built by *Khandekar et al. (2004)*. Fluid oscillation as well as flow reversals are reproduced and the error on the average temperature in the evaporator with respect to experimental data is always below 15%.

The effect of local pressure drops due to bends and U-turns on the thermal performance has been investigated and it has been proved that they should not be neglected by actual models *(Mameli et al. 2011b)*. Furthermore the local instabilities introduced by these minor losses seem to stabilize the PHP operation during critical tests (i.e. horizontal operation coupled high heat input level).

Finally a parametric numerical campaign has been performed in order to provide qualitative and quantitative validation on several parameters such as the heat input level, the number of turns, the inclination angle and the gravity level *(Mameli et al. 2012)*. The investigation shows that the horizontal and the microgravity operation are theoretically identical. If this clue will be proved experimentally, it will be possible to exploit ground experiment on horizontal PHP for the optimization of PHP for space applications. A real air cooled multi-turn PHP *(Yang et al. 2008)* has been simulated in vertical position for four different heat input levels and the error the average temperature in the evaporator with respect to experimental data is always below 10%.

A PHP experimental apparatus has been designed in the thermal physics laboratory of the University of Bergamo and assembled in the refrigeration and air condition laboratory at the Indian Institute of Technology Kanpur (IITK). The experimental campaign has been carried forward under the supervision of Prof. Sameer Khandekar at IITK and provided useful data regarding the flow patterns, the fluid local heat transfer coefficients in the evaporator zone, the overall PHP thermal performance and the stable working range *(Mameli et al. 2011c)*.

The roadmap for the quantitative validation of the numerical model have been drawn by comparing the actual experimental outcomes with the numerical results. The model is able to simulate the thermal-hydraulic behavior of PHPs with different geometries, boundary conditions and at different heat input levels.

Further modeling work will focus on reducing the number of assumptions in order to account for important physical phenomena such as the evaporative mass transfer from the liquid film, the advancing and receding contact angles at the liquid/vapor menisci interface. Finally the qualitative validation process must be carried forward by checking the model response to many other sensible parameters such as the number of turns, the tilting angle, the filling ratio.

When the present model will be capable of simulating a wide variety of PHPs operating in different modes, the target of developing a validated tool for the PHP assisted design will be fully achieved.

9.2 Future developments

It is clear that the PHP technology has not been considered for massive production yet because of its limited working range and inconstant thermal efficiency with respect to the standard HP so a big effort should be also devoted to improve the its reliability.

9.2.1 Thermal performance enhance by means of "Self-rewetting fluids"

Particular attention should be given to the so called "self-rewetting fluids" introduced by *Savino et al. (2009).* It is known that when a critical temperature gradient is exceeded, a slug thermo-capillary motion is established similarly to the case of a bubble migration in an unbounded liquid matrix. According to the theory, the slug velocity is given by:

$$U = -\frac{\Delta\sigma}{\Delta x}\frac{h^2}{r\mu} \tag{9.1}$$

where h is the liquid film thickness, r is the capillary radius, σ is the surface tension, μ is the dynamic viscosity of liquid and x is the axial direction.

Equation 9.1 shows that the velocity depends on the square of the film thickness between the capillary wall and the slug, linearly on the surface tension gradient and is inversely proportional to the diameter of the tube and to the dynamic viscosity of the liquid matrix.

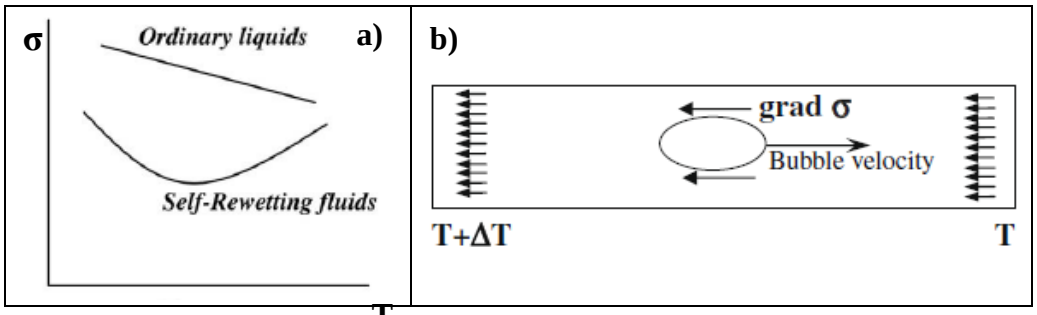

Figure 9. 1: a) surface tension behavior of ordinary liquids and self-rewetting fluids; b) anomalous bubble migration due to the inverse Marangoni effect in a self-rewetting fluid, *Savino et al. (2009).*

With ordinary liquids, since the surface tension is a decreasing function of the temperature, the slug moves in the direction of the temperature gradient, i.e. towards the warmer side. On the contrary, for a self-rewetting fluid with surface tension increasing with temperature, the slug is expected to move from the warmer to the cooler side (Figure 9.2).

The implementation of these binary and ternary mixtures of water and long-chain alcohols which seems to improve the thermal performance of the "wickless heat pipe" investigated by *Savino et al. (2009).*

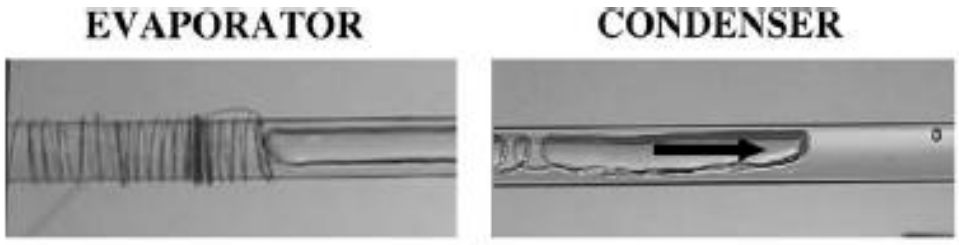

Figure 9. 2: anomalous bubble migration driven by the "inverse Marangoni effect" from the hot to the cold side in a 8mm I.D. glass tube, Savino (2009).

In order to explore and proof this concept an actual Pulsating Heat Pipe operated with self-rewetting fluids should be investigated.

9.2.2 Stabilization of the net fluid circulation

The present experimental work has shown that the fluid net circulation in the form of alternated slug down-comers and semi-annular up-comers ensures a stable and efficient working mode. Two possible clues for enhancing the fluid net circulation, are proposed here below.

The first method consists in altering the inner tube surface wettability in order to promote evaporation and condensation only in some desired strategic locations. In particular an alternated pattern of hydrophobic coatings may be deposed in the condenser section in such a way that the liquid phase may easily slide towards the uncoated evaporator section which is hydrophilic instead (pink color in Figure 9.3). The simpler and cost effective solution can be also explained referring to Figure 9.3.

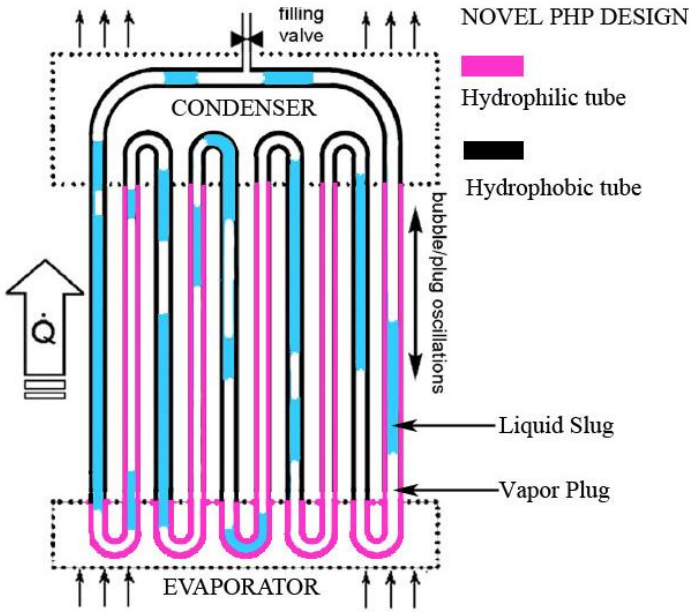

Figure 9. 3: Novel Pulsating Heat Pipe design based on hydrophilic and hydrophobic tubes.

In this case the pink colored channels are externally insulated by means of a plastic cover and the whole zone above the evaporator is fan cooled. Thus, axial heat conduction through the tube section keeps the insulated channels warmer and the up-coming semi-annular flow regime is promoted, while the down-coming slug flow is promoted in the cooled channels (black color).

Annex I

Numerical code for the thermal-hydraulic simulation of PHPs

Introduction

The present numerical code has been developed by Holley and Faghri (2005) and improved by the author. All the modifications and implementations are indicated with a grey background.

```
!     ...........................................................
!     BH_MM_PHP:
!     Brian Holley_Mauro Mameli(modifications)_Pulsating Heat Pipe.
!     Numerical Model Developed in Fortran 90
!     ...........................................................

!     ---------------------NOMENCLATURE (alphabetical order)-----------------
!     Variables followed by m: calculated at mean wall and fluid temperatures
!     bn = number of U-turns, [-];
!     Ca, Cb: Simpson rule coefficients, a previous b next;
!     cc: convergence criterion;
!     continue: whether this simulation continues a previous one;
!     converge: 1 if converged 0 if not;
!     Cptw: tube wall material specific heat, [J/kg.K];
!     Ct(min): (minimum) time step refinement factor;
!     D: increment change in;
!     del(tw/wk/lf):(tube wall/wick/liquid film) thickness, [m];
!     DP: Pressure difference(DPa DPc DPd DPg Dps DPv): pressure drops
!         due to slug accleleration, capillarity, dilatation, gravity,
!         shear, vapor, bends [Pa];
!     Dt: time step, [s];
!     DTmax: maximum plug temperature change between time steps, [K];
!     Dz, length step, [m];
!     Dza & Dzb: Convergence steps, [m];
!     Ea,Eb,Eo: Vapor plug energy iteration values, [J];
!     flag: whether to repeat with finer time step
!     g: gravity, [m/sq.s];
!     gamma: fill ratio;
!     h: heat transfer coefficient between wall and fluid, [W/sq.m.K];
!     hc: condensation heat transfer coefficient, [W/sq.m.K];
!     hcex: initial value for the condenser external htc, [W/sq.m.K];
!     hcex2: condenser external htc based on the heat input, [W/sq.m.K];
!     hm: mean heat transfer coefficient between wall and fluid, [W/sq.m.K];
!     hs: sensible heat transfer coefficient, [W/sq.m.K];
!     IIA: integral reciproical of A along flow path, [1/m];
!     kw: wall conductivity, [W/m.K];
!     K: (90,180,i,d,m): local pressure losses coefficients, [..];
!     L: path length, [m];
!     Lev: half evaporator length per loop [m];
!     Lc: half condenser length per loop [m];
!     Lp: plug length, [m];
!     ma,mb: convergence mass increments, [kg];
!     mdot: slug mass flow rate, [kg/s];
!     ml: liquid mass in heat pipe, [kg];
!     mom: total liquid momentum, [kg.m/s];
!     ms,mv: slug/plug mass [kg]
!     msev,mvev: liquid and vapor total mass in the evaporator section [kg]
!     n: maximum allowable number of slugs/plugs;
!     n(b/f): indices of (back/front) slug grids;
!     nk: index of the total n° of bends, nk = bn + 2
!     np: number of vapor plugs/liquid slugs;
!     n(s/w): number of (slug/wall) grids;
!     NuGN: Nusselt number Gnlieski correlation (1976);
!     NuDB: Nusselt number Dittus-Boelter Correlation;
!     NuST: Nusselt number Sieder-Tate Correlation;
!     Nu: Nusselt number;
!     Pr: Prandtl number;
!     qo: Interpolated heat flux, [W/sq.m];
```

```
!     Qhf/Qwp: heat rate from wall to liquid grids/vapor plugs, [W];
!     Qc(b,d,f): (back,inside,front) meniscus conduction from slug to plug, [W];
!     qin: evaporator heat flux, W/sq.m; Qt: total heat input, [W];
!     qwf(m): (mean) heat flux rate from wall to fluid per unit length, [W/sq.m];
!     R: ideal gas constant for water, [J/Kg.K];
!     Re: Reynolds number;
!     rfs: surface roughness features, [m];
!     rhotw: tube wall density, [kg/cu.m];
!     Sa, Sb: Integral values for two iterations, a new b old;
!     Ta,Tb: iteration temperature values, [K];
!     temp: temporary value; tend: final (stop) time, [s];
!     Tfm: mean fluid temperature, [K];
!     theta_in: inclination angle, (0°=BHM ; 90°=Horizontal; 180°=THM
!               allowed delta_theta_in = 1°), [deg];
!     Ti: initial temperature, [K];
!     Tinf: external temperature at condenser, [K];
!     tnow: elapsed time, [s];
!     To: interpolated temperature, [K];
!     Tp(a): (anticipated) back meniscus (plug) temperature, [K];
!     Ts: slug grid temperatures, [K];
!     twrite: write time, [s];
!     Tw(m): (mean) wall grid temperature, [K];
!     VarD/VarI: store double precision and integer variables if
!                iteration needs repeating with smaller time step;
!     Vp(a): (anticipated for next step) plug volume, [cu.m];
!     Vs: liquid slug volume [cu.m]
!     Vt: total path volume, [cu.m];
!     xqualco: istantaneous vapor mass quality in the vapor plug
!                passing through the condenser section [kg_vap/kg_tot]
!     xqualev: istantaneous vapor mass quality in the vapor plug
!                passing through the evaporator section [kg_vap/kg_tot]
!     z(1/2): dummy z variables, [m];
!     z(b/f/s): location of (back meniscus/front meniscus/slug grid
!               boundaries), [m];

!     ------------------------------------------------------------------------
!     CHOOSEFLUID VARIABLES MODULE
!     ------------------------------------------------------------------------
!     Choose one fluid from the list below and write it in 'fn'
!     which stays for "fluid name".
      module fluid
      implicit none
      integer, parameter :: n_coef = 6 , n_cond = 2
      integer :: status
            double precision
       coef_cpl(n_coef),cond_cpl(n_cond),coef_cpv(n_coef),cond_cpv(n_cond), &
       coef_hl(n_coef),cond_hl(n_cond),coef_hg(n_coef),cond_hg(n_cond), &
       coef_kl(n_coef),cond_kl(n_cond),coef_kv(n_coef), &
       cond_kv(n_cond),coef_mul(n_coef),cond_mul(n_cond),coef_muv(n_coef), &
       cond_muv(n_cond),coef_Psat(n_coef),cond_Psat(n_cond), &
       coef_rhol(n_coef),cond_rhol(n_cond),coef_rhov(n_coef),cond_rhov(n_cond), &
       coef_sigma(n_coef),cond_sigma(n_cond),coef_Tsat(n_coef),cond_Tsat(n_cond), &
       Pcr
      character(8), parameter :: fn = 'ethanol'
!       choose between
!       - 'water':    278.15-578.15 [K]
!       - 'ethanol':  255.0-475.0   [K]
!       - 'C6F14':    275.0-425.0   [K]
!       - 'R123':     200.0-440.0   [K]
!       - 'methanol': 220.0-470.0   [K]
!       - 'R134a':    170.0-360.0   [K]
!       - 'ammonia':  220.0-380.0   [K]
```

```
      end module

!     ------------------------------------------------------------------
!     INPUT PARAMETERS MODULE
!     ----------------------MM/15-09-2009-------------------------------
      module inputparameters
      implicit none
      double precision, parameter :: &
      cc = 1.0d-3, Cptw = 389.0, Ctmin = 1.0d-6, deltw = 0.001, delwk = 0.0005, &
      dellf = 0.00005, Dt = 1.0d-4, DTmax = 10.0, Dtwrite = 1.0d-1, g = 9.81, &
      gamma = 0.65, hcex = 10000, kw = 400.0, L = 1.168, L1 = 0.260, Lev = 0.025,&
      Lc = 0.035, pi = 3.1415927, Qt = 80.0, R = 461.9, rb = 0.01, rfs = 5.0d-6, &
      rhotw = 8960.0, tend = 600, theta_in = 0, Ti = 300.15, Tinf = 288.15, &
      xqualev = 0.3, xqualco =0.05, xqual0 = 0.0
      integer, parameter :: continue = 0, n = 100, nk = 5, ns = 225, nw = 1168, &
      bn = 3
      integer flag,j,nb(n),nf(n),np,VarI(n,3)
      double precision Ct,Dmdot(n),DPa(n),DPc(n),DPd(n),DPg(n),DPK(nw), &
      DPs(n),DPv(n),Dpbl(n),LOSSID(nw),LSid(nw),h(nw),hm(nw),ml,mdot(n),qin, &
      qwf(nw),qwfm(nw),Qcb(n),Qcd(ns),Qcf(n),Qhf(ns),Qwp(n),Tfm(nw), &
      tnow,Tw(nw),Twm(nw),Tp(n),Ts(ns),twrite,VarD(n,4),Vp(n),Vs(n), &
      Vt,zb(n),zf(n),zs(ns),Ls(n),ms(n),msev,mv(n),mvev,DP(nw)
      end module

!     ------------------------------------------------------------------
!     MAIN PROGRAM
!     ------------------------------------------------------------------
      program bphp
      use fluid
      use inputparameters
      implicit none
!     --------------------call choosefluid subroutine-------------------
!     Reads the fitting coefficient from the matlab output files,
!     get the coefficients and update the fitting general
!     functions with the chosen fluid.
      call choosefluid(coef_cpl,cond_cpl,coef_cpv,cond_cpv,coef_hl,cond_hl, &
                       coef_hg,cond_hg,coef_kl,cond_kl,coef_kv,cond_kv, &
                       coef_mul,cond_mul,coef_muv,cond_muv,coef_Psat,cond_Psat, &
                       coef_rhol,cond_rhol,coef_rhov,cond_rhov,coef_sigma, &
                       cond_sigma, coef_Tsat,cond_Tsat,Pcr)
      pause
!     ------------------------------------------------------------------
      call testprops
      call setvalues(Ct,Dmdot,DPa,DPbl,DPc,DPd,DPg,DPs,mdot,nb,nf,np,tnow,hm,DPK, &
      qwfm,Twm,Tfm)
      call meniscipositions(ml,nb,nf,np,Vt,zb,zf)
      call initialT(np,Tp,Ts,Tw)
      call evaporatorheatperlength(qin)
      call newpositions(Ct,Dmdot,mdot,ml,nb,nf,np,Tp,Ts,zb,zf,zs)
      if (continue.eq.1) call previous &
      (ml,mdot,nb,nf,np,qwfm,Tfm,tnow,Tp,Ts,Tw,Twm,zb,zf,zs)
      call plugvolume(Ct,np,Vp,zb,zf)
      twrite = tnow
      do while (tnow.le.tend)
      call refinet(Ct,mdot,nb,nf,np,Tp,VarD,VarI,Vp,zb,zf)
      call gravity(Ct,DPg,nb,nf,np,Tp,Ts,zb,zf,zs)
      call sheartotal(Ct,DPs,mdot,nb,nf,np,Tp,Ts,zb,zf,zs)
       if (tnow.gt.0.1) then
       call bendlossestot(Ct,DPbl,DPK,Lossid,LSid,mdot,nb,nf,np,Tp,Ts,zb,zf,zs)
       endif
      call pressurebalance(DPa,DPbl,DPc,DPd,DPg,DPs,DPv,mdot,np,Tp,zb,zf)
1     call mdotchange(Ct,Dmdot,DPa,mdot,nb,nf,np,VarD,VarI,Vp,zb,zf)
```

```
      call newpositions(Ct,Dmdot,mdot,ml,nb,nf,np,Tp,Ts,zb,zf,zs)
      call slugmerge(mdot,nb,nf,np,Tp,Vp,zb,zf)
      call heatwalltofluid(h,mdot,nb,nf,np,qwf,Tp,Ts,Tw,zb,zf,zs)
      call heatwalltoplug(Ct,nb,nf,np,qwf,Qwp,zb,zf)
      call heatplugtoslug(nb,nf,np,Qcb,Qcf,Tp,Ts,zb,zf,zs)
      call plugtemperature(Ct,flag,np,Qcb,Qcf,Qwp,Tp,Vp,Vt,zb,zf)
      if (flag.eq.1) goto 1
      call walltemperature(Ct,qin,qwf,Tw)
      call slugconduction(nb,nf,np,Qcb,Qcd,Qcf,Tp,Ts,zb,zf,zs)
      call heatwalltoslug(Ct,nb,nf,np,Qhf,qwf,Tp,Ts,zb,zf,zs)
      call slugtemperature(Ct,ml,Qcd,Qhf,Ts)
      call plugform(mdot,nb,nf,np,Tp,Ts,Vp,zb,zf,zs)
      call timeaverage(Ct,h,hm,nb,nf,np,qwf,qwfm,Tfm,tnow,Tp,Ts, &
      Tw,Twm,zb,zf,zs)
      tnow = tnow + Dt*Ct
      if (twrite+Dtwrite.le.tnow) then
      call output(Dmdot,DPa,DPbl,DPc,DPd,DPg,DPs,DPv,h,hm,ml,mdot,nf,nb, &
      np,qwf,qwfm,Tfm,tnow,Tp,Ts,Tw,Twm,zb,zf,zs)
      twrite = twrite+Dtwrite
      endif
      enddo
      end program

!     ------------------------------------------------------------------
!     FUNCTIONS
!     ------------------------------------------------------------------
!     ..................................................................
      double precision function A(z1)
!     User defined cross sectional area profile, sq.m
      use inputparameters, only : pi
      implicit none
      double precision dh, z1
      A = pi*dh(z1)**2.0/4.0
      return
      end
!     ..................................................................
      integer function between(a,b,c)
!     Determines if b lies between a and c on a loop
      implicit none
      double precision a,b,c
      if (a.lt.c.and.(a.le.b.and.b.le.c)) then
      between = 1
      elseif (c.lt.a.and.(a.le.b.or.b.le.c)) then
      between = 1 ! b lies between a and c
      else
      between = 0 !b does NOT lie between a and c
      endif
      return
      end
!     ..................................................................
      double precision function Cf(Re,z)
!     Evaluates Fanning friction factor based on Reynolds number for
!     laminar and turbulent (Colebrook) formula
      use inputparameters, only : cc, rfs
      implicit none
      double precision Cfa, dh, Re, Rea, z
      Rea = dabs(Re)
      if (Rea.lt.0.5) then
      Rea = 0.5
      endif
      if (Rea.le.2000) then
      Cf = 16.0/Rea
```

```
      else
      Cf = 0.0
      Cfa = 0.312*Rea**(-0.25)
      do while ((Cfa-Cf)/Cfa.gt.cc)
      Cf = Cfa
      Cfa = &
      (1.0/(1.74-2.0*dlog10(2.0*rfs/dh(z)+18.7/Rea/Cf**0.5)))**2.0
      enddo
      Cf = Cfa/4.0 !Convert from Darcy to Fanning friction factor
      if (Cf.gt.16.0/2000.0) Cf = 16.0/2000.0 !Transition region
      endif
      return
      end
!     .....................Mod.MM/17-09-2009.................................
      double precision function dh(z1)
!     User defined hydraulic diameter profile, m
      use inputparameters, only : pi
      implicit none
      double precision Dd, dn, z1, z2
      dh =0.002 ! nominal diameter
!      dn = 0.00185 ! nominal diameter
!      Dd = 0.00015 ! diamter deviation from nominal
!      z2 = z1
!      do while (z2.ge.0.250)
!      z2 = z2-0.250
!      enddo
!      if (z2.le.0.005) then
!      dh = dn + Dd*(sin(z2*pi/2.0/0.005))
!      elseif (0.005.le.z2.and.z2.le.0.120) then
!      dh = dn + Dd
!      elseif (0.120.le.z2.and.z2.le.0.130) then
!      dh = dn + Dd*cos((z2-0.120)*pi/0.01)
!      elseif (0.130.le.z2.and.z2.le.0.245) then
!      dh = dn - Dd
!      else
!      dh = dn + Dd*sin(((z2-0.245)/0.005-1.0)*pi/2.0)
!      endif
!      return
      end
!     ...................................................................
      integer function ninc(j,nb,nf)
!     determine number of liquid cells between nb and nf inclusive
      use inputparameters, only : n, ns
      implicit none
      integer j, nb(n), nf(n)
      if (nb(j).le.nf(j)) then
      ninc = nf(j)-nb(j)+1
      else
      ninc = nf(j)+ns-nb(j)+1
      endif
      return
      end
!     ...................................................................
      double precision function p(z)
!     User defined perimeter function of length, m
      use inputparameters, only : pi
      implicit none
      double precision dh, z
      p = pi*dh(z)
      return
      end
!     ...................................................................
```

```
      integer function plug(np,z,zb,zf)
!     Determines what plug point z lies on, otherwise 0
      use inputparameters, only : n
      implicit none
      integer i, j, np
      double precision z, zb(n), zf(n)
      j = 1
      plug = 0
      do while (j.le.np.and.plug.eq.0)
      i = mod(j+np-2,np)+1
      if (zf(i).lt.z.and.z.lt.zb(j)) then
      plug = j
      elseif (zb(j).lt.zf(i).and.(zf(i).lt.z.or.z.lt.zb(j))) then
      plug = j
      endif
      j = j + 1
      enddo
      return
      end
!     ................................................................
      double precision function rcap(z)
!     User defined capillary radius profile, m
      implicit none
      double precision dh, z
      rcap = dh(z)/2.0
      return
      end

!     ................................................................
      integer function slug(np,z,zb,zf)
!     Determines what slug point z lies on, otherwise 0
      use inputparameters, only : n
      implicit none
      integer j,np
      double precision z, zb(n), zf(n)
      j = 1
      slug = 0
      do while (j.le.np.and.slug.eq.0)
      if (zb(j).le.z.and.z.le.zf(j)) then
      slug = j
      elseif (zf(j).le.zb(j).and.(zb(j).le.z.or.z.le.zf(j))) then
      slug = j
      endif
      j = j + 1
      enddo
      return
      end
!     ................................................................
      double precision function wrap(z) ! to wrap = avvolgere
!     Used to allow slugs and plugs to pass between the length and
!     origin, m
      use inputparameters, only : L
      implicit none
      double precision z
      if (0.le.z.and.z.lt.L) then
      wrap = z
      elseif (z.lt.0.0) then
      wrap = z + L
      elseif (z.eq.L) then
      z = 0.0
      elseif (L.lt.z) then
      wrap = z - L
```

```
      endif
      return
      end

!     ------------------------------------------------------------------
!     FITTING FUNCTIONS FOR FLUID PROPERTIES
!     ------------------------------------------------------------------
!     ..................................................
      double precision function Cpl(Tsat,coef_Cpl,cond_Cpl)
!     Specific Heat of saturated liquid as a function of
!     temperature from NIST-REFPROP-8.0 data with matlab
!     polynomial fit coefficients and conditioning, J/kg
      implicit none
      integer j
      double precision coef_Cpl, cond_Cpl, Tsat
      dimension coef_Cpl(6), cond_Cpl(2)
      j = 1
      Cpl = 0.0
      do while (j.le.6)
      Cpl = Cpl + coef_Cpl(j)*((Tsat-cond_Cpl(1))/cond_Cpl(2))**(6-j)
      j = j+1
      enddo
      return
      end
!     ..................................................
      double precision function Cpv(Tsat,coef_Cpv,cond_Cpv)
!     Specific Heat of saturated vapor as a function of
!     temperature from NIST-REFPROP-8.0 data with matlab
!     polynomial fit coefficients and conditioning, J/kg
      implicit none
      integer j
      double precision coef_Cpv, cond_Cpv, Tsat
      dimension coef_Cpv(6), cond_Cpv(2)
      j = 1
      Cpv = 0.0
      do while (j.le.6)
      Cpv = Cpv + coef_Cpv(j)*((Tsat-cond_Cpv(1))/cond_Cpv(2))**(6-j)
      j = j+1
      enddo
      return
      end
!     ..........................................................
      double precision function hl(Tsat,coef_hl,cond_hl)
!     Enthalpy of saturated liquid as a function of temperature
!     from NIST-REFPROP-8.0 data with matlab polynomial fit
!     coefficients and conditioning, J/kg
      implicit none
      integer j
      double precision coef_hl, cond_hl, Tsat
      dimension coef_hl(6), cond_hl(2)
      j = 1
      hl = 0.0
      do while (j.le.6)
      hl = hl + coef_hl(j)*((Tsat-cond_hl(1))/cond_hl(2))**(6-j)
      j = j+1
      enddo
      return
      end
!     ..........................................................
      double precision function hg(Tsat,coef_hg,cond_hg)
!     Enthalpy of saturated vapor as a function of temperature
!     from NIST-REFPROP-8.0 data with matlab polynomial fit
```

```
!     coefficients and conditioning, J/kg
      implicit none
      integer j
      double precision coef_hg, cond_hg, Tsat
      dimension coef_hg(6), cond_hg(2)
      j = 1
      hg = 0.0
      do while (j.le.6)
      hg = hg + coef_hg(j)*((Tsat-cond_hg(1))/cond_hg(2))**(6-j)
      j = j+1
      enddo
      return
      end
!     ..................................................................
      double precision function kl(Tsat,coef_kl,cond_kl)
!     Thermal conductivity of saturated liquid as a function of
!     temperature from NIST-REFPROP-8.0 data with matlab polynomial
!     fit coefficients and conditioning, W/m.K
      implicit none
      integer j
      double precision coef_kl, cond_kl, Tsat
      dimension coef_kl(6), cond_kl(2)
      j = 1
      kl = 0.0
      do while (j.le.6)
      kl = kl + coef_kl(j)*((Tsat-cond_kl(1))/cond_kl(2))**(6-j)
      j = j+1
      enddo
      return
      end
!     ..................................................................
      double precision function kv(Tsat,coef_kv,cond_kv)
!     Thermal conductivity of saturated vapor as a function of
!     temperature from NIST-REFPROP-8.0 data with matlab polynomial
!     fit coefficients and conditioning, W/m.K
      implicit none
      integer j
      double precision coef_kv, cond_kv, Tsat
      dimension coef_kv(6), cond_kv(2)
      j = 1
      kv = 0.0
      do while (j.le.6)
      kv = kv + coef_kv(j)*((Tsat-cond_kv(1))/cond_kv(2))**(6-j)
      j = j+1
      enddo
      return
      end
!     ..................................................................
      double precision function mul(Tsat,coef_mul,cond_mul)
!     Viscosity of saturated liquid as a function of temperature
!     from NIST-REFPROP-8.0 data with matlab polynomial fit
!     coefficients and conditioning, Pa.s
      implicit none
      integer j
      double precision cond_mul, coef_mul, Tsat
      dimension coef_mul(6), cond_mul(2)
      j = 1
      mul = 0.0
      do while (j.le.6)
      mul = mul + coef_mul(j)*((Tsat-cond_mul(1))/cond_mul(2))**(6-j)
      j = j+1
      enddo
```

```
      return
      end
!     ..............................................................
      double precision function muv(Tsat,coef_muv,cond_muv)
!     Viscosity of saturated vapor as a function of temperature
!     from NIST-REFPROP-8.0 data with matlab polynomial fit
!     coefficients and conditioning, Pa.s
      implicit none
      integer j
      double precision cond_muv, coef_muv, Tsat
      dimension coef_muv(6), cond_muv(2)
      j = 1
      muv = 0.0
      do while (j.le.6)
      muv = muv + coef_muv(j)*((Tsat-cond_muv(1))/cond_muv(2))**(6-j)
      j = j+1
      enddo
      return
      end
!     ..............................................................
      double precision function Psat(Tsat,coef_Psat,cond_Psat)
!     Pressure of saturated liquid as a function of temperature
!     from NIST-REFPROP-8.0 data with matlab polynomial fit
!     coefficients and conditioning, Pa
      implicit none
      integer j
      double precision coef_Psat, cond_Psat, Tsat
      dimension coef_Psat(6), cond_Psat(2)
      j = 1
      Psat = 0.0
      do while (j.le.6)
      Psat = Psat + coef_Psat(j)*((Tsat-cond_Psat(1))/cond_Psat(2))**(6-j)
      j = j+1
      enddo
      Psat = dexp(Psat)
      return
      end
!     ..............................................................
      double precision function rhol(Tsat,coef_rhol,cond_rhol)
!     Density of saturated liquid as a function of temperature
!     from NIST-REFPROP-8.0 data with matlab polynomial fit
!     coefficients and conditioning, kg/cu.m
      implicit none
      integer j
      double precision coef_rhol, cond_rhol, Tsat
      dimension coef_rhol(6), cond_rhol(2)
      j = 1
      rhol = 0.0
      do while (j.le.6)
      rhol = rhol + coef_rhol(j)*((Tsat-cond_rhol(1))/cond_rhol(2))**(6-j)
      j = j+1
      enddo
      return
      end
!     ..............................................................
      double precision function rhov(Tsat,coef_rhov,cond_rhov)
!     Density of saturated vapor as a function of temperature
!     from NIST-REFPROP-8.0 data with matlab polynomial fit
!     coefficients and conditioning, kg/cu.m
      implicit none
      integer j
      double precision coef_rhov, cond_rhov, Tsat
```

```
      dimension coef_rhov(6), cond_rhov(2)
      j = 1
      rhov = 0.0
      do while (j.le.6)
      rhov = rhov + coef_rhov(j)*((Tsat-cond_rhov(1))/cond_rhov(2))**(6-j)
      rhov = dabs(rhov)
      j = j+1
      enddo
      return
      end
!     ..............................................................
      double precision function sigma(Tsat,coef_sigma,cond_sigma)
!     Surface Tension of saturated liquid as a function of
!     temperature from NIST-REFPROP-8.0 data with matlab polynomial
!     fit coefficients and conditioning, N/m
      implicit none
      integer j
      double precision cond_sigma, coef_sigma, Tsat
      dimension coef_sigma(6), cond_sigma(2)
      j = 1
      sigma = 0.0
      do while (j.le.6)
      sigma = sigma + coef_sigma(j)*((Tsat-cond_sigma(1))/cond_sigma(2))**(6-j)
      j = j+1
      enddo
      return
      end
!     ..............................................................
      double precision function Tsat(P,coef_Tsat,cond_Tsat)
!     Temperature of saturated liquid as a function of pressure from
!     NIST-REFPROP-8.0 data with matlab polynomial fit coefficients
!     and conditioning, K
      implicit none
      integer j
      double precision coef_Tsat, cond_Tsat, P
      dimension coef_Tsat(6), cond_Tsat(2)
      j = 1
      Tsat = 0.0
      do while (j.le.6)
      Tsat = Tsat + coef_Tsat(j)*((dlog(P)-cond_Tsat(1))/cond_Tsat(2))**(6-j)
      j = j+1
      enddo
      return
      end

!     ---------------------------------------------------------------------
!     GEOMETRY BUILDING FUNCTION
!     ---------------------------------------------------------------------
!     ............. MM/maj-2010.....................................
      integer function section(z)
!     Returns 1 if z lies in evaporator, 2-adiabatic, 3-condenser
      use inputparameters, only : bn,L1,pi,rb, Lc, Lev
      implicit none
      integer j,ii
      double precision  bm, L2, L3, L4, L5, Lfix, Lm ,z, z1, z2 !, zq
      real   zq
      dimension zq(5+5*(bn-1)/2)
      z1 = z
      ii = 0
      j = 0
      zq = 0.0
!     -----geometry definition-------
```

```
      bm = (bn-1)/2
      L2 = dnint(1000*pi*rb/2)/1000
      L3 = (bn-1)*2*rb
      L4 = 2*L2
      L5 = L1-2*rb
      Lm = 2*(L4+L5)
      Lfix = 2*(L1+L2)+L3+L4
!     -------------------------------
!      do while (z1.ge.L)
!      z1 = z1-L
!      enddo
!     -----------Heat I/O change location-----------------
      zq(1) = dnint(1000*(Lev - rb))/1000
      zq(2) = L1 - Lc + rb
      zq(3) = L1 + 2*L2 + L3 + Lc - rb
      zq(4) = Lfix - L4 -(Lev - rb)
      zq(5) = Lfix
      do ii = 0,(bm-1)
       zq(6+5*ii) = zq(5) + ii*Lm + (Lev - rb)
       zq(7+5*ii) = zq(6+5*ii) + L5 - Lev - Lc + 4*rb
       zq(8+5*ii) = zq(7+5*ii) + L4 + 2*(Lc - 3*rb)
       zq(9+5*ii) = zq(8+5*ii) - Lc - Lev + L5 + 4*rb
       zq(10+5*ii) = zq(9+5*ii) + Lev - rb + L4
      enddo
!     ---------------------------------------------------------
      if (0.0.le.z1.and.z1.lt.zq(1)) then
      section = 1
      elseif (zq(1).le.z1.and.z1.le.zq(2)) then
      section = 2
      elseif (zq(2).le.z1.and.z1.le.zq(3)) then
      section = 3
      elseif (zq(3).le.z1.and.z1.le.zq(4)) then
      section = 2
      elseif (zq(4).le.z1.and.z1.le.zq(5)) then
      section = 1
      else
      do j = 0,(bm-1)
       if ((zq(5) + j*Lm).le.z1.and.z1.le.zq(6+5*j)) then
       section = 1
       elseif (zq(6+5*j).le.z1.and.z1.le.zq(7+5*j)) then
       section = 2
       elseif (zq(7+5*j).le.z1.and.z1.le.zq(8+5*j)) then
       section = 3
       elseif (zq(8+5*j).le.z1.and.z1.le.zq(9+5*j)) then
       section = 2
       elseif (zq(9+5*j).le.z1.and.z1.le.zq(10+5*j)) then
       section = 1
       endif
      enddo
      endif
      return
      end
!     ..................................................................
      double precision function theta(z1)
!     User defined inclination angle profile
!     Angle of gravity vector from z axis, rad
!     bn >= 3 bends @180° plus 2 bends @90° profile
      use inputparameters, only : bn, L, L1, pi, rb, theta_in
      implicit none
      integer j,ii
      double precision  bm, L2, L3, L4, L5, Lfix, Lm, Ltot, theta1, z1, z2, zg
      dimension zg(6+2*(bn-1))
```

```
      z2 = z1
      ii = 0
      j = 0
      zg = 0.0
!     -----geometry definition-------
      bm = (bn-1)/2
      L2 = dnint(1000*pi*rb/2)/1000
      L3 = (bn-1)*2*rb
      L4 = 2*L2
      L5 = L1-2*rb
      Lm = 2*(L4+L5)
!     --------------------------------
      do while (z2.ge.L)
      z2 = z2-L
      enddo
!     -----------theta change location-----------------
      zg(1) = L1
      zg(2) = zg(1)+L2
      zg(3) = zg(2)+L3
      zg(4) = zg(3)+L2
      zg(5) = zg(4)+L1
      zg(6) = zg(5)+L4
      do ii = 0,(bm-1)
       zg(7+4*ii) = zg(6)+ ii*Lm + L5
       zg(8+4*ii) = zg(7+4*ii)+L4
       zg(9+4*ii) = zg(8+4*ii)+L5
       zg(10+4*ii) = zg(9+4*ii)+L4
      enddo
!     ------------------------------------------------------
      if (0.0.le.z2.and.z2.le.zg(1)) then
      theta = 1
      elseif (zg(1).le.z2.and.z2.le.zg(2)) then
      theta = 1.0-(z2-zg(1))/L4
      elseif (zg(2).le.z2.and.z2.le.zg(3)) then
      theta = 0.5
      elseif (zg(3).le.z2.and.z2.le.zg(4)) then
      theta = 0.5-(z2-zg(3))/L4
      elseif (zg(4).le.z2.and.z2.le.zg(5)) then
      theta = 0
      elseif (zg(5).le.z2.and.z2.le.zg(6)) then
      theta = (z2-zg(5))/L4
      else
      do j = 0,(bm-1)
       if ((zg(6) + j*Lm).le.z2.and.z2.le.zg(4*j+7)) then
       theta = 1
       elseif (zg(4*j+7).le.z2.and.z2.le.zg(4*j+8)) then
       theta = 1-(z2-zg(4*j+7))/L4
       elseif (zg(4*j+8).le.z2.and.z2.le.zg(4*j+9)) then
       theta = 0
       elseif (zg(4*j+9).le.z2.and.z2.le.zg(4*j+10)) then
       theta = (z2-zg(4*j+9))/L4
       endif
      enddo
      endif

!!---------------HOLLEY VERSION-------------------------------------------
!     theta = pi/2.0 ! top branch orientation does not depend on
                     ! theta. It is always in the horizontal position
!     else
!     theta = pi*(1.0-theta) !Top heat mode
!     theta = pi/2.0*(1.5-theta) !45 Degrees from top heat mode
!     theta = pi/2.0 !Horizontal heat mode
```

```
!      theta = pi/2.0*(0.5+theta) !45 Degrees from bottom heat mode
!      theta = pi*theta !Bottom heat mode
!       endif

       theta1 = theta_in/180 ! to be added in the local variable
        if (theta1.eq.0.5) then ! theta_in = 90°, Horizontal mode
        theta = pi/2.0 !Horizontal heat mode
        else ! other orientations
          if (zg(2).le.z2.and.z2.le.zg(3)) then
!    top branch orientation does not depend on theta.
          theta = pi/2.0 !theta is always 90°
          else ! other tube brances
          theta = pi*abs(theta -theta1)
          endif
        endif
       return
       end
!      ................................................................

!      ----------------------------------------------------------------
!      SUBROUTINES
!      ----------------------------------------------------------------
!      .......................MM/apr-2010.............................
        subroutine bendlosses(Ct,DPK,&
                  LScoef,Lossid,LSid,mdot,nb,nf,np,Tp,Ts,z,zb,zf,zs)
!      Minor Pressure Losses on the liquid phase due to the presence of bends
       use fluid
       use inputparameters, only : bn, cc, L, L1, n, ns, nw, pi, rb
       implicit none
       integer i,k,ii,j,jj,nb(n),nf(n),np,slug,between,converge
       double precision A,BDid(nw),bm,Ca,Cb,Ct,dh,DPK(nw),DPblt,jKb(bn+2), &
                        jKf(bn+2), KK(nw),LScoef(nw),LSid(nw),L2,L3,L4,L5,Lm, &
                        Lossid(nw),mdot(n),mul,Re(nw),rhol,Sa,Sb,To, &
                                Tp(n),Ts(ns),wrap,z,zb(n),zf(n),zKb(bn+2),zKf(bn+2),&
                                zs(ns),Km90,Km180,Ki90,Ki180,Kd90,Kd180
!      -----geometry definition-------
       bm = (bn-1)/2
       L2 = dnint(1000*pi*rb/2)/1000
       L3 = (bn-1)*2*rb
       L4 = 2*L2
       L5 = L1-2*rb
       Lm = 2*(L4+L5)
!      Three constants for the local pressure drop correlation
       Km180 = 1000
       Ki180 = 0.1
       Kd180 = 4
       Km90 = 800
       Ki90 = 0.091
       Kd90 = 4
!      Initialization
       LSid = 0.0 ! Liquid Slug Index vector init
       LScoef = 0.0 !Liquid Slug flag vector init
       BDid = 0.0 ! Bend coefficient init
       Lossid = 0.0
       Re = 1000

       do i = 1,nw     ! cycle for the tube discretized domain
       z = dble(i-1)/dble(nw)*L
       call Tfluid(nb,nf,np,To,Tp,Ts,z,zb,zf,zs)
       j = slug(np,z,zb,zf)
        if (j.gt.0) then
        LSid(i) = j
```

```
       LScoef(i) = LSid(i)**0.0 ! all the non-zero vector components are set to 1
       Re(i) = dabs(mdot(j))*dh(z)/mul(To,coef_mul,cond_mul)/A(z)
       else
       LSid(i) = 0
       LScoef(i) = 0
       Re(i) = 1000 ! cannot be zero!!(*)
       endif
!      Bends boundaries location
       zKb(1) = L1          ! 90° bend
       zKf(1) = zKb(1)+L2
       zKb(2) = zKf(1)+L3 ! 90° bend
       zKf(2) = zKb(2)+L2
       zKb(3) = zKf(2)+L1 ! 180° bend
       zKf(3) = zKb(3)+L4
       do ii = 0,(bm-1)
        zKb(4+2*ii) = zKf(3)+ ii*Lm + L5 ! 180° bend
        zKf(4+2*ii) = zKb(4+2*ii)+L4
        zKb(5+2*ii) = zKf(4+2*ii)+L5 ! 180° bend
        zKf(5+2*ii) = zKb(5+2*ii)+L4
       enddo
!      bends boundaries indexes
      k = 1
      do while (k.le.(bn+2))
       jKb(k) = nint(zKb(k)*dble(nw)/L) !index for the beginning of the 1st bend
       jKf(k) = nint(zKf(k)*dble(nw)/L) !index for the end of the 1st bend
       k = k + 1
      enddo
       ! the loss coefficient vector based only on the bends location is created
         if (jKb(1).le.i.and.i.le.jKf(1)) then
         KK(i) = (Km90/Re(i)) + Ki90*(1 + (Kd90/(dh(z)/0.0254)**0.3))!(*)
         BDid(i) = KK(i)/(jKf(1)-jKb(1))
         else if (jKb(2).le.i.and.i.le.jKf(2)) then
         KK(i) = (Km90/Re(i)) + Ki90*(1 + (Kd90/(dh(z)/0.0254)**0.3))!(*)
         BDid(i) = KK(i)/(jKf(2)-jKb(2))
         else if (jKb(3).le.i.and.i.le.jKf(3)) then
         KK(i) = (Km180/Re(i)) + Ki180*(1 + (Kd180/(dh(z)/0.0254)**0.3))!(*)
         BDid(i) = KK(i)/(jKf(3)-jKb(3))
         else
         do jj = 0,(bm-1)
          if (jKb(4+2*jj).le.i.and.i.le.jKf(4+2*jj)) then
          KK(i) = (Km180/Re(i)) + Ki180*(1 + (Kd180/(dh(z)/0.0254)**0.3))!(*)
          BDid(i) = KK(i)/(jKf(4+2*jj)-jKb(4+2*jj))
          else if (jKb(5+2*jj).le.i.and.i.le.jKf(5+2*jj)) then
          KK(i) = (Km180/Re(i)) + Ki180*(1 + (Kd180/(dh(z)/0.0254)**0.3))!(*)
          BDid(i) = KK(i)/(jKf(5+2*jj)-jKb(5+2*jj))
          endif
         enddo
         endif
       ! The loss coefficient vector is then multiplied with the
       ! Liquid Slug Vector in order to obtain a new loss
       ! coefficient vector whose components are non-zero
       ! only if liquid is present in the subelement.

       Lossid(i) = LScoef(i)*BDid(i)
        if (j.gt.0) then
       ! Differential Pressure relative to the single subvolume
         DPK(i) = -(Lossid(i)/2.0)*mdot(j)*dabs(mdot(j))/ &
                  (rhol(To,coef_rhol,cond_rhol)*A(z)**2.0)
       else
       DPK(i) = 0
       endif
      enddo
```

```
      end

!     ..................................................................
      subroutine bendlossestot(Ct,DPbl,DPK,Lossid,LSid,mdot,nb,nf,np, &
                 Tp,Ts,zb,zf,zs)
!     Total Pressure losses on the liquid phase due to the presence of bends
!     in given locations.
      use fluid
      use inputparameters, only : bn, cc, L, n, ns, nw
      implicit none
      integer i,j,nb(n),nf(n),np
      double precision BDid(nw),Ct,DPbl(n),DPblK(nw),DPK(nw),DPblt, &
                       KK(n),LSid(nw),LScoef(nw), Lossid(nw),mdot(n),Re(nw), &
                       Tp(n),Ts(ns),z,zb(n), zf(n),zKb(bn+2),zKf(bn+2),zs(ns)
       do j = 1,np ! cycle for all the liquid slugs
       call bendlosses(Ct,DPK,LScoef,Lossid,LSid,mdot,nb,nf,np,Tp,Ts,z,zb,zf,zs)
        i = 1
        DPblt = 0
         do while (i.le.nw) ! count for all the subvolumes
          ! select pressure losses relative to the same Liquid Slug
          if (LSid(i).eq.j) then
          DPblK(i) = DPK(i)
          else
          DPblK(i) = 0
          endif
          DPblt = DPblt + DPblK(i) ! sum the DP contributions relative to the i-th
                                   LS from different bends
         i = i + 1
         enddo
         DPbl(j) = DPblt
       enddo
       end
!     -------------------------CHOOSE FLUID SUBROUTINE----------------------------
!     Reads the fitting coefficient from the matlab output
!     files and update the fitting general functions n FIT_FUNCT with
!     the chosen fluid.
      subroutine choosefluid(coef_cpl,cond_cpl,coef_cpv,cond_cpv,coef_hl,cond_hl, &
                       coef hg,cond hg,coef kl,cond kl,coef kv,cond kv, &
                       coef_mul,cond_mul,coef_muv,cond_muv,coef_Psat,cond_Psat, &
                       coef_rhol,cond_rhol,coef_rhov,cond_rhov,coef_sigma, &
                       cond_sigma, coef_Tsat,cond_Tsat,Pcr)
      use fluid , only: n_coef,n_cond, fn, status
      implicit none
      double precision  coef_cpl(n_coef),cond_cpl(n_cond),coef_cpv(n_coef), &
                       cond_cpv(n_cond), coef_hl(n_coef),cond_hl(n_cond), &
                       coef_hg(n_coef), cond_hg(n_cond), coef_kl(n_coef), &
                       cond_kl(n_cond),coef_kv(n_coef), cond_kv(n_cond) &
                       coef_mul(n_coef),cond_mul(n_cond),&
                       coef muv(n coef),cond muv(n cond), &
                       coef Psat(n coef),cond Psat(n cond),&
                       coef_rhov(n_coef),cond_rhov(n_cond),&
                       coef_rhol(n_coef),cond_rhol(n_cond),&
                       coef_sigma(n_coef),cond_sigma(n_cond), &
                       coef_Tsat(n_coef),cond_Tsat(n_cond),&
                       Pcr
      if (fn.eq.'water') then
      Pcr = 22064000 ! Critical pressure for water [Pa]
      open (UNIT = 30 , FILE = &
       "C:\\Users\\mauro.mameli\\Documents\\MAURO\\DOTTORATO\\PHP_main
project\\HOLLEY IMPLEMENTATION\\BH MM PHP\\FLUIDS FIT COEF\\water.txt" , &
        STATUS = 'unknown', ACTION = 'read', IOSTAT = status)
       if (status.eq.0) then
```

```
      write (*,*) '"water.txt" opened succesfully'
      else
      write (*,*) 'Warning: an error occured in opening "water.txt" file!'
      end if
     pause
     read(30,*) coef_cpl(1),coef_cpl(2),coef_cpl(3),coef_cpl(4), &
                coef_cpl(5),coef_cpl(6), cond_cpl(1),cond_cpl(2)
     read(30,*) coef_cpv(1),coef_cpv(2),coef_cpv(3),coef_cpv(4), &
                coef cpv(5),coef cpv(6), cond cpv(1),cond cpv(2)
     read(30,*) coef_hl(1),coef_hl(2),coef_hl(3),coef_hl(4), &
                coef_hl(5),coef_hl(6), cond_hl(1),cond_hl(2)
     read(30,*) coef_hg(1),coef_hg(2),coef_hg(3),coef_hg(4), &
                coef_hg(5),coef_hg(6), cond_hg(1),cond_hg(2)
     read(30,*) coef_kl(1),coef_kl(2),coef_kl(3),coef_kl(4), &
                coef kl(5),coef kl(6), cond kl(1),cond kl(2)
     read(30,*) coef_kv(1),coef_kv(2),coef_kv(3),coef_kv(4), &
                coef_kv(5),coef_kv(6), cond_kv(1),cond_kv(2)
     read(30,*) coef_mul(1),coef_mul(2),coef_mul(3),coef_mul(4), &
                coef_mul(5),coef_mul(6), cond_mul(1),cond_mul(2)
     read(30,*) coef_muv(1),coef_muv(2),coef_muv(3),coef_muv(4), &
                coef muv(5),coef muv(6), cond muv(1),cond muv(2)
     read(30,*) coef_Psat(1),coef_Psat(2),coef_Psat(3),coef_Psat(4),coef_Psat(5), &
                coef_Psat(6),cond_Psat(1),cond_Psat(2)
     read(30,*) coef_rhol(1),coef_rhol(2),coef_rhol(3),coef_rhol(4),coef_rhol(5), &
                coef_rhol(6),cond_rhol(1),cond_rhol(2)
     read(30,*) coef_rhov(1),coef_rhov(2),coef_rhov(3),coef_rhov(4),coef_rhov(5), &
                coef rhov(6),cond rhov(1),cond rhov(2)
     read(30,*) coef_sigma(1),coef_sigma(2),coef_sigma(3),coef_sigma(4), &
                coef_sigma(5), coef_sigma(6),cond_sigma(1),cond_sigma(2)
     read(30,*) coef_Tsat(1),coef_Tsat(2),coef_Tsat(3),coef_Tsat(4),coef_Tsat(5), &
                coef_Tsat(6),cond_Tsat(1),cond_Tsat(2)
     close (unit = 30)
```

```
     else if (fn.eq.'ethanol') then
     Pcr = 6148000 ! Critical pressure for ethanol [Pa]
     open (UNIT = 21 ,FILE = &
      "C:\\Users\\mauro.mameli\\Documents\\MAURO\\DOTTORATO\\PHP main
project\\HOLLEY IMPLEMENTATION\PHP  9b ON\\FLUIDS FIT COEF\\ethanol.txt", &
       STATUS = 'unknown', ACTION = 'read', IOSTAT = status)
      if (status.eq.0) then
      write (*,*) '"ethanol.txt" opened succesfully'
      else
      write (*,*) 'Warning: an error occured in opening "ethanol.txt!'
      end if
      pause
     read(21,*) coef_cpl(1),coef_cpl(2),coef_cpl(3),coef_cpl(4), &
                coef_cpl(5),coef_cpl(6), cond_cpl(1),cond_cpl(2)
     read(21,*) coef_cpv(1),coef_cpv(2),coef_cpv(3),coef_cpv(4), &
                coef cpv(5),coef cpv(6), cond cpv(1),cond cpv(2)
     read(21,*) coef_hl(1),coef_hl(2),coef_hl(3),coef_hl(4), &
                coef_hl(5),coef_hl(6), cond_hl(1),cond_hl(2)
     read(21,*) coef_hg(1),coef_hg(2),coef_hg(3),coef_hg(4), &
                coef_hg(5),coef_hg(6), cond_hg(1),cond_hg(2)
     read(21,*) coef_kl(1),coef_kl(2),coef_kl(3),coef_kl(4), &
                coef kl(5),coef kl(6), cond kl(1),cond kl(2)
     read(21,*) coef_kv(1),coef_kv(2),coef_kv(3),coef_kv(4), &
                coef_kv(5),coef_kv(6), cond_kv(1),cond_kv(2)
     read(21,*) coef_mul(1),coef_mul(2),coef_mul(3),coef_mul(4), &
                coef_mul(5),coef_mul(6), cond_mul(1),cond_mul(2)
     read(21,*) coef_muv(1),coef_muv(2),coef_muv(3),coef_muv(4), &
                coef muv(5),coef muv(6), cond muv(1),cond_muv(2)
     read(21,*) coef_Psat(1),coef_Psat(2),coef_Psat(3), &
```

```
                coef_Psat(4),coef_Psat(5), coef_Psat(6),cond_Psat(1),cond_Psat(2)
     read(21,*) coef_rhol(1),coef_rhol(2),coef_rhol(3),coef_rhol(4),coef_rhol(5), &
                coef_rhol(6),cond_rhol(1),cond_rhol(2)
     read(21,*) coef_rhov(1),coef_rhov(2),coef_rhov(3),coef_rhov(4),coef_rhov(5), &
                coef_rhov(6),cond_rhov(1),cond_rhov(2)
     read(21,*) coef_sigma(1),coef_sigma(2),coef_sigma(3),coef_sigma(4), &
                coef_sigma(5), coef_sigma(6),cond_sigma(1),cond_sigma(2)
     read(21,*) coef_Tsat(1),coef_Tsat(2),coef_Tsat(3),coef_Tsat(4),coef_Tsat(5), &
                coef_Tsat(6),cond_Tsat(1),cond_Tsat(2)
     close (unit = 21)

     else if (fn.eq.'C6F14') then
     Pcr = 1830000 ! Critical pressure for C6F14 [Pa]
     open (unit = 32 ,file = &
      "C:\\Users\\mauro.mameli\\Documents\\MAURO\\DOTTORATO\\PHP main
project\\HOLLEY IMPLEMENTATION\PHP _9b_ON\\FLUIDS_FIT_COEF\\C6F14.txt" , &
       STATUS = 'old', ACTION = 'read', IOSTAT = status)
      if (status.eq.0) then
      write (*,*) '"C6F14.txt" opened succesfully'
      else
      write (*,*) 'Warning: an error occured in opening "C6F14.txt!'
      end if
     pause
     read(32,*) coef_cpl(1),coef_cpl(2),coef_cpl(3),coef_cpl(4), &
                coef_cpl(5),coef_cpl(6), cond_cpl(1),cond_cpl(2)
     read(32,*) coef_cpv(1),coef_cpv(2),coef_cpv(3),coef_cpv(4), &
                coef_cpv(5),coef_cpv(6), cond_cpv(1),cond_cpv(2)
     read(32,*) coef_hl(1),coef_hl(2),coef_hl(3),coef_hl(4), &
                coef_hl(5),coef_hl(6), cond_hl(1),cond_hl(2)
     read(32,*) coef_hg(1),coef_hg(2),coef_hg(3),coef_hg(4), &
                coef_hg(5),coef_hg(6), cond_hg(1),cond_hg(2)
     read(32,*) coef_kl(1),coef_kl(2),coef_kl(3),coef_kl(4), &
                coef_kl(5),coef_kl(6), cond_kl(1),cond_kl(2)
     read(32,*) coef_kv(1),coef_kv(2),coef_kv(3),coef_kv(4),coef&
                _kv(5),coef_kv(6), cond_kv(1),cond_kv(2)
     read(32,*) coef_mul(1),coef_mul(2),coef_mul(3),coef_mul(4), &
                coef_mul(5),coef_mul(6), cond_mul(1),cond_mul(2)
     read(32,*) coef_muv(1),coef_muv(2),coef_muv(3),coef_muv(4),coef_muv(5), &
                coef_muv(6), cond_muv(1),cond_muv(2)
     read(32,*) coef_Psat(1),coef_Psat(2),coef_Psat(3),coef_Psat(4),coef_Psat(5), &
                coef_Psat(6),cond_Psat(1),cond_Psat(2)
     read(32,*) coef_rhol(1),coef_rhol(2),coef_rhol(3),coef_rhol(4),coef_rhol(5), &
                coef_rhol(6),cond_rhol(1),cond_rhol(2)
     read(32,*) coef_rhov(1),coef_rhov(2),coef_rhov(3),coef_rhov(4),coef_rhov(5), &
                coef_rhov(6),cond_rhov(1),cond_rhov(2)
     read(32,*) coef_sigma(1),coef_sigma(2),coef_sigma(3),coef_sigma(4), &
                coef_sigma(5),coef_sigma(6),cond_sigma(1),cond_sigma(2)
     read(32,*) coef_Tsat(1),coef_Tsat(2),coef_Tsat(3),coef_Tsat(4),coef_Tsat(5), &
                coef_Tsat(6),cond_Tsat(1),cond_Tsat(2)
     close (unit = 32)

     else if (fn.eq.'methanol') then
     Pcr = 8215850 ! Critical pressure for methanol [Pa]
     open (unit = 33 ,file = &
      "C:\\Users\\mauro.mameli\\Documents\\MAURO\\DOTTORATO\\PHP main
project\\HOLLEY IMPLEMENTATION\\BH_MM_PHP\\FLUIDS_FIT_COEF\\methanol.txt" , &
       STATUS = 'old', ACTION = 'read', IOSTAT = status)
      if (status.eq.0) then
      write (*,*) '"methanol.txt" opened succesfully'
      else
      write (*,*) 'Warning: an error occured in opening "methanol.txt"!'
      end if
```

```
      pause
      read(33,*) coef_cpl(1),coef_cpl(2),coef_cpl(3),coef_cpl(4),coef_cpl(5), &
                 coef_cpl(6), cond_cpl(1),cond_cpl(2)
      read(33,*) coef_cpv(1),coef_cpv(2),coef_cpv(3),coef_cpv(4),coef_cpv(5), &
                 coef_cpv(6),  cond_cpv(1),cond_cpv(2)
      read(33,*) coef_hl(1),coef_hl(2),coef_hl(3),coef_hl(4), &
                 coef_hl(5),coef_hl(6), cond_hl(1),cond_hl(2)
      read(33,*) coef_hg(1),coef_hg(2),coef_hg(3),coef_hg(4), &
                 coef_hg(5),coef_hg(6), cond_hg(1),cond_hg(2)
      read(33,*) coef_kl(1),coef_kl(2),coef_kl(3),coef_kl(4), &
                 coef_kl(5),coef_kl(6), cond_kl(1),cond_kl(2)
      read(33,*) coef_kv(1),coef_kv(2),coef_kv(3),coef_kv(4), &
                 coef_kv(5),coef_kv(6), cond_kv(1),cond_kv(2)
      read(33,*) coef_mul(1),coef_mul(2),coef_mul(3),coef_mul(4),coef &
                  mul(5),coef_mul(6), cond_mul(1),cond_mul(2)
      read(33,*) coef_muv(1),coef_muv(2),coef_muv(3),coef_muv(4), &
                 coef_muv(5),coef_muv(6), cond_muv(1),cond_muv(2)
      read(33,*) coef_Psat(1),coef_Psat(2),coef_Psat(3),coef_Psat(4),coef_Psat(5), &
                 coef_Psat(6),cond_Psat(1),cond_Psat(2)
      read(33,*) coef_rhol(1),coef_rhol(2),coef_rhol(3),coef_rhol(4),coef_rhol(5), &
                 coef_rhol(6),cond_rhol(1),cond_rhol(2)
      read(33,*) coef_rhov(1),coef_rhov(2),coef_rhov(3),coef_rhov(4),coef_rhov(5), &
                 coef_rhov(6),cond_rhov(1),cond_rhov(2)
      read(33,*) coef_sigma(1),coef_sigma(2),coef_sigma(3),coef_sigma(4), &
                 coef_sigma(5), coef_sigma(6),cond_sigma(1),cond_sigma(2)
      read(33,*) coef_Tsat(1),coef_Tsat(2),coef_Tsat(3),coef_Tsat(4),coef_Tsat(5), &
                 coef_Tsat(6),cond_Tsat(1),cond_Tsat(2)
      close (unit = 33)

      else if (fn.eq.'R123') then
      Pcr = 3661800 ! Critical pressure for R123 [Pa]
      open (unit = 34 ,file = &
       "C:\\Users\\mauro.mameli\\Documents\\MAURO\\DOTTORATO\\PHP_main
project\\HOLLEY IMPLEMENTATION\PHP _9b_ON\\FLUIDS_FIT_COEF\\R123.txt" , &
        STATUS = 'old', ACTION = 'read', IOSTAT = status)
       if (status.eq.0) then
       write (*,*) '"R123.txt" opened succesfully'
       else
       write (*,*) 'Warning: an error occured in opening "R123.txt"!'
       end if
      pause
      read(34,*) coef_cpl(1),coef_cpl(2),coef_cpl(3),coef_cpl(4),coef_cpl(5), &
                 coef_cpl(6), cond_cpl(1),cond_cpl(2)
      read(34,*) coef_cpv(1),coef_cpv(2),coef_cpv(3),coef_cpv(4),coef_cpv(5), &
                 coef_cpv(6), cond_cpv(1),cond_cpv(2)
      read(34,*) coef_hl(1),coef_hl(2),coef_hl(3),coef_hl(4),coef_hl(5), &
                 coef_hl(6), cond_hl(1),cond_hl(2)
      read(34,*) coef_hg(1),coef_hg(2),coef_hg(3),coef_hg(4),coef_hg(5), &
                 coef_hg(6), cond_hg(1),cond_hg(2)
      read(34,*) coef_kl(1),coef_kl(2),coef_kl(3),coef_kl(4),coef_kl(5), &
                 coef_kl(6), cond_kl(1),cond_kl(2)
      read(34,*) coef_kv(1),coef_kv(2),coef_kv(3),coef_kv(4),coef_kv(5), &
                 coef_kv(6), cond_kv(1),cond_kv(2)
      read(34,*) coef_mul(1),coef_mul(2),coef_mul(3),coef_mul(4),coef_mul(5), &
                 coef_mul(6), cond_mul(1),cond_mul(2)
      read(34,*) coef_muv(1),coef_muv(2),coef_muv(3),coef_muv(4),coef_muv(5), &
                 coef_muv(6), cond_muv(1),cond_muv(2)
      read(34,*) coef_Psat(1),coef_Psat(2),coef_Psat(3),coef_Psat(4), &
                 coef_Psat(5), coef_Psat(6),cond_Psat(1),cond_Psat(2)
      read(34,*) coef_rhol(1),coef_rhol(2),coef_rhol(3),coef_rhol(4),coef_rhol(5), &
                 coef_rhol(6),cond_rhol(1),cond_rhol(2)
      read(34,*) coef_rhov(1),coef_rhov(2),coef_rhov(3),coef_rhov(4),coef_rhov(5), &
```

```
                coef_rhov(6),cond_rhov(1),cond_rhov(2)
     read(34,*) coef_sigma(1),coef_sigma(2),coef_sigma(3),coef_sigma(4), &
                coef_sigma(5), coef_sigma(6),cond_sigma(1),cond_sigma(2)
     read(34,*) coef_Tsat(1),coef_Tsat(2),coef_Tsat(3),coef_Tsat(4),coef_Tsat(5), &
                coef_Tsat(6),cond_Tsat(1),cond_Tsat(2)
     close (unit = 34)

     else if (fn.eq.'R134a') then
     Pcr = 4059280 ! Critical pressure for R134a [Pa]
     open (unit = 35 ,file = &
      "C:\\Users\\mauro.mameli\\Documents\\MAURO\\DOTTORATO\\PHP_main
project\\HOLLEY IMPLEMENTATION\\BH_MM_PHP\\FLUIDS_FIT_COEF\\R134a.txt" , &
       STATUS = 'old', ACTION = 'read', IOSTAT = status)
      if (status.eq.0) then
      write (*,*) '"R134a.txt" opened succesfully'
      else
      write (*,*) 'Warning: an error occured in opening "R134a.txt"!'
      end if
     pause
     read(35,*) coef_cpl(1),coef_cpl(2),coef_cpl(3),coef_cpl(4),coef_cpl(5), &
                coef_cpl(6), cond_cpl(1),cond_cpl(2)
     read(35,*) coef_cpv(1),coef_cpv(2),coef_cpv(3),coef_cpv(4),coef_cpv(5), &
                coef_cpv(6), cond_cpv(1),cond_cpv(2)
     read(35,*) coef_hl(1),coef_hl(2),coef_hl(3),coef_hl(4),coef_hl(5), &
                coef_hl(6), cond_hl(1),cond_hl(2)
     read(35,*) coef_hg(1),coef_hg(2),coef_hg(3),coef_hg(4),coef_hg(5), &
                coef_hg(6), cond_hg(1),cond_hg(2)
     read(35,*) coef_kl(1),coef_kl(2),coef_kl(3),coef_kl(4),coef_kl(5), &
                coef_kl(6), cond_kl(1),cond_kl(2)
     read(35,*) coef_kv(1),coef_kv(2),coef_kv(3),coef_kv(4),coef_kv(5), &
                coef_kv(6), cond_kv(1),cond_kv(2)
     read(35,*) coef_mul(1),coef_mul(2),coef_mul(3),coef_mul(4),coef_mul(5), &
                coef_mul(6), cond_mul(1),cond_mul(2)
     read(35,*) coef_muv(1),coef_muv(2),coef_muv(3),coef_muv(4),coef_muv(5), &
                coef_muv(6), cond_muv(1),cond_muv(2)
     read(35,*) coef_Psat(1),coef_Psat(2),coef_Psat(3),coef_Psat(4),coef_Psat(5), &
                coef_Psat(6),cond_Psat(1),cond_Psat(2)
     read(35,*) coef_rhol(1),coef_rhol(2),coef_rhol(3),coef_rhol(4),coef_rhol(5), &
                coef_rhol(6),cond_rhol(1),cond_rhol(2)
     read(35,*) coef_rhov(1),coef_rhov(2),coef_rhov(3),coef_rhov(4),coef_rhov(5), &
                coef_rhov(6),cond_rhov(1),cond_rhov(2)
     read(35,*) coef_sigma(1),coef_sigma(2),coef_sigma(3),coef_sigma(4), &
                coef_sigma(5), coef_sigma(6),cond_sigma(1),cond_sigma(2)
     read(35,*) coef_Tsat(1),coef_Tsat(2),coef_Tsat(3),coef_Tsat(4),coef_Tsat(5), &
                coef_Tsat(6),cond_Tsat(1),cond_Tsat(2)
     close (unit = 35)

     else if (fn.eq.'ammonia') then
     Pcr = 11333000 ! Critical pressure for ammonia [Pa]
     open (unit = 36 ,file = &
      "C:\\Users\\mauro.mameli\\Documents\\MAURO\\DOTTORATO\\PHP_main
project\\HOLLEY IMPLEMENTATION\\BH_MM_PHP\\FLUIDS_FIT_COEF\\ammonia.txt" , &
       STATUS = 'old', ACTION = 'read', IOSTAT = status)
      if (status.eq.0) then
      write (*,*) '"ammonia.txt" opened succesfully'
      else
      write (*,*) 'Warning: an error occured in opening "ammonia.txt"!'
      end if
     pause
     read(36,*) coef_cpl(1),coef_cpl(2),coef_cpl(3),coef_cpl(4),coef_cpl(5), &
                coef_cpl(6), cond_cpl(1),cond_cpl(2)
     read(36,*) coef_cpv(1),coef_cpv(2),coef_cpv(3),coef_cpv(4),coef_cpv(5), &
```

```
                  coef_cpv(6), cond_cpv(1),cond_cpv(2)
      read(36,*) coef_hl(1),coef_hl(2),coef_hl(3),coef_hl(4),coef_hl(5), &
                  coef_hl(6), cond_hl(1),cond_hl(2)
      read(36,*) coef_hg(1),coef_hg(2),coef_hg(3),coef_hg(4),coef_hg(5), &
                  coef_hg(6), cond_hg(1),cond_hg(2)
      read(36,*) coef_kl(1),coef_kl(2),coef_kl(3),coef_kl(4),coef_kl(5), &
                  coef_kl(6), cond_kl(1),cond_kl(2)
      read(36,*) coef_kv(1),coef_kv(2),coef_kv(3),coef_kv(4),coef_kv(5), &
                  coef_kv(6), cond_kv(1),cond_kv(2)
      read(36,*) coef_mul(1),coef_mul(2),coef_mul(3),coef_mul(4),coef_mul(5), &
                  coef_mul(6), cond_mul(1),cond_mul(2)
      read(36,*) coef_muv(1),coef_muv(2),coef_muv(3),coef_muv(4),coef_muv(5), &
                  coef_muv(6), cond_muv(1),cond_muv(2)
      read(36,*) coef_Psat(1),coef_Psat(2),coef_Psat(3),coef_Psat(4),coef_Psat(5), &
                  coef_Psat(6),cond_Psat(1),cond_Psat(2)
      read(36,*) coef_rhol(1),coef_rhol(2),coef_rhol(3),coef_rhol(4),coef_rhol(5), &
                  coef_rhol(6),cond_rhol(1),cond_rhol(2)
      read(36,*) coef_rhov(1),coef_rhov(2),coef_rhov(3),coef_rhov(4),coef_rhov(5), &
                  coef_rhov(6),cond_rhov(1),cond_rhov(2)
      read(36,*) coef_sigma(1),coef_sigma(2),coef_sigma(3),coef_sigma(4), &
                  coef_sigma(5), coef_sigma(6),cond_sigma(1),cond_sigma(2)
      read(36,*) coef_Tsat(1),coef_Tsat(2),coef_Tsat(3),coef_Tsat(4),coef_Tsat(5), &
                  coef_Tsat(6),cond_Tsat(1),cond_Tsat(2)
      close (unit = 36)

      endif

      end

!     ..................................................................
      subroutine evaporatorheatperlength(qin)
!     Determine evaporator heat flux from total heat input Qt
      use inputparameters, only : cc, L, Qt
      implicit none
      integer converge, ii, kk, section
      double precision p, qin, Sa, Sb, z
      converge = 0
      z = 0.0
      Sa = p(z)
      kk = 0
      do while ((converge.eq.0.or.kk.le.9).and.kk.lt.20)
      Sb = Sa
      Sa = 0.0
      kk = kk + 1
      do ii = 1, 2**(kk-1)
      z = dble(2*ii-1)*L/dble(2**kk)
      if (section(z).eq.1) Sa = Sa + p(z)
      enddo
      Sa = Sa/dble(2**kk) + Sb/2.0
      converge = 0
      if (Sa.eq.0.0.or.dabs((Sa-Sb)/Sa).lt.cc) converge = 1
      enddo
      if (Sa.ne.0.0) qin = Qt/L/Sa
      return
      end
!     ..................................................................
      subroutine gravity(Ct,DPg,nb,nf,np,Tp,Ts,zb,zf,zs)
!     Pressure difference due to gravity
      use fluid
      use inputparameters, only : cc,g,L,n,ns
      implicit none
      integer converge,ii,j,k,kk,nb(n),nf(n),np
```

```
      double precision Ca,Cb,Ct,DP,DPg(n),rhol,Sa,Sb,To,Tp(n),Ts(ns), &
      theta,wrap,z,z1,z2,zb(n),zf(n),zs(ns)
      do j = 1, np
      z1 = zb(j)
      z2 = zf(j)
      k = mod(j,np)+1 ! what for??
      Ca = 0.0
      call Tfluid(nb,nf,np,To,Tp,Ts,z1,zb,zf,zs)
      Sa = rhol(To,coef_rhol,cond_rhol)*dcos(theta(z1))
      call Tfluid(nb,nf,np,To,Tp,Ts,z1,zb,zf,zs)
      Sa = Sa + rhol(To,coef_rhol,cond_rhol)*dcos(theta(z2))
      kk = 0
!     mauro
      converge = 0
!
      do while ((converge.eq.0.or.kk.le.3).and.kk.lt.20)
      Sb = Sa
      Cb = Ca
      Ca = 0.0
      kk = kk + 1
      do ii = 1, 2**(kk-1)
      z = wrap(z1+dble(2*ii-1)*wrap(z2-z1)/dble(2**kk))
      call Tfluid(nb,nf,np,To,Tp,Ts,z,zb,zf,zs)
      Ca = Ca + rhol(To,coef_rhol,cond_rhol)*dcos(theta(z))
      enddo
      Sa = Sb/2.0 + (4.0*Ca - 2.0*Cb)/dble(2**kk)
      converge = 0
      if (dabs(Sa).lt.1.0.or.dabs((Sb-Sa)/Sa).lt.cc*Ct) converge = 1
      enddo
      DPg(j) = Sa*g*wrap(z2-z1)/3.0
      enddo
      return
      end
!     ..................................................................
      subroutine heatplugtoslug(nb,nf,np,Qcb,Qcf,Tp,Ts,zb,zf,zs)
!     Conduction at plug ends
      use fluid
      use inputparameters, only : n,ns
      implicit none
      integer i,is,j,k,ks,nb(n),nf(n),np
      double precision A,kl,Qcb(n),Qcf(n),Tp(n),Ts(ns),wrap,z1,z2, &
      zb(n),zf(n),zs(ns)
      do j = 1, np
      ks = mod(nb(j),ns)+1
      z1 = wrap(zs(nb(j))-zb(j))
      z2 = wrap(zs(ks)-zb(j))
      Qcb(j) = kl(Tp(j),coef_kl,cond_kl)*A(zb(j))* &
      ((z2**2.0-z1**2.0)*Tp(j)-z2**2.0*Ts(nb(j))+z1**2.0*Ts(ks))/ &
      (z1*z2*(z2-z1)) !Second order finite difference dT/dz
      k = mod(j,np)+1
      is = mod(nf(j)+ns-2,ns)+1
      z1 = wrap(zf(j)-zs(nf(j)))
      z2 = wrap(zf(j)-zs(is))
      Qcf(j) = kl(Tp(k),coef_kl,cond_kl)*A(zf(j))* &
      ((z2**2.0-z1**2.0)*Tp(k)-z2**2.0*Ts(nf(j))+z1**2.0*Ts(is))/ &
      (z1*z2*(z2-z1)) !Second order finite difference dT/dz
      enddo
      return
      end
!     ..................................................................
!     ..............Mod.MM/12-10-2009.............................
      subroutine heatwalltofluid(h,mdot,nb,nf,np,qwf,Tp,Ts,Tw, &
```

```
      zb,zf,zs)
!     Heat transfer from wall to fluid NON-HOMOGENEOUS_VMQ (Vapor Mass Quality
      Approach):
      use fluid
      use inputparameters, only : bn,L,Lev,n,ns,nw,pi,rb,Qt,xqual0,xqualev,xqualco
      implicit none
      integer i,j,nb(n),nf(n),np,plug,slug
      double precision A,alpha,beta,Bo,Cf,Cpl,dh,Gb,h(nw),hb,hc,hg,hl,hs,kl, &
                       Levtot,lambda,Ls(n),mdot(n),ms(n),msev,mv(n),mvev,mul &
                       Nu,NuDB,NuGN, NuSH,NuST,p,qflx,Prl,Prv,Psat,     &
                       qwf(nw),Relev,Relco,Rel,rhol,rhov,sigma,To,Tp(n), &
                       Ts(ns),Tw(nw),We,z,zb(n),zf(n),zs(ns)

      Levtot = (bn+1)*(dnint(1000*pi*rb/2)/1000 + Lev - rb)
!     Main cycle: sweep the tube along z
      do j = 1, nw
      z = dble(j-1)/dble(nw)*L
      call Tfluid(nb,nf,np,To,Tp,Ts,z,zb,zf,zs) ! calculate fluid temperature To
      for each tube position z

!       ---------------------------------------LIQUID SLUG--------------------------
        ! calculate sensible (single phase liquid) heat transfer coefficient
        if (plug(np,z,zb,zf).eq.0) then
        Rel = mdot(slug(np,z,zb,zf))*dh(z)/mul(To,coef_mul,cond_mul)/A(z) !Re
        Prl = mul(To,coef_mul,cond_mul)*Cpl(To,coef_cpl,cond_cpl)/ &
              kl(To,coef_kl,cond_kl)!Pr
!          ------------------------LAMINAR CORRELATIONS-----------------------------
!          Shah correlation for thermally developping laminar flow
           beta = dabs(Rel)*Prl*dh(z)/Levtot
           if (beta.lt.33.3) then
            NuSH = 4.364 + 0.072*beta
           else
            NuSH = 1.953*(beta**(0.333))
           endif
!          ------------------------TRANSIENT/TURBOLENT CORRELATION-----------------
           NuGN = (Cf(Rel,z)/2.0*(dabs(Rel)-1000.0)*Prl/ &
                 (1.0+12.7*(Cf(Rel,z)/2.0)**0.5)/(Prl**(2.0/3.0)-1.0)) ! Gnielinski
!          ------------------------TURBOLENT CORRELATIONS--------------------------
           NuDB = 0.023*(dabs(Rel)**0.8 )*(Prl**0.4) ! Dittus-Boelter
!          NuST = 0.023*(dabs(Rel)**0.8 )*(Prl**(0.333))* &
!                ((mul(To,coef_mul,cond_mul)/mul(Tw(j),coef_mul,cond_mul))**0.14)
!                  Sieder-Tate
!          -------------------------------------------------------------------------
        if (dabs(Rel).lt.2000) then
         Nu = NuSH
        elseif (2000.lt.dabs(Rel).lt.10000) then
         Nu = NuGN
        elseif (dabs(Rel).gt.10000) then
         Nu = NuDB
        endif
        if (Nu.lt.4.36) Nu = 4.36 !set the minimum limit for Nusselt
         hs = (Nu*kl(To,coef_kl,cond_kl)/dh(z)) ! liquid phase HTC

!       If TWALL < TFLUID set the SENSIBLE HTC
         if (Tw(j).lt.To) then
         h(j) = hs
         else
!       Otherwise TWALL > TFLUID  set the BOILING HTC with Gungor and
!       Winterton correlation with vapor mass quality set to zero
         Gb = mdot(slug(np,z,zb,zf))/A(z)
         qflx = Qt/(pi*dh(z)*0.040)
         Bo = qflx/(dabs(Gb)*(hg(To,coef_hg,cond_hg)-hl(To,coef_hl,cond_hl)))
```

```
          alpha = 1 + 3000*(Bo**0.86) + ((xqual0/(1-xqual0))**0.75)* &
          ((rhol(To,coef_rhol,cond_rhol)/rhov(To,coef_rhov,cond_rhov))**0.41)
          hb = alpha*hs
           if (hb.gt.1.0d6) hb = 1.0d6 ! boiling HTC upper limit
          h(j) = hb
          endif

        else

!       ---------------------------------------VAPOR PLUG---------------------------
          Relev = mdot(plug(np,z,zb,zf))*dh(z)*(1 - xqualev)/ &
          mul(To,coef_mul,cond_mul)/A(z) !Reynolds numb. (adjacent liquid slug)
          Relco = mdot(plug(np,z,zb,zf))*dh(z)*(1 - xqualco)/ &
          mul(To,coef_mul,cond_mul)/A(z) !Reynolds numb. (adjacent liquid slug)
          Prl = mul(To,coef_mul,cond_mul)*Cpl(To,coef_cpl,cond_cpl)/ &
          kl(To,coef_kl,cond_kl) !Prandtl numb. (liquid)
!         If TWALL>TFLUID set the BOILING HTC with Gungor and Winterton correlation
!         and vapor quality set to xqualev
          if (Tw(j).gt.To) then
!           ------------------------LAMINAR CORRELATIONS----------------------------
!           Shah correlation for thermally developping laminar flow
            beta = dabs(Relev)*Prl*dh(z)/Levtot
            if (beta.lt.33.3) then
             NuSH = 4.364 + 0.072*beta
            else
             NuSH = 1.953*(beta**(0.333))
            endif
!           ------------------------TRANSIENT/TURBOLENT CORRELATION-----------------
            NuGN = (Cf(Relev,z)/2.0*(dabs(Relev)-1000.0)*Prl/ &
                  (1.0+12.7*(Cf(Relev,z)/2.0)**0.5)/(Prl**(2.0/3.0)-1.0)) ! ! !
!            Gnielinski
!           ------------------------TURBOLENT CORRELATIONS---------------------------
            NuDB = 0.023*(dabs(Relev)**0.8 )*(Prl**0.4) ! Dittus-Boelter
!           NuST = 0.023*(dabs(Relev)**0.8 )*(Prl**(0.333))* &
!                 ((mul(To,coef_mul,cond_mul)/mul(Tw(j),coef_mul,cond_mul))**0.14) !
!                 Sieder-Tate
!           ------------------------------------------------------------------------
         if (dabs(Relev).lt.2000) then
          Nu = NuSH
         elseif (2000.lt.dabs(Relev).lt.10000) then
          Nu = NuGN
         elseif (dabs(Relev).gt.10000) then
          Nu = NuDB
         endif
          if (Nu.lt.4.36) Nu = 4.36 !set the minimum limit for Nusselt
           hs = (Nu*kl(To,coef_kl,cond_kl)/dh(z)) ! liquid phase HTC
           Gb = mdot(plug(np,z,zb,zf))/A(z) ! NOT SURE!!!
           qflx = Qt/(pi*dh(z)*0.040)
           Bo = qflx/(dabs(Gb)*(hg(To,coef_hg,cond_hg)-hl(To,coef_hl,cond_hl)))
           alpha = 1 + 3000*(Bo**0.86) + ((xqualev/(1-xqualev))**0.75)* &
           ((rhol(To,coef_rhol,cond_rhol)/rhov(To,coef_rhov,cond_rhov))**0.41)
           hb = alpha*hs
           if (hb.gt.1.0d6) hb = 1.0d6 ! boiling HTC upper limit
           h(j) = hb

!         Otherwise if TWALL < TFLUID set the condensation HTC with SHAH correlation
!         and vapor mass quality set to xqualco
          else
!           ------------------------LAMINAR CORRELATIONS----------------------------
!           Shah correlation for thermally developping laminar flow
            beta = dabs(Relco)*Prl*dh(z)/Levtot
            if (beta.lt.33.3) then
```

```
            NuSH = 4.364 + 0.072*beta
           else
            NuSH = 1.953*(beta**(0.333))
           endif
!          ------------------------TRANSIENT/TURBOLENT CORRELATION-----------------
           NuGN = (Cf(Relco,z)/2.0*(dabs(Relco)-1000.0)*Prl/ &
                 (1.0+12.7*(Cf(Relco,z)/2.0)**0.5)/(Prl**(2.0/3.0)-1.0)) !
!                Gnielinski
!          ------------------------TURBOLENT CORRELATIONS--------------------------
           NuDB = 0.023*(dabs(Relco)**0.8 )*(Prl**0.4) ! Dittus-Boelter
!          NuST = 0.023*(dabs(Relco)**0.8 )*(Prl**(0.333))* &
!                ((mul(To,coef_mul,cond_mul)/mul(Tw(j),coef_mul,cond_mul))**0.14) !
!           Sieder-Tate
!          ------------------------------------------------------------------------
         if (dabs(Relev).lt.2000) then
          Nu = NuSH
         elseif (2000.lt.dabs(Relev).lt.10000) then
          Nu = NuGN
         elseif (dabs(Relev).gt.10000) then
          Nu = NuDB
         endif
          if (Nu.lt.4.36) Nu = 4.36 !set the minimum limit for Nusselt
           hs = (Nu*kl(To,coef_kl,cond_kl)/dh(z)) ! liquid phase HTC
!        Set CONDENSING HTC wit SHAH correlation
           lambda = ((1 - xqualco)**0.8 + ((3.8*(xqualco**0.76)* &
                    (1 - xqualco)**0.04)/ (Psat(To,coef_Psat,cond_Psat)/Pcr)**0.38))
           hc = lambda*hs
           h(j) = hc
          endif
        endif
        qwf(j) = h(j)*(Tw(j)-To)

        enddo
        return
        end
!       ..................................................................
        subroutine heatwalltoplug(Ct,nb,nf,np,qwf,Qwp,zb,zf)
!       Integrate heat into each plug by adaptive simpson integration
        use fluid
        use inputparameters, only : cc,n,nw
        implicit none
        integer converge,i,ii,is,j,kk,ks,nb(n),nf(n),np,plug
        double precision Ca,Cb,Ct,Lp,p,qo,qwf(nw),Qwp(n),Sa,Sb,wrap,z, &
        zb(n),zf(n)
        do j = 1, np
        i = mod(j+np-2,np)+1
        Lp = wrap(zb(j)-zf(i))
        call interp(qwf,qo,zf(i))
        Sa = qo*p(zf(i))
        call interp(qwf,qo,zb(j))
        Sa = Sa + qo*p(zb(j))
        Ca = 0.0
        kk = 0
!       mauro
        converge = 0
!
        do while ((converge.eq.0.or.kk.lt.5).and.kk.lt.20)
        Sb = Sa
        Cb = Ca
        Ca = 0.0
        kk = kk + 1
        do ii = 1, 2**(kk-1)
```

```
      z = wrap(zf(i) + dble(2*ii-1)*Lp/dble(2**kk))
      call interp(qwf,qo,z)
      Ca = Ca + qo*p(z)
      enddo
      Sa = Sb/2.0 + (4.0*Ca - 2.0*Cb)/dble(2**kk)
      converge = 0
      if (Sa.eq.0.0.or.dabs((Sa-Sb)/Sa).lt.cc*Ct) converge = 1
      enddo
      Qwp(j) = Sa*Lp/3.0
      enddo
      return
      end
!     ..................................................................
      subroutine heatwalltoslug(Ct,nb,nf,np,Qhf,qwf,Tp,Ts,zb,zf,zs)
!     Heat flux entering liquid slugs adaptive trapezoidal integration
      use fluid
      use inputparameters, only : cc,n,ns,nw
      implicit none
      integer back,converge,j,jo,js,ii,jj,kk,nb(n),nf(n),np,slug
      double precision Ct,Dz,p,Qhf(ns),qo,qwf(nw), &
      Sa,Sb,Tp(n),Ts(ns),wrap,zb(n),zf(n),z,zs(ns)
      do jo = 1, ns !counter
      js = mod(nb(1)+jo-2,ns)+1 !slug cell index
      j = slug(np,zs(js),zb,zf) !slug index
      back = 0
      if (j.gt.0.and.nb(j).eq.js) back = j
      if (back.gt.0) then
      Dz = wrap(zs(js)-zb(j))
      z = zb(j)
      else
      Dz = wrap(zs(js)-zs(mod(js+ns-2,ns)+1))-Dz
      z = wrap(zs(js)-Dz)
      endif
      call interpq(qo,qwf,z,zb(j),zf(j))
      Sa = qo*p(z)
      z = wrap(z+2.0*Dz)
      call interpq(qo,qwf,z,zb(j),zf(j))
      Sa = (Sa + qo*p(z))/2.0
      kk = 0
!     mauro
      converge = 0
!
      do while ((converge.eq.0.or.kk.le.3).and.kk.lt.20)
      Sb = Sa
      Sa = 0.0
      kk = kk + 1
      do ii = 1, 2**(kk-1)
      z = wrap(zs(js)-Dz+2.0*Dz*dble(2*ii-1)/dble(2**kk))
      call interpq(qo,qwf,z,zb(j),zf(j))
      Sa = Sa + qo*p(z)
      enddo
      Sa = Sb/2.0 + Sa/dble(2**kk)
      converge = 0
      if (Sa.eq.0.0.or.dabs((Sb-Sa)/Sa).lt.cc*Ct) converge = 1
      enddo
      Qhf(js) = Sa*2.0*Dz
      enddo
      end
!     ..................................................................
      subroutine initialT(np,Tp,Ts,Tw)
!     Initial fluid and wall temperature values
      use inputparameters, only : n, ns, nw, Ti
```

```
      implicit none
      integer i,j,np
      double precision Tp(n),Ts(ns),Tw(nw)
      do j = 1, np
      Tp(j) = Ti
      enddo
      do j = 1, ns
      Ts(j) = Ti
      enddo
      do j = 1, nw
      Tw(j) = Ti
      enddo
      return
      end
!     ..................................................................
      subroutine interp(x,xo,zo)
!     Center interpolate n values of x with to find xo=x(zo)
!     A higher Heat Input Causes an error in the code: zo comes somehow to be
!     negative and so i is also negative. x has a negative argument
!     and this is not possible because it had been defined as xv(nw).
!     the function wrap is applied to zo in order to get always a positive value.
      use inputparameters, only : L,nw
      implicit none
      integer i
      double precision Dz,x(nw), xo, zo,wrap
      Dz = L/dble(nw)
      i = idint(wrap(zo)/Dz)+1
      if (i.eq.nw) then
      xo = x(nw)+(x(1)-x(nw))/Dz*(wrap(zo)-dble(i-1)*Dz)
      else
      xo = x(i)+(x(i+1)-x(i))/Dz*(wrap(zo)-dble(i-1)*Dz)
      endif
      return
      end
!     ..................................................................
      subroutine interpq(x,xv,z,zb,zf)
!     Return interpolated value (x) of a vector of values (xv)
!     corresponding to wall locations from zb to zf
      use inputparameters, only : L,n,ns,nw
      implicit none
      integer between,j
      double precision Dz,x,x1,x2,xv(nw),z,z1,z2,zb,zf,wrap
      Dz = L/dble(nw)
!     A higher Heat Input Causes an error in the code: z comes somehow to be
!     negative and so j is also negative. xv has a negative argument
!     and this is not possible because it had been defined as xv(nw).
!     the function wrap is applied to z in order to get always a positive value.
      j = idint(wrap(z)/Dz) !"idint(number)" is a function that returns the
                            ! largest integer whose absolute value
                            ! does not exceed the absolute value of the argument
                            ! and has the same sign as the argument.
      if (between(Dz*dble(j),zb,Dz*dble(mod(j+1,nw))).eq.1) then
      z1 = Dz*dble(j+1) !backward interpolate
      x1 = xv(mod(j+1,nw)+1)
      x2 = xv(mod(j+2,nw)+1)
      !x = x1-(x2-x1)/Dz*(z-z1)
      x = x1-(x2-x1)/Dz*(wrap(z)-z1)
      elseif (between(Dz*dble(j),zf,Dz*dble(mod(j+1,nw))).eq.1) then
      z2 = Dz*dble(j) !forward interpolate
      x1 = xv(mod(j+nw-1,nw)+1)
      x2 = xv(j+1)
      !x = x2+(x2-x1)/Dz*(z-z2)
```

```
      x = x2+(x2-x1)/Dz*(wrap(z)-z2)
      else
      z1 = Dz*dble(j) !central interpolate
      x1 = xv(j+1)
      x2 = xv(mod(j+1,nw)+1)
      !x = x1+(x2-x1)/Dz*(z-z1)
      x = x1+(x2-x1)/Dz*(wrap(z)-z1)
      endif
      return
      end
!     ..................................................................
      subroutine intinvA(Ct,IIA,z1,z2)
!     Integrate the recipriocal of A along a slug from the back meniscus
!     to location z
      use inputparameters, only : cc,n
      implicit none
      integer converge,ii,j,kk
      double precision A,Ca,Cb,Ct,IIA,Sa,Sb,wrap,z,z1,z2
      Ca = 0.0
      Sa = 1.0/A(z1) + 1.0/A(z2)
      kk = 0
!     mauro
      converge = 0
!
      do while ((converge.eq.1.or.kk.le.5).and.kk.lt.20)
      Sb = Sa
      Cb = Ca
      Ca = 0.0
      kk = kk + 1
      do ii = 1, 2**(kk-1)
      z = wrap(z1+dble(2*ii-1)*wrap(z2-z1)/dble(2**kk))
      Ca = Ca + 1.0/A(z)
      enddo
      Sa = Sb/2.0 + (4.0*Ca - 2.0*Cb)/dble(2**kk)
      converge = 1
      if (dabs((Sa-Sb)/Sa).lt.cc*Ct) converge = 0
      enddo
      IIA = Sa/3.0*wrap(z2-z1)
      return
      end
!     ..................................................................
      subroutine massincrement(Ct,Dza,k,ma,Ts,zo)
!     Integrate mass increment using adaptive Simpson quadrature
      use fluid
      use inputparameters, only : cc,ns
      implicit none
      integer ii, k, kk
      double precision A,Ca,Cb,Ct,Dza,ma,rhol,Sa,Sb,Ts(ns),wrap,z,zo
      Sa = rhol(Ts(k),coef_rhol,cond_rhol)*A(zo)+rhol(Ts(k),coef_rhol,cond_rhol)* &
      A(wrap(zo+Dza))
!     mauro
      Sb = Sa
!
      Ca = 0.0
      kk = 0
      do while (dabs((Sa-Sb)/Sa).gt.cc*Ct.or.kk.le.2)
      Sb = Sa
      Cb = Ca
      Ca = 0.0
      kk = kk + 1
      do ii = 1, 2**(kk-1)
      z = wrap(zo+dble(2*ii-1)*Dza/dble(2**kk))
```

```
      Ca = Ca + rhol(Ts(k),coef_rhol,cond_rhol)*A(z)
      enddo
      Sa = Sb/2.0 + (4.0*Ca - 2.0*Cb)/dble(2**kk)
      enddo
      ma = Sa*Dza/3.0
      return
      end
!     ..................................................................
      subroutine &
      mdotchange(Ct,Dmdot,DPa,mdot,nb,nf,np,VarD,VarI,Vp,zb,zf)
!     Change in mass flow rate by adaptive Simpson integration
      use fluid
      use inputparameters, only : Dt, n
      implicit none
      integer j,nb(n),nf(n),np,VarI(n,3)
      double precision Ct,Dmdot(n),DPa(n),IIA,mdot(n),VarD(n,4),Vp(n), &
      z1,z2,zb(n),zf(n)
      np = VarI(1,3)
      do j = 1, np
      nb(j)=VarI(j,1); nf(j)=VarI(j,2); Vp(j)=VarD(j,4)
      zb(j)=VarD(j,1); zf(j)=VarD(j,2); mdot(j)=VarD(j,3)
      z1 = zb(j)
      z2 = zf(j)
      call intinvA(Ct,IIA,z1,z2)
      Dmdot(j) = DPa(j)*Dt*Ct/IIA
      enddo
      return
      end
!     ..................................................................
      subroutine menisciposition(ml,nb,nf,np,Vt,zb,zf)
!     Initial menisci locations
      use fluid
      use inputparameters, only : gamma, L, n, Ti
      implicit none
      integer j, nb(n), nf(n), np
      double precision A,D,Dz,ml,rhol,Vt,z,zb(n),zf(n)
!     Total internal volume by trapeziodal integration, cu.m
      Dz = 0.00001
      z = 0.0
      Vt = 0.0
      do while ((z+Dz).le.L)
      Vt = Vt + Dz*(A(z) + A(z+Dz))/2.0
      z = z + Dz
      enddo
      if (z.lt.L) Vt = Vt + (L-z)*(A(z) + A(L))/2.0
!     Mass of liquid
      ml = Vt*gamma*rhol(Ti,coef_rhol,cond_rhol)
!     Compute initial locations of front and back menisci
!     depending on the initial number of LSs/VPs and on the
!     filling ratio gamma.
      np = 3 ! initial number of LSs/VPs
      do j = 1, np
      nb(j) = 1 + (j-1)*75
      nf(j) = j*75
      zb(j) = (dble(j-1) + 0.5 - 0.5*gamma)*L/dble(np)
      zf(j) = (dble(j-1) + 0.5 + 0.5*gamma)*L/dble(np)
      enddo
      return
      end
!     ..................................................................
      subroutine newpositions(Ct,Dmdot,mdot,ml,nb,nf,np,Tp,Ts,zb,zf,zs)
!     Back meniscus displacement
```

```
      use fluid
      use inputparameters, only : cc, Dt, n, ns
      implicit none
      integer ii,j,jn,js,kk,nb(n),nf(n),ninc,np
      double precision A,Ca,Cb,Ct,dh,Dmdot(n),Dza,Dzb,ma,mb,ml, &
      mdot(n),rhol,temp,Tp(n),Ts(ns),wrap,z1,zb(n),zf(n),zs(ns)
      do j = 1, np
      Dzb = Dt*Ct*(mdot(j)+Dmdot(j))/rhol(Tp(j),coef_rhol,cond_rhol)/A(zb(j))
1     Dza = Dt*Ct/2.0*((mdot(j)+Dmdot(j))/rhol(Tp(j),coef_rhol,cond_rhol) &
      /A(wrap(Dzb+zb(j))) + mdot(j)/rhol(Tp(j),coef_rhol,cond_rhol)/A(zb(j)))
      if (dabs(Dza-Dzb)/dh(zb(j)).gt.cc*Ct) then
      Dzb = Dza
      goto 1
      endif
      mdot(j) = mdot(j) + Dmdot(j)
      zb(j) = wrap(zb(j) + Dza)
      z1 = zb(j)
      Dza = ml/rhol(Ts(nb(j)),coef_rhol,cond_rhol)/A(z1)/dble(ns)
      do js = 1, ninc(j,nb,nf) !Secant Method
      jn = mod(nb(j)+js-2,ns)+1
      Dzb = 0.0
      mb = 0.0
      call massincrement(Ct,Dza,jn,ma,Ts,z1)
      do while (dabs(ma-ml/dble(ns))*dble(ns)/ml.gt.cc*Ct)
      temp = (Dza-Dzb)/(ma-mb)
      Dzb = Dza
      mb = ma
      Dza = Dza + temp*(ml/dble(ns)-ma)
      call massincrement(Ct,Dza,jn,ma,Ts,z1)
      enddo
      zs(jn) = wrap(z1+Dza/2.0)
      z1 = wrap(z1+Dza)
      enddo
      zf(j) = z1
      enddo
      return
      end
!     ..................................................................
      subroutine output &
      (Dmdot,DPa,DPbl,DPc,DPd,DPg,DPs,DPv,h,hm,ml,mdot,nf,nb,np, &
      qwf,qwfm,Tfm,tnow,Tp,Ts,Tw,Twm,zb,zf,zs)
!     Output data
      use fluid
      use inputparameters, only : L,Lev,Lc,Tinf,Ti,Qt,hcex,gamma,n,ns,nw
      implicit none
      integer i,ii,j,js,k,nb(n),nf(n),np,slug
      double precision Dmdot(n),DPa(n),DPbl(n),DPc(n),DPd(n),DPg(n),DPs(n), &
      DPv(n),h(nw),hm(nw),mdot(n),ml,mom,qwf(nw), &
      qwfm(nw),Tfm(nw),tnow,Tp(n),Ts(ns),Tw(nw),Twm(nw),wrap, &
      zb(n),zf(n),zmin,zs(ns),Cpl,dh,hg,kl,mul,Psat,rhol,sigma, &
      qin,To,Res,zz,A,Prs,NuDB,NuSH,NuGN,beta,Cf,Nu

!      open(unit=19,file='Initial_Conditions_B.txt',status='unknown')
!!      initial conditions
!      write(19,"(i4)")  np
!      write(19,"(i4)") (nb(i),nf(i),i=1,np)
!      write(19,1) tnow,ml,(mdot(i),i=1,np),(hm(i),i=1,nw), &
!      (qwfm(i),i=1,nw),(Tfm(i),i=1,nw),(Tp(i),i=1,np), &
!      (Ts(i),i=1,ns),(Tw(i),i=1,nw),(Twm(i),i=1,nw),(zb(i),i=1,np), &
!      (zf(i),i=1,np),(zs(i),i=1,ns)
!1     format(d17.10)
!      open(unit=20,file='status-B-_DPbl_test.m',status='unknown')
```

```
!       write(20,1) tnow;
              open(unit=21,file='mom_eq_terms_et_BHM_80W.txt',position='append', &
                   status='unknown')
        do j = 1, np
         write(21,2) tnow, zb(j), zf(j), mdot(j), Dmdot(j), Tp(j), &
         DPa(j), DPc(j), DPd(j), DPg(j), DPs(j), DPv(j), DPbl(j), j
        enddo
2       format(1x,13(' ',e13.6),i4)

        mom = 0.0 !momentum
        do j = 1, np
         mom = mom+mdot(j)*wrap(zf(j)-zb(j))
        enddo
         open(unit=25,file='tnow_T_mom_et_BHM_80W.txt',position='append', &
              status='unknown')
        write(25,6) tnow,minval(Tw),maxval(Tw),Tw(1152),h(1152),hm(1152),mom
6       format(1x,e13.6,6(' ',e13.6))

!       open(unit=20,file='hcex2.txt',position='append',status='unknown')
!       write(20,7) tnow,maxval(hcex2)
!7      format(1x,e13.6,(' ',e13.6))

        do i = 1, 25
         close(i)
        enddo
        return
        end
!       ......................................................................
        subroutine plugform(mdot,nb,nf,np,Tp,Ts,Vp,zb,zf,zs)
!       Account for formation of vapor plugs at maximum (max) T on slug
        use fluid
        use inputparameters, only : rfs,n,ns
        implicit none
        integer i,is,j,jo,js,k,ks,nb(n),nf(n),ninc,nmax,np
        double precision Dz,mdot(n),Psat,rcap,sigma,Tsat,Tsh, &
        Tshmax,To,Tp(n),Ts(ns),Vp(n),wrap,zb(n),zf(n),zmax,zo,zs(ns)

!       mauro
        Dz = 0
!
        j = 1
        do while (j.le.np)
        k = mod(j,np)+1
        Tshmax = 0.0
        if (ninc(j,nb,nf).gt.4) then
        do jo = 1, ninc(j,nb,nf)-3
        js = mod(nb(j)+jo-2,ns)+1
        is = mod(js+ns-2,ns)+1
        ks = mod(js,ns)+1
        Dz = wrap(zs(js)-zs(is))-Dz
        if (jo.eq.1) Dz = wrap(zs(js)-zb(j))
        zo = wrap(zs(js)+Dz)
        call Tfluid(nb,nf,np,To,Tp,Ts,zo,zb,zf,zs)
        Tsh = dmax1(Tp(j),Tp(k))
        Tsh = Tsat(Psat(Tsh,coef_Psat,cond_Psat)+2.0* &
        sigma(Tsh,coef_sigma,cond_sigma)/rcap(zo),coef_Tsat,cond_Tsat)
        if (jo.ge.3.and.To.gt.Tsh.and.To.gt.Tshmax) then
        Tshmax = To
        nmax = js
        zmax = zo
        endif
        enddo
```

```
      endif
      if (Tshmax.gt.0.0) then
      do i = np+1, j+1, -1
      zb(i) = zb(i-1); zf(i) = zf(i-1); nb(i) = nb(i-1);
      nf(i) = nf(i-1); Tp(i) = Tp(i-1); mdot(i) = mdot(i-1)
      Vp(i) = Vp(i-1);
      enddo
      zf(j) = zmax; zb(j+1) = zmax; Tp(j+1) = Tshmax; Vp(j+1) = 0.0
      nf(j) = nmax; nb(j+1) = mod(nmax,ns)+1; j = j+1; np = np+1
      endif
      j = j+1
      enddo
      return
      end
!     ..................................................................
      subroutine plugtemperature(Ct,flag,np,Qcb,Qcf,Qwp,Tp,Vp,Vt,zb,zf)
!     Vapor plug temperature based on heat, volume using secant method
!     and pressure change
      use fluid
      use inputparameters, only : cc,Ctmin,Dt,DTmax,n,nw,R
      implicit none
      integer converge,flag,i,j,np
      double precision Ct,Ea,Eb,Eo,hg,Psat,Qcb(n),Qcf(n),Qwp(n), &
      qwf(nw),Ta,Tb,temp,Tp(n),Tpa(n),Vp(n),Vpa(n),Vt,wrap,zb(n),zf(n)
      call plugvolume(Ct,np,Vpa,zb,zf)
      flag = 0
      do j = 1, np
      i = mod(j+np-2,np)+1
      Tpa(j) = Tp(j)
      Ta = Tp(j)
      Eo = Psat(Ta,coef_Psat,cond_Psat)*Vp(j)*hg(Ta,coef_hg,cond_hg)/R/Ta + &
      (Qwp(j)-Qcf(i)-Qcb(j))*Dt*Ct
      if (Eo.gt.0.0.and.Vp(j).gt.0.0.and.Vpa(j).gt.Vt*cc) then
      Ea = Eo - Psat(Ta,coef_Psat,cond_Psat)*Vpa(j)*hg(Ta,coef_hg,cond_hg)/R/Ta
      Tb = Tp(j) + 1.0
      Eb = Eo - Psat(Tb,coef_Psat,cond_Psat)*Vpa(j)*hg(Tb,coef_hg,cond_hg)/R/Tb
      converge = 0
      do while(converge.eq.0)
      temp = Ta - (Ta-Tb)*Ea/(Ea-Eb)
      Tb = Ta
      Ta = temp
!     ------------------------------------------------------------------
!     Temperature limit check
      if (fn.eq.'water') then
       if (Ta.gt.578.15) then
       Ta = 578.15
       write (*,*) 'WARNING: Temperature exceeds the maximum limit!'
       else if (Ta.lt.288.15) then
       Ta = 288.15
       write (*,*) 'WARNING: Temperature is lower then the minimum limit!'
       end if
      else if (fn.eq.'ethanol') then
       if (Ta.gt.475.0) then
       Ta = 475.0
       write (*,*) 'WARNING: Temperature exceeds the maximum limit!'
       else if (Ta.lt.265.0) then
       Ta = 265.0
       write (*,*) 'WARNING: Temperature is lower then the minimum limit!'
       end if
       else if (fn.eq.'C6F14') then
       if (Ta.gt.425.0) then
       Ta = 425.0
```

```
        write (*,*) 'WARNING: Temperature exceeds the maximum limit!'
        else if (Ta.lt.275.0) then
        Ta = 275.0
        write (*,*) 'WARNING: Temperature is lower then the minimum limit!'
        end if
        else if (fn.eq.'methanol') then
        if (Ta.gt.470.0) then
        Ta = 470.0
        write (*,*) 'WARNING: Temperature exceeds the maximum limit!'
        else if (Ta.lt.220.0) then
        Ta = 220.0
        write (*,*) 'WARNING: Temperature is lower then the minimum limit!'
        end if
        else if (fn.eq.'R123') then
        if (Ta.gt.440.0) then
        Ta = 440.0
        write (*,*) 'WARNING: Temperature exceeds the maximum limit!'
        else if (Ta.lt.210.0) then
        Ta = 210.0
        write (*,*) 'WARNING: Temperature is lower then the minimum limit!'
        end if
        else if (fn.eq.'R134a') then
        if (Ta.gt.360.0) then
        Ta = 360.0
        write (*,*) 'WARNING: Temperature exceeds the maximum limit!'
        else if (Ta.lt.180.0) then
        Ta = 180.0
        write (*,*) 'WARNING: Temperature is lower then the minimum limit!'
        end if
        else if (fn.eq.'ammonia') then
        if (Ta.gt.380.0) then
        Ta = 380.0
        write (*,*) 'WARNING: Temperature exceeds the maximum limit!'
        else if (Ta.lt.220.0) then
        Ta = 220.0
        write (*,*) 'WARNING: Temperature is lower then the minimum limit!'
        end if
      end if
!     ------------------------------------------------------------------------
      Eb = Ea
      Ea = Eo - Psat(Ta,coef_Psat,cond_Psat)*Vpa(j)*hg(Ta,coef_hg,cond_hg)/R/Ta
      converge = 0
      if (Ea.eq.0.0.or.dabs((Ea-Eb)/Eo).lt.cc*Ct) converge = 1
      enddo
      Tpa(j) = Ta
      endif
      if (dabs(Tp(j)-Tpa(j)).gt.DTmax) flag = 1
      if (flag.eq.1.and.Tpa(j).gt.Tp(j)) Tpa(j) = Tp(j) + DTmax
      if (flag.eq.1.and.Tpa(j).lt.Tp(j)) Tpa(j) = Tp(j) - DTmax
      if (Ct.lt.Ctmin) flag = 0
      enddo
      if (flag.eq.0) then
      do j = 1, np
      Vp(j) = Vpa(j)
      Tp(j) = Tpa(j)
      enddo
      else
      Ct = Ct/10.0
      endif
      return
      end
!     ...............................................................
```

```
      subroutine pressurebalance(DPa,DPbl,DPc,DPd,DPg,DPs,DPv,mdot,np, &
      Tp,zb,zf)
!     Pressure difference across liquid slugs
      use fluid
      use inputparameters, only : n
      implicit none
      integer i,j,k,np
      double precision A,DPa(n),DPbl(n),DPc(n),DPd(n),DPg(n),DPs(n), &
      DPv(n),mdot(n),Psat,rcap,rhol,sigma,Tp(n),wrap,zb(n),zf(n)
      do j = 1, np
      i = mod(j+np-2,np)+1
      k = mod(j,np)+1
!     Overall pressure difference across slug
      DPv(j) = Psat(Tp(j),coef_Psat,cond_Psat) - &
      Psat(Tp(k),coef_Psat,cond_Psat)
!     Capillary
      DPc(j) = 2.0*(sigma(Tp(k),coef_sigma,cond_sigma)/ &
      rcap(zf(j))-sigma(Tp(j),coef_sigma,cond_sigma)/rcap(zb(j)))
!     Dilatation
      DPd(j) = mdot(j)*dabs(mdot(j))/2.0* &
      (1.0/rhol(Tp(k),coef_rhol,cond_rhol)/A(zf(j))**2.0 - &
       1.0/rhol(Tp(j),coef_rhol,cond_rhol)/A(zb(j))**2.0)
!     Acceleration
      DPa(j) = DPv(j)+DPc(j)-DPd(j)+DPg(j)+DPs(j)+DPbl(j)
      enddo
      return
      end
!     ..................................................................
      subroutine previous &
      (ml,mdot,nb,nf,np,qwfm,Tfm,tnow,Tp,Ts,Tw,Twm,zb,zf,zs)
!     Conditions from a previous simulation
!     with mean values (followed by m)
      use fluid
      use inputparameters, only : n,ns,nw
      implicit none
      integer i,j,nb(n),nf(n),np
      double precision hm(nw),ml,mdot(n),qwfm(nw),Tfm(nw),tnow, &
      Tp(n),Ts(ns),Tw(nw),Twm(nw),zb(n),zf(n),zs(ns)
      open(unit=19,file='Initial_Conditions.txt',status='old')
      read(19,"(i4)")  np
      read(19,"(i4)") (nb(i),nf(i),i=1,np)
      read(19,1) tnow,ml,(mdot(i),i=1,np),(hm(i),i=1,nw), &
      (qwfm(i),i=1,nw),(Tfm(i),i=1,nw),(Tp(i),i=1,np), &
      (Ts(i),i=1,ns),(Tw(i),i=1,nw),(Twm(i),i=1,nw),(zb(i),i=1,np), &
      (zf(i),i=1,np),(zs(i),i=1,ns)
1     format(d17.10)
      close(19)
      return
      end
!     ..................................................................
      subroutine refinet(Ct,mdot,nb,nf,np,Tp,VarD,VarI,Vp,zb,zf)
!     Anticipate collisions to allow for least amount of slug overlap
      use fluid
      use inputparameters, only : Dt,n
      implicit none
      integer i,j,nb(n),nf(n),np,VarI(n,3)
      double precision A,Ct,mdot(n),rhol,temp,Tp(n), &
      VarD(n,4),Vp(n),wrap,zb(n),zf(n)
      Ct = 1.0
      VarI(1,3) = np
      do j = 1, np
      VarI(j,1) = nb(j); VarI(j,2) = nf(j); VarD(j,4) = Vp(j)
```

```
      VarD(j,1) = zb(j); VarD(j,2) = zf(j); VarD(j,3) = mdot(j)
      i = mod(j+np-2,np)+1
      temp = mdot(i)/rhol(Tp(j),coef_rhol,cond_rhol)/A(zf(i))-mdot(j)/ &
      rhol(Tp(j),coef_rhol,cond_rhol)/A(zb(j))
      if (temp.ne.0.0) temp = wrap(zb(j)-zf(i))/Dt/temp
      if (temp.gt.0.0.and.temp.lt.1.0.and.temp.lt.Ct) Ct = temp
      enddo
      return
      end
!     ..................................................................
      subroutine &
      setvalues(Ct,Dmdot,DPa,DPbl,DPc,DPd,DPg,DPs,mdot,nb,nf,np,tnow,hm,DPK, &
      qwfm,Twm,Tfm)
!     Initial conditions
      use inputparameters, only : hcex,n,ns,nw
      implicit none
      integer jjj,iii, nb(n),nf(n),np
      double precision Ct,Dmdot,DPa,DPbl,DPc,DPd,DPg,DPs,mdot,tnow,DPK,hm, &
      qwfm,Twm,Tfm,qwf
      dimension Dmdot(n),DPa(n),DPbl(n),DPc(n),DPd(n),DPg(n),DPs(n), &
      mdot(n),DPK(nw), hm(nw),qwfm(nw),Twm(nw),Tfm(nw),qwf(nw)
!     Time, s

!      Ct = 1.0
!      tnow = 0.0
!      np = 1
!      nb(1) = 1
!      nf(1) = ns
!      Dmdot(1) = 0.0
!      mdot(1) = 0.0
!      DPa(1) = 0.0
!      DPc(1) = 0.0
!      DPd(1) = 0.0
!      DPg(1) = 0.0
!      DPs(1) = 0.0

      Ct = 1.0   !initialize time step refinement factor
      tnow = 0.0 !initialize time now
      np = 3     !initial number of vapor plugs/liquid slugs (3 LSs + 3 VPs)
      nb(1) = 1  !initial position of the 1st LS back meniscus
      nf(1) = ns !initial position of the 1st LS front meniscus

!     Cycle added in order to initialize every possible variable component
      do jjj = 1,n
      Dmdot(jjj) = 0.0
      mdot(jjj) = 0.0
      DPa(jjj) = 0.0
      DPbl(jjj) = 0.0
      DPc(jjj) = 0.0
      DPd(jjj) = 0.0
      DPg(jjj) = 0.0
      DPs(jjj) = 0.0

      enddo

      do iii = 1,nw
      DPK(iii) = 0.0
      hm(iii) = 0.0
      qwfm(iii)= 0.0
      Twm(iii)= 0.0
      Tfm(iii)= 0.0
      qwf(iii) = 0.0
```

```
      enddo
!
      return
      end
!     ..................................................................
      subroutine shear(Ct,DP,mdot,nb,nf,np,Tp,Ts,z1,z2,zb,zf,zs)
!     Differential pressure along slug due to shear from back meniscus
!     to given location
      use fluid
      use inputparameters, only : cc, n, ns
      implicit none
      integer converge,ii,j,k,kk,nb(n),nf(n),np,slug
      double precision A,Ca,Cb,Cf,Ct,dh,DP,mdot(n),mul,Re,rhol,Sa,Sb,To, &
      Tp(n),Ts(ns),wrap,z,z1,z2,zb(n),zf(n),zs(ns)
      call Tfluid(nb,nf,np,To,Tp,Ts,z1,zb,zf,zs)
      j = slug(np,z1,zb,zf)
      Re = mdot(j)*dh(z1)/mul(To,coef_mul,cond_mul)/A(z1)
      Sa = Cf(Re,z1)/(dh(z1)*rhol(To,coef_rhol,cond_rhol)*A(z1)**2.0)
      call Tfluid(nb,nf,np,To,Tp,Ts,z2,zb,zf,zs)
      Re = mdot(j)*dh(z2)/mul(To,coef_mul,cond_mul)/A(z2)
      Sa = Sa + Cf(Re,z2)/(dh(z2)*rhol(To,coef_rhol,cond_rhol)*A(z2)**2.0)
      Ca = 0.0
      kk = 0

!     mauro
      converge = 0
!
      do while ((converge.eq.0.or.kk.le.3).and.kk.lt.20)
      Sb = Sa
      Cb = Ca
      Ca = 0.0
      kk = kk + 1
      do ii = 1, 2**(kk-1)
      z = wrap(z1+dble(2*ii-1)*wrap(z2-z1)/dble(2**kk))
      call Tfluid(nb,nf,np,To,Tp,Ts,z,zb,zf,zs)
      Re = mdot(j)*dh(z)/mul(To,coef_mul,cond_mul)/A(z)
      Ca = Ca + Cf(Re,z)/(dh(z)*rhol(To,coef_rhol,cond_rhol)*A(z)**2.0)
      enddo
      Sa = Sb/2.0 + (4.0*Ca - 2.0*Cb)/dble(2**kk)
      converge = 0
      if (Sa.lt.cc*Ct.or.dabs((Sa-Sb)/Sa).lt.cc*Ct) converge = 1
      enddo
      DP = -2.0*Sa*mdot(j)*dabs(mdot(j))*wrap(z2-z1)/3.0
      return
      end
!     ..................................................................
      subroutine sheartotal(Ct,DPs,mdot,nb,nf,np,Tp,Ts,zb,zf,zs)
!     Differential pressure across slug due to shear dP/dz
      use inputparameters, only : n,ns
      implicit none
      integer j, nb(n), nf(n), np
      double precision Ct,DP,DPs(n),mdot(n),Tp(n), &
      Ts(ns),z1,z2,zb(n),zf(n),zs(ns)
      do j = 1, np
      z1 = zb(j)
      z2 = zf(j)
      call shear(Ct,DP,mdot,nb,nf,np,Tp,Ts,z1,z2,zb,zf,zs)
      DPs(j) = DP
      enddo
      return
      end
!     ..................................................................
```

```
      subroutine slugconduction(nb,nf,np,Qcb,Qcd,Qcf,Tp,Ts,zb,zf,zs)
!     Conduction along slug
      use fluid
      use inputparameters, only : n,ns
      implicit none
      integer back,front,is,j,js,k,ks,nb(n),nf(n),np,slug
      double precision A,kl,Qcb(n),Qcd(ns),Qcf(n),Tp(n),Ts(ns),wrap, &
      zb(n),zf(n),zs(ns)
      do js = 1, ns
      back = 0
      front = 0
      j = slug(np,zs(js),zb,zf)
      if (js.eq.nb(j)) back = j
      if (js.eq.nf(j)) front = j
      if (back.gt.0) then
      ks = mod(js,ns)+1
      Qcd(js) = Qcb(j) + kl(Ts(js),coef_kl,cond_kl)*A(zs(js))* &
      (Ts(ks)-Ts(js))/wrap(zs(ks)-zs(js))
      elseif (front.gt.0) then
      is = mod(js+ns-2,ns)+1
      k = mod(j,np)+1
      Qcd(js) = Qcf(j) + kl(Ts(js),coef_kl,cond_kl)*A(zs(js))* &
      (Ts(is)-Ts(js))/wrap(zs(js)-zs(is))
      else
      is = mod(js+ns-2,ns)+1
      ks = mod(js,ns)+1
      Qcd(js) = kl(Ts(js),coef_kl,cond_kl)*A(zs(js))* &
      ((Ts(is)-Ts(js))/wrap(zs(js)-zs(is)) + &
      (Ts(ks)-Ts(js))/wrap(zs(ks)-zs(js)))
      endif
      enddo
      return
      end
!     ..................................................................
      subroutine slugmerge(mdot,nb,nf,np,Tp,Vp,zb,zf)
!     account for any two slugs merging this time step
      use inputparameters, only : cc,Dt,n
      implicit none
      integer between,i,j,k,nb(n),nf(n),np
      double precision A,dh,Dz,mdot(n),rhol,Tp(n),Vp(n),wrap,zb(n),zf(n)
      j = 1
      do while (j.le.np)
      i = mod(j+np-2,np)+1
      if (np.gt.1.and.(between(zb(j),zf(i),zf(j)).eq.1.or. &
      wrap(zb(j)-zf(i)).lt.dh(zb(j))*cc)) then
      mdot(j) = (mdot(i)*wrap(zf(i)-zb(i))+ &
      mdot(j)*wrap(zf(j)-zb(j)))/wrap(zf(j)-zb(i))
      zb(j) = zb(i)
      nb(j) = nb(i)
      Tp(j) = Tp(i)
      Vp(j) = Vp(i)
      if (i.lt.np) then
      do k = i, np-1
      zb(k) = zb(k+1)
      zf(k) = zf(k+1)
      nb(k) = nb(k+1)
      nf(k) = nf(k+1)
      Tp(k) = Tp(k+1)
      Vp(k) = Vp(k+1)
      mdot(k) = mdot(k+1)
      enddo
      endif
```

```
      np = np-1
      else
      j = j+1
      endif
      enddo
      return
      end
!     ..................................................................
      subroutine slugtemperature(Ct,ml,Qcd,Qhf,Ts)
!     Fluid temperature based on axial convection and convection to wall
      use fluid
      use inputparameters, only : Dt,ns
      implicit none
      integer js
      double precision Cpl,Ct,ml,Qcd(ns),Qhf(ns),Ts(ns)
      do js = 1, ns
      Ts(js) = Ts(js) + &
      (Qcd(js)+Qhf(js))*dble(ns)*Dt*Ct/ml/Cpl(Ts(js),coef_cpl,cond_cpl)
      enddo
      return
      end
!     ..................................................................
      subroutine testprops
!     Output file to check diameter variation across the length and
!     gravity angle profile.
      use fluid
      use inputparameters !, only:L,Lev,Lc,Ti,Tinf,hcex,Qt,gamma,nw
      implicit none
      double precision theta,theta1,dh,Cpl,Cpv,hl,hg,kl,kv,mul,muv,Psat, &
                       rhol,rhov,sigma,z4
      integer section,section1
      open(unit=1,file='test_geom_prop@Ti_et_BHM_80W.txt',status='unknown')
      write(1,10) 'Ti',Ti,'[K]','Tinf',Tinf,'[K]','hcex',hcex,'[W/m2.K]', &
                  'Qt',Qt,'[W]','gamma',gamma,'[-]','L',L,'[m]','Le',Lev,'[m]', &
                  'Lc',Lc,'[m]','Cpl(Ti)',Cpl(Ti,coef_cpl,cond_cpl),'[J/kg.K]', &
                  'Cpv(Ti)',Cpv(Ti,coef_cpv,cond_cpv),'[J/kg.K]', &
                  'hl(Ti)',hl(Ti,coef_hl,cond_hl),'[J/kg]', &
                  'hg(Ti)',hg(Ti,coef_hg,cond_hg),'[J/kg]', &
                  'kl(Ti)',kl(Ti,coef_kl,cond_kl),'[W/m.K]', &
                  'kv(Ti)',kv(Ti,coef_kv,cond_kv),'[W/m.K]', &
                  'mul(Ti)',mul(Ti,coef_mul,cond_mul),'[Pa.s]', &
                  'muv(Ti)',muv(Ti,coef_muv,cond_muv),'[Pa.s]', &
                  'Psat(Ti)',Psat(Ti,coef_Psat,cond_Psat),'[Pa]', &
                  'Pcr',Pcr,'[Pa]', &
                  'rhol(Ti)',rhol(Ti,coef_rhol,cond_rhol),'[kg/m3]', &
                  'rhov(Ti)',rhov(Ti,coef_rhov,cond_rhov),'[kg/m3]', &
                  'sigma(Ti)',sigma(Ti,coef_sigma,cond_sigma),'[N/m]', &
                  'deltw',deltw,'[m]','dellf',dellf,'[m]','rfs',rfs,'[m]' , &
                  'xqualev',xqualev,'[kgv/kg]','xqualco',xqualco,'[kgv/kg]'
10    format(1x, A9, ' = ' e13.6, '      ' A8)
      write(1,15) 'nw' , nw , 'theta_in' , theta_in
15    format(1x, A9, ' =  ' i4)
      write(1,16) 'fn' , fn
16    format(1x, A9, ' =' A10)
      open(unit=2,file='z_theta_section_et_BHM_80W.txt',status='unknown')
      z4 = 0.0
      do while (z4.le.L)
      write(2,20) z4,theta(z4), section(z4)
20    format(1x, f5.3, ',', f5.3, ',', i1)
      z4 = z4 + 0.001
      enddo
      close(unit=1)
```

```
      close(unit=2)
      return
      end
!     ..................................................................
      subroutine Tfluid(nb,nf,np,To,Tp,Ts,z,zb,zf,zs)
!     Interpolate fluid temperatures for
      use inputparameters, only : n,ns
      implicit none
      integer between,i,is,j,js,ks,nb(n),nf(n),np,plug,slug
      double precision To,Tp(n),Ts(ns),wrap,z,zb(n),zf(n),zs(ns)
      j = slug(np,z,zb,zf) !determines what slug lies in the actual z
!                          position j = 0 means that there is not a
!                          LS on the actual z position.
      if (j.eq.0) then
      To = Tp(plug(np,z,zb,zf)) !indeed if j = 0 then the fluid
!                               temperature is equal to the temperature
!                               of the plug that lies in that z position.
      elseif (between(zb(j),z,zs(nb(j))).eq.1) then
      js = nb(j)
      ks = mod(js,ns)+1
      To = Ts(js)-(Ts(ks)-Ts(js))/ &
      wrap(zs(ks)-zs(js))*wrap(zs(js)-z)
      elseif (between(zs(nf(j)),z,zf(j)).eq.1) then
      js = nf(j)
      is = mod(js+ns-2,ns)+1
      To = Ts(js)+(Ts(js)-Ts(is))/ &
      wrap(zs(js)-zs(is))*wrap(z-zs(js))
      else
      js = nb(j)
      ks = mod(js,ns)+1
      do while (between(zs(js),z,zs(ks)).eq.0)
      js = mod(js,ns)+1
      ks = mod(js,ns)+1
      enddo
      To = Ts(js)+(Ts(ks)-Ts(js))/ &
      wrap(zs(ks)-zs(js))*wrap(z-zs(js))
      endif
      return
      end
!     ..................................................................
      subroutine timeaverage(Ct,h,hm,nb,nf,np,qwf,qwfm,Tfm,tnow, &
      Tp,Ts,Tw,Twm,zb,zf,zs)
!     Mean (variables followed by m) wall and fluid temperatures
      use fluid
      use inputparameters, only : Dt,L,n,ns,nw
      implicit none
      integer i,j,nb(n),nf(n),np
      double precision Ct,h(nw),hm(nw),qwf(nw), &
      qwfm(nw),Tfm(nw),tnow,To,Tp(n),Ts(ns),Tw(nw),Twm(nw),z,zb(n), &
      zf(n),zs(ns)
      do i = 1, nw
      hm(i) = (hm(i)*tnow+h(i)*Dt*Ct)/(tnow+Dt*Ct)
      qwfm(i) = (qwfm(i)*tnow+qwf(i)*Dt*Ct)/(tnow+Dt*Ct)
      z = L*dble(i-1)/dble(nw)
      Twm(i) = (Twm(i)*tnow+Tw(i)*Dt*Ct)/(tnow+Dt*Ct)
      call Tfluid(nb,nf,np,To,Tp,Ts,z,zb,zf,zs)
      Tfm(i) = (Tfm(i)*tnow+To*Dt*Ct)/(tnow+Dt*Ct)
      enddo
      return
      end
!     .............Mod.MM/17-09-2009.....................................
      subroutine walltemperature(Ct,qin,qwf,Tw)
```

```
!     New wall temperature based on heat transfer to or from fluid, from
!     evaporator, or to condenser
      use fluid
      use inputparameters, only : Cptw,deltw,delwk,Dt,hcex,kw,L,nw,pi, &
      rhotw,Tinf
      implicit none
      integer i,j,k, section
      double precision A,Atw,Awk,Cp,Cpl,Ct,dh,Dz,kl,p,rhol,qin,Qwc, &
      qwf(nw),Tw(nw),Twn(nw),z
      Dz = L/dble(nw)
      do j = 1, nw
      i = mod(j+nw-2,nw)+1
      k = mod(j+nw,nw)+1
      z = dble(j-1)*Dz
!     -------holley's wick---------------------------------
!      Awk = pi/4.0*(dh(z)+2.0*delwk)**2.0-A(z)
!      Atw = pi/4.0*(dh(z)+2.0*(delwk+deltw))**2.0-Awk-A(z)
!      Qwc = (kw*(Atw)+kl(Tw(j))*Awk)/Dz*(Tw(i)-2.0*Tw(j)+Tw(k))
!      Cp = (rhotw*Cptw*Atw+rho(Tw(j))*Cpl(Tw(j))*Awk)*Dz
!      if (section(z).eq.1) then
!      Twn(j) = Tw(j) + Dt*Ct/Cp*(Qwc+p(z)*Dz*(qin-qwf(j)))
!      elseif (section(z).eq.2) then
!      Twn(j) = Tw(j) + Dt*Ct/Cp*(Qwc-qwf(j)*p(z)*Dz)
!      else
!      Twn(j) = Tw(j) + Dt*Ct/Cp*(Qwc-qwf(j)*p(z)*Dz- &
!      hcex*pi*(dh(z)+2.0*(deltw+delwk))*(Tw(j)-Tinf)*Dz)
!     -----------------------------------------------------
!      Awk = pi/4.0*(dh(z)+2.0*delwk)**2.0-A(z)
      Atw = pi/4.0*(dh(z)+2.0*(deltw))**2.0-A(z)
      Qwc = (kw*(Atw))/Dz*(Tw(i)-2.0*Tw(j)+Tw(k))
      Cp = (rhotw*Cptw*Atw)*Dz
      if (section(z).eq.1) then
      Twn(j) = Tw(j) + Dt*Ct/Cp*(Qwc+p(z)*Dz*(qin-qwf(j)))
      elseif (section(z).eq.2) then
      Twn(j) = Tw(j) + Dt*Ct/Cp*(Qwc-qwf(j)*p(z)*Dz)
      else
      Twn(j) = Tw(j) + Dt*Ct/Cp*(Qwc-qwf(j)*p(z)*Dz- &
      hcex*pi*(dh(z)+2.0*(deltw))*(Tw(j)-Tinf)*Dz)
      endif
      enddo
      do j = 1, nw
      Tw(j) = Twn(j)
      enddo
      return
      end
```

Annex II

Experimental apparatus: technical drafts

Introduction

Many details of the experimental test-rig described in Chapter 7 have been designed by the author. Here is the list of all the technical drafts provided to the workshop in order to obtain the constitutive element of the presented PHP.

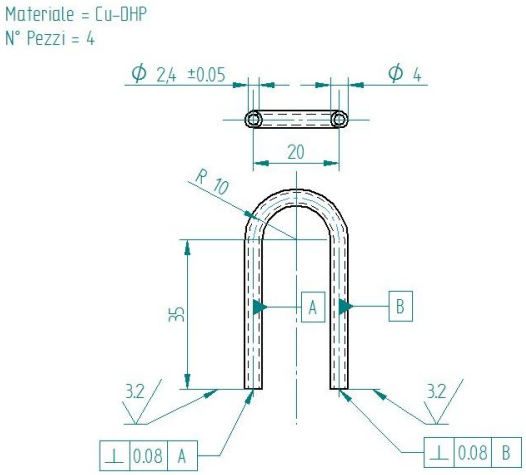

Figure AII. 1: Condenser copper U-tube.

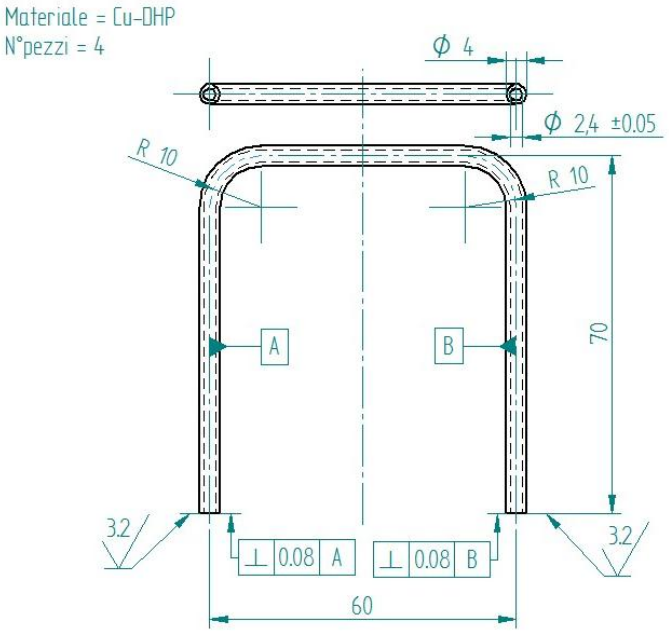

Figure AII. 2: condenser copper tube.

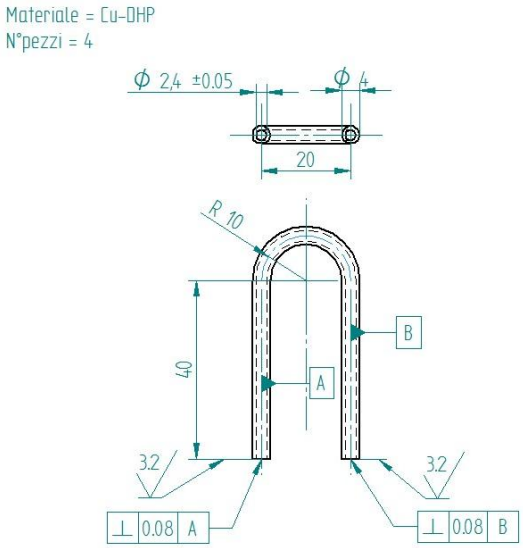

Figure AII. 3: evaporatorator copper tube.

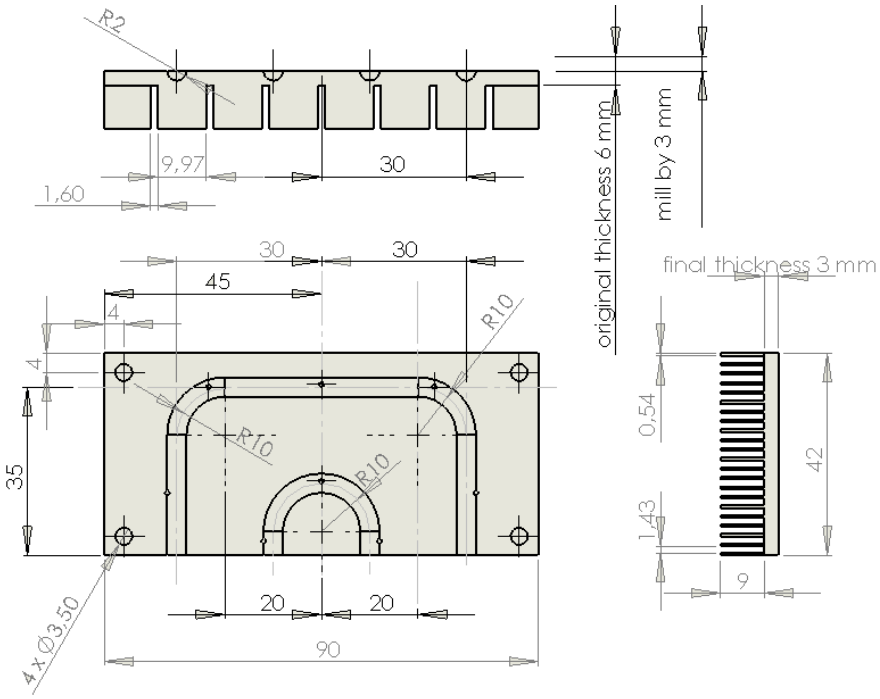

Figure AII. 4: condenser heat sink

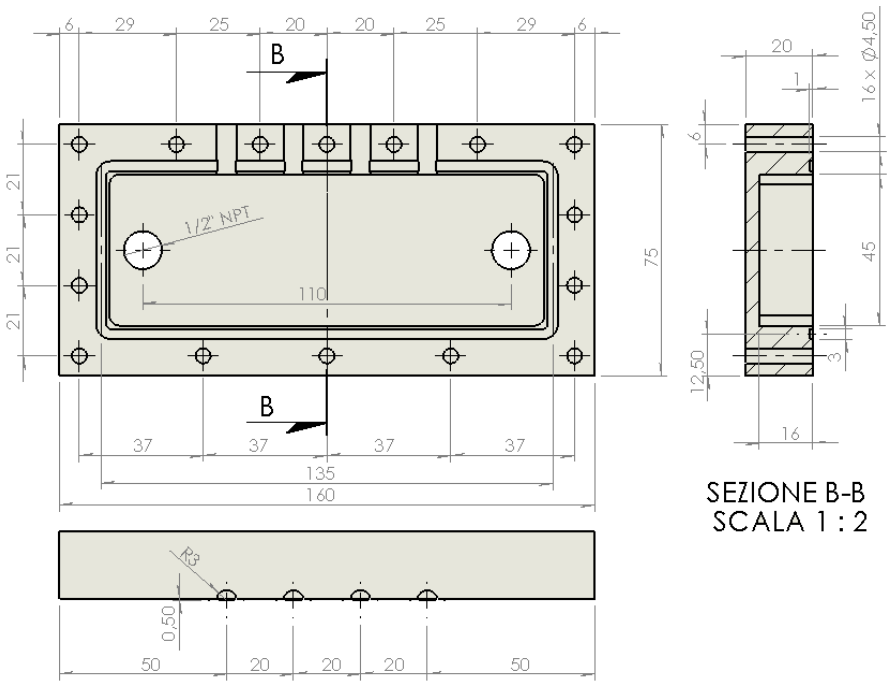

Figure AII. 5: condenser shell

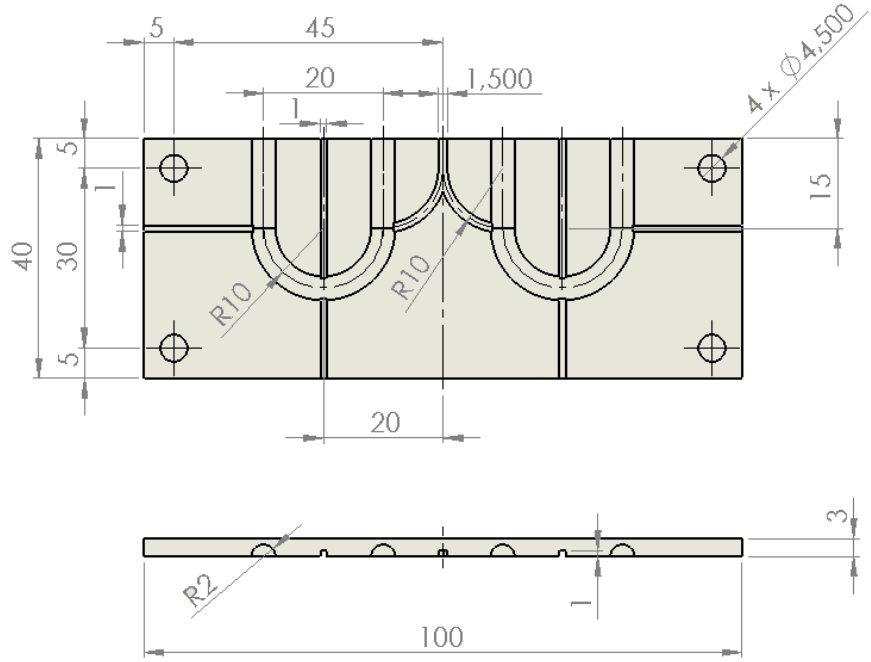

Figure AII. 6: evaporator copper block.

List of tables

List of figures

List of publications

International journals

1. Mameli, M., Marengo, M. & Zinna, S., 2011. Numerical model of a multi-turn Closed Loop Pulsating Heat Pipe: Effects of the local pressure losses due to meanderings. *International Journal of Heat and Mass Transfer*, 55(4), pp.1036-1047.
2. Mameli, M., Marengo, M. ,Zinna, S., 2012, Thermal Hydraulic Simulation of a Pulsating Heat Pipe Effects of Different Liquid Properties on a Simple Geometry, *Heat Transfer Engineering Int. J*., Vol. 33 (14).
3. Mameli, M., Marengo, M. ,Zinna, S**.,** 2012, Numerical investigation of the effects of orientation and gravity in a Closed Loop Pulsating Heat Pipe. *Microgravity Science and Technology Int. J*., DOI: 10.1007/s12217-011-9293-2.

Conference proceedings

1. Mameli M., Marengo M., Vassiliev L., Zinna S., 2008, Advanced design of a pulsating heat pipe: numerical Simulations and proposal for an experimental apparatus, *1st European Conference on Microfluidics*, Bologna, December 10-12.
2. Mameli M., Marengo M., Vassiliev L., Zinna S., 2009, Lumped Parameters Modeling Of A Single Closed Loop Pulsating Heat Pipe, *XXVII UIT Congress*.
3. Mameli M., Marengo M., Zinna S. Thermal Simulation Of A Pulsating Heat Pipe: Effects Of Different Liquid Properties On A Simple Geometry, 2009, *7th International Conference on Heat Transfer, Fluid Mechanics and Thermodynamics*, 19-21 July, Antalya, Turkey.

4. Mameli M., M. Marengo, S. Zinna, How orientation affects the Closed Loop Pulsating Heat Pipe thermal performance: a numerical investigation, *5th International Topical Team Workshop on Two-Phase Systems For Ground And Space Applications*, Kyoto, Japan, September 26-29, 2010.
5. Mameli, M., Marengo, Khandekar S., Flow Patterns and Corresponding Local Heat Transfer Coefficients in a Pulsating Heat Pipe, *XXIX Congresso UIT*, Torino.
6. Mameli, M., Marengo, Khandekar S., (2011b) An Exploratory Study Of A Pulsating Heat Pipe Operated With A Two Component Fluid Mixture, *ISHMT and ASME conference, ITTM, Chennai, India,* ISHMT_IND_16_033.

Bibliography

Akachi, H., 2000. Heat transfer device having metal band formed with longitudinal holes. *US Patent 6,026,890*.

Akachi, H., 1996. L-type heat sink. *US Patent 5,490,558*.

Akachi, H., 1998. Method of manufacturing tunnel-plate type heat pipes. *US Patent 5,737,840*.

Akachi, H., 1997a. Ribbon-like plate heat pipes. *US Patent 5,642,775*.

Akachi, H., 1990. Structure of a heat pipe. *US Patent 4,921,041*.

Akachi, H., 1993. Structure of micro-heat pipe. *US Patent 5,219,020*.

Akachi, H., 1997b. Tunnel-plate type heat pipe. *US Patent 5,697,428*.

Akachi, H., Polasek, F., Stulc P., 1996, Pulsating Heat Pipe, *5th International Heat Pipe Symposium,*. Melbourne, Australia , pp. 208–217.

Akachi H., Polasek F., 1997. Thermal control of IGBT modules in traction drives by Pulsating Heat Pipes, *10th heat pipe conference Stuttgart*, vol. 3, pp. 8-12.

Asfia, J.F., Chen, C. & Cai, Q., 2007. Cooling Apparatus, System, And Associated Method. *EP Patent 1,834,515*.

Begg, E., Holley, B., Faghri, A., 2003. Condensation heat transfer and pressure drop measurements in miniature horizontal tubes with low mass flux rates, *J. Enhanced Heat Transfer* 10 (3), 335–354.

Bhuwakietkumjohn, N. & Rittidech, S., 2010. Internal flow patterns on heat transfer characteristics of a closed-loop oscillating heat-pipe with check valves using ethanol and a silver nano-ethanol mixture. *Experimental Thermal and Fluid Science*, 34(8), pp.1000-1007.

Bretherton, 1961. The motion of long bubbles in tubes, *J. Fluid Mech.*, Vol. 10, pp. 167-188.

Cao, Y. & Gao, M., 2002. Wickless network heat pipes for high heat flux spreading applications. *International Journal of Heat and Mass Transfer*, 45(12), pp.2539-2547.

Charoensawan, P., 2003. Closed loop pulsating heat pipes Part A: parametric experimental investigations. *Applied Thermal Engineering*, 23(16), pp.2009-2020.

Chen, P.-H., Lee, Y.-W. & Chang, T.-L., 2009. Predicting thermal instability in a closed loop pulsating heat pipe system. *Applied Thermal Engineering*, 29(8-9), pp.1566-1576.

Cotter, T.P., 1965. Theory of heat pipes. Los Alamos Scientific Laboratory Report No. LA-3246-MS.

Das, S.P. et al., 2010. Thermally induced two-phase oscillating flow inside a capillary tube. *International Journal of Heat and Mass Transfer*, 53(19-20), pp.3905-3913.

Delil, A.A.M., 2001. *Pulsating & oscillating heat transfer devices in acceleration environments from microgravity to supergravity Pulsating & oscillating heat transfer devices in acceleration environments from microgravity to supergravity*,

Darby R., 1999. Correlate pressure drop through fittings. Chem. Eng., Vol. 106 (7), pp.101–104.

Darby R., 2001. Correlate pressure drop through fittings. Chem. Eng., Vol. 108 (4), pp.127–130.

Dobson, R, 2004. Theoretical and experimental modelling of an open oscillatory heat pipe including gravity. *International Journal of Thermal Sciences*, 43(2), pp.113-119.

Dobson, RT, 2003. An open oscillatory heat pipe steam-powered boat. *International Journal of Mechanical Engineering Education*, 31(4), pp.339–358.

Dobson, R.T., 2005. An open oscillatory heat pipe water pump. *Applied Thermal Engineering*, 25(4), pp.603-621.

Dobson, R.T. & Harms, T.M., 1999. Lumped parameter analysis of closed and open oscillatory heat pipes. In *Proceedings of the 11th International heat pipe Conference.*

Van Es, J. & Woering, A., 2000. High-acceleration performance of the flat swinging heat pipe, *American Technical Publishers Ltd*.

Faghri, A., 1995. Heat Pipe Science and Technology, Taylor & Francis, Washington, DC.

Filippeschi S., 2006. On Periodic Two-phase Thermosyphons Operating Against Gravity, *Int. J. of Thermal Sciences*, Vol. 45, No. 2, pp. 124-137.

Gaugler, R.S., 1944. US Patent 2350348.

Givler, R.C. & Martinez, M.J., 2009. *Modeling of Pulsating Heat Pipes*,

Groll, M., and Khandekar, S., 2003. Pulsating Heat Pipes: Progress and Prospects, *International Conference on Energy and Environment*, Shanghai, China, vol. 1, pp. 723–730.

Grover, G.M., 1963. US Patent 3229759.

Grover, G.M., Cotter, T.P. and Erickson, G.F., 1964. Structures of very high thermal conductance. J. App. Phys., Vol. 35, p. 1990.

Gu, J., Futamata, R. & Kawaji, M., 2004. Effects of Gravity on the Performance of Pulsating Heat Pipes. *Journal of Thermophysics and Heat Transfer*, 18(3), pp.370-378.

Gu, J., Kawaji, M. & Futamata, R., 2005. Microgravity performance of micro pulsating heat pipes. *Microgravity - Science and Technology*, 16(1-4), pp.181-185.

Gungor K.E. and Winterton R.K.S., 1987. Simplified general correlation for saturated flow boiling and comparisons of correlations with data, *Chem. Eng. Res. Des.*, Vol. 65, pp. 148-166.

Han, X. et al., 2008. Investigations on the heat transport capability of a cryogenic oscillating heat pipe and its application in achieving ultra-fast cooling rates for cell vitrification cryopreservation. *Cryobiology*, 56(3), pp.195-203.

Han Y., Shikazono N., 2009. Measurement of the liquid film thickness in micro tube slug flow, International Journal of Heat and Fluid Flow, Vol. 30, pp. 842–853.

Holley, B. & Faghri, Amir, 2005. Analysis of pulsating heat pipe with capillary wick and varying channel diameter. *International Journal of Heat and Mass Transfer*, 48(13), pp.2635-2651.

Hosoda, M., Nishio, S., and Shirakashi, R., 1999. Meandering Closed Loop Heat Transport Tube (Propagation Phenomena of Vapor Plug), *Proc. 5th ASME/JSME Joint Thermal Engineering Conference*, AJTE99-6306, pp. 1–6, San Diego, California, USA.

Ji, Y. et al., 2011. Particle shape effect on heat transfer performance in an oscillating heat pipe. *Nanoscale research letters*, 6(1), p.296.

Kammuang-Lue, N., Hudakorn, T. & Terdtoon, Pradit, 2010. Establishment , Verification and Application of a Correlation to Predict the Maximum Heat Flux of a Horizontal Closed-Loop Pulsating Heat Pipe. *Energy Research Journal*, 1(2), pp.96-103.

Karimi, G., 2004. Review and assessment of pulsating heat pipe mechanism for high heat flux electronic cooling. *in Electronic Systems*, pp.52-59.

Katpradit, T. et al., 2005. Correlation to predict heat transfer characteristics of a closed end oscillating heat pipe at critical state. *Applied Thermal Engineering*, 25(14-15), pp.2138-2151.

Khandekar, S, 2004. An insight into thermo-hydrodynamic coupling in closed loop pulsating heat pipes. *International Journal of Thermal Sciences*, 43(1), pp.13-20.

Khandekar, S, 2003. Closed loop pulsating heat pipes Part B: visualization and semi-empirical modeling. *Applied Thermal Engineering*, 23(16), pp.2021-2033.

Khandekar, S, Gautam, a & Sharma, P., 2009. Multiple quasi-steady states in a closed loop pulsating heat pipe. *International Journal of Thermal Sciences*, 48(3), pp.535-546.

Khandekar, S, Groll, M, et al., 2002. Pulsating heat pipes: thermo-fluidic characteristics and comparative study with single phase thermosyphon. In

12th International Heat Transfer Conference, Grenoble, France., pp. 459–464.

Khandekar, S. & Cui, X., 2002. Thermal performance modeling of pulsating heat pipes by artificial neural network. *12th Int. Heat Pipe Conf.-Moscow-Kostroma-Moscow*, pp.215-219.

Khandekar, S. & Groll, M., 2004. Pulsating Heat Pipes: Attractive Entrants in the Family of Closed Passive Two-Phase Systems. *Journal of Energy Heat and Mass Transfer*, 26(1/4), p.99.

Khandekar, S., Schneider, M. & Groll, M., 2002. Mathematical modeling of pulsating heat pipes: state of the art and future challenges. In *5th ASIVTE/TSHMT Joint International Heat and Mass Transfer Conference. Kolkata, India: Kolkata Press Club*. pp. 856-862.

Khandekar, Sameer, 2010. Pulsating heat pipe based heat exchangers. In *Proc. 21st Int. Symp. Transport Phenomena, Kaohsiung City, Taiwan*.

Khandekar, Sameer & Groll, Manfred, 2008. Roadmap to realistic modelling of closed loop pulsating heat pipes. In *Proceedings of the 9th International Heat Pipe Symposium*. pp. 17–20.

Khandekar, Sameer & Gupta, A., 2007. Embedded pulsating heat pipe radiators. In *14th International Heat pipe Conference (14th IHPC), Florianopolis, Brazil*. pp. 4-9.

Khandekar, Sameer, Dollinger, N. & Groll, Manfred, 2003. Understanding operational regimes of closed loop pulsating heat pipes: an experimental study. *Applied Thermal Engineering*, 23(6), pp.707-719.

Kim, J.-H., Kim, J.-W. & Kim, Jong-Su, 2002. The Study on Pressure Oscillation and Heat Transfer Characteristics of Oscillating Capillary Tube Heat Pipe Using Mixed Working Fluid. *Transactions of the Korean Society of Mechanical Engineers B*, 26(2), pp.318-327.

Kim, J.S. et al., 2003. Flow visualization of oscillation characteristics of liquid and vapor flow in the oscillating capillary tube heat pipe. *Journal of Mechanical Science and Technology*, 17(10), pp.1507–1519.

Kim, Jong-Soo, Im, Y.-B. & Bui, N.-H., 2005. Numerical analysis of pulsating heat pipe based on separated flow model. *Journal of Mechanical Science and Technology*, 19(9), pp.1790-1800.

Lee, Y.-W. & Chang, T.-L., 2009. Application of NARX neural networks in thermal dynamics identification of a pulsating heat pipe. *Energy Conversion and Management*, 50(4), pp.1069-1078.

Lemmon, E.W., Huber, M.L., McLinden, M.O., 2007. NIST Standard Reference Database 23: Reference Fluid Thermodynamic and Transport Properties-REFPROP, Version 8.0, *National Institute of Standards and Technology*, Standard Reference Data Program, Gaithersburg.

Liang, S. & Ma, HB, 2004. Oscillating motions of slug flow in capillary tubes. *International communications in heat and mass transfer*, 31(3), pp.365–375.

Lin, L., 2001. *Experimental Investigation of Oscillating heat Pipe for Actuator Cooling*,

Lin, Y., Kang, S. & Chen, H, 2008. Effect of silver nano-fluid on pulsating heat pipe thermal performance. *Applied Thermal Engineering*, 28(11-12), pp.1312-1317.

Lin, Y.-H., Kang, S.-W. & Wu, T.-Y., 2009. Fabrication of polydimethylsiloxane (PDMS) pulsating heat pipe. *Applied Thermal Engineering*, 29(2-3), pp.573-580.

Lin, Z., Wang, S. & Zhang, W., 2009. Experimental study on microcapsule fluid oscillating heat pipe. *Science in China Series E: Technological Sciences*, 52(6), pp.1601-1606.

Liu, S. et al., 2007. Experimental study of flow patterns and improved configurations for pulsating heat pipes. *Journal of Thermal Science*, 16(1), pp.56-62.

Ma, H.B., Hanlon, M. a. & Chen, C.L., 2005. An investigation of oscillating motions in a miniature pulsating heat pipe. *Microfluidics and Nanofluidics*, 2(2), pp.171-179.

Ma, Y. & Zhang, H., 2006. Analysis of Heat Transfer Performance of Oscillating Heat Pipes Based on a Central Composite Design1. *Chinese Journal of Chemical Engineering*, 14(2), pp.223-228.

Maezawa, S., Izumi, T. & Gi, K., 1997. Experimental chaos in oscillating capillary tube heat pipes. In *10th International Heat Pipe Conference, Stuttgart, Germany*.

Mameli, M., Marengo, M. & Zinna, S., 2011a. Numerical model of a multi-turn Closed Loop Pulsating Heat Pipe: Effects of the local pressure losses due to meanderings. *International Journal of Heat and Mass Transfer*, 55(4), pp.1036-1047.

Mameli, M., Marengo, Khandekar S., 2011b An Exploratory Study Of A Pulsating Heat Pipe Operated With A Two Component Fluid Mixture, *ISHMT and ASME conference, ITTM, Chennai, India,* ISHMT_IND_16_033.

Mameli, M., Marengo, M. ,Zinna, S., 2012a, Thermal Hydraulic Simulation of a Pulsating Heat Pipe Effects of Different Liquid Properties on a Simple Geometry, *Heat Transfer Engineering Int. J*., Vol. 33 (14).

Mameli, M., Marengo, M. ,Zinna, S**.,** 2012b, Numerical investigation of the effects of orientation and gravity in a Closed Loop Pulsating Heat Pipe. Microgravity Science and Technology Int. J., DOI: 10.1007/s12217-011-9293-2.

Miyazaki, Y., 2005. Cooling of Notebook PCs by Flexible Oscillating Heat Pipes. In *Proceedings of ASME InterPACK, San Francesco, USA*. pp. 1-5.

Nasonov, E.A., Bondarenko, Y.I., 1980, Heat transmission device for solar heating systems, Geliotekhnika 16, pp. 56–61.

Nikolayev, V.S., 2011. A Dynamic Film Model of the Pulsating Heat Pipe, *J. Heat Transfer*, ASME, Vol. 133 (8), 081504.

Nuntaphan, A. et al., 2010. Use of oscillating heat pipe technique as extended surface in wire-on-tube heat exchanger for heat transfer enhancement.

International Communications in Heat and Mass Transfer, 37(3), pp.287-292.

Qu, W. & Ma, H, 2007. Theoretical analysis of startup of a pulsating heat pipe. *International Journal of Heat and Mass Transfer*, 50(11-12), pp.2309-2316.

Qu J., Wu H., Cheng P., 2010. Thermal performance of an oscillating heat pipe with Al_2O_3–water nanofluids, Int. Commun. Heat and Mass Transfer, Vol. 17, pp. 111-115.

Reay D.A., Kew P.A., 2006. Heat Pipes Theory Design and Applications, Elsevier, fifth edition.

Riehl, R., 2004. Characteristics of an open loop pulsating heat pipe.

Rittidech, S. & Wannapakne, S., 2007. Experimental study of the performance of a solar collector by closed-end oscillating heat pipe (CEOHP). *Applied Thermal Engineering*, 27(11-12), pp.1978-1985.

Rittidech, S., Boonyaem, A. & Tipnet, P., 2005. CPU cooling of desktop PC by closed-end oscillating heat-pipe (CEOHP). *American journal of applied sciences*, 2(12), pp.1574–1577.

Rittidech, S., Pipatpaiboon, N. & Terdtoon, P., 2007. Heat-transfer characteristics of a closed-loop oscillating heat-pipe with check valves. *Applied Energy*, 84(5), pp.565-577.

Rittidech, S. et al., 2003. Correlation to predict heat transfer characteristics of a closed-end oscillating heat pipe at normal operating condition. *Applied Thermal Engineering*, 23(4), pp.497-510.

Roberts, C.C., 1981. A review of heat pipe liquid delivery concepts. Advances in Heat Pipe Technology. *Proceedings of IV International Heat Pipe Conference*. Pergamon Press, Oxford.

Sakulchangsatjatai, P., 2004. Operation modeling of closed-end and closed-loop oscillating heat pipes at normal operating condition. *Applied Thermal Engineering*, 24(7), pp.995-1008.

Sakulchangsatjatai, P. et al., 2008. Mathematical Modeling of Closed-End Pulsating Heat Pipes Operating with a Bottom Heat Mode. *Heat transfer engineering*, 29(3), pp.239–254.

Savino, R., Cecere, A. & Di Paola, R., 2009. Surface tension-driven flow in wickless heat pipes with self-rewetting fluids. *International Journal of Heat and Fluid Flow*, 30(2), pp.380-388.

Shah, R.K., 1975. Thermal entry length solutions for the circular tube and parallel plates". *Proc. 3rd Natnl. Heat Mass Transfer Conference*, IIT Bombay, Vol. I, Paper HMT-11-75.

Shah M.M., 1979. A general correlation for heat transfer during film condensation inside of pipes, *Int. J. Heat and Mass Transfer*, Vol. 22, pp. 547-556.

Shafii, M.B., Faghri, A & Zhang, Y., 2002. Analysis of heat transfer in unlooped and looped pulsating heat pipes. *International Journal of Numerical Methods for Heat &Fluid Flow*, 12(5), pp.585–609.

Shafii, Mohammad B., Faghri, Amir & Zhang, Yuwen, 2001. Thermal Modeling of Unlooped and Looped Pulsating Heat Pipes. *Journal of Heat Transfer*, 123(6), p.1159.

Smyrnov G. F. and Savchenkov G. A., 1971. USSR patent 504065.

Smyrnov, G., 2004. Method of action of the PHP, its construction and the devices on its base.

Song, Y. & Xu, J., 2009. Chaotic behavior of pulsating heat pipes. *International Journal of Heat and Mass Transfer*, 52(13-14), pp.2932-2941.

De Souza, F.A.S., Destri, J.F.A. & Colle, S., 2007. An Experimental Investigation of a Co2 Pulsating Heat Pipe. In *14th International Heat Pipe Conference (14th IHPC), Florianópolis, Brazil, April 22-27, 2007.*

Swanepoel, G., 2001. Thermal Management of Hybrid Electrical Vehicles Using Heat Pipes. , (November).

Tamburini P., 1978, T-System proposal of a new concept heat transport system, *3rd IHPC Palo Alto*.

Tong, B.., Wong, T.N & Ooi, K.., 2001. Closed-loop pulsating heat pipe. *Applied Thermal Engineering*, 21(18), pp.1845-1862.

Wannapakhe, S. et al., 2010. Heat transfer rate of a closed-loop oscillating heat pipe with check valves using silver nanofluid as working fluid. *Journal of Mechanical Science and Technology*, 23(6), pp.1576-1582.

Webb, R.L., 1994. Principles of Enhanced Heat Transfer, Wiley Interscience, New York.

Weislogel, M.M., 2002. Passive oscillatory heat transport systems. *AIP Conference Proceedings*, 608, pp.241-249.

White and Breadmore, 1962. The velocity of rise of single cylindrical air bubbles through liquids contained in vertical tubes, Chem. Eng. Science, Vol. 17, pp. 351-361.

Wong, T.N., Tong, B.. & Lim, S.M., 1999. Theoretical modeling of pulsating heat pipe. *Heat Pipe Conference, Tokyo, Japan*.

Wyatt, T. A., 1965. Controllable heat pipe experiment for the SE-4 satellite JHU Tech. Memo APL-SDO-1134, John Hopkins University. Appl. Phys. Lab., AD 695433.

Xu, J.L. & Zhang, X.M., 2005. Start-up and steady thermal oscillation of a pulsating heat pipe. *Heat and Mass Transfer*, 41(8), pp.685-694.

Xu, J.L., Li, Y.X. & Wong, T.N., 2005. High speed flow visualization of a closed loop pulsating heat pipe. *International Journal of Heat and Mass Transfer*, 48(16), pp.3338-3351.

Yang, H., Khandekar, S & Groll, M, 2008. Operational limit of closed loop pulsating heat pipes. *Applied Thermal Engineering*, 28(1), pp.49-59.

Yang, H., Khandekar, S & Groll, M, 2009. Performance characteristics of pulsating heat pipes as integral thermal spreaders. *International Journal of Thermal Sciences*, 48(4), pp.815-824.

Zhang, Yuwen & Faghri, Amir, 2007. Advances and Unsolved Issues in Pulsating Heat Pipes. *Heat Transfer Engineering*, 29(1), pp.20-44.

Zhang, Yuwen & Faghri, Amir, 2002. Heat transfer in a pulsating heat pipe with open end. *International Journal of Heat and Mass Transfer*, 45(4), pp.755-764.

Zhang, Yuwen & Faghri, Amir, 2003. Oscillatory Flow in Pulsating Heat Pipes with Arbitrary Numbers of Turns. *Journal of Thermophysics and Heat Transfer*, 17(3), pp.340-347.

Zhang, Yuwen, Faghri, a. & Shafii, M.B., 2002. Analysis of liquid–vapor pulsating flow in a U-shaped miniature tube. *International Journal of Heat and Mass Transfer*, 45(12), pp.2501-2508.

Zuo, Z.J., North, M.T. & Wert, K.L., 2001. High heat flux heat pipe mechanism for cooling of electronics. *ITHERM 2000. The Seventh Intersociety Conference on Thermal and Thermomechanical Phenomena in Electronic Systems (Cat. No.00CH37069)*, 24(2), pp.122-128.